MECHANISMS OF HEAT AND MASS TRANSFER TO AND FROM SINGLE DROPS FREELY-SUSPENDED IN AN AIR STREAM

George Oteng-Attakora

Submitted for the degree of

Doctor of Philosophy

Department of Chemical Engineering and Applied Chemistry

The University of Aston in Birmingham

July 1995

MECHANISMS OF HEAT AND MASS TRANSFER TO AND FROM SINGLE DROPS FREELY-SUSPENDED IN AN AIR STREAM

George Oteng-Attakora

Doctor of Philosophy 1995

SUMMARY

A critical review is presented of the literature pertaining to drop evaporation, drying and dynamics in air.

Information on the dynamics of drops freely suspended in an air stream and their effects on mass transfer rate is limited. There is no model in the literature to adequately describe the effects of droplet surface instability on heat and mass transfer rates. In spray drying the prediction of mass transfer rates immediately after atomisation and prior to skin or crust formation is very important since a great deal of aroma or other volatile flavours may be lost during this period.

A specially-designed vertical wind tunnel was used to freely suspend individual liquid drops of 5 mm initial diameter to investigate drop dynamics, terminal velocity and heat and mass transfer rates. Droplets of distilled, de-ionised water, n-propanol, iso-butanol, monoethanolamine and heptane were studied over a temperature range of 50°C to 82°C. The effects of substances that may provide drop surface rigidity (e.g. surface active agents, binders and polymers) on mass transfer rates were investigated by doping distilled de-ionised water drops with sodium di-octyl sulfo-succinate surfactant. Mass transfer rates decreased with reduced drop oscillation as a result of surfactant addition, confirming the importance of droplet surface instability. Rigid naphthalene spheres and drops which formed a skin were also studied; the results confirmed the reduced transfer rates in the absence of drop fluidity.

Following consideration of fundamental drop dynamics in air and experimental results from this study, a novel dimensionless group, the Oteng-Attakora, (OT), number was included in the mass transfer equation to account for droplet surface behaviour and for prediction of heat and mass transfer rates from single drops which exhibit surface instability at Re>=500. The OT number and the modified mass transfer equation are respectively :

$$OT = \left(\frac{\rho_a v_a^2}{\mu_d}\right).d_e^{1.5}\sqrt{\left(\frac{\rho_d}{\sigma}\right)}$$

$$Sh = 2 + 0.02OT^{0.15}Re^{0.88}Sc^{0.33}$$

Under all conditions drop terminal velocity increased linearly with the square root of drop diameter and the drag coefficient was ≈ 1. The data were correlated with a modified equation by Finlay as follows:

$$C_D = 0.237.\left(\frac{Re}{P^{0.13}}\right)^{1.55}\left(\frac{1}{We.P^{0.13}}\right)$$

The relevance of the new model to practical evaporative spray processes is discussed.

Key Words: Drop Dynamics, Drop Evaporation, Spray Drying.

DEDICATION

Dedicated to my family and friends; both in Britain and in Ghana for their continual support and inspiration.

ACKNOWLEDGEMENT

I acknowledge with gratitude the valued guidance and assistance of Dr. C. J. Mumford who provided me with a broad perspective and deep insight into the mechanisms of drop drying and the science in research in general.

I would also like to thank Dr. E. L. Smith for his immense contribution during the preparation of this thesis and for his diligence in proof-reading and uncomplainingly checking the contents of this thesis. "A good thesis is one that is terse and boasts of clarity and brevity whilst maintaining the underlying science", he would say. Dr. Smith, you are magnificent.

I would also like to thank Mr. Winston Witter for his input and assistance with the organisation and typing of this thesis.

Lastly I would like to thank Aston University for the award of a Supplementary Studentship to top up my S.E.R.C. grant and for financing the greater part of my trip to The 9th International Drying Symposium , IDS'94, in Australia, the proceedings of which proved invaluable to the development of this thesis.

CONTENTS

page

APPENDICES.

LIST OF FIGURES

LIST OF PLATES

LIST OF TABLES

CHAPTER ONE

"Just as a great river is fed by small streams, some even barely noticeable at its source and along its banks, so science and technology proceed from small individual contributions until they become an ever-increasing flow of knowledge with inventions."

G. Oteng-Attakora

INTRODUCTION

1.1 *An Introduction to Evaporative Spray Processes*

Nature provides an invaluable source of models from which analogies can be drawn for most engineering processes. A fish with a streamlined shape, adapted to its environment to reduce drag forces, serves as a useful model upon which the design of aerodynamic and hydrodynamic aircraft, submarines and rockets has been based.

The all-familiar phenomena of rainfall and hailstones also provide one such model for process engineers. In fact Reynolds in 1861 began the study of coalescence by observing the behaviour of a raindrop resting momentarily on the surface of a pond. Rainfall consists of the fall of water droplets through air and during their travel, some evaporation takes place. If the surrounding air temperature is below freezing, the droplets are frozen before they hit the ground and therefore fall as hailstones of varying size. The quality or purity of these stones is undoubtedly affected by pollutants in the atmosphere, e.g. SO_2, making them rather acidic.

The principles underlying the evaporation from, condensation and freezing of droplets are utilised in most industrial liquid/gas operations, e.g. combustion of atomised liquid fuel. In the chemical and biochemical industries, many of the downstream processes involve evaporation and drying of the

product in a particulate form. One such process is spray drying. Masters[1] lists a range of products that have been successfully processed in this way (e.g. dairy products, fruit juice, coffee, vegetable extracts, pharmaceutical products). Spray drying involves the atomisation of a solution or suspension into a myriad of droplets (typically 10-1000 μm) and their contact with hot gas. Not unlike rain drops and/or hail stones, the quality of product is affected by composition, moisture content, retention of volatile compounds, size, shape and physical structure of the particles, which in turn depend upon fluid dynamics and transport conditions during drying.

The complex situation resulting from the atomisation and drying of droplets moving in an air stream provides a challenge for researchers involved in fundamental investigation. Initial mass transfer rates are very high, the process is non-steady state and occurs in a medium with uneven temperature and vapour concentration driving forces. The drops move irregularly relative to the drying medium, are more or less deformed, and exhibit internal circulation. A skin may form: eventually a crust develops around the surface, and in some cases the surface may expand or shrink. Heat transfer between the drops and the medium may occur by a combination of convection and radiation and once a crust is formed, transfer through the surface is by conduction. The overall process is therefore very complex. Unless simplifications are made, the mathematical exposition becomes so complex that its connection with physical reality is obscured. However, the simplifications necessary to set up a real model upon which to base mathematical analyses are numerous and often unrealistic. As a consequence, design criteria are based on empirical correlations and progressive scale-up procedures; spray processes designed in this way very often have narrow operating ranges and can be used only for a limited range of products.

An attempt to study the transport and evaporating characteristics of the individual droplets produced in an atomiser spray is not feasible. However contributions towards understanding the mechanisms of evaporation and drying

of droplets and to improved design criteria can be made by the study of heat and mass transfer between a single droplet and its surrounding gas stream under conditions similar to those encountered in practice. If the method employed displays the salient behaviour of actual systems, the fruitfulness of the approach is established and the resultant theory, although it may be simplified, will provide the ground work needed for handling more complex models. Many investigators have therefore invested considerable effort in examining the transport phenomena pertinent to drops and to particles of various shapes and sizes. What is lacking in the literature is attention to the surface hydrodynamics of droplets, i.e. the effects of drop oscillation, surface tension and viscosity on mass transfer from drops in free-flight. Most of the studies in the past have been mainly of evaporation with the droplet motionless relative to the drying medium, so that the hydrodynamic factor is absent. Such conditions have unprecedented disadvantages and never occur in practice. The author's experimental work[168] and that of others demonstrate that a drop in free flight presents different major and minor axes ratios. These ratios subject the drop to drag forces of different magnitudes inducing internal circulation, drop rotation and vibration which lead to an extension of its surface. The extension of droplet surface requires that molecules be brought from the interior of the droplet to the surface against the inward attractive force perpendicular to the surface to increase the surface area. The ease or otherwise of this phenomenon will depend invariably on the physical properties of the droplet. The mass transfer rates of drops exhibiting this behaviour deviate from predictions using existing correlations derived by Frossling[2] and Ranz and Marshall[3]. A new, or modified, mass transfer correlation is therefore required which takes into account droplet behaviour. This thesis reports on both theoretical considerations, and experimental investigations carried out to develop a new dimensionless group and a modified mass transfer equation for prediction of mass transfer rates from atomised oscillating drops.

1.2 *The Objectives of the Thesis*

The objectives of this work were to define more precisely the mechanisms of drop behaviour in free-flight and to develop a model for predicting heat and mass transfer rates immediately after atomisation.

Masters[1] in a schematic illustration of the stages involved in an open-cycle co-current spray dryer, presented four main stages as in Figure 1.1. This

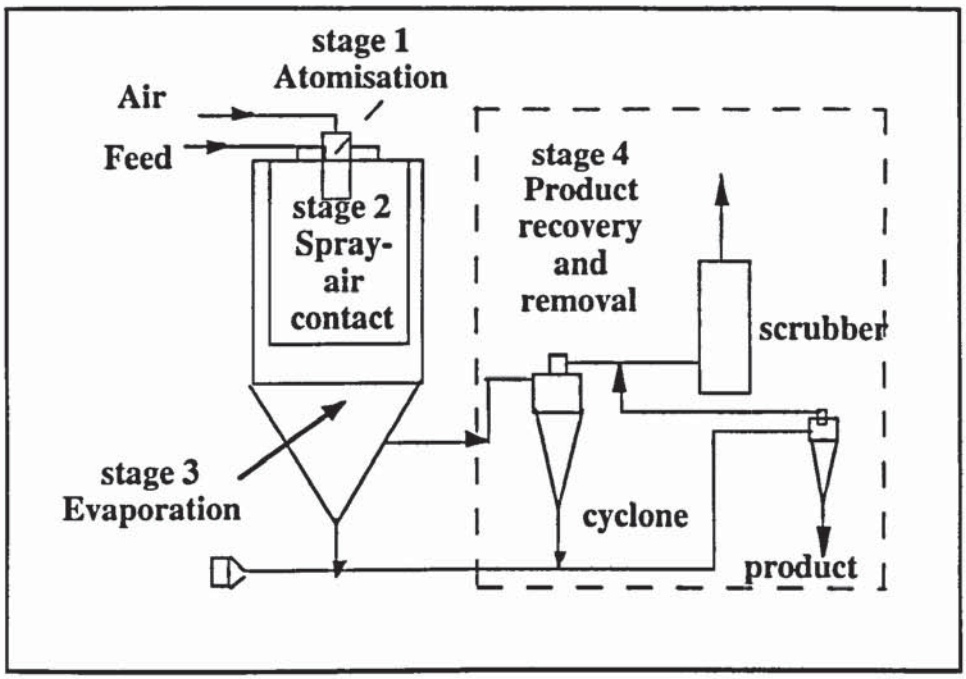

Figure 1.1 Basic layout of an open-cycle co-current spray dryer.[1]

presentation is misleading. It tends to suggest that in the spray air/mixing stage; stage 2, no evaporation occurs, and that evaporation commences at stage 3 during which droplets have assumed a stable spherical shape. The present work seeks to provide a correction to this postulation. The approach employed is given in section 1.3.

1.3 *Approach to the Problem*

An improved correlation for heat and mass transfer from single drops clearly requires appropriate experimental data. The present studies made use of a vertical wind tunnel provided with an angled mirror to produce a three-dimensional image of each droplet. Droplet surface behaviour and age were

monitored with a Mitsubishi Video Camera Recorder equipped with a fast shutter speed of up to 1/10000 sec. The camera was fitted with a X5 zoom magnification and gave an exposure of 100 frames per second. An in-built timer allowed each frame to be studied.

The study was divided into two parts:

(i) drop visualisation and hydrodynamic study, and,

(ii) a study of the effects of surface tension, drop viscosity and drop surface behaviour on heat and mass transfer rates.

By following this programme it was hoped to shed more light on the following questions:

(1) When air/liquid drop phases are separated by an interface how do interfacial instabilities, and rates of heat and mass transfer across an interface element, depend upon the bulk state of the phases and their properties?

(2) When air/liquid drop phases are present in a finite volume, how do the variations with time of interfacial behaviour depend on the initial states and on operating conditions?

(3) When air/liquid drop phases are present as process streams through an extensive piece of equipment, how do the selection of inlet and outlet streams depend on each other and upon the flow conditions and drop behaviour in the equipment?

1.4 *Organisation of The Thesis*

Liquid as it leaves the nozzle of an atomiser is still in a continuous body in the form of a cylinder or a sheet. The mutually opposing surface tension and aerodynamic forces acting upon the surface of the liquid body, give rise to oscillations and perturbations and cause the liquid to break up into drops. If the drops so formed are bigger than the stable maximum limit, they disintegrate further into smaller droplets. This confirms that the forces causing liquid disintegration do not diminish once droplets are formed. Before the droplets

attain their final velocity, they have often experienced a much higher initial velocity and gone through a series of shape oscillations. Considerable evaporation takes place during this period over and above that which would occur without drop oscillation. Owing to the complexity of the interaction between hydrodynamic behaviour of the bulk phases, interfacial dynamics and mass transfer, no satisfactory method has as yet been developed for the prediction of mass transfer rates in the presence of interfacial oscillation.

To promote a better understanding of the physical dynamics underlying these processes, a review of the literature pertaining to atomisation and liquid break-up, and the experiments leading to some of the fundamental theories of mass transfer is presented in Chapter Two. This is followed by a discussion of the development of fundamental momentum transport equations, mass transfer theory and interfacial phenomena in Chapter Three.

Chapter Four is devoted to a critical review of evaporation from spheres and drops. Previous work is described and evaluated in terms of its generality and practicality.

Chapter Five describes the experimental programme followed in the present work.

Chapter Six presents representative experimental results with explanations of the technique used. It also compares present findings with those in previous work. The results of this work are then applied to the analyses and development of a model to correlate mass transfer data and to predict mass transfer rates from spray droplets in Chapter Seven.

Finally Chapter Eight presents conclusions and recommendations for further work arising from the work in this thesis.

In the Appendices are detailed experimental data and the listing of the program, SURFACE_TEMPERATURE, written in turbo pascal, to calculate droplet surface temperature.

CHAPTER TWO

2 DYNAMICS OF LIQUID-GAS SPRAY SYSTEMS

CHAPTER TWO

DYNAMICS OF LIQUID-GAS SPRAY SYSTEMS

2.1 *Introduction*

Liquid disintegration into droplets is the first stage of all liquid-gas spray processes. Spray processes are performed to achieve greater surface area, to produce a homogeneous dispersion and to enhance heat and mass transfer rates. There are three types of liquid-in-gas dispersions that are of practical interest in the process industries. These are: (1) sprays produced by nozzles or by other atomisation systems for combustion, fire fighting, evaporation/drying or coating of surfaces; (2) mist due to entrainment generated by gas bubbling through a liquid as in distillation towers or kettle reboilers; and (3) fogs generated from gases that are super-saturated. The first two are of interest to the present study. They share a dependency on mechanical break-up of the liquid mass which is frequently a combination of processes involving disintegration of liquid columns, sheets and filaments. In spray evaporation/drying, the feed is dispersed by some form of atomisation device, mixed with a gas and evaporated by a process of simultaneous heat and mass transfer. Within a spray, there is a distribution of drop sizes, the size range of which is dependent on the physical properties of the liquid and the type and operating parameters of the atomisation device employed. The droplet size spectrum determines droplet behaviour and droplet trajectory which in turn determines the residence time and hence the extent of evaporation or drying.

The initial size of droplet in a spray dryer does not necessarily represent the size of resultant dried particle at the end of the drying process, since the droplet may shrink, collide with the wall of the drying chamber, rupture or agglomerate. It is therefore important that droplets immediately following release from the atomiser, when droplet behaviour is still affected by the liquid physical

properties and turbulence, are partially dried before impinging on the walls of the drier to prevent undesirable wall build-up or agglomeration of droplets.

A knowledge of droplet atomisation and droplet behaviour therefore facilitates better understanding of droplet evaporative mechanisms immediately after atomisation and the prediction of wall impingement and drop coalescence which are critical considerations in product specification and in spray dryer design. The intent of this chapter is not to give a detailed analysis of atomiser design and droplet formation but to provide a general review of liquid break-up and its implications for droplet behaviour. The effects of droplet hydrodynamics, drop shape oscillation and break-up and internal circulation are discussed in section 2.2. and 2.3. Section 2.4 continues the discussion of the effects of momentum transfer, wake shedding and superimposed mass on droplet aerodynamic drag and drop motion. A summary of the discussion is provided in section 2.5.

2.2 *The Mechanisms Of Droplet Atomisation*

Liquid disintegration may be brought about by one or a combination of the following atomisation processes: (1) hydraulic; (2) pneumatic, and (3) electrical. More recently, sonic or acoustic atomisation and turbulent impinging jets have also been used successfully. Liquid disintegration by turbulent opposing jets is achieved by impinging two jets head on such that the shear force is large enough to break the jet into droplets[4]. However, such techniques have not reached commercialisation and are not included in the present discussion. For the purposes of this study, only hydraulic and pneumatic atomisation will be considered. Special attention is paid in this chapter to liquid jet and sheet break-up, but the principles discussed here are applicable to most commercial methods of atomisation.

The break-up of liquid discharged from an orifice of a nozzle is effected by three factors. These are (1) the initial disturbances to the liquid in the atomiser

which affect the turbulence in the jet or sheet; (2) the properties of the medium into which the droplet is discharged; and (3) the physical properties of the discharged liquid. Each of these contributes to the process of spray formation but the precise contribution of each in the disruption of the liquid is a subject of debate. A change in the physical properties is thought to have an effect not only on the process of droplet formation and hence droplet size but also influences the spray indirectly by its influence upon the flow through the nozzle. This flow phenomenon depends primarily on the value of the Reynolds number and hence the kinematic viscosity.

2.2.1 *Disintegration of Liquid Jets*

One of the earliest theories of the disruption of liquid jets is attributed to Lord Rayleigh [163]. He considered laminar liquid flow with a velocity potential and with a jet only under the influence of surface tension forces. It was concluded that a jet would be unstable and ready to disrupt if its length were greater than its circumference i.e. $L > 2\pi r$. Although the conditions considered by Rayleigh do not exist in practice, i.e. (a) the flow in an actual jet is turbulent, (b) the liquid is viscous, and (c) the effect of the surrounding air is not negligible, the general conclusions from his work regarding jet stability have been accepted by later theorists. The basis of Rayleigh's solution assumes irrotational flow of a non-viscous jet such that any small disturbance or distortion of the jet in its flight results in an imbalance in the forces acting on the jet. Under certain conditions, this imbalance is self-perpetuating and leads to an increased disturbance until necking or jet break-up occurs. The force required to continue this imbalance is that of surface tension. Mathematically stated:

$$\eta = \eta_o \exp(qt) \qquad (2.1)$$

where η = amplitude of disturbance, η_o = initial amplitude and q, the growth rate is given by;

$$q = \sqrt{\frac{\sigma}{\rho_l R_o^3}}\, f\left(\frac{2R_o}{l}\right) \qquad (2.2)$$

R_o = jet orifice radius, l = wavelength of the disturbance, and t = time.

In their analyses of spray formation from liquid jets, Weber[5] and Ohnesorge[6] highlighted the importance of turbulent flow in the atomiser. According to Ohnersorge, the turbulence gives the liquid jet a radial velocity component which helps to overcome the surface tension forces and leads to break away from the main jet, thus accelerating the process of atomisation. Liquid break-up was correlated in terms of the Reynolds number (Re) and the Z number of the liquid jet. The Reynolds number represents in part the flow characteristics of the jet and the Z number, the ratio between the Reynolds and the Weber number (We). The greater the value of We, the greater the external force compared with the counteracting interfacial tension; at a critical value, We_{crit}, break-up occurs. Weber[5] calculated the break-up time and found it to be proportional to $d^{1.5}$ for non-viscous liquids and proportional to d for viscous liquids (d = jet diameter).

The manner in which the air forces participate in the disruption of a high speed jet has been analysed by Hinze[7]. Hinze identified three ways in which forces associated with air flow can cause detachment of a droplet from the main jet. These are: (a) the action of normal forces; (b) the action of tangential forces; and (c) the action of local turbulence in the air. The tangential air forces are caused by the friction of the air on the surface of the liquid similar to the normal air forces. They become effective when any ruffling or distortion of the surface of the jet occurs.

Holfelder[8], Haelein[9] and later Dombrowski and Frazer [10] used high speed photography to investigate the formation of spray droplets and identified four stages of liquid disruption:

(1) break-up into droplets caused by rotationally symmetrical oscillations of the jet surface due to the effect of primary disturbances and surface tension forces, (Figure 2.1);

(2) break-up into droplets due to oscillation with the additional effect of air friction, (Figure 2.2);

(3) break-up through undulation of the jet, assisted by air friction, (Figure 2.3); and

(4) complete and immediate disruption of the jet. The cross-section of the jet can become deformed in such a way that successive deformations are displaced by 90 degrees.

If the distance between one deformation and the other as indicated by l (wave length) is less than the circumference of the jet, then surface tension forces can prevent further increase in deformation and thus prevent disruption of the jet. However, if l is greater than the circumference, then surface tension forces contribute to further increase deformation and the disruption of the jet. The most favourable wave length for jet disruption was calculated by Weber [5] to be:

for non-viscous liquids, $$l_{opt} = \sqrt{2\pi d} \qquad (2.3)$$

and for viscous liquids, $$l_{opt} = \sqrt{2\pi d}\ \{1+(2\mu^2-d)^{0.5}\}^{0.5} \qquad (2.4)$$

2.2.2 *Liquid Sheet Break-up*

The mechanism of droplet formation by liquid sheet break-up is prevalent in atomisers like the fan nozzle, swirl nozzle and rotational discs. The basic principle is to form a thin sheet which can break via a variety of mechanisms to

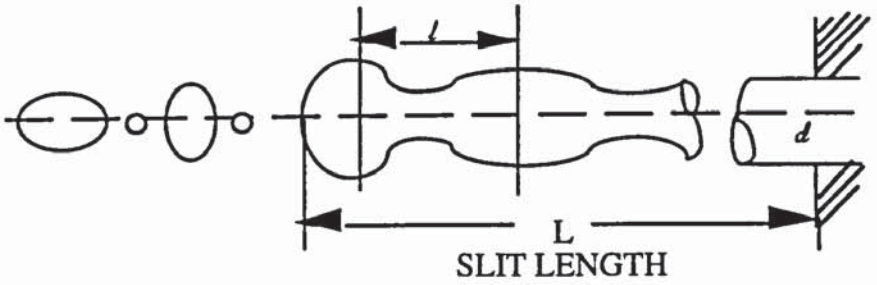

Figure 2.1 Oscillation Causing Disruption of Jets.

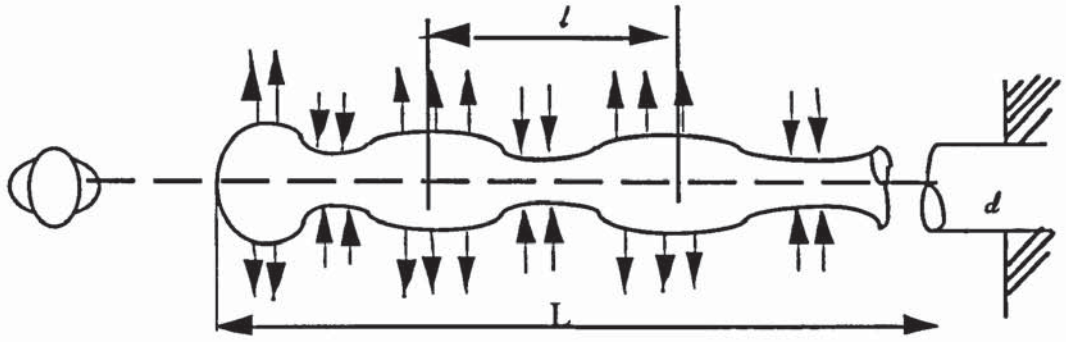

Figure 2.2 Jet Disruption by Oscillation with Air Friction.

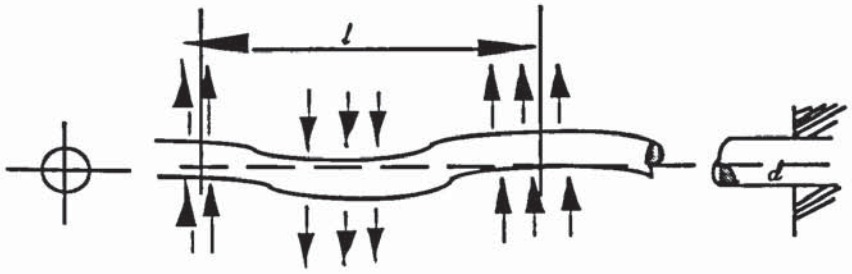

Figure 2.3 Wave-like Break-up of Jet with Air Friction

form threads of liquid which in turn yield chains of droplets. Dombrowski et al[11] and Castleman [12], have argued that to create a disrupted state, a continuous change in the bulk fluid must occur forming unstable ligaments or short films which collapse to yield drops. The collapse of the unstable ligaments to droplets is taken to proceed in a manner analogous to that described for liquid jet break-up. However, there are three main mechanisms that individual atomisers may follow in attenuating the fluid to some unstable form:

(1) rim disintegration, in which the free edge of the sheet contracts into a cylinder which then breaks from the surface as large drops (the breakdown is restrained by high viscosity);

(2) perforated sheet disintegration in which depressions due to turbulence puncture the sheet; cavities then grow rapidly with their rims joining to form threads which break into droplets (Figure 2.4);

(3) wave disintegration in which reinforcement of surface waves by drag forces builds up until the sheet ruptures (Figure 2.5).

It is clear that liquid disintegration is based on the conversion of pressure energy within the bulk of the liquid into kinetic energy of the liquid leaving the nozzle or the edge of a rotating disc. The aerodynamics of the liquid surface generate turbulence and sinuous and dilational instabilities which ultimately lead to the formation of droplets of varying sizes. Liquid viscosity resists drop formation at all stages. However, whilst the effect of surface tension is to resist sheet deformation, it assists drop formation after the sheet is broken down. Surface tension helps the drop attain the minimum surface area as a sphere. As the drop is originally elongated and deformed during the drop formation and detachment stage, the tendency to create the minimum surface area leads to oscillations in shape.

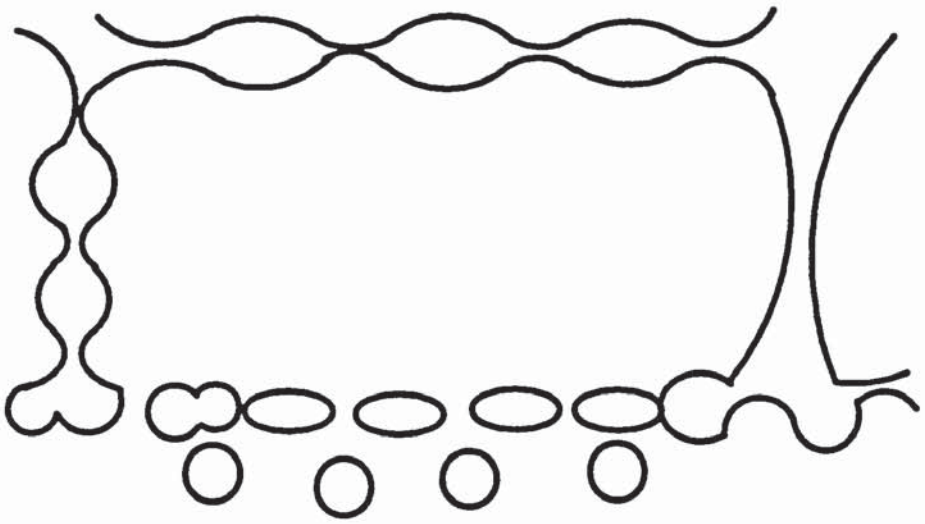

Figure 2.4 Liquid sheet subjected to aerodynamic sinuous waves

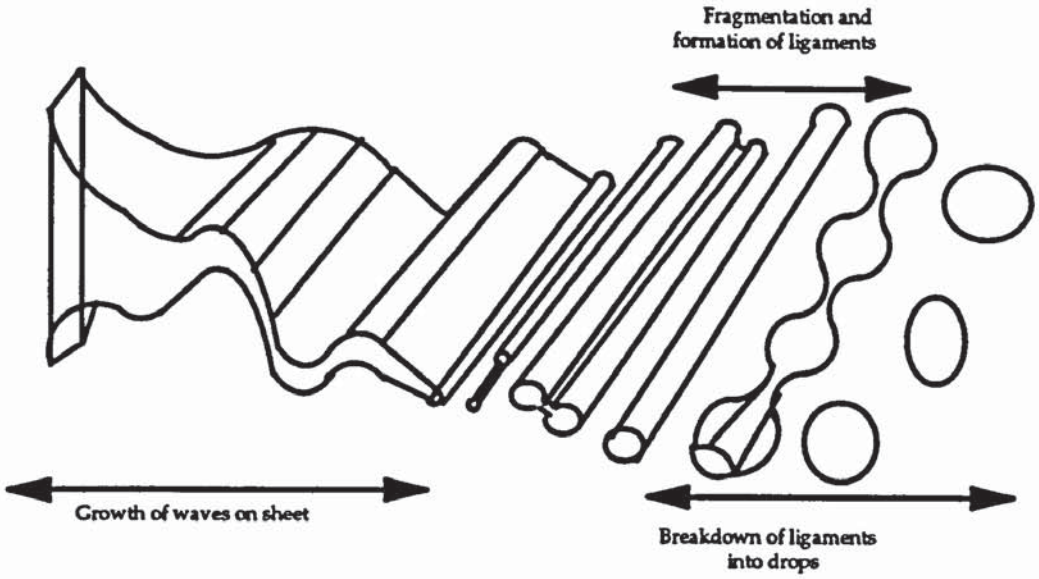

Figure 2.5 Drop Formation; perforated sheet disintegration

2.3 *Droplet Hydrodynamics*

In spray processes, there are two different aerodynamic zones through which the droplet must travel; a region in the vicinity of the atomising nozzle where the liquid jet or sheet has just disintegrated, and a region downstream where the liquid exists as stable droplets almost at their terminal velocity and where spray-air mixing is complete. Pham and Keey [13] refer to the former as the jet zone and to the latter as the principal zone. The effects of the jet zone are four-fold:

(1) the relative velocity between a droplet and the air is higher than in the main zone owing to the larger air velocity gradient;

(2) the absolute velocity of the droplet is also higher since it is still decelerating;

(3) the kinetic energy of the droplet and the turbulence on the liquid surface of the parent liquid jet or sheet which is determined by liquid viscosity, surface tension and aerodynamic forces will maximise drop oscillation and increase the degree of turbulence on the droplet surface;

(4) the confined geometry of the jet and the limited amount of air in it will tend to diminish the effective driving force and hence minimise possible heat and mass transfer processes.

Effects 1, 2 and 3 tend to increase the rate of material transfer whilst effect 4 will decrease it. As the droplets travel downstream in the principal zone, they entrain the ambient gas and consequently set up an overall induced gas flow field. This induced gas motion in turn modifies the droplet trajectory. The subsequent behaviour of the principal zone is then governed by the interaction between the droplets and the gas space. The dynamics of the jet zone or the atomisation region is of particular interest to the present study in relation to evaporative spray systems. A knowledge of the hydrodynamics of liquid droplets

in this zone should therefore precede any study of the heat and mass transfer mechanisms within such systems.

2.3.1 *Drop Oscillation & Break-up*

In the jet zone, droplets are ejected into the gas stream at high initial velocities, and are elongated and deformed during formation and detachment. The external gas resistance force and the internal forces determined by the droplet viscosity and surface tension subject it to opposing forces which induce further deformation, internal circulation, drop shape oscillation and rotation. It is possible that mass may separate from the droplet surface in an extremely fine mist as the equilibrium between the aerodynamic forces and surface tension is upset. This phenomenon is itself of great interest in relation to the internal combustion engine, agricultural spraying, production of aerosols and spray drying. An accurate description of the deformation is impossible to formulate from theory alone because of the lack of information on the pressure distribution around small moving droplets. As the shape of a droplet changes, the pressure distribution around it also changes: either a state of equilibrium is reached between the external and the internal pressures or further deformation follows which may result in splitting of the droplet.

The mode of break-up appears to depend upon the initial Weber number, which relates inertial forces to the forces of surface tension. For We less than 10, the drop will deform without breaking, indicating the dominance of surface tension. Lane[14] determined the critical air stream velocity at which drops would just shatter to be inversely proportional to the square root of the initial drop diameter. Shattering was considered to be due to either boundary layer stripping or the production of unstable waves on the surface of the drop, but calculations based on the former did not agree with experimental results.

Further studies of critical Weber number were made by Morrell[15] who observed that when jet or drop break-up is achieved by the stripping mechanism,

a critical value of dynamic pressure, rather than the Weber number, is important. Hanson et al.[16] used a shock tube to provide a sudden flow over drops of either water, methyl alcohol, or three viscous oils. They observed a 'bag-type' break-up, in which the air stream flattens the drop until, at a critical relative air speed the drop is blown out in the downstream direction like a bag attached to a rigid rim. It was proposed that the mode of break-up changes only when the air stream velocity exceeds the critical value by an appreciable amount. In such cases the drop takes the shape of a plano-convex with the plane surface leeward upon further deformation. Liquid is drawn downstream from the edges of the drop into a thin sheet which is eventually torn into ligaments and then into smaller drops. However, the mere passage of a shock wave over the drop will not cause break-up. Rather, a sustained large relative air velocity is necessary to form the drop. Rabin et al.[17] also observed both bag-type and shear shattering and proposed a critical Weber number proportional to $\sqrt{Re}$ for the latter.

According to Klusener [18] if a droplet is in a state of equilibrium, the outer pressure (Pa) and the surface tension (Ps) give rise to a pressure (Pi) inside the droplet, i.e. Pi = Ps + Pa = constant. At a point where Pa increases, the droplet will become flatter, thus decreasing the value of Ps and vice versa, (Fig. 2.6). For a sphere, Ps equals $2\sigma/r$. If Ps<Pa any appreciable change in Pa cannot be balanced by a corresponding change in Ps to maintain the value of Pi constant. The outer pressure may therefore change the shape of the droplet in such a way that a further decrease occurs in Ps at certain points resulting finally in it splitting into two or more smaller droplets.

The deformation of moving droplets has been considered further by Hinze [19], who analysed mathematically the balance between the dynamic force of the environment and the surface tension of the liquid and the effect of viscosity on the splitting of droplets. It was concluded that, although a droplet would tend to split if the Weber number is greater than ten, viscosity could delay and dampen excessive deformation such that splitting is averted. It was postulated that, if the

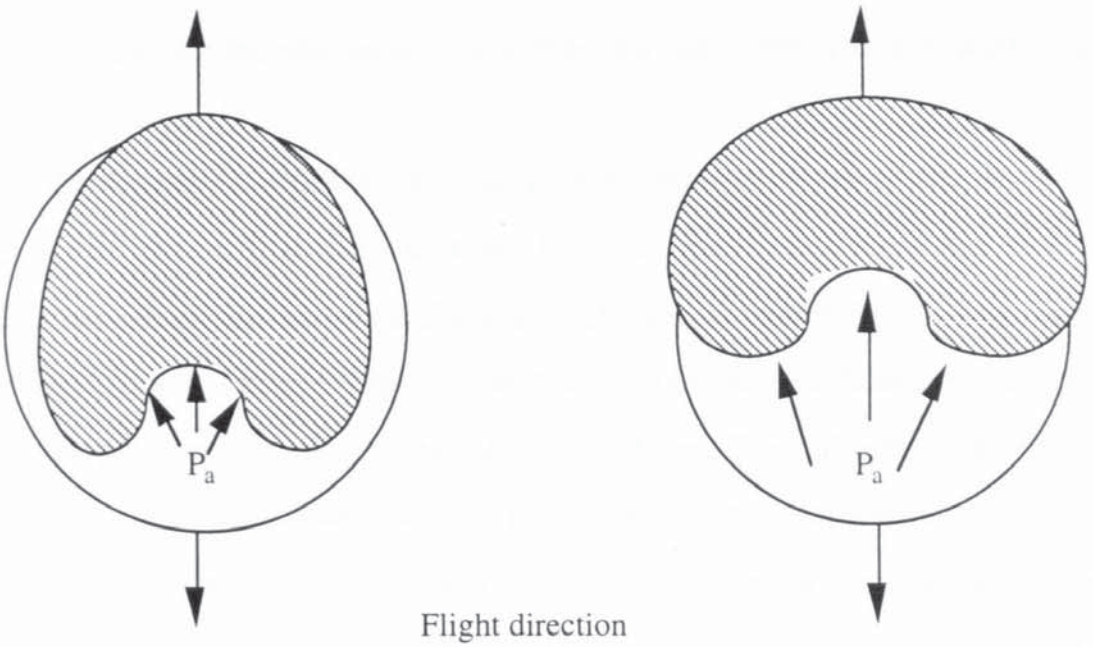

Figure 2.6 Deformation of droplet in turbulent air flow

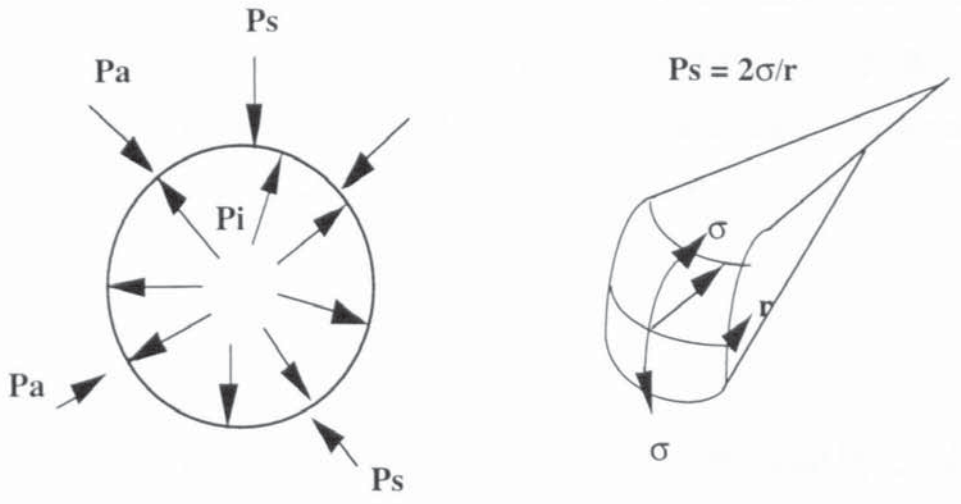

Figure 2.7 Forces acting on droplet surface.

rate of deformation is substantially decreased by viscosity effects, there may be sufficient time for the relative air velocity to fall below the critical value so that no splitting occurs.

Photographic studies, especially of multiple pictures of the same liquid drop in air, reveal that during travel in air drops do not have any particular equilibrium shape but show oscillations in shape and even rotation. Blanchard[20], Srikrishna[21] and Akbar [22] investigated the shapes and oscillations of individual liquid drops in air by taking stroboscopic pictures. They all presented values of major and minor axes. Blanchard[20] in his investigation suspended water drops in an open wind tunnel and studied drop size, suspension time, maximum drop diameter before break-up, aerodynamic effects as a cause of drop collision, and drop break-up by collision. Brass plates and mesh screens were used inside the wind tunnel to lower the velocity in the central portion of the air core. He thus obtained the conditions necessary for the suspension of drops of water and observed both drop oscillation and rotation.

Srikrishna[21] studied the shapes and oscillation of individual acetone drops in air by employing photographic techniques. The oscillation frequencies of liquid drops in air were found to decrease with an increase in drop diameter. For some drop sizes, Srikrishna reported more than one oscillatory frequency. He proposed the following correlation for the frequency of oscillation,

$$f_n = [(8\sigma)/(3\pi m)]^{0.48} \qquad (2.5)$$

Equation 2.5 is very close to the theoretical correlation proposed by Lamb

$$f_n = [(8\sigma)/(3\pi m)]^{0.5} \qquad (2.6)$$

with about 7% maximum deviation.

Garner and Lane[23] determined experimentally the frequency of oscillation of water drops and seven organic liquids (drop size: 3-5 mm) in a vertical air stream and found that the values agreed with the theoretical values obtained using Equation 2.6. However, the oscillation frequencies reported by Costan and Calvert [24] for drops of water and three organic liquids did not agree with the theoretical values using Equation 2.6. A "Ciné-Kodak Special" 16 mm camera fitted with a 63 mm f/2 lens, and run at 64 frames/sec was used by Garner and Lane[23] to study drop behaviour. The camera gave an individual exposure of 1/500 sec. Costan and Calvert[24] on the other hand used separately, a 16 mm high speed motion picture camera at 400 to 1,200 frames/sec, and a 16-mm camera at 64 frame/sec with exposure of 1/500 sec. Drop diameter studied was between 2 to 3 mm. The discrepancy in the two results could be due to the limitation of the Ciné Kodak camera used by Garner and Lane. However, Costan and Calvert attributed the deviation of experimental data from Equation 2.6 to effective diffusivity, but no satisfactory means were established to correlate the oscillation to effective diffusivity.

Earlier descriptions of drop behaviour by some investigators [25, 26] assumed an oscillation between prolate and oblate ellipsoids of revolution in which the drop was viewed in two dimensions and the concept of symmetric oscillation applied. Based on these assumptions, Garner and Lane[23] correlated the mean values of the major and minor axes (a/b) with the Eotvos group $(g\Delta\rho d_e^2/\sigma)$ and produced the correlation;

$$\left(\frac{a}{b}\right) = 0.12(g\Delta\rho d_e^2/\sigma) + 1 \qquad (2.7)$$

Gunn [27] investigated the behaviour of water droplets in vertical fall and plotted the natural oscillation frequency of a drop and the frequency with which eddies were shed from the wake of the drop against drop size. The results

support the theory of drop oscillation being a function of periodic wake shedding.

Grace et al[28] classified droplet behaviour into four shape regimes, plotting the Reynolds number and the Morton number against the Eotvos number. These drop shape regimes are: (a) spherical, (b) ellipsoidal, (c) wobbling and (d) spherical-cap and ellipsoidal-cap. In the spherical regime, drops are closely approximated by spheres if interfacial tension or viscous forces are much more important than inertial forces, i.e. the Re is sufficiently low that there is no wake at the rear of the drop. Drops in this regime are generally very small, usually less than 1 mm in diameter, and exhibit no internal circulation. They tend to obey Stokes' law.

As the drop size is increased above the laminar flow region ($10 < Re < 100$) with an increase in Eo number, a size is reached at which the drop flattens and assumes a generally oblate ellipsoidal shape, thus marking the beginnings of the ellipsoidal regime. Drops in this regime are unstable especially at low viscosity, and begin to oscillate. The oscillation may be triggered by the shedding of vortices in the wake.

With larger drops, of diameter greater than 1 mm, a series of oscillations accompanied by waves moving over the interface is typical. Surface behaviour is thus typified by fluttering surface instabilities which cause the droplet to dilate and recede in a random wobbly manner. Spherical and ellipsoidal cap drops are marked with indentations at the rear and flat bases at high Re and Eo numbers. Such drops resemble segments cut from spheres or from oblate spheroids of low eccentricity. These classifications are, however, limited to the motion of drops and bubbles through liquids and as such the boundaries of shape regimes may not strictly apply to droplets in air.

Many investigators[29, 30] have attempted to refine the calculation of drop shape by considering the internal circulation of the liquid induced by surface forces. McDonald[31] investigated the following factors in connection with shapes

of drops; surface tension, hydrostatic pressure, external aerodynamic pressure, circulation and electrostatic charges. He concluded that only the first three factors were important.

2.3.2 *Drop Internal Circulation*

The phenomenon of internal circulation occurring in liquid drops falling in air has been investigated by Hadamard[32] and Rybczynski[33]. Garner and Lane[23] measured internal circulation velocities of individual drops falling in a gas by observing the movement of aluminium particles inside each drop. The measured circulation velocities were found to be of the same order as those calculated using the Rybczynski-Hadamard model.

The Rybczynski-Hadamard model considers a fluid sphere with its interface assumed to be completely free from surface-active contaminants so that the interfacial tension is constant. The interfacial boundary is assumed to move over the surface of the sphere in axial symmetry from a front stagnation point to a rear stagnation point such that new area is being continuously created in the forward regions and an equivalent area destroyed in the rear of the drop. The above assumptions summarised as:

(i) stresses through the interface are continuous,

(ii) tangential velocity is continuous through the interface,

(iii) there is no movement of fluid across the interface,

(iv) the interfacial tension is zero,

lead to the internal motion of the drop given by:

$$\psi_p = \frac{u\, r^2 \sin^2\theta}{4\left(1 + \left(\mu_d/\mu_c\right)\right)}\left[1 - \frac{r^2}{a^2}\right] \tag{2.8}$$

and the terminal velocity as:

$$u_t = \frac{3\mu_d + 3\mu_c}{3\mu_d + 2\mu_c}\cdot\left(\frac{(\rho_d - \rho_c)gd^2}{18\mu_c}\right) \tag{2.9}$$

For a liquid drop falling in air or for a very viscous drop in a low viscosity field liquid, Equation 2.9 becomes equivalent to Stokes' law. It must be mentioned that surface-active contaminants are present in most systems of practical importance and for this reason the Hadamand-Rybczynski equation is not obeyed in practice.

Bond and Newton[34] suggested that a circulating drop required energy locally to stretch interfacial area elements over the leading deformed shape, while these shrink over the rear surface. This process was hypothesised to cause additional tangential stresses which retard the droplet with surface tension playing the dominant role in determining whether the terminal velocity follows Stokes' law or Rybczinski's model. Bond and Newton[34] proposed that internal circulation would only occur for Eo>4. However, subsequent experimental work[35, 36] has demonstrated that the so-called Bond criterion is not always applicable. On the other hand the surface energy argument has been shown by Harpel et al[37] to be valid if the tangential gradients of temperature and surface tension are considered.

The lack of internal circulation in small droplets was proposed by Boussinesq[38] to be due to an interfacial monolayer which acts as a viscous membrane. A model commonly called the "Newton surface fluid model" was proposed by Boussinesq which involves surface shear viscosity and surface dilation in addition to surface tension. The problem with Boussinesq's model is that it is difficult to obtain reliable measurements of the surface viscosity.

Frumkin and Levich[39] proposed a surface contamination theory. According to this theory, the absence of internal circulation in small drops is due to surfactant contamination. When drops move through a continuous phase, absorbed surface active materials are swept to the rear leaving the frontal region relatively uncontaminated. The concentration gradient is most profound for small drops, in agreement with the tendency for small fluid particles to be particularly subjected to retardation. The theory further suggests that irrespective of size all drops will exhibit internal circulation if the system is sufficiently free of surface

active contamination. Experimental evidence from observations of small drops in liquid-liquid systems tends to support this view[40].

The criterion commonly used for characterising the droplet hydrodynamic state is the drop Reynolds number. i.e.

(i) stable droplet, $Re_{drop}<1.0$

(ii) circulating droplet, $1<Re_{drop}<200$

(iii) oscillating droplet, $Re_{drop}>200$

However, it is apparent from the above review that complex interactions and other property characteristics should be considered in order to classify the hydrodynamic state of drops. The Weber number, the Strouhal number, the Ohnesorge number or a new property group may need to be included to characterise drop behaviour. In order to fully characterise drop behaviour and to predict the momentum transfer associated with it, the aerodynamic drag on the droplet must also be considered.

2.4 *Aerodynamic Drag & Drop Motion.*

The flow of a real fluid (except at extremely low pressure) has two fundamental characteristics. One is that there is no continuity of velocity; the second is that, at a solid surface, the velocity of the fluid relative to the surface is zero. As a result, a region exits close to the surface, in which the velocity increases rapidly from zero and approaches the velocity of the main stream. The increase in velocity with increasing distance from the solid surface involves relative movement between the particles in the boundary layer and thus shear stress is in evidence. Since the layer is usually very thin the velocity gradient, i.e. the rate of change of velocity with increasing distance from the surface is high and the shear stresses are important.

Drag is the result of shear stress forces and pressure difference. This in turn determines droplet velocity and momentum with respect to the continuous phase and hence material transfer rates.

2.4.1 *Momentum Transfer*

The phenomena of momentum transfer arising from droplet motion in a fluid is the key to understanding heat and mass transfer processes from spray droplets. Determination of droplet trajectory, residence time and momentum transport in forced convection depends upon the evaluation of the drag force exerted by the fluid on the droplet. For any surface in contact with a flowing fluid, skin friction or drag will exist. Skin friction results from the transfer of momentum from the continuous phase perpendicular to the droplet surface which gives rise to a tangential shear stress on the surface parallel to the direction of flow.

If a fluid is not flowing parallel to the surface but must change direction to pass round the body of some geometric shape, significant additional frictional losses will occur in addition to skin friction; and this is termed form drag. The forces in the boundary layer which oppose the fluid flow are: (1) viscous forces, (2) frictional forces causing retardation, and (3) a pressure gradient causing retardation. Whereas the skin friction drag is the resultant of the forces tangential to the surface, the form drag is the resultant of the forces normal to the surface.

In almost all cases in which flow takes place around a solid body, the boundary layer separates from the surface towards the rear of the body. Downstream of the separation position the flow is greatly disturbed by large-scale eddies, and this region of eddying motion is known as the wake (Fig. 2.8, Fig. 2.9). As a result of the highly turbulent motion in the wake the pressure there is reduced and the form drag is thus increased. The magnitude of the form drag

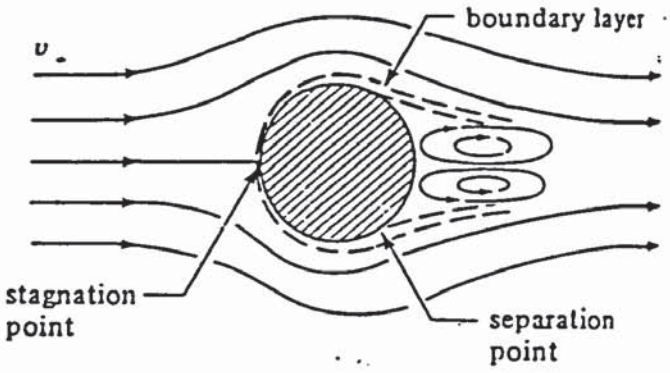

Figure 2.8

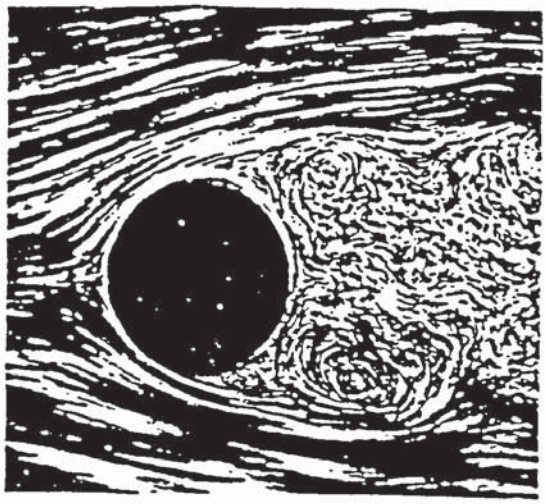

Figure 2.9

Figures 2.8 and 2.9. Flow pattern and development of wake behind spheres.

depends on the size of the wake and this, in turn, depends on the shape of the object and the position of separation. For a bluff body, the flow is separated over much of the surface, the wake is large and the form drag much greater than the skin friction. Undoubtedly, therefore, droplet shape oscillation will contribute to the total drag force.

Results obtained from investigations on the drag force are normally represented by the standard drag coefficient (C_D), which is defined as the ratio of the total drag force per unit area to the dynamic force of the continuous phase, $C_D = \frac{F_D/A_p}{\rho v^2/2}$. The Reynolds number for a given object immersed in a flowing fluid is given by $Re = \frac{D_p v \rho_a}{\mu}$. For each, particular shape of object and orientation of the object with the direction of flow, a different relationship of C_D vs. Re exists. Correlation of C_D vs. Re is shown in Figure 2.10. In the laminar region corresponding to low Reynolds numbers, the experimental drag force of which two-thirds is attributed to skin friction is the same as the theoretical Stokes law Equation as follows;

$$F_D = 3\pi\mu D_p v \qquad (2.10)$$

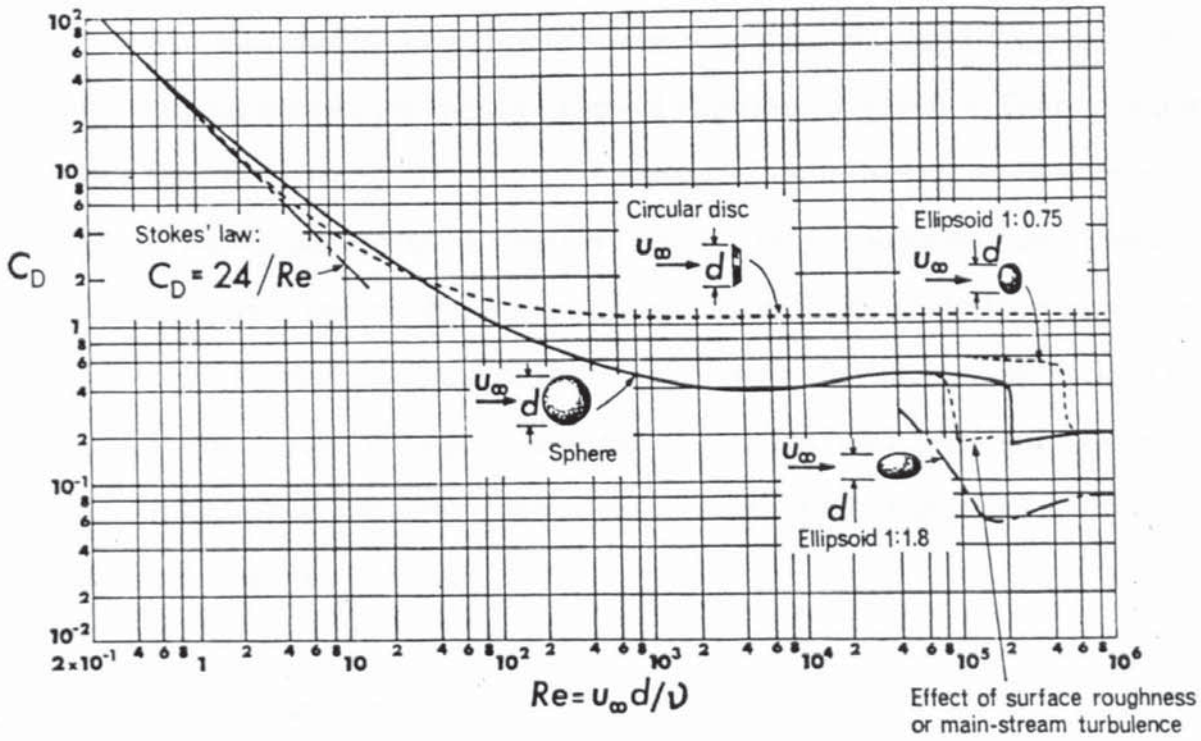

Figure 2.10. Drag coefficient as a function of Re .

thus solving for a spherical droplet, C_D, the drag coefficient predicted by Stokes law is;

$$C_D = \frac{24}{D_p v_o \rho/\mu} = \frac{24}{Re} \tag{2.11}$$

This result, because of the neglect of the inertia terms, agrees closely with experiment only for Re<0.1. Oseen[41] improved the correlation by accounting in part for the inertia terms which Stokes had omitted. Oseen's solution, valid for Re<1, is:

$$C_D = \frac{24}{Re}\left(1 + \frac{3}{16}Re\right) \tag{2.12}$$

An empirical solution acceptable up to about Re =100 is:

$$C_D = \frac{24}{Re}\left(1 + \frac{3}{16}Re\right)^{1/2} \tag{2.13}$$

The highly idealised conditions under which the standard drag coefficient curve is derived are seldom met in chemical engineering practice. Therefore data obtained from the standard drag curve may in some instances be extremely inaccurate. At higher Reynolds numbers such as those found in many chemical engineering applications, the variation of C_D with Re is quite complicated because of the interaction of the factors that control skin drag and form drag e.g. drop oscillation, wake shedding, internal circulation, and superimposed mass transfer. As a result the drag coefficient of solid spheres is often used as an approximate basis for analysis.

2.4.2 *Effects of Wake Shedding*

As the Reynolds number for a sphere is increased beyond the Stokes' law range separation occurs and a wake is formed. The precise Re at which circulation or wake formation begins has been the subject of debate [42]. The best estimate for the onset of circulation is according to Clift et al.[43] Re = 20.

Development of the wake is evident in photographs of flow passed a rigid sphere produced by Teneda[44]. At Reynolds numbers 20<Re<130 there is steady wake shedding, the wake changing from convex to a concave shape at Re = 35. As Re is increased beyond about Re = 130, diffusion and convection of vorticity no longer keep pace with vorticity generation; instead, discrete pockets of vorticity begin to be shed from the wake.

Teneda [44] reported that at Re = 130 oscillations appear in the tip of the wake. According to Goldberg et al.[45] and Seeley et al.[46] vortex shedding appears to result from flow instability originating in the free surface layer and moving downward to affect the position of the wake. As Re increases beyond about 400, vortices are shed in regular succession, i.e. the Strouhal number for vortex shedding increases, (the Strouhal number, Sr =(fd/v)), see Figure 2.11.

Further increase in Re causes a shift in the separation point at about Re = $3x10^5$. The sudden drop in C_D (Fig. 2.10) is a result of the boundary layer

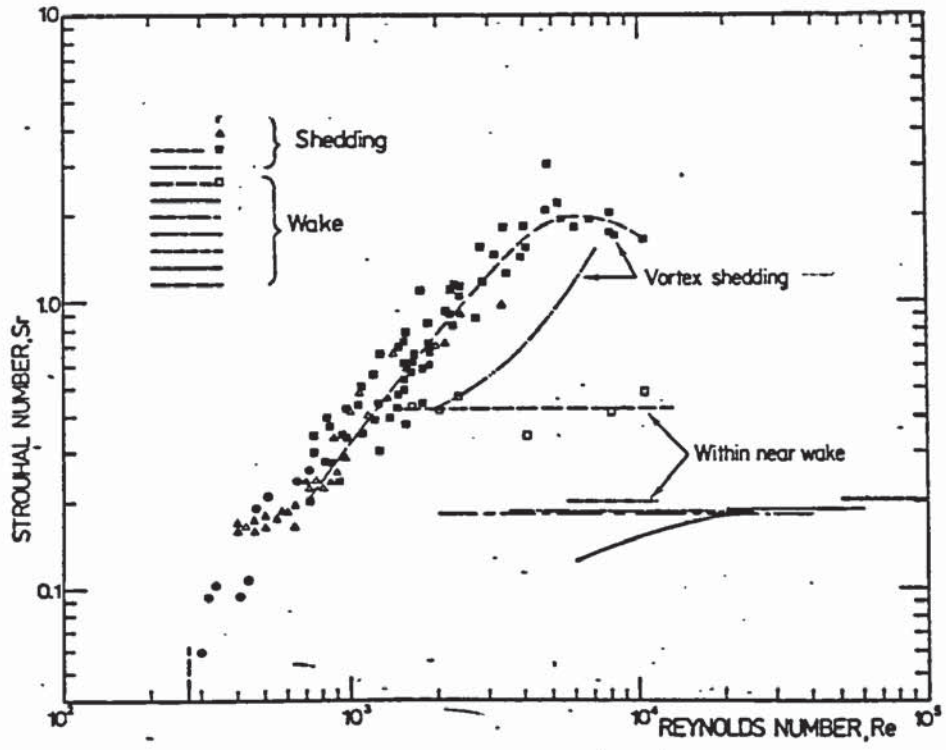

Figure 2.11. Vortex shedding as a function of Strouhal number Sr. A phenomena in sphere wake.

becoming completely turbulent and the point of separation moving downstream. In the region of Re of 10^3 to $2x10^5$, the drag coefficient is approximately constant for each type of geometry, $C_D = 0.445$ for spheres.

When the relative velocity between a droplet and fluid changes with time the drag coefficient may differ considerably from the standard value at the appropriate instantaneous velocity. The force balance around a liquid drop falling in air may be written as;

$$V(\rho_l-\rho_a)g = C_D A_f(\rho_a u^2/2)+V\rho_l\left(\frac{\partial u}{\partial t}\right), \qquad (2.14)$$

where $\partial u/\partial t$ = acceleration or deceleration of droplet. For a small droplet the terminal velocity is equal to that of a solid sphere. Larger droplet attains its terminal velocity much faster than a rigid sphere of equal volume due to vortex shedding, and oscillation of the drop.

A correlation relating drop size, surface tension and terminal velocity has been proposed by Spilhaus[47], assuming that the drag coefficient for a liquid drop is intermediate between that of a flat plate and a sphere. The equations are:

$$C_D = C_{do}(\gamma - E(\gamma - 1)) \tag{2.15}$$

$$u_t^2/r_e = (4\rho_l g)(3\rho_a C_{do})[\gamma - E(\gamma - 1)]^{-1}E^{2/3} \tag{2.16}$$

where $\gamma = C_{fp}/C_{do}$, C_D = drag coefficient, C_{do} = drag coefficient for a sphere of the same volume, C_{fp} = drag coefficient of a flat plate, E = a/b, ratio of semi-major and semi-minor axes, r_e = radius of spherical drop of equivalent volume. For drops of equivalent diameter<1.3 mm, Spilhaus assumed that the shape remained spherical. For larger drops he assumed constant values for C_{fp}=0.6 and C_{do}=0.21.

Narasimhamurty[48] developed a generalised correlation for the motion of liquid drops in gases:

$$We = C(Re)^n \tag{2.17}$$

where $We = (du_t\rho_a/\sigma)$ and $Re = (du_t\rho_a/\mu_a)$. Equation(2.14) is valid for $4.0 \le We \le 1.0$. For $We \le 1.0$ the values for C and n are correlated by:

$$We = 0.252(M)^{0.338}Re^{1.602} \tag{2.18}$$

where $M = (g\mu_a^4)/(\sigma^3\rho_a)$. Clearly however the accuracy is not that implied by the number of significant figures in the exponents.

Finlay[49] proposed an equation of the type;

$$C_D We P^{0.13} = \omega(Re/P^{0.13})^n \tag{2.19}$$

where P = property group given by $(\rho_a^2\sigma^3/g\mu^4(\rho_l-\rho_a))$, n= 1.26 for water drops and 1.55 for other liquids and ω is a correlation constant.

When the relative velocity between droplet and the continuous phase changes with time, as in Equation 2.12, the drag coefficient may differ considerably from the standard value, as the unsteady motion may increase the fluid resistance and hence C_D.

2.4.3 *Effects of Superimposed Mass Transfer.*

In a liquid(dispersed)-vapour system the vapour cloud surrounding a droplet undergoing mass transfer may be expected to reduce the skin friction due to a thickening of the boundary layer and may also affect the position of the boundary layer separation. Ingebo [50] found that for small mass transfer rates, the same equation could be used to express drag coefficient for both evaporating and non-evaporating droplets. For higher mass transfer rates, Eisenklam et al.[51] asserted that mass transfer reduces skin friction and has some effect on the pressure distribution around an evaporating drop. Eisenklam et. al. measured the drag coefficient for burning and evaporating drops initially of 25 μm diameter in high temperature air. The mass transfer was expressed in terms of the Spalding number defined for evaporation as:

$$B = \frac{C_p \Delta T}{\lambda} \tag{2.20}$$

Their results showed a considerable decrease in the drag coefficient with increasing values of B. This was attributed to the momentum of the diffusing vapour, and the drag coefficient was related to B according to the relationship:

$$C_{DM} = \frac{C_D}{(1+B)} \tag{2.21}$$

Chuchottaworm et al [52, 53, 54] modified Equation 2.19 by solving the Navier-Stokes Equation, using numerical techniques. They proposed the following correlation for drag coefficient of an evaporating or condensing droplet:

$$\left(1+\frac{C_{DM}}{C_D}\right)=\frac{Re^{0.257}}{\left(3.83+1.1\left(\frac{\Psi_m}{C_D}\right)\right)} \tag{2.22}$$

where ψ_m represented the surface mass injection ratio. In terms of mass transfer number B_M;

$$\frac{C_{DM}}{C_D}=\left(1+B_M-0.19Sc^{-0.74}(1+B_M)^{-0.29}\right) \tag{2.23}$$

where $B_M=\frac{(x_{vs}-x_{vo})}{(1-x_{vs})}$ and x_{vs} and x_{vo} are the mass fractions of the vapour at the droplet surface and in the flow respectively.

2.5 *Conclusion*

From this short review of liquid disintegration, discrepancies can be noted in the importance attributed to different factors by different investigators. e.g. Re, the Z-number, Weber number, Ohnesorge number and liquid pressure. However from all the work on liquid atomisation the following summarises the primary stages of liquid disintegration and drop oscillation. Liquid disintegration is caused primarily by aerodynamic interaction and liquid turbulence which generate waves and render the liquid surface unstable. Continued aerodynamic interaction and the tendency of the droplet to maintain a minimum drop surface, leads to drop shape oscillation and internal circulation. This affects the total drag force of droplets, their residence time, their exposed surface area and consequently heat and mass transfer rates.

Although a great deal of experimental and theoretical work has been done on droplet motion, there are omissions, in particular, in the field of drop shape oscillation and the factors responsible for such movements.

Finlay's[49] correlation for terminal velocity and drag coefficient does take into consideration the physical properties of the liquid drop by incorporating the property group, P, but the correlation has the disadvantage that the correlation constant, ω, varies for different liquids and therefore limits its general use. Subsequent chapters examine drop surface hydrodynamics and explore their possible inclusion in the general transport equations.

CHAPTER THREE

3 TRANSPORT AND INTERFACIAL PHENOMENA

3.1 Introduction

3.2 General Molecular Transport

3.2.1 Momentum Transport

3.2.2 Heat Transfer

3.2.3 Mass Transfer

3.3 The Stagnant-Film Theory

3.4 The Surface Renewal Theory

3.5 The Penetration Theory

3.6 The Film-Penetration Theory

3.7 Introduction to Interfacial Phenomena

3.7.1 Convective Instability

3.7.2 Surface Turbulence

3.7.3 Effect of Surface-active Agents

3.8 Conclusion

CHAPTER THREE

TRANSPORT AND INTERFACIAL PHENOMENA

3.1. *Introduction*

Liquid drops exhibit several interesting phenomena as they travel through a gas phase. They may travel in the laminar region in which they assume a nearly spherical shape, show little or no deformation and may exhibit internal circulation. Alternatively they may travel in the turbulent region in which they no longer maintain a spherical shape but go through a series of shape oscillations with eddies in their wake.

The motion of molecules or fluid element of droplets caused by these phenomena, or by some form of potential or driving force, is very important in most chemical engineering operations. Many industrial processes depend on material transfer involving one or more fluids in turbulent flow; e.g. gas absorption, liquid/liquid extraction, evaporation and drying of spray droplets.

The general subject of mass transfer across an interface may be divided into two broad areas: molecular diffusion in the laminar region of low Re number, and turbulent diffusion and mixing. The first has been the subject of much study by scientists and the supportive theory is well developed. However, current understanding of turbulence is not sufficient to form a basis for the development of a practically-useful theory for forced convective mass transfer. Hence the factors determining the rate of interfacial transfer have been the particular concern of many investigators. Some of these studies have good theoretical bases for limited situations; in others, use has been made of simplifications, often with little reference to the surface hydrodynamics and mechanisms by which property (momentum, heat, and mass) is transferred between phases. Models for dispersed liquid systems which attempt to explain

mass transfer under forced convection conditions should address the phenomena of drop mechanics, including drop shape, drop deformation, internal circulation and vibration. To fully appreciate some of these models, and of course the factors giving rise to surface turbulence and mass transfer, it is convenient to first discuss the relatively simple phenomena involved in the general molecular transport processes of momentum, heat, and mass.

3.2 *General Molecular Transport*

Molecular transport is generally concerned with the transfer of a given property by molecular movement through a system or medium comprising a fluid or in some cases a solid. The property transferred may be mass, thermal energy or the momentum associated with it. When a difference of concentration exits for any of these from one region to an adjacent region, a net transport of the property occurs. In gases, in which the molecules are relatively far apart, the rate of transport of the molecules should be relatively fast since few molecules are present to block the transport or interact. In liquids, the molecules are close-together and transport or diffusion proceeds more slowly. In solids the molecules are even more close-packed than in liquids and molecular migration is even more restricted. All molecular transport processes of momentum, thermal energy and mass are usually described fundamentally by the same general type of transport equation:

$$\text{rate of a transfer process} = \text{driving force/resistance.} \qquad (3.1)$$

The kinetic theory of gases provides a good physical interpretation of the motion of individual molecules in fluids. As a result of their kinetic energy the molecules are in rapid random movement often colliding with each other. Molecular transport or molecular diffusion occurs in a fluid because of these random movements of individual molecules. Hence, if there are spatial

differences in a property, there will be a net flux of that property between high and low regions.

3.2.1 *Molecular Momentum Transport*

A fluid flowing freely past a phase boundary as discussed in Chapter Two, Figure 2.8, has x-directed momentum of concentration $v_x\rho$ kg.m/sm^3. As the fluid is deflected round the immersed body, the random motion of molecules in the faster-moving layer translates some of the molecules into the slower-moving layer, where they increase momentum in the z-direction. Molecules in the slower layer (close to the boundary) also tend to retard those in the faster layer. The equation for the transport of this momentum is given by;

$$\tau_{zx} = -\nu\frac{\delta(v_x\rho)}{\delta z} \tag{3.2}$$

where τ_{zx}, is the flux of x-directed momentum in the z-direction. τ_{zx} in Equation 3.2 can be interpreted as the shear force in which each layer immediately adjacent to the other is carried along at a slightly slower velocity than the top layer. The negative sign in Equation 3.2 indicates that momentum is transferred down the gradient from high to low velocity regions.

Above a certain flow velocity, the flow changes from laminar to turbulent. The turbulence of the flow field makes the effective viscosity larger than the molecular viscosity, μ, and neighbouring layers of different velocity not only transmit momentum to each other by molecular interaction but also by cross-currents, (eddies). These cross currents increase in intensity to the third power away from the phase boundary, (i.e. eddy diffusivity, $E_d = C_1y^3$)[55, 56, 57, 58]. This results in a steep velocity gradient next to the boundary layer. The decrease in turbulence towards the phase boundary has led to the concept of the hydrodynamic boundary layer of thickness ∂_h in which the velocity gradient is constant. The shear stress in the boundary layer is given by;

$$\tau = \mu \frac{v_x}{\partial_h} \tag{3.3}$$

The shear stress depends on the Reynolds number which can be interpreted as the ratio of the momentum transport by convection (ρv^2) to the momentum transport by diffusion ($\mu v/D$). In turbulent flow the transport by convection (eddies) prevails. From the definition of ∂_h, and Re, it can be inferred that eddy momentum transfer overrides viscous transfer if:

$$E_d = C_1 y^3 \geq \frac{\mu}{\rho} = \nu \tag{3.4}$$

Hence

$$C_1 \partial_h^3 = \nu \tag{3.5}$$

3.2.2 *Heat Transport*

The molecular transport of heat within the boundary layer can be written using Fourier's law for constant density, ρ, and heat capacity, C_p, as;

$$Q_f = -k \frac{\partial T}{\partial_T} = -\alpha \partial \left(\frac{C_p \rho T}{\partial_T} \right) \tag{3.6}$$

where $(k/\rho C_p) = \alpha$ is the thermal diffusivity.

Outside the thermal boundary layer, eddies disperse the heat so efficiently that a uniform temperature exists in the core of the flow. The term convective heat transfer is used when heat flow is by mixing of warmer portions with colder portions of the same fluid. The convective heat flux through a fluid is written as;

$$Q_f = h_c (T_a - T_s) \tag{3.7}$$

where h_c is the convective heat transfer coefficient, and $T_a > T_s$.

By analogy with the eddy currents in momentum transport discussed in the preceding section, the diffusivity of heat by eddies can also be described by: $E_d = C_1 \partial_T^3$. Hence by similar reasoning, the distance ∂_T from the interface at which the contribution to heat transfer by convection (heat transfer by eddies) overtakes that due to conduction is:

$$C_1 \partial_T^3 = \alpha \tag{3.8}$$

A relationship between the thermal thickness, ∂_T, and the hydrodynamic thickness, ∂_h, can therefore be established as;

$$\frac{\partial_h}{\partial_T} = \left(\frac{\nu}{\alpha}\right)^{1/3} = \left(\frac{\rho C_p \nu}{k}\right)^{1/3} = \left(\frac{C_p \mu}{k}\right)^{1/3} \tag{3.9}$$

$C_p\mu/k$ is the Prandtl number, Pr.

The Prandtl number gives a measure of the thermal dissipation in the boundary layer independent of fluid motion. It is a function of the properties of the interface and indicates the predominance or otherwise of kinematic diffusivity over thermal diffusivity. The temperature drop through the boundary layer decreases in proportion to the total temperature drop as the Prandtl number decreases from a large value to a lower one. The turbulent core and the boundary (viscous) layer coincid when Pr = 1, whilst if Pr>1 there is significant turbulent diffusion of heat within the viscous layer. If Pr<1, the thermal diffusion layer, ∂_T, is thicker than the viscous layer.

3.2.3 *Mass Transport*

A common example of molecular diffusion of a gaseous component is that of diffusion of water vapour from an air/water interface, Figure 3.1.

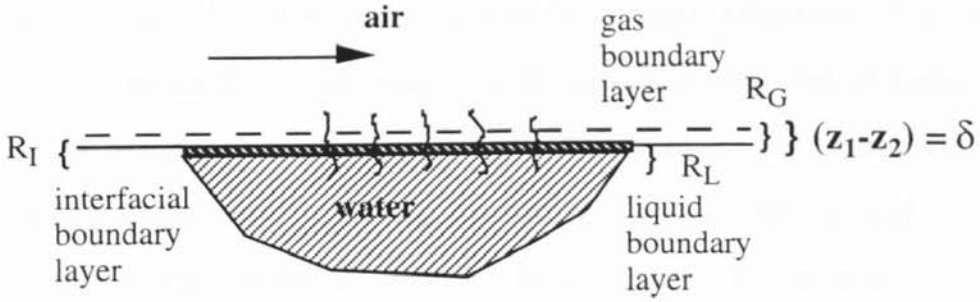

Figure 3.1. **Molecular diffusion from an air/water interface.**

The basic equation describing the molecular diffusion across the interface is Fick's law;

$$N_A = -D_v \frac{\partial C}{\partial z} \tag{3.10}$$

where N_A represents the mass flux of diffusing component, C the concentration of diffusing component and z the direction of diffusion; D_v = mass diffusivity. A mass balance on an element of interest at unsteady state yields Fick's second:

$$\frac{\partial C}{\partial t} = -D_v \frac{\partial^2 C}{\partial z^2} \tag{3.11}$$

By assuming that the perfect gas laws will apply, Equation 3.10 can be written;

$$N_A = -\frac{D_v}{RT}\frac{\partial p}{\partial z} \tag{3.12}$$

where p is the partial pressure of the diffusing water vapour. Integration of Equation 3.12 leads to the following expression for the mass flux of the diffusing gas;

$$N_A = -\frac{D_v}{RT}\left(\frac{p_2 - p_1}{z_2 - z_1}\right) \tag{3.13}$$

As a molecule passes across the liquid-gas interface (Figure 3.1), it encounters in general a total resistance R^1 which is the sum of three separate diffusional resistance due respectively to diffusion in the liquid phase, across the monolayer (monomolecular region constituting the interface), and through the gas film above the interface. In pure liquids as in the above example, the resistance in the liquid phase is approximately zero. The resistance of the gas/liquid interface and of the gas phase make up a concentration boundary layer of thickness ∂_c or (z_1-z_2), analogous to those described in previous sections, through which mass transfer must occur. By similar reasoning a relationship can be found between the hydrodynamic boundary layer, ∂_h, and the concentration boundary layer, ∂_c, thus;

$$\frac{\partial_h}{\partial_c} = \left(\frac{\nu}{D_v}\right)^{1/3} \tag{3.14}$$

(ν/D_v) = the Schmidt number Sc. Sc represents the ratio of momentum diffusivity (ν) to molecular diffusivity (D_v) and has a similar physical significance to the Prandtl number in heat transfer. In all these cases, the effective boundary thickness, ∂, cannot be measured. It is therefore convenient to employ a mass transfer coefficient which must be measured experimentally. This is defined as the ratio of molal, or mass, flux to the potential or driving force, responsible for mass transport. Equation 3.13 may therefore be rewritten as;

$$N_A = k_G(p_2 - p_1) \tag{3.15}$$

or

$$N_A = k_c(C_{A1} - C_\infty) \tag{3.16}$$

where k_G or k_c is the mass transfer coefficient. The ratio of the actual rate of mass transfer given by the mass transfer coefficient to that due to molecular diffusion is the Sherwood number, Sh;

$$Sh = \frac{k_G D}{D_v} \qquad (3.17)$$

Since the mass transfer coefficient must be evaluated experimentally, most researchers have attempted to developed empirical equations which relate it to the properties of the fluid, the flow characteristics and the hydrodynamics of the interface. But, conditions in the immediate region of the interface are difficult both to observe and to explore experimentally. In such a situation it is helpful to develop mathematical models of the process drawing on some of the basic facts discussed above. Some of these models are reviewed in section 3.3.

3.3 *The Stagnant Film Model*

According to this model material is transferred within the bulk phases by convection currents and concentration gradients are regarded as negligible, except in the vicinity of the interface between the phases. It is assumed that the currents die out on either side of the interface, and that a thin film of fluid exists through which the transfer is effected only by molecular diffusion. This film is of such a thickness (∂) as will explain the experimentally-observed magnitude of the mass transfer resistance. The film model was first proposed by Nernst [59]. It has been applied to both heat and mass transfer and it forms the basis of Whitman's [60] Two Film Theory of gas absorption.

The Stagnant Film Theory employs the assumption that the phases are in equilibrium at the interface, i.e. that there is no diffusional resistance at the phase boundary. It was recognised very early that this concept was an oversimplification of the actual conditions near the phase boundary. Although it does not provide a basis for the prediction of the boundary thickness (∂) needed to estimate mass transfer, it has been a remarkably useful concept. The correlation of mass transfer data using dimensionless groups stems from the Film Theory.

The Film Theory predicts a first power dependence of mass flux on the molecular diffusion coefficient, i.e.;

$$k_c = \frac{N_A}{(C_{A1} - C_\infty)} \alpha D_v \tag{3.18}$$

3.4 *The Penetration Model*

As noted above, the Film Theory assumes that there is no diffusional resistance at the phase boundary. It neglects the accumulation of the diffusing species in the film, the local flux across the area in contact, interfacial movement or turbulence. Higbie[61] experimented on the absorption of carbon dioxide bubbles in a vertical column of water in a three millimetre diameter glass tube and suggested that, since liquid-gas contacting equipment operates with repeated brief contact of the two phases, the contact times are too short to permit the attainment of a steady state. It was observed that as carbon dioxide rose through the column, the displaced liquid ran back as a thin film between the bubble and tube. Higbie attributed this largely to fresh material being brought to the interface by the eddies where a process of unsteady state transfer took place from the freshly-exposed surface for a fixed period. This analysis is similar to that of diffusion or conduction in a semi-infinite slab. Higbie used an average residence time over the interface and expressed the mass transfer coefficient as:

$$k_c = \frac{N_A}{(C_{A1} - C_\infty)} = 2\sqrt{\frac{D_v}{\pi t}} \tag{3.19}$$

Except in special cases, Equation 3.19 cannot be used to predict mass transfer coefficient since the time, t, is seldom known in practice. The same difficulty is encountered as in the Film Theory which involves the unknown film thickness, ∂. The Penetration Theory predicts that the mass flux and k_c vary as the square root of the molecular diffusivity, whereas the Film Theory indicates the first power.

Several investigators [62, 63, 64] have reported powers for D_v ranging generally between 0.5 to 0.75.

The derivation of Equation 3.19 assumes that the fluid in contact with the interface is substantially stagnant during its brief exposure. Brunson and Wellek[65] reported that the time average k_c for a droplet system may be approximated by Equation 3.19 only when there is internal stagnation and no drop shape oscillation. However, as discussed in Chapter 2, in most practical applications drop mechanics is more complicated than is assumed in the Penetration Theory.

Angelo et al [66] have extended the Penetration Theory to cases where the surface area varies with time, as in drop formation and drop oscillation, in liquid-liquid systems expressing k_c as;

$$k_c = \frac{N_A}{(C_{A1} - C_\infty)} = \left(\frac{4D_v f_N(1+\varepsilon_o)}{\pi}\right) \tag{3.20}$$

where f_N is the frequency of drop shape oscillation and ε_o is a dimensionless constant given by;

$$\varepsilon_o = \varepsilon + \frac{3}{8}\varepsilon^2 \tag{3.21}$$

ε = the amplitude of the surface stretch calculated from a knowledge of the maximum and minimum surface area per cycle. The stretched surface area of the droplet was given by;

$$A = A_o(1 + \varepsilon \sin^2(\theta)) \tag{3.22}$$

where θ is dimensionless time.

This solution assumes a short exposure time for any surface element, and neglects diffusional transfer of solute by convection in the interface; it makes no

allowances for circulatory motion or surface turbulence. The theory is based on droplet oscillation, typically from nearly spherical to oblate then back again. Drop mechanics is more complicated than this simplistic model.

Handlos and Baron[67] and later Orlander[68], and Patel and Wellek[69], made theoretical analyses of diffusion in oscillating drops. These led to the expression:

$$k_c = \frac{3.75 \times 10^{-3} v}{1 + \mu_d/\mu_c} \tag{3.23}$$

where v (m/s) is the drop velocity relative to the continuous phase. Clearly however since it omits other essential physical properties, e.g. ρ_c, ρ_d, and σ, this correlation is restricted to the range of liquid-liquid systems for which it was validated.

3.5 *The Surface Renewal Model*

A significant extension of the Penetration Theory was proposed by Danckwerts[70]. Whereas Higbie[61] had taken the exposure time to be similar for all the repeated contacts of the fluid within the interface, Danckwerts suggested that the material brought to the surface will remain there for a wide spectrum of times and averaged the varying degrees of penetration. It was assumed that the probability of any element at the surface becoming mixed with the bulk of the fluid was independent of the age of the element. Thus, the fractional rate of renewal, s, of the area exposed to penetration followed the surface age distribution function:

$$\varphi = se^{-st} \tag{3.24}$$

where φ represents the probability that any element of the area will be exposed by the time, t, before being replaced by freshly-mixed fluid from the bulk. The calculated mass transfer rate based on this Surface Renewal model is given by:

$$N_A = (C_{A1} - C_\infty)\sqrt{D_v} \int_0^\infty \frac{se^{-st}}{\sqrt{\pi t}} \partial t = (C_{A1} - C_\infty)\sqrt{D_v s} \qquad (3.25)$$

Hence k_c is

$$k_c = \sqrt{D_v s} \qquad (3.26)$$

Since values of s, the rate of surface renewal are not generally available, its appearance in the analysis presents the same problem as the boundary layer thickness, ∂ and t, in the Film Theory and Higbie models respectively.

3.6 *The Film Penetration Model*

A theory which takes into account some of the principles of both the Film Theory and the Penetration Theory was put forward by Toor and Marchello [71]. Like the Stagnant Film Theory, the mass transfer resistance is regarded as lying within a laminar film at the interface but the mass transfer process is regarded as one in an unsteady state. Toor and Marchello assumed that fresh fluid is formed at intervals and brought from the bulk of the fluid to the interface by the action of eddy currents. Mass transfer then takes place as in the Penetration Theory with the exception that resistance is confined to a finite film and material which traverses the film is immediately mixed completely with the bulk of the fluid. For short times of exposure, when none of the diffusing materials has reached the far side of the layer, the process is identical to that postulated in the Penetration Theory. For long periods of exposure, when a steady concentration gradient has developed, conditions are similar to those considered in the Stagnant Film Model.

3.7 *Introduction to Interfacial Phenomena*

The Film Theory described in the preceding section employs the assumption that the phases in contact are in equilibrium whilst the Surface Renewal and the Penetration theories deal with the phenomenon of continuous surface movement. With reference to mass transfer from droplet surfaces, the Surface Renewal concept appears more appealing as drop surface behaviour is known not to be static. The extension by Angelo et. al.[66] of the Penetration Theory to include surface stretch is also of great interest; however it does not include surface turbulence or circulation. None of the above models incorporates fully the surface phenomena of turbulence or the physical properties which contribute to such behaviour. A strategy for developing a better model (discussed in later chapters) is to consider droplet behaviour at the interface and the physical properties of the bulk phases which govern such behaviour.

Surface phenomena should by definition refer to any activity which either originates from the bulk fluids, in the interface or is specific to it. It should take account of induced gradients of pressure and surface tension on the flow characteristics of the interface and consequently on heat and mass transfer.

The fundamental mass transfer rate $\delta w/\delta t$, is proportional to the mass transfer coefficient, k_c, the interfacial area and the driving force. Interfacial movement or turbulence will therefore affect predominantly the interfacial area and internal circulation which in turn will affect the mass transfer coefficient and increase the mass transfer rates above those which would otherwise occur in the absence of interfacial motion. Lewis[72, 73] in the course of measurement of interfacial tension of drops by the pendant method, noted ripples, erratic pulsation and surface motion. He observed that abnormally high mass transfer rates were associated with marked interfacial turbulence. It is clear that changes in the interfacial behaviour of a droplet greatly affect the mass transfer rates.

3.7.1 *Convective Instability*

Sterling and Scriven[74] grouped liquid surface behaviour into two regimes. Even though their studies involved flat interfaces and liquid-liquid systems, the observed disturbances are thought to be similar to those observed at round interfaces[75], and are therefore discussed here to serve as a basis for understanding droplet behaviour in air. The first instability, the convective instability or stationary regime, is characterised by surface disturbance without oscillation or translation. Surface movement in this regime is confined to small ripples at the interface; they are often not induced by motion of the bulk fluid. Ordered cell-like motion or cellular interfacial motion and the Marangoni effect fall into this category.

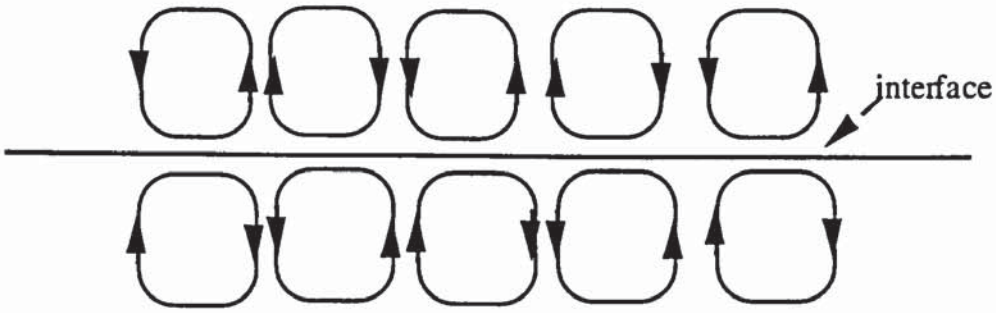

Figure 3.2. Convective Instability; assumed roll-cell structure near a liquid-gas boundary.

Cellular interfacial motion is characterised by a roll cell motion which is generated by the motion of the elements of liquid along the interface followed by a motion inside the phase in question. The presence of these cell-like motions (Figure 3.2) enhances the rate of mass transfer[76] as fresh fluid is continuously being brought to the interface. The mass transfer during the contact with the interface is followed by that taking place when the liquid elements are moving along the inside path. The motion along this "inside path" of the roll cell may be accompanied by complete or partial refreshing[77]. If a chemical or thermal difference along an interface causes an interfacial tension gradient, surface flow

in the direction of low surface tension will result. This phenomenon is known as the Marangoni effect, first discovered by Thompson[78] and adopted by Marangoni[79, 80] who noted that liquid of lower surface tension would spread over liquid of higher surface tension. It has been shown by Sherwood and Wei[81] that pronounced convective instability occurs when a chemical reaction occurs simultaneously with mass transfer between phases.

3.7.2 *Surface Turbulence*

The second regime is the oscillatory regime. This is typified by surface movement with random drop shape oscillation. The interface is often in such a state of intense agitation that it is referred to as interfacial turbulence. Rose and Kinter[82] measured the amplitude of oscillation of organic liquid drops in water, based on the dimensions of the major and minor axes. The amplitude of drop oscillation proposed was:

$$Amp = \frac{d_{max}}{2} - d_{min} \tag{3.27}$$

d_{max} = length of major axis, d_{min} = length of minor axis.

Angelo et. al.[66] in their study of surface stretch proposed the relationship given as Equation 3.22. Schroeder and Kinter[83] modified Lamb's correlation for frequency of oscillation by the addition of an empirical amplitude coefficient, b, estimated by:

$$b = 1 - \frac{d_{max} - d_{min}}{2d_{av}} \tag{3.28}$$

giving droplet oscillation frequency as:

$$f_N = \sqrt{\left(\frac{48b\sigma}{(3\rho_d - 2\rho_c)d_e^3\pi^2}\right)} \tag{3.29}$$

Haberman[84] argued that the factor, b, in Equation 3.28 should be used to predict the frequency of oscillation and not the amplitude. Al-Hassan[85] correlated the

amplitude of drop oscillation as a function of vortex shedding and the Weber number:

$$Amp = 0.434\ Sr^{-0.46}\ We^{-0.53}\sigma^{0.11} \tag{3.30}$$

Using the principle of eccentricity rather than the amplitude of drop oscillation, Kintner[86] correlated the area of a deformed droplet as:

$$A = \frac{\pi}{2}\left[d_h^2 + \frac{d_v d_h}{E^2-1}\,\mathrm{In}\left(E + \sqrt{E^2-1}\right)\right] \tag{3.31}$$

E = eccentricity of drop, (d_h/d_v). He presented the ratio of the area of an ellipsoid to that of a sphere of equal volume

as:

$$\frac{A}{A_e} = \frac{1}{2}\left[E^{2/3} + \frac{1}{E^{1/3}\sqrt{E^2-1}}\,\mathrm{In}\left(E + \sqrt{E^2-1}\right)\right] \tag{3.32}$$

Sterling and Scriven[74] proposed a number of conditions under which interfacial turbulence may occur:

(i) solute transfer out of the phase of higher viscosity,

(ii) solute transfer out of the phase in which its diffusivity is lower,.

(iii) large difference in solute diffusivity between the two phases,

(iv) steep concentration differences near the interface,

(v) interfacial tension highly sensitive to solute concentration,

(vi) low viscosity and diffusivities in both phases,

(vii) absence of surface active agents, and

(viii) interfaces of large extent.

Sawistowski[87] found on the contrary that the intensity of interfacial turbulence was higher when phenol and propionic acid were transferred into water in which the kinematic viscosity is higher and diffusivity lower; Sawistowski challenged

the reliability of Sterling et. al's criteria and suggested that they were oversimplified.

3.7.3 *Effects Of Surface Active Agents*

The introduction of any surface active agent affects the properties of the interface, increasing the so called Gibbs Marangoni elasticity modulus[88] and adversely affecting surface renewal. In addition, surface viscosity will slow down any movement in the interface. This phenomenon has been analysed theoretically by Berg and Acrivos[89] who extended Pearson's [90] stability analysis of surface tension induced convection to account for the presence of a surfactant.

A surfactant may have two important effects on the rate of mass transfer through a surface. It may reduce and often eliminate the Marangoni effect, i.e. suppressing interfacial convection. Simultaneously it introduces a surface resistance to diffusion across the interface. It has been shown by Plevan and Quinn[91] that, for gas absorption, the action of a surfactant on a liquid surface is entirely hydrodynamic in nature. The early work of Lindland and Terjesen[92] showed that mass transfer from drops of carbon tetrachloride (CCl_4) falling in water to be reduced by 68% by the addition of only $6x10^{-5}$g surfactant/100ml water. Similar reductions in the rate of mass transfer by the addition of various surfactants are reported by Thompson[93] who studied the absorption of either NH_3, SO_2 or CO_2 into water in an unstirred container. It has been shown by many investigators that surface active material renders droplets more rigid so that the mass transfer rates approach those of stagnant drops.[94, 95, 96]. Thus the results for mass transfer in industrial systems, with commercial rather than pure chemicals and with extraneous contaminants exhibiting surfactant effects, often differ from those from laboratory experiments. However, it is futile to attempt to generalise the effects of surface active agents in a simple equation because of the complex interactions between hydrodynamics, surface chemistry and mass transfer.

The interfacial phenomena between a drop and a gas are qualitatively similar to those described for situations where the continuous phase is a liquid. The quantitative differences stem largely from the fact that molecular diffusion coefficients are several orders of magnitude greater in gases than in liquids resulting in larger continuous phase coefficients; the viscosity ratio μ_d/μ_c, and ρ_d/ρ_c are also enormous, reducing but not eliminating internal circulation. References have been made to liquid-liquid systems because of the extensive literature on both theoretical and experimental studies with photographic evidence. (97, 98, 99).

Gas-liquid systems are affected by surfactant addition in a similar way to liquid-gas systems. As in drops, bubbles exhibit internal circulation and the velocity of rise, or terminal velocity, is greater than for solid spheres. Garner(36) observed circular motions inside bubbles > 2.2 mm by the addition of ammonium chloride fog during formation. For bubbles below 1 mm no circulation was observed; they behaved like rigid spheres. Bubbles of intermediate size (1-1.5 mm) were flattened and distorted, with oblate spheroids or ellipsoidal shapes; these oscillated and wobbled as they rose. Large bubble diameters, > 1.5 mm formed spherical caps.

In studies of single bubbles, the gas is introduced at the bottom of a liquid column through an orifice or small capillary. A bubble is released when the buoyancy force just overcomes the surface tension, at which time the bubble diameter is given by;(173, 174).

$$d_p = \left(\frac{6d_o\sigma}{\Delta\rho g}\right)^{1/3} \tag{3.33}$$

d_p = bubble diameter, $\Delta\rho$ = difference in density of liquid and gas, d_o = orifice diameter, and σ=surface tension.

Mass transfer within bubbles is rapid because molecular diffusivities in gases are larger and the resistance to mass transfer on the liquid side of the

interface is controlling. The work of Johnson et al[175] gives the mass transfer rate in terms of the Sherwood number as:

$$Sh = \frac{k_c d_p}{D_v} = 1.13\, Pe^{1/3}\left(\frac{d_p}{0.45 + 0.2 d_p}\right)^{1/3} \qquad (3.34)$$

3.8 *Conclusion*

The fundamental theoretical development of equations to describe mass transfer to, and from, drops have been discussed. In most practical situations the flow is turbulent and the drop behaviour and flow field are inadequately specified; both molecular and eddy diffusivity may be involved and a rigorous treatment is not usually possible from theory alone. The most important factor pertaining to mass transfer to, or from, drops in a liquid-gas system in turbulent flow is that the resistance to mass transfer is confined largely to a thin region adjacent to the interface and that interfacial instability grossly affects transfer rates. The principal effects of a surfactant on the interface are the formation of a relatively rigid interface, with suppression or elimination of interfacial turbulence, and the introduction of a surface barrier to mass transfer.

In bubbles, the effect is to reduce the liquid flow over the surface during rise, with the result that the velocity of free rise is appreciably reduced. In the case of drops the internal circulation and drop oscillation are reduced and small drops behave as rigid spheres. Since the mass transfer coefficient must be evaluated experimentally, it is important that all the physical properties which regulate drop surface behaviour are included in the experimental investigation and adequately characterised. The following chapter critically reviews previous experimental studies of mass transfer to, and from, spheres and drops taking the above phenomena into account and evaluates published correlations for mass transfer coefficients in terms of their generality and practicality.

CHAPTER FOUR

4 EVAPORATION FROM SPHERES AND DROPLETS

CHAPTER FOUR

EVAPORATION FROM SPHERES AND DROPLETS.

4.1 *Introduction*

Evaporation of a spray of water to cool air and the vaporisation of a spray of liquid fuel for combustion are widely-practised processes. In those processes where the droplet surface is saturated, the rate of material transfer is largely dependent upon the rate of heat transfer to the evaporating surface. Depending on its direction the process of mass transfer can either raise or lower the rate of heat transfer. Thus a surface exposed to a hot gas can be partially protected from rapid heating if the surface is kept wet with a volatile liquid which evaporates ("film or sweat cooling"). This phenomenon which is utilised in drying provides spray drying with an overwhelming advantage over most contact dryers.

Studies of the evaporation of pure liquids dates as far back as 1877 when Maxwell[100] proposed a theoretical expression for the rate of diffusion from a spherical drop of radius r_o, diffusing through a radial distance r, in quiescent air as;

$$\dot{E}_r = -4\pi r^2 D_v \frac{\partial C}{\partial r} \tag{4.1}$$

where $r > r_o$. Integrating between the limits $C = C_i$ at $r = r_o$ and $C = C_\alpha$ at $r = r_\alpha$,

$$\frac{\dot{E}_r}{4\pi D_v}\left(\frac{1}{r_o} - \frac{1}{r_\alpha}\right) = C_i - C_\alpha \tag{4.2}$$

In the limits as $1/r_\alpha \approx 0$, and $r_o = D/2$,

$$E_r = 2\pi D_v D(C_i - C_\alpha) \tag{4.3}$$

From Equation 3.16,

$$\dot{E}_r = k_G A(C_i - C_\alpha) \tag{4.4}$$

$$\therefore \quad k_G \pi D^2 = 2\pi D_v D \tag{4.5}$$

$$\Rightarrow \quad \frac{k_G D}{D_v} = 2 \tag{4.6}$$

The dimensionless group $k_G D/Dv$ is the Sherwood number, Sh, and for vaporisation from a sphere into quiescent air, Sh = 2.

For a system which has attained dynamic equilibrium the rate of mass transfer from the saturated surface is exactly balanced by the rate of heat transfer. Hence following the Nusselt analogy, $Nu = h_c D/k = 2$.

Srezvenski[101], in 1882, studied the evaporation rates of liquid drops of 3 mm diameter placed on the flat top of a cylindrical column such that the drop completely covered the top. He expressed the transfer rate in terms of volume change as;

$$\frac{\partial V}{\partial t} = \frac{\pi}{2}(V^2 + h^2)\frac{\delta h}{\delta t} = \frac{s}{2}\frac{\delta h}{\delta t} \tag{4.7}$$

$$V = \frac{\pi h}{6}(3r^2 + h^2) \tag{4.8}$$

$$s = \pi(r^2 + h^2) \tag{4.9}$$

s = the free surface of a spherical segment of height h and radius of base r.

Using this theorem Srezvenski determined the rate of evaporation of hemispherical droplets of water, benzene, ether, chloroform and carbon disulphide with varying column radius r (3.6 -7.2 mm). It was observed that the evaporation rate of a hemispherical drop with a surface area of 1 cm^2 and resting

on a plane is the same as that of a free drop with the same radius of curvature. This confirms Maxwell's[100] finding that the rate of evaporation from a spherical droplet is inversely proportional to its radius.

Powell[102] studied the evaporation of water from saturated and spherical surfaces to establish the effects of air speed and vapour pressure on the evaporation rate. He presented results for two forms of wet surface; a horizontal plane subjected to a tangential wind stream and a vertical cylinder subjected to a wind stream at right angles to its axis. In each case the rate of evaporation was found to be proportional to (p_2-p_1), the difference between the vapour pressure at the saturated surface and the partial pressure of water vapour in the incident air stream. Powell plotted the rate of evaporation per unit area (in grams of water evaporated per unit area per second per (p_2-p_1)) against u, the air speed in cm per second from spheres of 1.96, 3.65. 6.35, 9.05 and 15.5 cm diameter. The rate of evaporation per unit area was found to increase as the diameter decreased. For a particular sphere the rate of evaporation was proportional to $u^{0.62}$ whilst at a constant value of u it varied approximately as $d^{-0.5}$. He correlated the transfer rate for values of ud ranging from 100 to 700 in the form;

$$\frac{E_v}{(p_2-p_1)} = 2.1\times10^{-7}(ud)^{0.59} \qquad (4.10)$$

Powell's investigation was significant in establishing the dependency of transfer rates on the velocity of the continuous phase. It is interesting to note that for a constant velocity of the incident air the evaporation rate varied inversely with diameter, a phenomenon which was observed by both Maxwell and Srezvenski.

Lurie and Michailoff[103] also investigated evaporation from a free water surface and found the evaporation rate to be proportional to the so-called 'drying potential', i.e. the pressure difference between saturated steam at the temperature of the wet bulb, p_2, and the partial pressure of the steam, p_1, at the temperature and saturation of the moving air.

The resistance to mass transfer in processes such as those described above is predominantly in the boundary layer of the continuous phase. In the case of pure liquid-gas or pure solid-gas systems this is often referred to as 'gas film control'. Evaporation rate is found to increase with an increase in relative velocity between phases from laminar to turbulent flow. Dimensional analyses have been applied to problems involving the transfer of mass and heat from bodies immersed in fluid streams. In the case of a single sphere the results are;

$$Nu = f(Pr,Re,Gr) \tag{4.11}$$

$$Sh = f(Re,Sc,Gr) \tag{4.12}$$

These analyses are based on the Stagnant Film Theory, and the actual forms of the functions are not obtainable by dimensional analysis techniques.

Many investigators have therefore concentrated on the study of liquid-gas, solid-gas and solid-liquid systems, both by theory and experiment in an attempt to establish a model based primarily on radial diffusion due to natural and forced convection. The literature pertaining to this area of study is reviewed in two sections; heat and mass transfer from solid surfaces and studies on liquid droplet/air systems.

4.2 *Heat and Mass Transfer from Solid Surfaces*

Mathers et al.[104] studied the simultaneous transfer of heat and mass from coated and uncoated spheres to air under natural convection. The coated sphere was of diameter 0.127 cm. and the uncoated sphere 0.254 cm. The spheres were constructed of brass with an internal resistor, so that the surface temperature could be elevated above that of the surrounding air by regulation of the current passing through the resistor.

Immediately preceding a run, the sphere for coating was dipped into a melt of naphthalene or benzene. It was then suspended via one of the current leads on a balance. The temperature was adjusted until sufficient current was passed through the sphere heater to bring it to the desired temperature. The rate of mass transfer was determined by measuring the loss in weight of the heated sphere over a period of time, and the heat transfer rate determined electrically from the value I^2R across the internal resistor of the sphere. The following correlations were proposed:

$$Nu = 2 + 0.282(Gr.Pr)^{0.37} \tag{4.13}$$

$$Sh = 2 + 0.282(Gr.Sc)^{0.37} \tag{4.14}$$

for GrSc(Pr)<100. For 100 ≤GrSc(Pr)≤100 the correlations were;

$$Nu = 2 + 0.5(Gr.Pr)^{0.25} \tag{4.15}$$

$$Sh = 2 + 0.5(Gr.Sc)^{0.25} \tag{4.16}$$

It may have been a sounder procedure to use spheres of identical initial diameter; in any event it is likely that the systemic error introduced in this investigation was high since there was no provision to ensure that the sphere was given a smooth and even coating. In addition no data were provided to account for the heat transfer by conduction and radiation to the coating of naphthalene or benzene.

In a similar study, Tsubouchi and Sato[105] suspended thermistor beads (0.3 to 2 mm diameter), in a wind tunnel. Current was passed through the thermistor and from measurements of current, voltage and resistance, the

temperature and the rates of heat transfer were obtained. Their results were correlated by;

$$Nu = Nu_o + 0.29(Re^{0.5} + 1.41Gr^{0.25}) \qquad (4.17)$$

for $0.3 \leq Re \leq 3000$. Nu_o relates heat transfer under natural convection conditions.

Yuge[106] also studied heat transfer from brass and carbon-chrome steel spheres in different wind tunnels at Re in the range of 3.5 to 1.44×10^5. Spheres 6 mm in diameter were pre-heated in an electric furnace before being introduced into the wind tunnel. The spheres were suspended in the wind tunnel by the chromel-alumel thermocouple wires. Larger spheres(≥60 mm), were internally heated. Heat transfer correlations were found not to differ significantly from those of Tsubouchi and Sato[105];

$$Nu = 2 + 0.493Re^{0.5}, \qquad 10 \leq Re \leq 1.8 \times 10^3 \qquad (4.18)$$

and

$$Nu = 2 + 0.3Re^{0.5664}, \qquad 1.8 \times 10^3 \leq Re \leq 1.5 \times 10^5 \qquad (4.19)$$

However the implied accuracy of the exponent on Re is obviously spurious given that the two anemometers mounted 2 mm apart in the wind tunnel showed a 20% scatter in their readings.

Steinberger and Treybal[107] studied rates of dissolution of cast benzoic acid spheres into liquids under natural and forced convection conditions. Spheres of 12.7,17, and 25.4 mm. were individually mounted in a vertical, cylindrical test section of a flow apparatus 10.16 cm in diameter and made of Pyrex pipe. An upward flow of solvent at constant temperature and flow rate contacted the sphere for a measured time interval. Upon removing the sphere and re-weighing

when dry, the loss in weight versus time and hence the mass transfer rate were determined. Water and aqueous propylene glycol were used as solvents in both laminar and turbulent flows. Steinberger and Treybal correlated their data according to whether GrSc was less, or greater, than 10^8 in the form;

$$Sh = A + B.Re^n \tag{4.20}$$

For GrSc< 10^8, A was given by;

$$A = Sh_o + 0.569.(GrSc)^{0.25} \tag{4.21}$$

The average deviation of Equation 4.21 was 12.7%. For GrSc>10^8, A was;

$$A = Sh_o + 0.254.(GrSc)^{1/3}Sc^{2.44} \tag{4.22}$$

B was correlated by:

$$B = 0.347Sc^{0.312} \tag{4.23}$$

A combined correlation for both laminar and turbulent mass transfer was given as:

$$Sh = Sh_o + 0.347.(ReSc^{1/2})^{0.62} \tag{4.24}$$

Equation(4.24) is based on the additivity of the mass transfer contributions from natural and forced convection processes and correlates the heat and mass transfer data for both liquid and gas streams. It was found to be independent of the

laminar-turbulent transition point, contrary to previous studies by many investigators.

Maisel and Sherwood[108] studied the evaporation of liquids into turbulent gas streams. The studies were carried out using wetted plane surfaces, cylinders, spheres and discs. Water was evaporated into air from each of these shapes. The spheres were made by binding sand with precipitated calcium silicate using a spherical mould. Liquid was fed continuously from a burette through a hypodermic feed tube to the top of the sphere so as to maintain a constant level. Mass transfer was correlated by;

$$J_D = 0.3Re^{-0.44}, \quad \text{for} \quad Re = 2x10^3 \text{ to } 5x10^4 \tag{4.25}$$

Pasternak and Gauvin[109] used a similar technique involving suspended 3.8 to 10 mm diameter spheres of Celite saturated with water. The wetted spheres were supported in a glass column through which hot air was passed. Celite changes colour from orange to pale yellow on drying, and this gave a qualitative picture of the rate of mass transfer around a particle. For spheres of 5.6 mm diameter, the data were correlated using a modified Reynolds number:

$$J_D = 0.692Re_1^{-0.486} \tag{4.26}$$

where the dimensional length, D, in Re_1 = surface area/maximum perimeter to account for particle shape and orientation. However, the use of the Celite colour indicator was rather tentative so that the implied accuracy of the exponent on the Re number is debatable.

In another study by Pasternak and Gauvin[110], acetone was evaporated from an acetone-impregnated, radio-active Celite particle accelerating co-currently in a hot turbulent air stream at 190°C. The column was made of a Pyrex glass 536.4 cm long and 45.7 cm in diameter. High speed photography at two

positions along the column permitted measurement of the rate of particle rotation. A particle of known weight (impregnated with sufficient acetone to ensure free-surface evaporation) was introduced into the air stream under equilibrium conditions. On reaching the end of the column it fell into a flask containing 200 cm^3 of cold distilled water. The evaporation rate was determined by analysing the amount of acetone left in the particle. This was done by bringing the solution in the flask to boil under reflux for 10 min to allow acetone to diffuse from the particle into the water. An aliquot of the water-acetone was then withdrawn and titrated with iodium-sodium thiosulphate. The data were correlated with Equation 4.26 with a maximum deviation of ±15%.

It was concluded that particles rotated in a random manner. It is unclear to what degree sufficient acetone was used to ensure free-surface evaporation since acetone migration from within the Celite is likely to affect evaporation rates. Furthermore, it is doubtful if Equation 4.26 generally applies to freely moving particles.

Rowe et al.[111] presented results, ($10 \leq Re \leq 10^4$), for the dissolution of spheres of benzoic acid in water and the sublimation of naphthalene in air. The results were correlated for naphthalene in air as;

$$Sh = 2 + 0.69Re^{0.5}Sc^{0.33} \tag{4.27}$$

$$Nu = 2 + 0.69Re^{0.5}Pr^{0.33} \tag{4.28}$$

and for benzoic acid in water as;

$$Sh = 2 + 0.79Re^{0.5}Sc^{0.33} \tag{4.29}$$

$$Nu = 2 + 0.79Re^{0.5}Pr^{0.33} \tag{4.30}$$

Skelland and Cornish[112] studied mass transfer from oblate naphthalene spheroids to an air stream over a Reynolds number range of 130 to 6,000; eccentricities varied from 1:1 to 3:1. Individual spheres were supported on a suspension device and vaporised in a wind tunnel. It was observed that for 25.4 mm spheroids, the effects of natural convection were negligible at Re>15. Skelland and Cornish[112] correlated their results, adopting the modified Reynolds number proposed by Pasternak and Gauvin [109], as;

$$J_D = 0.74 Re_1^{-0.5} \tag{4.31}$$

The maximum deviation of Equation(4.31) was ±6.4%

A theoretical study of methods of calculation for shear stress and heat transfer in external flows was considered by Acrivos[113] for combined laminar free and forced convection. It was suggested that the parameter Gr/Re^2 was of fundamental importance in determining whether laminar free or forced convection transfer predominated. Natural convection was found to be negligible as $Gr/Re^2 \approx 0$, and forced convection to have little influence as $Gr/Re^2 \approx \infty$.

Sandoval-Robles et al.[114] measured mass transfer coefficients from a sphere submerged in a fluid. Brass spheres of 5, 7, 9 and 10 mm. in diameter and coated with gold film 5μm thick were rotated in a motionless electrolytic solution. The mass transfer coefficient was related to the limit current intensity, I_{lim}, by the expression;

$$k_c = \frac{I_{lim}}{(e.F.tr.C_{sol})} \tag{4.32}$$

tr = transfer area

F = Faraday current

e = No. of electrons

C_{sol} = electrochemical species concentration.

Results were correlated by;

$$Sh = 1.032Re^{0.385}Sc^{1/3} \qquad 2 \leq Re \leq 20 \qquad (4.33)$$

$$Sh = 0.803Re^{0.474}Sc^{1/3} \qquad 20 \leq Re \leq 2000 \qquad (4.34)$$

$$Sh = 0.300Re^{0.593}Sc^{1/3} \qquad 2000 \leq Re \leq 23,000 \qquad (4.33)$$

It is interesting to note that the exponent on Re increased with Re. The values range from 0.385 for 2<Re<20 to 0.593 for 2000<Re<23,000 which compares with the theoretical predictions of 0.33 for the creeping flow region, 0.5 for the boundary layer theory (which represents the transfer mechanism in the frontal part of the sphere) and 0.66 for the surface renewal mechanism.

In a later study Sandoval-Robles et al.[115] correlated the mass transfer coefficient in terms of the turbulent intensity, Tu, for 330≤Re≤1720 as;

$$Sh = 6.82Re^{0.559}Tu^{0.069} \qquad (4.35)$$

for Tu, 0.04<Tu<0.30. As is common in such studies extraordinary accuracy is implied by the numerical constant and exponents. Experiments were carried out in a 94 mm diameter vertical column closed at the bottom by a fixed bed of glass spheres. Turbulence in the column was generated by a polyethylene porous plate of 80μm pore diameter. The intensity of turbulence was measured with a hot film anemometer. Not surprisingly, mass transfer rates, were found to increase with an increase in turbulence intensity.

4.3 *Evaporation From Pure Liquid Drops*

The analysis of the evaporation of drops has been considered by many investigators; Hughes and Gilliland[116] have reviewed the mechanics of drops.

Maxwell[100] and later Langmuir[117] postulated the basic relationship for the evaporation of spherical drops into quiescent air. Fuchs[118] extended the work to include the behaviour of much smaller drops. Frossling[2] developed from simple boundary layer theory an expression for evaporation rate in a turbulent stream. Ingebo[50, 119] followed Frossling's analysis and developed an empirical expression of the same general form. Ranz and Marshall[3] considered the evaporation of drops and confirmed the earlier work of Beddingfield and Drew[120] concerning the relative independence of the wet bulb temperature on the Reynolds number of the flow around a drop. In all these studies the method of investigation invariably affected the final correlation of results. Therefore in the next section, a review of liquid-air systems is divided into the two principal methods of study; of a droplet in free fall and of a droplet supported on a suspending device.

4.3.1 *Evaporation From Suspended Liquid Droplets*

Morse[121] showed experimentally that the rate of evaporation from a stationary drop in a gas was proportional to its diameter, (D). His results were analysed by Langmuir[117] who presented the following theoretical equation;

$$-\frac{\partial m}{\partial t} = \partial_h \int D_v D\rho^1 \qquad (4.36)$$

in which the factor ∂_h accounted for the thickness of the film surrounding the drop through which diffusion of the vapour occurred. It was defined by;

$$\partial_h = \frac{4\pi r_1 r_2}{(r_2 - r_1)} \qquad (4.37)$$

D_v = diffusivity coefficient, ρ^1 is the partial density of the vapour of the evaporating substance, r_2 is the radius of the outside of the film of gas and, r_1, the

radius of the evaporating sphere. If r_2 is assumed to be very large compared to r_1, then $\partial_h = 4\pi r_1$ and the rate of evaporation becomes;

$$-\frac{\partial m}{\partial t} = \frac{4\pi r_1 D_v M_w P}{RT} \tag{4.38}$$

which leads to the result that the rate of evaporation is directly proportional to the radius of the sphere.

Houghton[122] in his study of the liquid water content of a foggy atmosphere presented a theoretical expression for the evaporation of small spherical water drops in still air. Measurements were made of the evaporation rates of drops ranging from 25 to 2600 μm, at temperatures ranging from 3°C-32°C. The electrostatic analogy of Jeffrey's[123] general diffusion equation was applied, which for a sphere is,

$$\frac{\partial}{\partial t}(\rho_l V) = -2\pi D_v D(\rho^l_o - \rho^l_\alpha) \tag{4.39}$$

where $\rho^1{}_o$ and $\rho^1{}_\alpha$ are water vapour densities, ρ_l = liquid density, D = droplet diameter and D_v, diffusivity coefficient.

Drops were observed at rest, suspended from a fine wire or glass filament within a small chamber in which the relative humidity was maintained constant. Larger drops of 2000 μm and above were observed to deviate from a spherical form whilst drops smaller than 25 μm could not be accurately observed because of the limitation imposed by the smallest available support. To reduce the area of contact, and to limit heat transfer by conduction between the drop and the support, the support was given a thin coating of paraffin. Drop diameter was measured by means of an ocular micrometer in a low power microscope. The evaporation rate from small droplets (<2000 μm) was found to be directly proportional to drop diameter. The total time for evaporation was given as;

$$T_{tot} = \frac{D^2}{8D_v}(\rho^1_o - \rho^1_\alpha) \qquad (4.40)$$

where D is the initial drop diameter and D_v the diffusivity coefficient.

Houghton does not give the dimensions of his experimental chamber. However the paraffin coating used to limit conduction of heat along the fibre would invariably have reduced the distortion of the spherical surface of the drop at the point of contact therefore restricting drop dynamics. Moreover the fall in temperature of the drops was neither measured nor calculated; it was assumed that the temperature of the drop equalled the temperature shown by the wet bulb thermometer placed in the chamber. It appears likely that the real temperature of the drop, and hence $(\rho^1_o - \rho^1_\alpha)$, was considerably lower than calculated with the result that the application of Equation 4.40 is limited.

Frazier[124] considered a model to fit the data of Houghton[122]and Duguid and Stampfer[125]. It was found that the surface tension effect on vapour pressure was negligible for drops of the size of several microns. The proposed correlation for the evaporation of water was;

$$\frac{\partial m}{\partial t} = m_o[1 + f(GrPr)] \qquad (4.41)$$

where $f(GrPr)) = A(GrPr)^{1/n}$; for $Gr<4.22/Pr$, $A=0.15$ and $n = 2$; for $(4.22/Pr)<Gr<10^5$, $A = 0.215$, $n = 4$. Good agreement was observed with Houghton's[122] results. However, the model underestimates the results for relatively small droplets (6-18μm) of Duguid and Stampfer[125], even allowing for 2% forced convection effects and the influence of surface tension on the vapour pressure in the transition zone between macroscopic and microscopic behaviour. It was concluded that Brownian motion can lead to a continuous distortion of the film around a drop. Thus the heat and mass transfer rates can be enhanced above those given by macroscopic continuous motion.

Theoretical and experimental investigations of droplet evaporation were performed by Frossling[2]. Individual droplets of water, nitrobenzene or aniline of diameter 0.2 to 1.8 mm were suspended on a thin glass fibre rod in a wind tunnel with an upward flow of air of velocity ranging from 0.2 to 7 m/s and Re in the range of 2 to 800. Using convection boundary layer theory, the evaporation rate of moving drops was shown to be expressed by the product of evaporation in quiescent air and a wind factor (1+f). The results were expressed as;

$$-\frac{\partial m}{\partial t} = 2\pi D_v D M_w \frac{\Delta P}{RT}(1 + f) \qquad (4.42)$$

f was expressed as a function of Re thus;

$$f = K\sqrt{Re} = 0.276 Sc^{1/3} Re^{1/2} \qquad (4.43)$$

The mass transfer equation in terms of the Sherwood Number was given by;

$$Sh = 2(1 + 0.276) Re^{0.5} Sc^{0.33} \qquad (4.44)$$

and the Nusselt number by;

$$Nu = 2(1 + 0.276) Re^{0.5} Pr^{0.33} \qquad (4.45)$$

From the sublimation of naphthalene beads, Frossling demonstrated that the local rate of mass transfer projected from the boundary layer theory agreed well with actual distribution of rates around the sphere. The mass transfer rate is a maximum at the front axis of the drop facing the oncoming flow and decreases to a minimum value near the equator, where the wake separates, before increasing again to a maximum at the rear axis where velocities occur in the reverse direction.

Ranz and Marshall[3] investigated the evaporation of water drops of 0.06-0.11 cm initial diameter by suspending individual drops from a glass capillary tube (microburrette) in an upward flowing stream of air. The rate of evaporation was determined in two ways: (1) by measuring the rate of feed through the burette necessary to maintain a constant drop diameter and (2) using a cine camera to photograph the drops at 24 frames per second. Drop temperature was measured by imbedding a thermoelement junction inside the drop. The Re range for the experiments was from 2 to 200. Results were correlated by:

$$Sh = 2 + 0.6Re^{0.5}Sc^{0.33} \qquad (4.46)$$

and, by analogy, the Nusselt number was correlated as;

$$Nu = 2 + 0.6Re^{0.5}Pr^{0.33} \qquad (4.47)$$

The results of Frossling and Ranz and Marshall are very significant from the boundary layer theory considerations, and have become the most widely-quoted equations for heat and mass transfer rate calculations from single drops and spheres. However, these models neglect the effects of drop dynamics and interfacial turbulence during transfer processes. Not surprisingly surface phenomena and drop dynamics were not observed in the study by Ranz and Marshall because individual drops were supported on a suspending device such that the hydrodynamic factor was reduced to a minimum. In addition the cine camera used in the study was capable of recording only 24 frames per sec, rendering it impossible to observe and hence correlate droplet behaviour. As a result evaporation rates from drops which exhibit drop oscillation are higher than predicted by equations 4.44 and 4.46.

Kinard et al[126] analysed the forced convection in front of, and behind, the separation zone of the boundary layer. Since the boundary layer theory makes no

provision for the transfer from the rear surface of a sphere, an additional term was introduced to account for the transfer in the wake of the drop. Using data from Ranz and Marshall[3], Garner and Suckling[127], and Steinberger and Treybal[108], the following correlation was proposed;

$$Sh = Sh_o + 0.45Re^{0.5}Sc^{0.33} + 0.00484ReSc^{0.33} \qquad (4.48)$$

where Sh_o is the Sherwood number under natural conditions.

Hsu et al.[129] followed a similar experimental procedure to that used by Ranz and Marshall[3] and suspended individual drops of n-heptane of volume 7.155×10^{-12} m^3 on a small glass tube (micro pipette). The evaporation rate was measured as the rate of introduction of the evaporating component which was required to maintain the drop at a constant volume. The investigation was intended to highlight the effect of drop behaviour on mass transfer. Twenty six different drop configurations were observed; the shapes ranged from pendant contours with a large value of the height/diameter ratio to oblate spheroids with small values of this ratio. In all cases, the evaporation rate as measured by the Sherwood number was observed to increase rapidly with deviation from sphericity. The oblate spheroids yielded higher evaporation rates than the pendant drops. By a trial and error procedure, Hsu et al[129] correlated their data by;

$$Sh = 2\left[1 + 0.178Re^{0.56}Sc^{0.33}\right]\left[1 + 2.292(1-E_1)\right]\left[1 - 0.257(1-E)\right] \qquad (4.49)$$

where E_1 = drop sphericity = $\frac{6V}{A_e d_e}$,

The disadvantages of using techniques whereby a droplet is supported on a suspension device are:

(1) the elimination or reduction of drop mechanics, which have a considerable effect on mass transfer rates,

(2) conduction of heat along the suspension device which can represent a significant amount of heat transfer and

(3) the uneven exposure of droplet surface to the incident continuous phase.

Audu[130] in an attempt to overcome some of these problems suspended a droplet from a rotating nozzle in a horizontal wind tunnel. The rotating suspension device supposedly exposed all sides of the evaporating droplet to the air stream, overcoming the problem of uneven droplet exposure. However, the problem of conduction of heat along the suspension device and the fact that the suspended droplets were not spherical were not addressed. Audu[130] expressed his results as;

$$Sh = 2 + 0.473 Re^{0.5} Sc^{0.33} \tag{4.50}$$

Hassan[131] modified Audu's[130] approach to enable a simultaneous measurement of droplet weight and temperature. The drop shape was assumed to be hemispherical and allowances were made for thermal conduction along the suspending glass fibre. Heat transfer data were correlated by:

$$Nu = 2 + 0.27(1/B)^{0.18} Re^{0.5} Sc^{0.33} \tag{4.51}$$

where $B = \frac{C_p \Delta T}{\lambda}$. For mass transfer:

$$Sh = 2 + 0.575[(T_a - T_s)/T_{amb}]^{-0.04} Re^{0.5} Sc^{0.33} \tag{4.52}$$

Equation 4.52 is essentially a reproduction of the Frossling equation[2] since $[(T_a - T_s)/T_{amb}]^{-0.04}$ for most practical purposes ≈ 1.

4.3.2 *Evaporation from Single Droplets in Free -Fall*

It is evident from previous discussions that although they provide an insight into transfer phenomena, and have enabled skin-formation[131] and particle morphology to be evaluated[132], investigations based on suspended droplets do not adequately represent the behaviour of liquid droplets in heat and mass transfer processes. A more practical approach to the study of droplet behaviour is by observing droplets in free fall. The earliest of such studies was the work of Woodland and Mack[132] and Gudris and Kulikova[133] who freely-suspended charged droplets in a Milikan condenser. Individual particles, previously charged, were introduced into the Milikan apparatus and the potential across the condenser varied until the electrostatic and gravitational fields were balanced such that the drop remained stationary. The loss in weight of the droplet with time (evaporation rate) was followed as the decrease in electric potential. The maximum size of droplet which could be studied by this method was 1.5μm (Re; 10^{-5} to 10^{-4}). These limitations render results from the Milikan experiment of limited value. Furthermore, the technique does not lend itself to the study of the effects of relative movement of drop and drying medium.

To overcome these problems, Kinzer and Gunn [134] studied the evaporation rate of charged particles that fell freely through detector rings. By employing this method they were able to study larger droplets of diameter 10-140 μm. Droplets greater than 1 mm were also studied by supporting them in free flight by hydrodynamic forces. They analytically developed the expressions;

$$Sh = 2\left[\left(\frac{1+F_t}{4\pi}\right)(ReSc)^{1/2}\right] \tag{4.53}$$

$$Nu = 2\left[\left(\frac{1+F_t^1}{4\pi}\right)(RePr)^{1/2}\right] \tag{4.54}$$

where F_t and $F^1{}_t$ were designated wind factors. Kinzer and Gunn[134] first considered mass transfer under stagnant conditions and then modified it to the

situation where the surrounding fluid swept continually over the surface. A contact time was introduced as the time required for small amounts of the moving fluid to transverse one diameter of the equivalent sphere. This assumption was, of course, first introduced by Higbie[61]. It is interesting to note that Kinzer and Gunn arrived at a factor which has been obtained by workers using the potential flow approach. The wind factor was found to be a function of Re. It was a maximum at Re = 4, then fell to a lower value before rising again with increasing Re.

Finlay[49] used a vertical wind tunnel to study droplet behaviour. Individual drops of water, iso-butanol, heptane or iso-octanol were suspended in an air stream within the tunnel. Drops were collected and weighed after a known period of time and Sh numbers calculated for drop diameter in the range of 0.1 to 0.5 cm. In order to compare the data with those of Ranz and Marshall, Finlay plotted Sh against $Sc^{0.33}Re^{0.5}$ and found a marked discrepancy which was attributed to droplet shape oscillation. He presented the approximate correlation:

$$J_D = \frac{(k_c Sc^{2/3})}{V} = BRe^n \qquad (4.55)$$

for which B and n were different for each system and therefore of limited application as to its generality.

Jones and Smith[135] studied mass transfer from solid spheres of naphthalene, camphor or benzoic acid suspended in an air stream within a rotameter tube. Radial and axial spinning motions of the particles were observed. To compare the mass transfer rates with those for stationary spheres, a ball bearing was inserted inside the spheres to prevent spinning; no differences in mass transfer rates were observed. It was concluded that when a particle is spinning, one side is stationary relative to the gas whilst the other meets the gas at twice its linear velocity, hence cancelling out any effect. Experimental data were correlated by;

$$Sh = 2 + 25(ReScRe_t^{0.5})^{0.33} \qquad \text{for laminar flow} \qquad (4.56)$$

$$Sh = 2 + 0.055(ReScRe_t^{0.5})^{0.55} \qquad \text{for turbulent flow} \qquad (4.57)$$

where Re_t is flow Reynolds number.

Hattangady[136] used a similar technique to Finlay[49] to investigate the heat transfer rate from Freon drops of size range 0.3 to 1.0 mm at high pressures, e.g. 8-9 atmospheres. Droplet oscillation was observed. However, it was concluded that the rate of heat transfer was independent of drop history and size. He proposed the correlation:

$$Nu = \frac{Pr^m Re^n}{(1+B)^{2/3}} \qquad (4.58)$$

where n was found to be between 1 and 0.5. Values of m were obtained by regression analysis and were found to be between 0.70 and 0.85, higher than the frequently-obtained value of 0.33. This, he attributed to random oscillation of drops, which actually contradicts his conclusion about the effects of drop history and size.

Using the same apparatus, Garner and Lihou[137] investigated droplet behaviour in a vertical wind tunnel. From cine films, they determined the mean drop shape, terminal velocity and its mode and frequency of oscillation. It was noted that, as drop shape oscillation increased, so did the surface area and hence mass transfer rate. The oscillation number, $OD = (\pi\mu_d d_e/\sigma T^1)$, was proposed to allow for such effects. However droplet oscillation in general does not conform to a harmonised periodic change and it is therefore difficult to evaluate the period of oscillation T^1 even at low Re regimes, which suggests the correlation of OD must be limited to the experimental conditions employed.

Miura et al [138] presented experimental results in support of the Ranz-Marshall equation, (4.46). They studied the evaporation of water drops of initial diameter 2.9 to 3.3 mm, floating in an ascending air current of velocity 7.5 to 9 m/s. It was concluded that, even though floating droplets experienced shape oscillation, the heat and mass transfer rates correlated well with the Ranz-Marshall[3] equation. However inspection of the experimental data shows very few results, which are clustered at one point on the plot of Sh vs $Re^{0.5}.Sc^{0.33}$. It was concluded that an experimental correlation could not be proposed but nevertheless Miura et al fitted the experimental data with the equation by Ranz-Marshall.

Yao and Schrock[139] conducted an experiment to study the effect of drop oscillation on evaporative cooling from falling droplets. An apparatus was designed to provide accurate data on the mean temperature of the drop and its position in free-fall. The initial drop diameter, and the temperature and humidity of the air through which it fell, were also measured. The apparatus consisted of a drop generator, a plastic column 3m in height and a calorimeter that could be positioned at any elevation to collect a drop and measure its temperature. Drop size and oscillation were determined from photography of the drops. An oil-free white paint was added to the water to provide better illumination; whether, as many paints do, this had any surface active characteristics which would affect surface fluidity is unclear. The observed oscillations were found to be in 2 modes; a prolate-oblate oscillation for smaller drops and for drops larger than 4 mm and at a distance $x/d_e<50$, (x is the falling distance and d_e the drop diameter), a distinct point was formed alternately at the top and bottom. Experimental results showed much higher rates of evaporative cooling from oscillating drops than predicted by the Ranz and Marshall model[3]. A correction factor, g, was suggested to modify the Ranz and Marshall equation, where $g = 25\ (x/d_e)^{0.7}$ yielding;

$$Nu = 2 + 15Pr^{1/3}Re^{1/2}(x/d_e)^{0.7} \quad (4.59)$$

$$Sh = 2 + 15Sc^{1/3}Re^{1/2}(x/d_e)^{0.7} \quad (4.60)$$

for $3 \leq d_e \leq 6$ mm and $10 \leq x/d_e \leq 600$.

Ahmadzadeh and Harker[140] investigated the evaporation rates of acetone and water droplets in free-fall. Drops were allowed to fall down a vertical column into a collecting device designed to prevent further evaporation of acetone. Nozzles of different diameters (0.107, 0.173, 0.235 and 0.313 cm) were used for drop formation. Mass transfer rates were measured by passing the ensuing gas through wash bottles to absorb all the acetone evaporated and the resulting solution was then analysed chemically and spectro-photochemically. Drop volumes and residence times were evaluated using high-speed photographic techniques. The mass transfer rate was correlated by;

$$Sh = 3.0\,(0.345d_e - 0.744)Re \quad (4.61)$$

Ahmadzadeh and Harker do not give the initial drop diameter produced by the various nozzles used. Drop volume was evaluated by photographing it just after it had left the nozzle and presumably drop diameter was calculated from this. Since the drop diameter was not directly measured the implied accuracy in Equation 4.61 is surprising. In the event it was concluded that the Ranz and Marshall correlation did not fully describe mass transfer from a falling drop and that the effect of increased oscillation with larger drops must be further investigated.

More recently, Akbar[22] studied droplets drying in free-flight using apparatus based on the previous design by Lihou[137]. Droplets of 2.8-4.6 mm in diameter were suspended in a vertical wind tunnel at Re in the range 500 to 1380,

and over a temperature range from 37-97°C. Photographic techniques were used to observe and record droplet behaviour. The data were correlated by:

$$Sh = -105 + 3.9\,[(T_a - T_s)/T_{amb}]^{0.18} Re^{0.5} Sc^{0.33} \qquad (4.62)$$

for Re > 1380. Obviously this equation is limited to the range of properties studied since otherwise Sh would become negative; in fact for Re < 1060, Sh was correlated by;

$$Sh = 2 + 0.71\,[(T_a - T_s)/T_{amb}]^{0.18} Re^{0.5} Sc^{0.33} \qquad (4.63)$$

In any event equations 4.62 and 4.63 do not appear to accurately correlate Arkbar's experimental data. A plot of the experimental data demonstrates a non linear correlation with $Re^{0.5}Sc^{0.33}$. However, Equation 4.63 gives a linear relationship of Sh vs. $Re^{0.5}Sc^{0.33}$, since for pure liquid droplets$[(T_a - T_s)/T_{amb}]^{0.18}$ is essentially constant.

4.3.3 *Evaporation From a Spray of Droplets*

Dloughy and Gauvin[141] investigated evaporation rates from a spray of water droplets produced by pneumatic atomising nozzles within a purpose-built co-current spray tower of 20.32 cm diameter. The drop sizes were in the range of 11.5 -38.5 μm. The spray was considered to go through three distinct zones: the nozzle zone, in which the droplets decelerate from the initial release to their settling velocity; the evaporating zone, where the mechanism of evaporation is the same as that from a free liquid surface; and finally the drying zone, in which internal diffusion in the drying particle becomes the governing factor. To calculate the rates of heat and mass transfer in the evaporating zone, samples of air and droplets were taken from a succession of points down the tower and instantaneous heat and mass transfer coefficients calculated from energy and

material balances. It was concluded that the presence of a swarm of droplets within a spray had no influence on the rate of evaporation. For the range of droplet size of 11.5 to 38.5 μm considered, the heat and mass transfer coefficients were observed to be the same as for single stationary droplets evaporating in quiescent air, i.e. Sh = 2, Nu = 2.

The conclusions drawn by Dloughy and Gauvin[141] were contradicted by Bose and Pei[128] in a later study. Both of these studies were similar in nature except that in the latter a larger range of drop sizes, 40 to 125 μm, was considered. Boss and Pei found that the experimentally-determined values of heat and mass transfer coefficients could not be accurately correlated by Sh = Nu = 2. They therefore proceeded to evaluate droplet relative velocities and compared the experimentally-determined values with the Ranz-Marshall correlation. An improved correlation of data was obtained, which suggested that the relative velocity between the droplet and the surrounding air is of significant importance. It was concluded that for industrial applications where the droplet diameters are within a larger range, relative velocities between air and particle must be taken into consideration in the calculation of the heat and mass transfer rates.

Dickinson and Marshall[142] performed a computational study on the rates of evaporation of sprays of non-uniform drop size distribution. Cases of negligible and appreciable relative velocities were considered. Among the assumptions made to justify the modelling were no back-mixing, and more importantly that the spray comprised drops of pure liquids, implying that the drop temperatures remained constant at the wet bulb temperature. For sprays moving at negligible relative velocity the investigation showed that:

(a) the air temperature falls as the spray evaporates resulting in a decrease in evaporation rate,

(b) sprays with less uniform drop size distribution evaporate more rapidly at first than more homogeneous sprays with the same diameter,

(c) no mean diameter can adequately characterise a spray with respect to evaporation,

(d) the size distribution of droplets changes during evaporation; for non-uniform sprays, the mean diameter is higher and then decreases until completion of the operation.

For sprays moving with significant relative velocity the study highlighted additional features:

(i) to achieve a given degree of evaporation the spray must travel a far greater distance,

(ii) the effect of relative velocity is more significant at high initial velocities and at higher drying temperatures,

(iii) for higher initial velocities, the relative error in neglecting drop velocity is greatest for small drops. This is because such drops evaporate extremely rapidly and a larger proportion of the evaporation occurs during droplet deceleration.

Manning and Gauvin[143] conducted a similar study using water sprays in both co-current and counter-current air flows. The evaporation rates from the sprays were followed by measuring the colorimetric increase in the concentration of a red dye used. Drop size distribution was determined from samples obtained by traversing the spray with an immersion cell containing varsol. They correlated their results with the equation proposed by Frossling[2] and Ranz and Marshall[3] for stationary droplets supported in moving air but there was a considerable scatter. Evidently this was due to the fact that relative velocity plays a significant role especially in the vicinity of the atomising nozzle.

Marshall[144] presented a detailed method for the evaluation of droplet distribution in a spray process. The spray size distribution was divided into size groups and the change in average drop diameter was studied over short periods of time under zero relative velocity conditions. It was concluded that in the majority of sprays about 90% of the evaporation is completed during the first 1.5

seconds after release. This is the period during which sheet to ligament to drop, and drop dynamic behaviour, are the predominant factors.

4.3.4 *Evaporation of Single Droplets in High Temperature Surroundings.*

In the process of drop evaporation there is obviously a balance between the heat lost by the drop as a result of vaporisation and the heat transferred to the drop from the surrounding air by convection or radiation. In a high temperature environment the sensible heat required to raise the temperature of the vapour leaving the drop surface to the surrounding gas temperature becomes significantly larger. There is therefore a reduction in the actual amount of heat reaching the drop surface. It has been shown by Ranz[145] that, as little as about 25% of the total heat transferred in a high temperature environment reaches the surface of an evaporating drop; the rest is absorbed by the cold vapour in its radial flow from the drop. Ranz[145] proposed the following correlation;

$$\text{Corrected evaporation} = \frac{1}{Z}\ln(1+Z)\frac{\partial V}{\partial t} \tag{4.64}$$

$$\text{where } Z = \frac{k_a C_p}{k_v}\Delta T \text{ and } k_v = \text{heat capacity of vapour.} \tag{4.65}$$

Spalding[146] developed the following equation;

$$Nu_m = Nu(1+B)^{0.4} \tag{4.66}$$

$$\text{where } B = \frac{C_p \Delta T}{\lambda}$$

A differential equation describing the heat balance over a spherical shell through which heat was transferred inward to the drop and mass was transferred outward was developed by Marshall[144]. In a study of droplet evaporation in high temperature surroundings (>150°C), Marshall solved the equation to give

the temperature T as a function of distance x, through the gas film surrounding the drop:

$$\frac{T-T_s}{T_g-T_s}=\frac{\exp\left(\frac{E_T}{x}\right)-\exp\left(\frac{-E_T}{r_1}\right)}{\exp\left(\frac{-E_T}{r_2}\right)-\exp\left(\frac{-E_T}{r_1}\right)} \tag{4.67}$$

where $E_T=\frac{mC_p}{4\pi k_v}$, r_1 = radius of evaporating drop, r_2 = outer radius of the gas film. Ignoring the variation in thermal conduction and heat capacity of the gas film caused by temperature and concentration gradients, differentiation of Equation 4.67 with respect to the drop surface gives Nu;

$$Nu=\frac{2(E_T/r_1)}{\exp\left(E_T\left(\frac{1}{r_1}-\frac{1}{r_2}\right)\right)-1} \tag{4.68}$$

Downing[177] studied the evaporation of 1 mm diameter drops of water, acetone, benzene or hexane in a high temperature stream of air, (from 27°C-340°C) with Re in the range 24 to 325. The results were correlated by;

$$Nu=M^1N\left(\frac{\ln(1+B^1)}{B^1}\right)(2+0.6Re^{0.5}Pr^{0.33}) \tag{4.69}$$

$$Sh=M^1(2+0.6Re^{0.5}Sc^{0.33}) \tag{4.70}$$

where $M^1=1-0.4(1-T_s/T_a)$ and $N=1-0.4\left(1-\ln\frac{(1+B^1)}{B^1}\right)$

All physical and transport properties were calculated at an average film temperature T_f, defined as 0.6 (T_a - T_s). The term B^1 was related by,

$$B^1=\frac{C_p\Delta T}{\left(\lambda-\frac{q_{rad}}{N_A}\right)} \tag{4.71}$$

Hoffman and Gauvin[146] measured the evaporation rates of liquid drops of initial diameter 0.4 to 1.4 mm supported on the tip of a thin glass fibre inside a 9.5 mm thick wall stainless steel sphere of radius 114.5 mm. The sphere was electrically heated to temperatures between 100 and 500°C. Mass transfer rate in each case was followed by photographing the evaporating droplet at constant time intervals through a number of viewing ports on the sides of the steel wall. It was concluded that the Nusselt number was not dependent on the Grashof number. The experimental data were correlated in terms of the Spalding number as;

$$Nu = \frac{3.2\, B^{0.97}\, Pr^{0.33}}{B^{1}} \qquad (4.72)$$

Pei and Gauvin[147], however, in a later study presented the heat transfer coefficient as a function of the Grashof number. Pei and Gauvin[147] used porous Celite spheres of radius between 6.35 to 12.7 mm in diameter at temperatures in the range of 204°C to 537°C. The proposed correlation was;

$$Nu = \frac{3.32\, Re^{0.5}\, Pr^{0.33}}{B}(Gr/Pr^{2})^{0.007} \qquad (4.73)$$

However the low power of the group (Gr/Pr^2) in Equation 4.73 clearly renders it superfluous.

Maltosz et al.[148] investigated the evaporation of drops of n-heptane in a high temperature environment of nitrogen or argon at 286°C with gas pressures ranging from 6.8 to 102 atmospheres. Initial drop diameters were within the range of 720 to 910 mm, or 1470 to 1780μm. They found the effect of the non-ideal behaviour of the gas phase to be important for the theoretical prediction of drop temperature especially at high pressures. At low pressures(6.8 atm) the effective molecular diffusion coefficient was found to be in good agreement with the

calculated molecular diffusion coefficient. At high pressures(102 atm), the effective molecular diffusion coefficient was six times greater than the calculated molecular diffusion coefficient, suggesting that molecular mass transport may not have been the controlling factor.

Lee and Ryley[149] used a 50 μm diameter glass fibre to suspend water drops of 230 to 1130μm initial diameter in a horizontal brass tunnel through which superheated steam of 1 to 2 atmospheres was passed. The Re was in the range of 64 to 250. The data were correlated by;

$$Nu = 2 + 0.74\, Re^{0.5}\, Pr^{0.33} \qquad (4.74)$$

Trommelen and Crosby[150] evaporated water droplets into air and superheated steam. The air velocity was between 1.5 to 2.1m/s and the temperature ranged from 150 to 250°C. Drops of 1.56 mm diameter were suspended at the junction of a chrome-constantan thermocouple which was attached to a fine horizontal glass fibre. This technique allowed the simultaneous measurement of drop weight and temperature. The evaporation rate was observed to be slower in superheated steam but followed a pattern similar to those observed by Ranz and Marshall[3] and Lee and Ryley[149]. It was concluded that the Ranz-Marshall equation for stagnant droplets in an air stream was also valid for evaporation in superheated vapour.

Yen and Chen[151] measured the heat transfer rates of porous spheres saturated with either water or ethanol in a vertical hot air flow at 2.1-11.4 m/s, Re of 200-2000, and air temperatures of 150-960°C. The data were correlated by;

$$Nu(1 + B) = 2 + 0.6\, Re^{0.5}\, Pr^{0.33} \qquad (4.75)$$

i.e. evaporation reduced the heat transfer rate by a factor (1+B).

Renkzibulut and Yuen[152] repeated the studies of Yen and Chen[151] using methanol, heptane and water droplets. They extended the range of Re to cover 25 to 2000 and the Spalding transfer number B, from 0.07 to 2.79. Results were correlated by:

$$Nu(1 + B)^{0.7} = 2 + 0.57\, Re^{0.57}\, Pr^{0.33} \qquad (4.76)$$

4.4 *Evaporation From Drops Containing Dissolved Substances*

The presence of dissolved solids in a liquid drop leads to a decrease in the vapour pressure of the drop.

The vapour pressure of a pure liquid is the measure of the number of molecules in the vapour phase. It is thus a measure of the escaping tendency of the 'surface molecules' and also the strength of the inter-molecular attraction between molecules. With the addition of a solute to a solvent, the molecules of both the solute and the solvent are both present on the surface of the solution. Since by Dalton's law the total vapour pressure above the solution is the sum of the individual vapour pressures, it is clear that the number of molecules of the solvent in the vapour phase will be < than the number of molecules of solvent present on the surface of the pure solvent. The driving force for mass transfer is therefore reduced resulting in a reduction in the mass transfer rate. The surface temperature of the evaporating drop consequently increases above the thermodynamic wet bulb temperature.

As the solvent is evaporated from the surface a skin or deposition of solute may commence on its surface. This affects equilibrium conditions and may increase resistance to heat and mass transfer with increasing thickness. In most cases the skin begins as a porous monolayer which thickens and hardens to form a crust on the surface during drying. It becomes increasingly impervious and consequently retards drying. Depending on the porosity or rheological properties of the crust, if the outer layer is not permeable, the particle may fracture under

internal pressure. The rise in pressure occurs due to an increase in temperature associated with lower mass transfer rates. If the skin is less porous and has elastic mechanical properties, it may be inflated by the rise in internal pressure and a hollow particle may form. Alternatively the skin may stretch, rupture and reform, allowing a surge of vapour to escape.

For a saturated surface, evaporation occurs only from the wetted surface exposed and moisture movement from within the material is of little importance. Once the liquid has been concentrated beyond saturation, the mechanisms of moisture movement from within the material become important. The entire process may be further complicated by internal circulation and drop oscillation. Consequently, evaporation of drops containing dissolved substances is very complex and does not lend itself to simple analysis.

Hassan[131] has classified skin-forming materials into three groups; (I) materials which form a skin by gelatinisation at high temperatures, i.e. > 150°C, e.g. starch and custard, (II) materials which form a skin immediately on exposure to the drying medium at any temperature, e.g. gelatine drops, and (III) materials which form a skin due to solute deposition on the surface as evaporation proceeds, e.g. skimmed milk, glucose, etc. The actual mechanism of skin formation is however product specific.

Shepherd et al.[153] divided the drying of most solutions/suspensions into two main zones:

(i) The constant rate period, during which moisture movement within the material is rapid enough to maintain saturation at the evaporating surface. Evaporation proceeds by diffusion of vapour from the saturated surface of the material across the stagnant film at the interface; the controlling factors are the mass transfer coefficient for diffusion across the film and the driving force provided by the difference between the saturated vapour pressure at the interface and the pressure in the bulk gas stream. The constant rate is

often observed immediately following atomisation and drop mechanics is important in determining the mass transfer coefficient.

(ii) The falling rate period. This is further divided into the zone of unsaturated surface drying and the zone of internal moisture movement control. The first zone of the falling rate period commences after the critical moisture content is exceeded and the entire evaporating surface is no longer maintained at saturation by moisture movement within the solid. In the second zone, the plane of evaporation recedes into the solid. The drying rate is then controlled by the rate, and hence the specific mechanism, of internal moisture movement within the solid. If the reduced moisture content is larger than the critical moisture content, only the constant rate period will occur. In other cases, for example the drying of soap[154], the initial moisture content is lower than the critical moisture content and the entire drying process takes place in the falling rate period.

Some of the theories advanced to explain the various mechanisms of moisture movement are reviewed below.

4.4.1 *Mechanisms of Moisture Movement.*

The diffusion theory, the capillary theory and the receding evaporation front are the three commonly-used theories to describe the mechanisms of moisture movement once the surface has been concentrated beyond saturation, i.e. in the falling-rate periods.

(i) The diffusion theory: Fundamentally, diffusion occurs when there is a concentration gradient between any point deep within the material and at the surface. This method of transport of moisture is usually found in non-porous solids in which single phase solutions are formed with the moisture, e.g.. paste, soap, gelatine or glue. It is also found in the removal of the last portion of moisture from clay, flour, wood leather, paper, starch and textiles[154]. This process is considered to take place in two characteristically different ways;

(a) diffusion of liquid from within the solid surface followed by evaporation of the liquid at the surface, and

(b) evaporation of liquid at a point beneath the surface of the solid followed by diffusion of water vapour through the pores to the surface and into the ambient air. A theory based on this approach has been developed by Harmathy[155] to predict the drying rate of clay.

(ii) Capillary movement in porous solids: A porous material contains interconnecting pores and channels of varying pore size. As water is evaporated, a meniscus of liquid water is formed across each pore in the depth of the solid. This sets up capillary forces between the water and solid which provide the driving force in moving water through the pores to the surface.

(iii) Effect of shrinkage: Another factor affecting internal moisture movement and hence the drying rate is any shrinkage of the solid as moisture is removed. Rigid drops do not shrink appreciably but colloidal and fibrous materials such as vegetables and other foodstuffs do undergo shrinkage. Shrinkage may be accompanied by a sudden release of moisture and in some cases this may cause the material to warp or change its structure.

(iv) In the receding evaporation theory, internal moisture migration is explained in terms of the creation of a receding front which divides the system into a dry zone and a wet zone. Choeng et al[156] presented a model for predicting crust thickness, core temperature and mass transfer rate following the assumptions that; (1) the evaporation interface, r=z, recedes into the wet core as evaporation proceeds, (2) the core temperature is uniform throughout the core, and (3) the moisture is transferred from the evaporation interface by vapour diffusion through the pores at a rate related to an effective diffusivity, D_{eff}. A mass balance over the evaporating interface was given by:

$$-4\pi r^2 \rho_{co} x \frac{\partial z}{\partial \theta} = -4\pi r^2 D_{eff}\left(\frac{M_w}{RT_c}\right).\frac{\partial P}{\partial r}\Big]_{r=z} \qquad (4.77)$$

The crust thickness rate was expressed as:

$$\frac{\partial z}{\partial \theta} = \frac{D_{eff}}{\rho_{co}{}^{x}}\left(\frac{M_w}{RT_c}\right)\cdot\frac{\partial P}{\partial r}\Bigg]_{r=z}, \tag{4.78}$$

Assuming that heat was transferred through the crust by conduction, the change in core temperature was given by:

$$\frac{\partial T_c}{\partial \theta} = \left(\frac{{}^{a}1/a_4}{a_2z^2 + a_3z}\right)\left(\frac{T_g - T_c}{2}\right) + \left(\frac{{}^{b}1/a_4}{b_2z^2 + b_3z}\right)\left(\frac{P_g - P_c}{T_c z}\right), \tag{4.79}$$

and the rate of weight loss expressed as;

$$-\frac{\partial w}{\partial \theta} = -4\pi z^2 \rho_{co}{}^{x}\left(\frac{b_1}{b_2z^2 + b_3z}\right)\left(\frac{P_g - P_c}{T_c}\right) \tag{4.80}$$

All the variables are as defined in the Nomenclature. The above equations were solved simultaneously by the Runge-Kutta fourth-order method to give the crust thickness, core temperature and weight of drop as a function of time.

Audu and Jeffreys[157] studied droplet drying of sodium sulphate detergent slurries and expressed the crust mass transfer coefficient as:

$$k_c = \frac{D_v \varepsilon_1^{1.5}}{\psi_1} \tag{4.81}$$

where ε_1 = crust porosity, and ψ_1 = crust thickness proposed as:

$$\psi_1 = R_e - \left[R_e^3 - \frac{3G}{2\pi C_o}(H_d - H_u)\Delta\theta\right]^{0.33} \tag{4.82}$$

where C_o = initial concentration, R_e = external drop radius, G = air flow rate and H_d and H_u downstream and upstream humidity respectively. However, the calculated values were as much as 20% more than experimental results.

Esubiyi[158] in a theoretical study expressed the crust mass transfer coefficient, k_c as:

$$k_c = \frac{\varepsilon^3 \rho}{5(1-\varepsilon)^2 \mu s_b^2 \psi_1} \tag{4.83}$$

where s_b = specific surface area. This correlation was based on an assumed vapour velocity through the pore of a solid crust described by the Kozeny equation:

$$\varepsilon = \left[\frac{5G.s_b^2 v \psi_1}{2\pi d_c \Delta P}\right]^{0.33} \tag{4.84}$$

The mechanisms of moisture movement in a solid are however extraordinarily difficult to correlate and will always be product-specific, and vary to some extent with drier operating parameters e.g. initial moisture content, modes of heat transfer, driving force and even the ratio of free surface area to volume. In addition to the phenomenon of shrinkage referred to above, there may be crack formation, which provides an additional route for moisture loss. Alternatively expansion may occur effectively reducing the bulk density and thinning any film formed but increasing the mean distance for moisture migration. In solids containing other volatile compounds as well as water, selective diffusion phenomena may occur as moisture content is reduced significantly resulting in preferential retention of the larger volatile molecules. As implied in page 98 in some solids with extreme drying conditions, a series of explosions may occur resulting in rapid transient moisture transfer and leaving blow holes or surface imperfections. Thus analyses of solutions/slurry/solid drying phenomena are considerably more complex than for pure liquids.

4.5 *Conclusion*

A considerable amount of analytical and experimental work has been carried out on evaporation from the surface of both solid particles and liquid drops to allow prediction of heat and mass transfer rates. Although most of the work presented follows a similar pattern in terms of method, the diversity of correlations presented emphasises the complexity of the phenomena involved, or possibly in some cases the limitations of the experimental technique.

Common to most of the papers reviewed, are the effects of the Reynolds number, the Prandtl number, the Schmidt number, and turbulence. Therefore as a first approximation, it may be assumed that the general Equations 4.85 and 4.86 are suitable engineering correlations:

$$Nu = C + B\, Re^{n} Pr^{m} \tag{4.85}$$

$$Sh = C + B\, Re^{n} Sc^{m} \tag{4.86}$$

for which the evaporation for droplets in quiescent air or with no relative flow of the continuous phase has been theoretically shown to be equal to 2, i.e. Sh=Nu=2.

Inherent in these correlations is the assumption that the hydrodynamic conditions close to the interface, that is in the region where most of the resistance to transfer is located, are uniquely described by the Reynolds number of the continuous phase. The above models assume either that the interface does not interfere with the transfer process or that surface oscillation does not affect the exposed surface area for transfer. However as noted in Chapter Three, surface instability grossly affects transfer rates. On occasions when interaction between the phases is considered, it is accounted for by introducing into the mass transfer equation the Reynolds number raised to some spurious power of up to four decimal places. The shortcomings of these models can be readily demonstrated by comparison of a transfer process where there is interfacial movement due to

drop oscillation with one which shows little or no interfacial movement, (e.g. sublimation of naphthalene spheres or water drops treated with surfactant, see Chapter Six). In the latter case it can be assumed that the phases are in equilibrium at the interface. This state of equilibrium refers not only to concentration and thermal equilibrium but also to the forces acting in the interface, (c.f. Chapter Two). One of these forces, the interfacial tension, is a characteristic feature of the interface. Should its value be locally affected by the transfer process, in terms of the pressure it exerts on the surface, the equilibrium between the forces will be locally affected and movements within the interface may result. Such movements are transferred by continuity of stress to the adjoining sublayer and in turn affect the rate of transfer. Hence the bulk Reynolds number can no longer be used to represent hydrodynamic conditions existing in the close vicinity of the interface. Consequently correlations of the type given in equations 4.85 and 4.86 will cease to satisfactorily describe the mass transfer process.

As the dynamic force of the continuous phase becomes important, a value of Re is reached where the boundary layer separates and a wake is formed. The flow becomes turbulent. The turbulence may lead to vortex shedding, the frequency of which is a function of Re, (c.f. Chapter Two). Many investigators have shown that turbulence has a significant effect on drop shape oscillation and on heat and mass transfer rates. It has also been shown that the Reynolds number alone is insufficient for the complete correlation of droplet behaviour[22, 49, 136, 140]. However, in the widely-used experimental technique including suspension of a single drop on the tip of a glass filament the effects of drop shape, oscillation and circulation are largely ignored.

Shape oscillations become evident when a drop is studied in free fall. These oscillations tend to thin the boundary layer characterised by Pr for heat transfer and Sc for mass transfer processes. The exponent applicable to these groups as predicted by the boundary layer and penetration theories increases

from 0.33 to 0.50 at higher mass transfer rates. However, most workers[2, 3, 22, 135, 170, 171, 172] have found no dependence of transfer rates on Pr and Sc beyond the power of a third, even though higher mass transfer rates have been recorded attributable to drop shape oscillation. It is evident that, for a more comprehensive correlation of mass transfer to and from droplets which exhibit shape oscillation or interfacial movement, an additional factor or group needs to be developed in order to modify Equations 4.84 and 4.85.

The present study was carried out to investigate droplet behaviour for a range of pure liquid droplets freely suspended in an air stream. The succeeding chapters describe the experimental programme and the development of a new dimensionless group for incorporation into the mass transfer equations.

CHAPTER FIVE

5 INTRODUCTION TO THE EXPERIMENTAL PROGRAMME

5.1 Introduction

5.2 The Vertical Wind Tunnel

5.2.1 Drop Collecting Device

5.2.2 The Inverted Velocity Profile

5.2.3 The Working Section(Drying Chamber)

5.2.4 The Drop-Forming System

5.2.5 Video Recording of Floating Droplets

5.3 Measurement of Liquid Physical Properties

5.3.1 The Torsion Meter

5.3.2 The Haake Viscometer

5.3.3 Air Temperature and Humidity

5.3.4 Drop Dimensions

5.3.5 Drop Surface Temperature

5.4 Radiation Effects

5.5 The Moulding of Naphthalene Spheres

5.5.1 Sphere Preparation

5.6 Experimental Procedure

CHAPTER FIVE

INTRODUCTION TO EXPERIMENTAL PROGRAMME

5.1 *Introduction*

This research programme studied the fluid dynamics of pure liquid drops as an essential part of the mechanics of mass transfer which have also been studied concurrently. The literature search revealed that drop behaviour has an important effect on mass transfer rates, but that this effect has not been properly quantified and incorporated into the mass transfer equation. Some of the assumptions made when estimating the rate of heat and mass transfer to and from spray droplets are that,

1) droplets upon release from the atomiser are stable and spherical,

2) there is no evaporation in the preliminary heating up period, and

3) evaporation in the constant rate period takes place from a stable spherical droplet.

In practise this is not usually the case. In droplet drying operations in which the constant rate period is significant, these assumptions could result in a dryer height greater than is actually necessary to evaporate the water. Although the additional length may provide capacity for variations in moisture content and for occasional overload, it has the disadvantage that the material may rise in temperature beyond the wet bulb and approach the inlet air temperature which may cause product degradation.

Many researchers have been unable to incorporate droplet behaviour into the mass transfer equation partly because the majority of the experimental techniques have rendered the evaporating droplet virtually motionless. Such a technique is not representative of droplet behaviour in an actual spray process. Consequently, models derived from such studies tend to be of limited use. Other researchers have used a technique in which the droplet is allowed to fall through

stagnant air. With this method, the drop has to fall large heights of the order of 12-15 metres in order to attain its terminal velocity. As the terminal velocities of liquid drops in air vary usually from 400-1000 cm/sec, the time available for observation is very small and data collection difficult.

The experimental programme followed in this study was as follows;

1) Droplet hydrodynamic visualisation study:- the objective of this work was to investigate the aerodynamic effects of air flow on droplet shape.

2) Heat and mass transfer study:- this was to ascertain the effects of droplet hydrodynamics or shape oscillation on heat and mass transfer rates.

3) Study of the effect of surfactants on droplet shape stability and mass transfer rates:- this was to confirm the effects of drop shape stability on heat and mass transfer rates.

The technique used in this study involved a vertical wind tunnel. Individual droplets were retained in the tunnel in a upward flowing gas stream which had an axial minimum velocity. Studies were carried out under carefully-controlled conditions of humidity and temperature. Droplet behaviour was studied using a high speed video recorder of shutter speed 1/10,000 sec; an arrangement of mirrors enabled droplet surface behaviour to be monitored in three dimensions. Experiments were carried out with a range of different liquids (water, n-propanol, iso-butanol, heptane, monoethanolamine). Initial drop diameters were 5 mm. Rigid spheres of naphthalene and water droplets doped with sodium dioctyl sulfo-succinate to reduce surface movement were also studied.

5.2 *The Vertical Wind Tunnel*

The vertical wind tunnel is shown in Figure 5.1. The lower section, A, (24 cm by 29 cm square) housed two rows of eight electric bar heaters, five in the top row and three at the bottom. Each heater had a heating power of 1kW. The

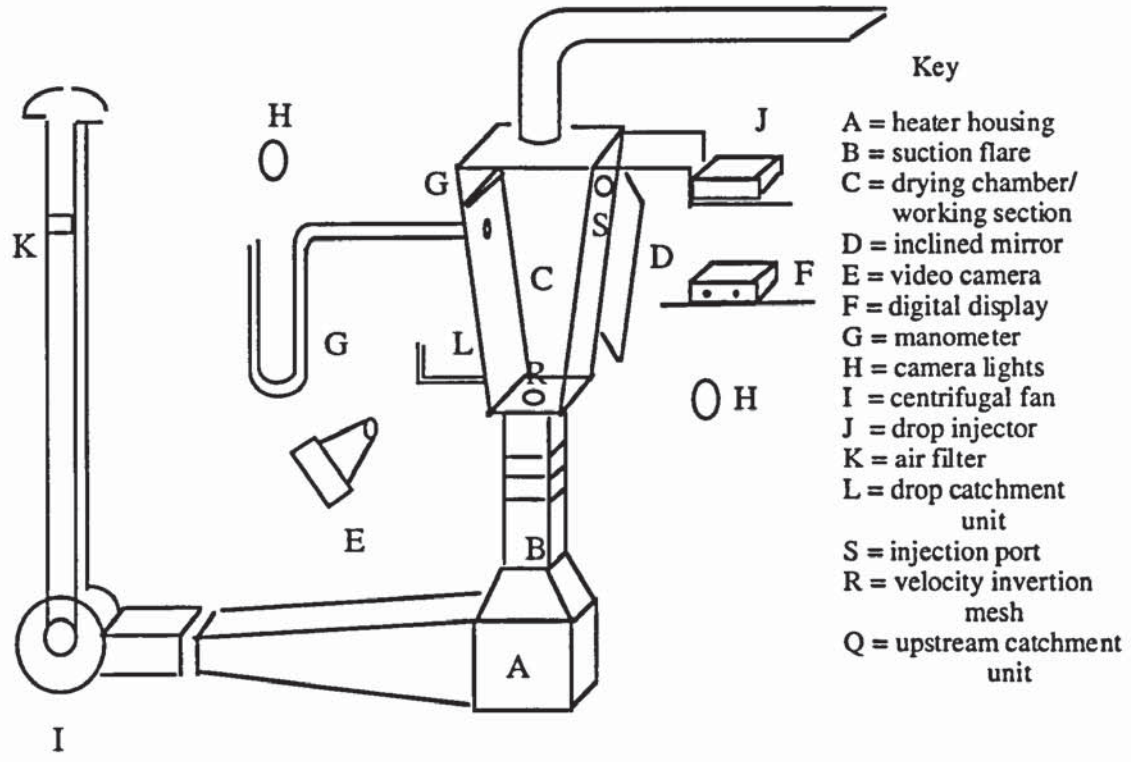

Figure 5.1 **The Vertical Wind Tunnel**

incoming air propelled by I, an 0.75 kW centrifugal fan, was heated and expanded through a venturi-shaped tunnel of length 51 cm, which diverged at an angle of 13° to section A. A fine stainless steel gauze of 30/30 mesh was placed diagonally across the flow and at the entrance to section A to reduce eddies and to assist the 90° change in direction of the air flow. Section B was 100 cm in height and comprised four stainless steel gauze meshes arranged in series to dampen turbulence. The smooth contraction of B (suction flare) accelerated the gas without introducing any further turbulence. The gas entered the drying chamber through an aluminium 20/20 screen mesh, R, which was specifically shaped to invert the air velocity into a U-shaped profile. Section C was of aluminium with transparent glass windows. In this section, the drop could be observed, filmed and withdrawn for analysis of the amount of mass transfer which had occurred during its residence time in the tunnel. The sides of the drying chamber had a divergence of 5.4° which provided a vertical velocity gradient such that the velocity decreased in the upward direction of flow, thus enabling the droplet to

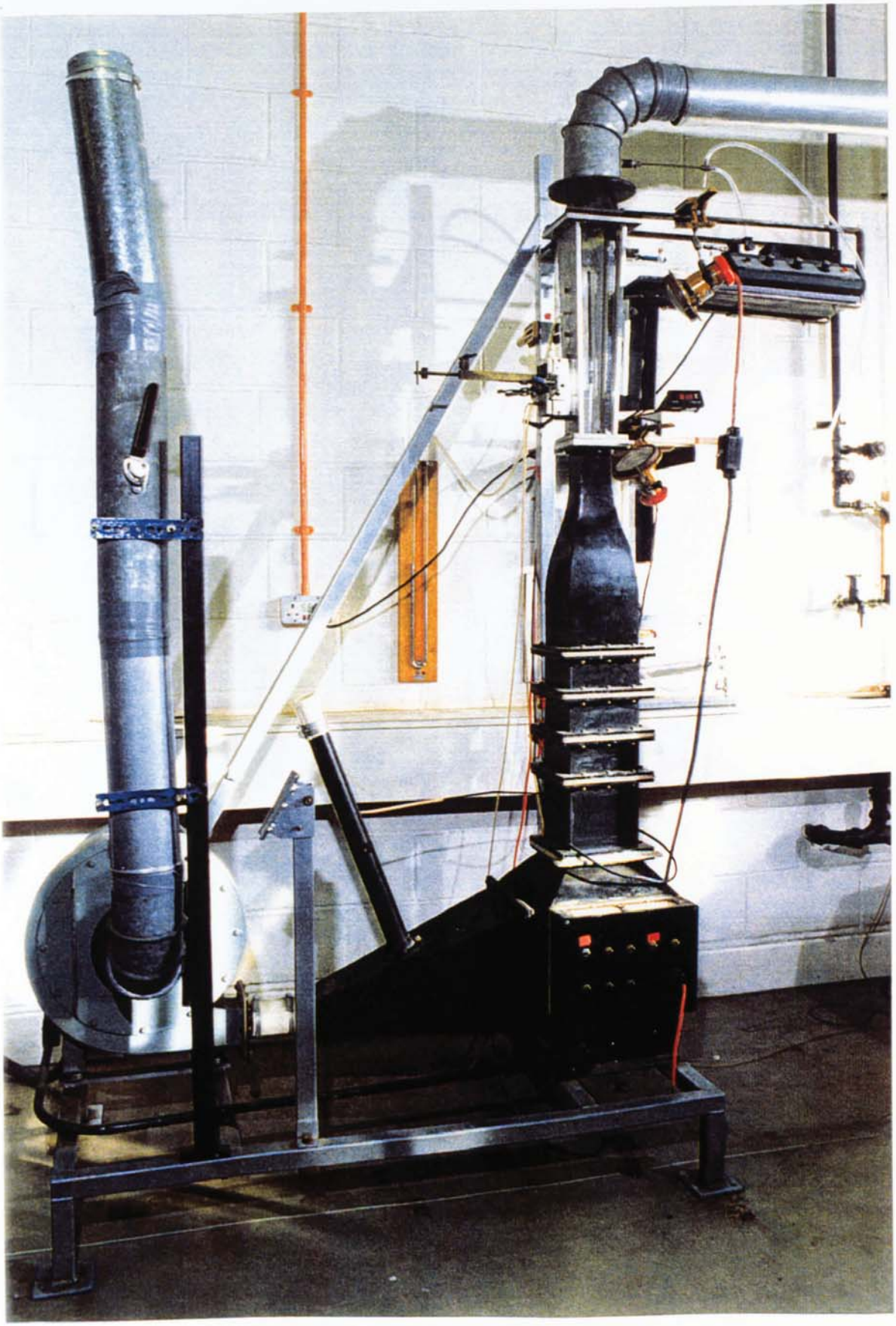

Plate 5.1. **The Vertical Wind Tunnel**

find its own level. A plane mirror, D, was mounted at an angle of 45^{o} to provide the third dimensional image of the drop. This arrangement provided a three dimensional image of the droplet which could be recorded using a video recorder, E. Droplets were injected through the injection port, S, a circular hole of 5.2 cm in diameter at the top right hand wall of section C. After injection, the syringe pump was withdrawn and the hole sealed by sliding shut a flat circular aluminium plate door of 6.5 cm diameter hinged to the top edge of C. An upstream collection unit, Q, was fitted to C to trap small liquid droplets. The entire apparatus was supported on a platform raised 16 cm above floor level.

The wet and dry bulb temperatures of the drying air were measured by five thermocouples located at the suction and discharge ends of the air line and the readings from which were displayed on an L.C.D. panel, F. The mounted manometer, G, measured the pressure differential between the drying chamber and atmosphere. Camera lights, H, were well-positioned around the equipment to provide illumination and to prevent shadows and tail images during recording. The collection unit at the bottom, L, was fitted with internal cooling coils to prevent continuous evaporation once the droplet was captured.

5.2.1 *Drop Collection Device*

The drop collection device consisted of a brass rod handle of 28 cm length joined to a rectangular cup 4.5 cm x 3 cm and 6.5 cm deep. Inside this cup was a cylindrical cavity of 3 cm diameter and 6 cm deep. Lined within the cavity was a cooling coil of bore diameter 1.5 mm made of stainless steel. The cooling coil left a cylindrical clearance of 2.5 cm within which a pre-weighed glass bottle was placed to collect floating droplets. The cooling water entered via the bottom of the coil and exited from the top, (Plate 5.2).

A trigger mounted on the brass handle was used to release the cup into the drying chamber after a predetermined time for drop collection. When not in use it remained in a retracted position on the side of the drying chamber. The presence

Plate 5.2 **The Drop Collection Device, (lined with a cooling coil).**

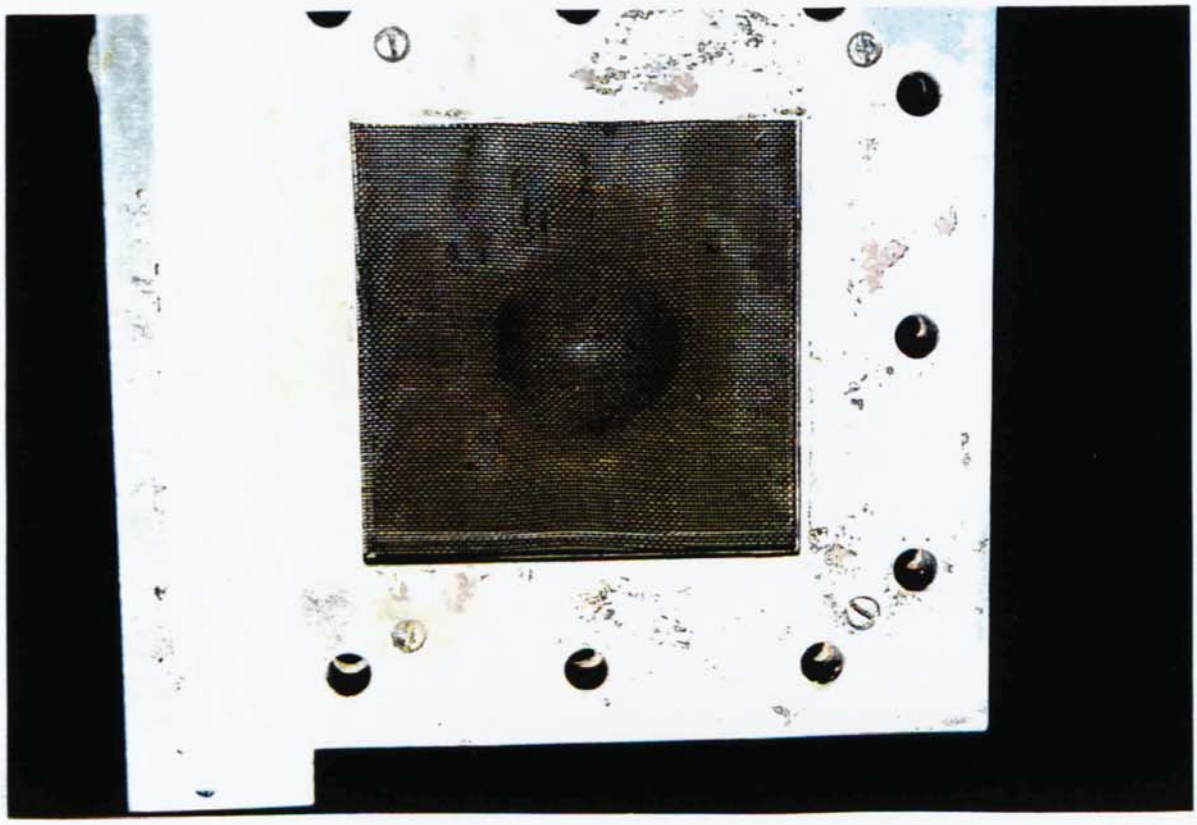

Plate 5.3 **The Convex Shaped Screen Mesh. (Aerial view).**

of the collection device in the drying chamber, on release, cut off the air flow supporting the droplet in free-flight. The droplet therefore fell into the glass bottle and was quickly withdrawn for weighing.

5.2.2 *The Inverted Velocity Profile.*

In theory, a droplet will float in an upward stream of air if its terminal velocity is equivalent to the velocity of the air current. In practice, the terminal velocity of an evaporating drop varies continuously as the shape and size of the droplet is reduced. Consequently, the droplet is immediately carried away by the air stream. However, a droplet can be made to float for a much longer time period. By inserting a hump shaped screen mesh (Plate 5.3 and 5.4), the velocity in the central part of the air stream was decreased leaving the annular region that surrounded it at a relatively higher velocity. This was achieved by trial and error to ensure that droplets in the wind tunnel stayed within view of the camera. The velocity of the gas rose sharply from the wall to a maximum just outside the boundary layer then fell to a minimum in the centre. As the droplet evaporated and its size diminished, it gradually moved upwards to regions of lower air velocity in the axis of the tunnel. The drop was thus retained for a much longer time.

5.2.3 *The Working Section*

The working section is shown in Plate 5.5. It was made of an aluminium frame; 7 cm square at the bottom, rising through a height of 46 cm and terminating in a 10 cm square at the top. In order to insert the velocity profile shaping gauze, the wind tunnel was in two sections and connected at the top and bottom ends by flanges.

The front end of the working section facing the camera and the right side wall were of glass, cemented to the aluminium frame(10 mm thick). A narrow glass window measuring 4 cm wide and 29 cm in length was inserted at the back and used for illumination purposes. Drilled in the left side wall (made of

Plate 5.4 **The 20/20 Screen Mesh in Working Section.**

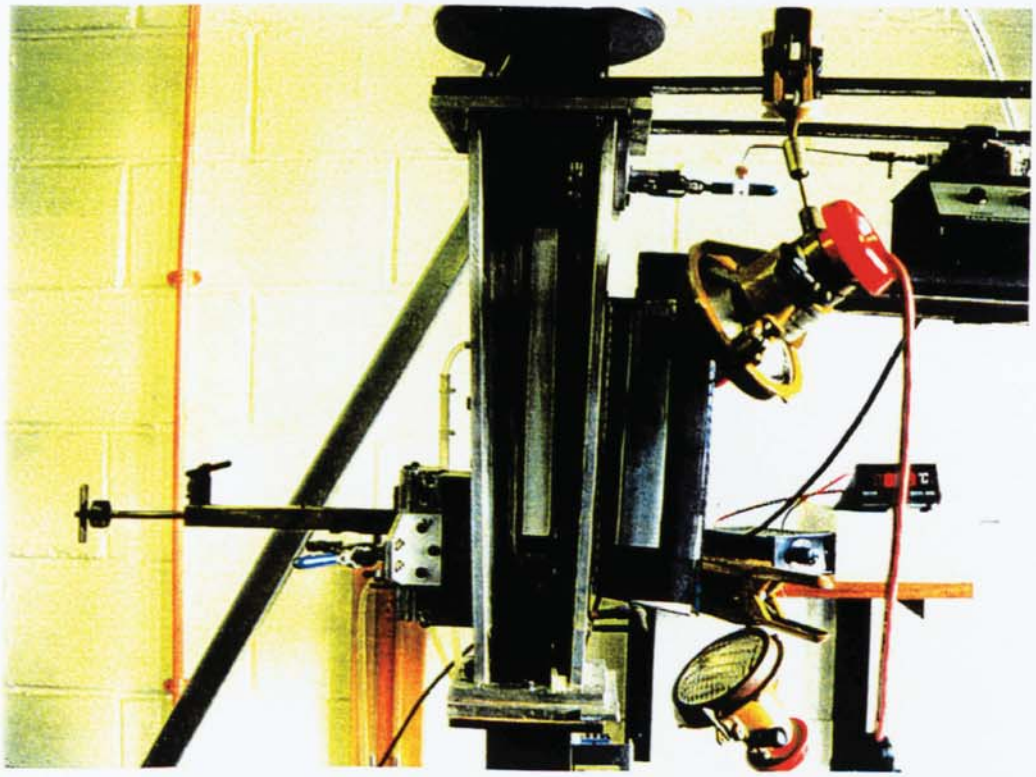

Plate 5.5 **Drying Chamber (Working Section), mounted with the Drop Injection Device (top right).**

aluminium) and spaced approximately 5.2 cm apart in a vertical plane were 6 mm holes. These allowed insertion of a pitot tube and thermocouples for dynamic pressure and temperature measurements. When not in use, these holes were sealed with removable bolts. A polished mirror was bolted at 45° adjacent to the right window to reflect the side view of the floating droplet.

The velocity profile in the working section was determined by traversing a pitot tube across the test section at various positions. The air velocity was given by;

$$V = 1.291\sqrt{\frac{1000.T_a P_v}{B.289}} \qquad (5.1)$$

where B is the barometric pressure and P_v, the dynamic pressure of air.

A mathematical correlation, Equation 5.2, was formulated which related the vertical position of the droplet to the air velocity;

$$V = -0.244h_d + 12.48 \qquad (5.2)$$

h_d = vertical position of droplet above base of drying chamber, (cm).

The air flow rate was regulated by a butterfly valve fitted to the inlet air duct. Figures 5.2 and 5.3 show the velocity distribution in the wind tunnel.

5.2.4 *The Drop-Forming System.*

The drop forming system comprised a 10 ml glass syringe connected to a stainless steel nozzle of 2 mm bore. The stainless steel nozzle was equipped with a three way valve which was used to rid the syringe of air bubbles. The glass syringe filled with the liquid under study was mounted on an electrically-controlled syringe pump (Sage instrument, model 351). After selection of the syringe size and flow rate, the syringe plunger was automatically controlled to give a fixed flow rate. The nozzle when used in the wind tunnel for repeated runs

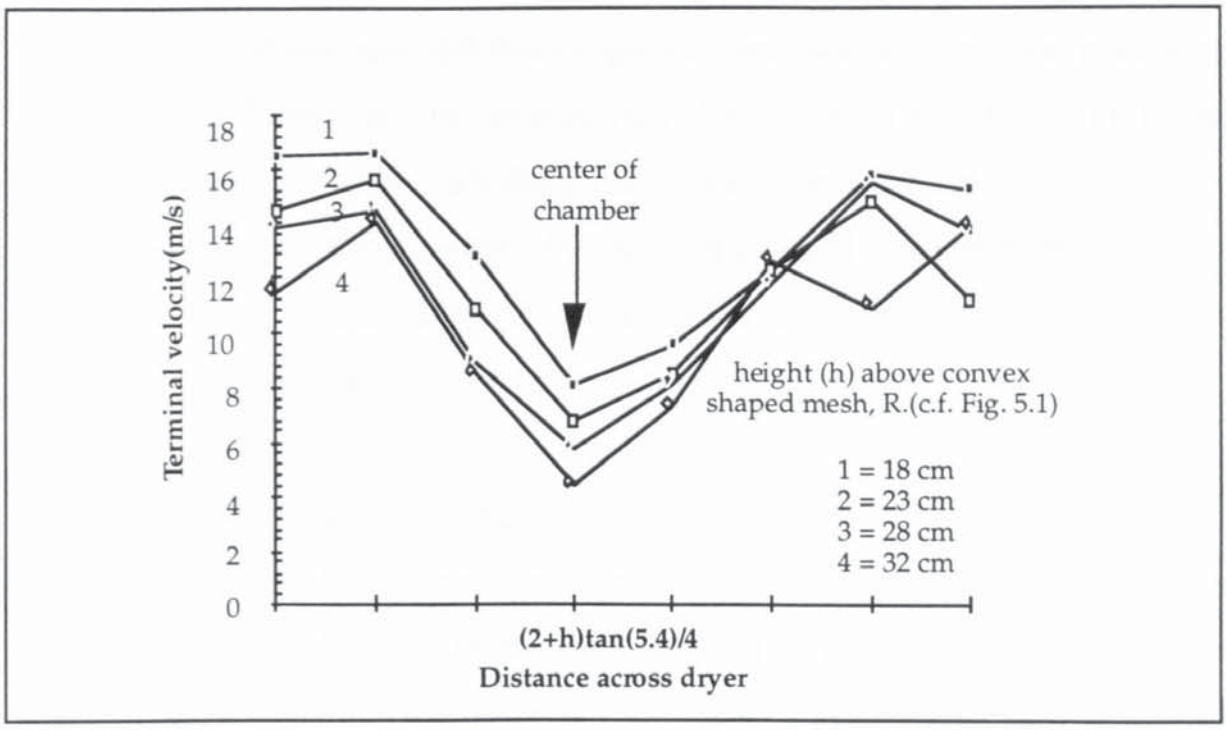

Figure 5.2. **Air velocity profile in the drying chamber,(working section).**

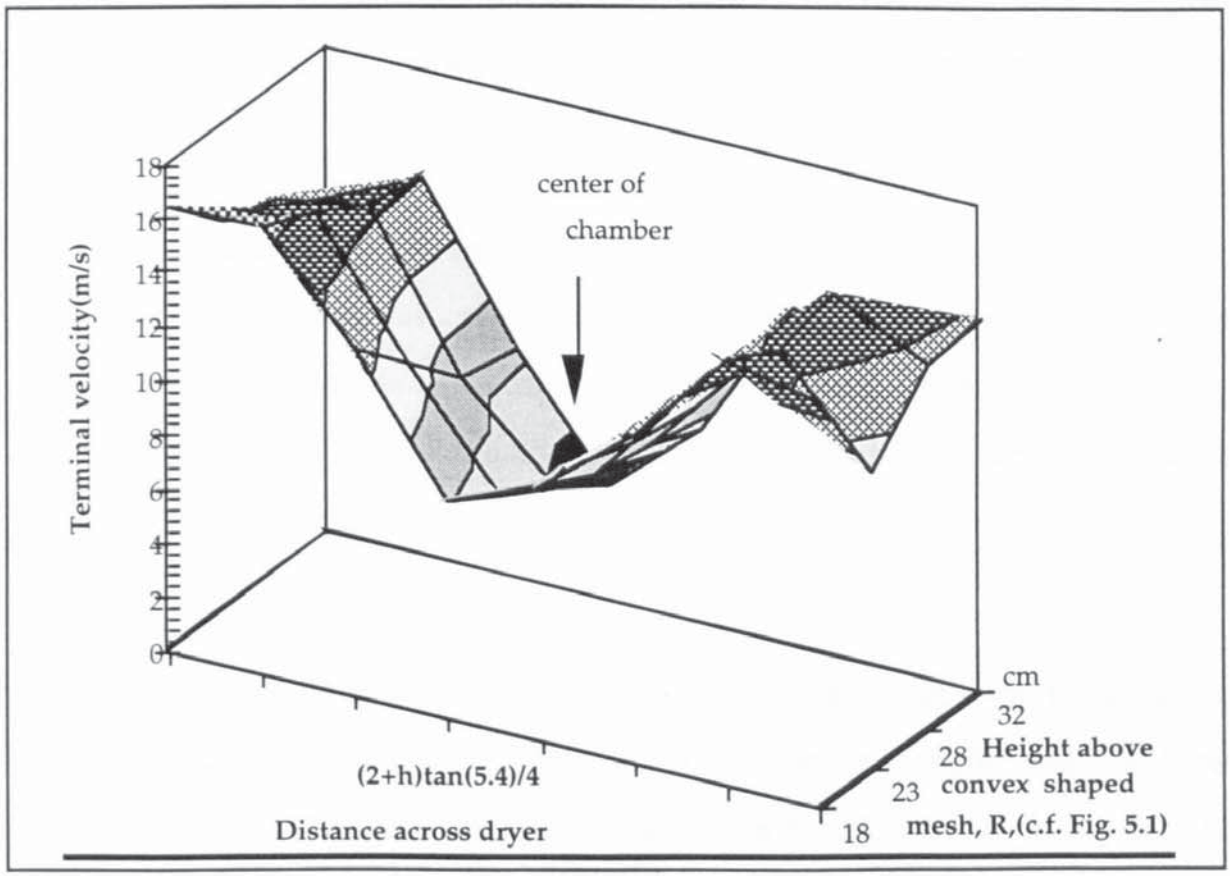

Figure 5.3 **Air velocity distribution in the working section of the Wind Tunnel.**

was inserted into the same position each time. This reduced error in drop size repeatability and also ensured that drops were released into the axial minimum velocity area. There was also an insulated plastic shroud around the tip of the nozzle to protect the drops from the gas stream during formation.

The entire unit was mounted upon a support rail attached to the top right section of the drying chamber. This arrangement facilitated quick withdrawal of the syringe pump after drop injection.

5.2.5 *Video Recording of Floating Droplets.*

Floating droplets were filmed using a Mitsubishi video camera HS C35B. It had a 100 mm focal length and a shutter speed of 1/10000 sec. This gave an effective magnification of up to 10 when viewed on a 14" television set.

The camera was mounted on a stand specially built to ensure that, when positioned, it remained at a fixed distance away from the working section but was movable in the vertical direction to keep track of the evaporating droplet in the wind tunnel.

5.3. *Measurement of Liquid Physical Properties.*

Relevant physical properties of each liquid were determined experimentally. Densities were determined by means of a hydrometer at room temperature, ($\approx 20^{o}C$). Liquid viscosity was measured using a plate viscometer at $30^{o}C$. A torsion balance was used for surface tension measurements.

5.3.1 *The Torsion Balance*

The interfacial tension of liquids used was measured at room temperature ($\approx 20^{o}C$) with a Torsion balance (Plate 5.6). It consisted of a scale calibrated from 0-0.12 N/m with 240 equal divisions. It had three knurled screws in the base to level the balance. Two devices were available for measuring surface and interfacial tension; a platinum ring and a glass test plate.

About 20-30 ml of the liquid to be examined was put into the concave glass provided and the glass placed on the platform below the platinum ring marked F. The platform was lowered to the maximum extent by means of adjusting screw D. The position and level of the platform were adjusted by means of clamp screw E so that the surface of the liquid was about 1 cm below the platinum ring. The beam clamp was slowly released by means of screw (D) until the platinum ring was in contact with the liquid. The height of the liquid was then lowered gradually by adjusting screw D with one hand whilst moving the index pointer, B, in an anticlockwise direction with the other so as to maintain the balance pointer C at zero. After a degree of movement dependant upon the surface tension of the liquid, the platinum ring would suddenly part from the surface of the liquid. The value indicated by the index pointer B at the moment when the platinum ring parted from the liquid was recorded as the surface tension of the liquid. Measurements were repeated three fold and the average taken.

5.3.2 *The Viscometer.*

A Haake viscometer, RV12, was used to measure the viscosity of liquids studied (Plate 5.7). The viscometer comprised (i) the driving unit, (ii) temperature vessel, (iii) the sensor system and (iv) the recorder.

(i) The measuring drive unit comprised the motor, tachogenerator, reduction gear, calibrated spring, transducer and pre-amplifier, all of which were connected to the recorder(basic unit) by means of a multi-core cable. The angle of twist measured by the calibrated spring when the liquid was sheared was picked up by the sensor system which was then displayed on a chart recorder or on an L.C.D.

(ii) The temperature vessel had three main functions:

(a) it connected the sensor system to the measuring drive unit,

(b) it centred the rotor and cup, and

(c) it controlled the temperature of test substance.

Plate 5.6. **The Torsion Balance**

Aston University

Illustration removed for copyright restrictions

Aston University

Illustration removed for copyright restrictions

Aston University

Illustration removed for copyright restrictions

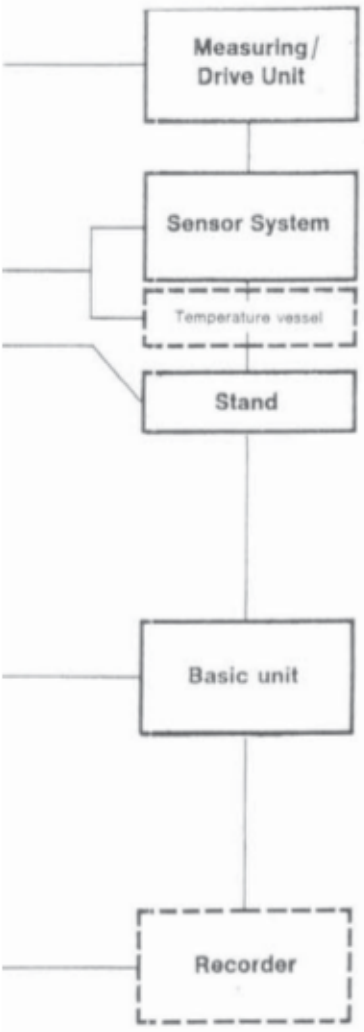

Plate 5.7 The Plate Viscometer.

(iii) The sensor system consisted of a coaxial cylindrical temperature vessel with three different rotors to provide different viscosity measuring ranges. The rotor was mechanically centred. The top and the bottom surfaces of the rotor were recessed to minimise "end effects". Sample volume required was about 40 cm^3 .

5.3.3 *Air temperature & Humidity*

The air temperature was measured at various points along the apparatus; at the entrance to the suction end, just before it entered the drying chamber, and within the drying chamber. These were measured using type K Ni-Cr/Ni-Al thermocouples. A digital twelve-way manual selector was used to select the required thermocouple and display readings on a Digitron L.C.D. panel(Digitron Instrument, model 3900). By varying the position of the thermocouples, the temperature distribution within the drying chamber was ascertained.

Air humidity was calculated from readings of the wet bulb and dry bulb temperatures of the air stream. The wet bulb temperature was measured by shrouding a type K Ni-Cr/Ni-Al thermocouple in a cotton wool wick with the tip dipped in a water reservoir. The assembly was placed in-line across the air stream, (Plate 5.8). An air/water psychometric chart was used to calculate the air humidity.

5.3.4 *Drop Dimensions*

A perfectly spherical plastic ball of uniform dimensions was introduced into the drying chamber of the wind tunnel at the beginning of each experiment and recorded using the fast shutter speed, video camera recorder. The camera was placed at a fixed distance away from the wind tunnel. The magnification of the ball was measured on a 24" Panasonic colour monitor using a perpex rule and a transparent 2 mm grid. The measurements served as the calibration for the subsequent set of runs.

Plate 5.8 **The Wet bulb Thermometer Assembly.**

5.3.5 *Drop Surface Temperature*

For pure liquids drops, the surface temperature attained when heat is transferred by contact with a large quantity of a gas at a given temperature and humidity is constant. It arises from the condition under which the energy associated with mass transfer from the saturated surface of the liquid by evaporation is exactly balanced by the heat supply from the gas.

The rate of transfer of heat from the gas to the liquid can be written as;

$$Q = A(h_c+h_r)(T-T_s) \tag{5.3}$$

where Q is the rate of heat flow, h_c represents the heat transfer coefficient from the air to the wetted surface by convection, h_r is the heat transfer coefficient corresponding to radiation from the surroundings (assumed to be at the same temperature as the drying gas) to the wetted surface, A is the area for heat transfer, and T and T_s are the temperatures of the gas and liquid phases respectively.

The liquid evaporating into the gas is transferred by diffusion from the interface to the gas phase as a result of a concentration difference (C_o - C), where C_o is the concentration of the vapour at the surface (mass per unit volume) and C is the concentration in the gas stream. The rate of evaporation is therefore given by;

$$W = k_G A(C_o - C) = (k_G A)\left(\frac{M_w}{RT}\right)(p_2 - p_1) \tag{5.4}$$

For small values of p_2 and p_1 the rate of evaporation can be written in the form;

$$W = k_G A(H_s - H)\frac{pM_a}{RT} = k_G A\rho_a(H_s - H) \tag{5.5}$$

Snce the heat supply maintains this rate of mass transfer, Equation 5.3 and 5.5 can be equated on introducing λ, to give:

$$(H_s - H) = (h/k_G\rho_a\lambda)(T - T_s) \tag{5.6}$$

where $$(h/k_G\rho_a) = c_s\left(\frac{\mu/\rho_a D_v}{C_p\mu/k}\right)^{2/3}, \tag{5.7}$$

and $h = (h_c + h_r)$.

Fortuitously for air-water vapour $h/k_G\rho_a = c_s$ when the air speed is ≥ 5 m/s Hence for the air-water system;

$$(H - H_s) = -\left(\frac{c_s}{\lambda}\right)(T - T_s) \tag{5.8}$$

where c_s is the humid heat. At a humidity of 0.047, c_s for air-water ≈ 1, i.e. the surface temperature of pure water droplets evaporating freely in a sufficient flow of air may be assumed to be the wet-bulb temperature. However, for any humidity above and below 0.047, there is a divergence between the two temperatures and for accurate work, droplet surface temperatures for liquids used were calculated using a computer program based on Equation 5.7 and 5.8. (Appendix C).

5.4 *Radiation Effects*

Radiation is occasionally the dominant mode of heat transfer in certain types of dryer but usually in convective dryers it represents a relatively minor enhancement of the heat transfer by convection, or with suspension by conduction. Radiation is therefore considered here as a correction to the mechanism for pure convection.

Radiation from the hot gas to the liquid drop is unhampered by any resistance in the viscous film and does not depend on the velocity, density or other characteristics of the gas stream or droplet behaviour. The quantity of heat transferred is dependant only on the temperature of the hot gas and the area of the hot surface exposed to unit area of cold surface. In Equation 5.3, radiant heat transfer was treated in terms of a fictitious radiant heat-transfer coefficient, h_r, defined as;

$$h_r = \sigma_\Sigma \frac{\{(T-273)^4 - (Ts-273)^4\}}{T - T_s} \qquad (5.9)$$

5.5 *The Moulding of Naphthalene Spheres.*

In the present work, spheres were cast from naphthalene. After the dimensions and weight of a single sphere had been measured, it was freely-suspended in the wind tunnel with air flowing at constant temperature. Upon removing the sphere and re-weighing at specific time intervals, the loss in weight was determined.

5.5.1 *Sphere Preparation.*

Molten naphthalene at 90°C was injected into a clay (plasticine) mould with a hypodermic syringe to form spheres. The cavity was made by pressing a 10 mm stainless steel ball bearing between two halves of 10 cm x 5 cm x 15 cm clay blocks forming two hemispherical depressions. To ensure sphericity and alignment of the two halves, the steel ball bearing was kept in place and the entire assembly kept in a refrigerator for about two hours (Plate 5.9, 5.10). Upon solidification, the two halves were clamped and a sprue hole and a thermocouple cavity drilled radially between the two clamped halves, the ball bearing serving to align the assembly. The ball bearing was later removed and the two halves put together again. Spheres of naphthalene were then cast by charging the mould with molten naphthalene at 90°C. To prevent voids forming within the spheres

during cooling, the mould was cooled slowly from the bottom upwards so that the molten naphthalene could flow downward into the cavity. This was achieved by placing the bottom half of the mould on a cold metal plate with a hot metal plate on the top.

In order to facilitate clean removal of spheres from the mould, the mould was returned to the refrigerator for about two hours to solidify. The cast spheres were inspected and excess sprue material removed with a file and the sphere polished. By this procedure contamination associated with the use of a mould release agent was avoided. Six micrometer measurements of diameter, to the nearest 0.001 mm, were taken at intervals around the equator. An average deviation of 0.002 mm was considered acceptable.

5.6 *Experimental Procedure*

Experimental studies consisted of two parts. In the first part, a set of experiments was carried out in which an individual droplet was evaporated in free-flight and its surface behaviour, i.e. shape oscillation, recorded using a fast shutter speed of 1/10000 sec until it either became so small that it was no longer visible or it was carried away by the air stream. In the second part, individual drops were collected from the wind tunnel after specific time intervals and weighed.

Part I

The following procedure was adopted for part I:

(1) Check water in wet bulb reservoir. Start fan and turn on heating switches. Allow fan to run until the desired temperature of experiment is attained and all the thermocouple readings within the working section of the wind tunnel are identical. Record hot air temperature, the wet bulb temperature and the ambient temperature. Record pitot tube reading for conversion to air flow rate.

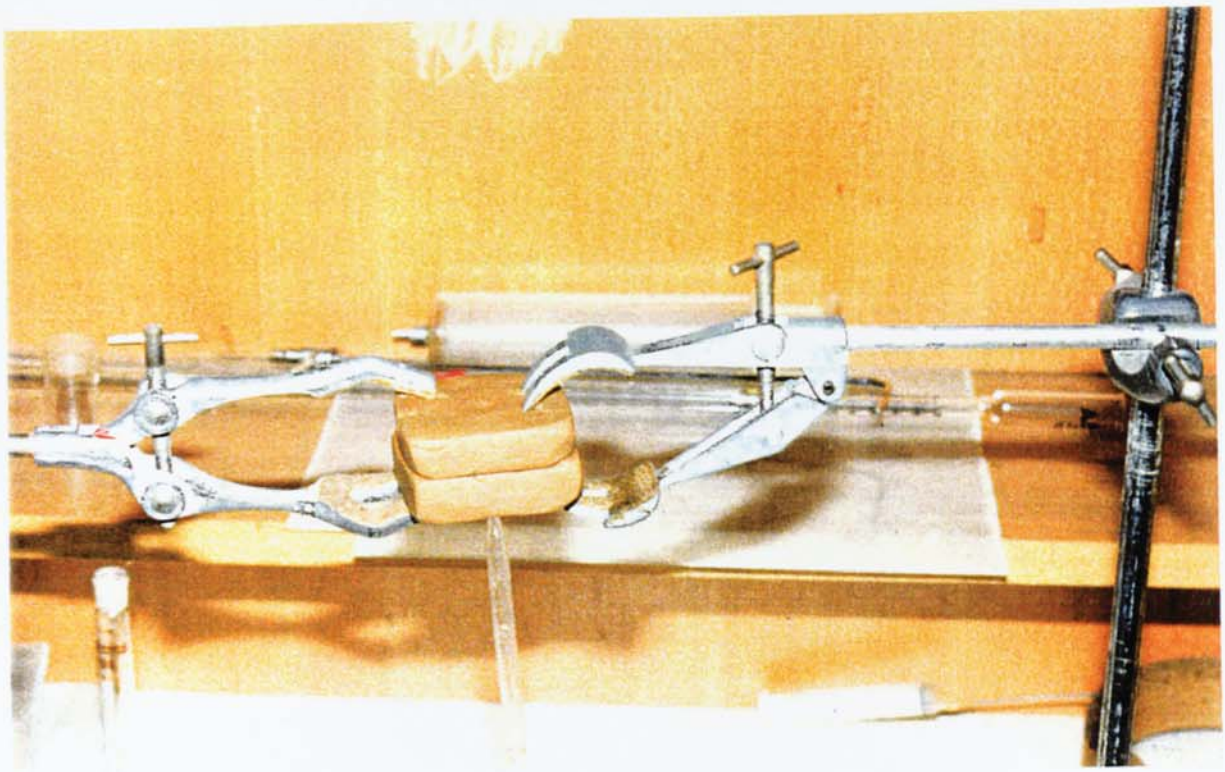

Plate 5.9. **Naphthalene Moulding Assembly.**

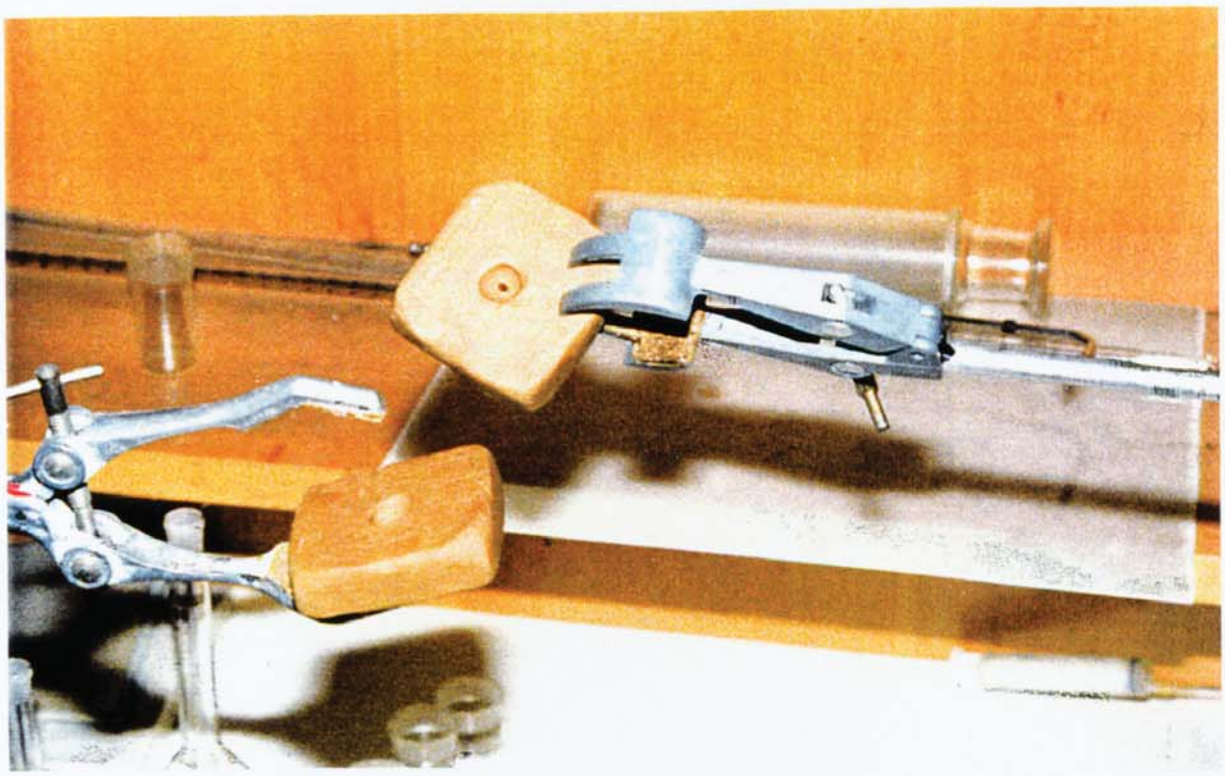

Plate 5.10. **Naphthalene Moulding Assembly showing spruce hole.**

(2) Load the video camera with an "Super VHS" tape, mount it on the video stand and position it focused on the wind tunnel. Turn on camera lights and adjust light intensity. Float the heat resistant spherical plastic ball in the wind tunnel, using the injection port. Adjust focal length of camera, set shutter speed to 1/10000sec, readjust focus. When satisfactory, clamp camera stand in a fixed position by releasing brakes. Press the record button on the video camera to record the floating spherical plastic ball for calibration purposes. Reset video after about 3 min. of recording.

(3) *Test run:* (i) Load syringe with liquid to be studied. Mount syringe on syringe pump. Set syringe size and flow rate to desired position. Open drop injection port.

(ii) Slide syringe pump to insert nozzle into the centre of the wind tunnel. Turn the inject switch to the infuse mark to inject a drop into the wind tunnel. Withdraw syringe pump quickly. Shut injection port door.

(iii) Adjust air flow with butterfly valve such that the drop is in full view of the video camera. Adjust illumination to enhance video recording. When satisfied, flush droplet.

(4) Ensure video is reset. Check the hot air and the wet bulb temperatures again and record pitot reading. Activate video record button to start recording, start in-built video clock. Repeat step 3(i). Adjust the position of the camera to track the drop as it evaporates and as its vertical position changes until it becomes too small to observe.

Part II

(5) Repeat experimental conditions as for part one. Turn on the tap to supply cold water to the cooling coils of the drop collection device. Insert a pre-weighed weighing bottle in the collection unit and retain it in the retracted position. Inject droplet following the same procedure as in 3(i) and (ii). Start stop watch (set to desired time interval) simultaneously with drop release. Collect drop for weighing at set time interval by releasing the drop collection unit. Repeat experiments to reduce experimental and systematic errors.

Accuracy and Reproducibility of Results.

All experimental results reported in Chapter Six were based on an average of at least 5 runs. The expereiments were replicated for three main reasons;

(a) to establish from the data an estimate of error of the measurement, i.e. drop diameter and weight.

(b) to make possible some protection against out-of-line measurements, and

(c) to gain the benefits of the increased precision of averages over that of individual measurements.

Maximum variation of droplet weight produced by the Syringe pump.was ±2.4%. Measurement of droplet dimensions from the TV screen at a magnification of X5 and to an accuracy of ± 0.5 mm produced a maximum propagation variation in volume of ± 1.50 mm^3.

CHAPTER SIX

6 EXPERIMENTAL RESULTS

6.1 Introduction

6.2 Drop Diameter and Terminal Velocity

6.3 Evaporation of Liquid Drops

- 6.3.1 Evaporation of Distilled De-ionised Water Drops
- 6.3.2 Evaporation of Iso-butanol Liquid Drops
- 6.3.3 Evaporation of Heptane Liquid Drops
- 6.3.4 Evaporation of n-Propanol Liquid Drops
- 6.3.5 Evaporation of n-Monoethanolamine Liquid Drops
- 6.3.6 Evaporation of Distilled de-ionised Water doped with Sodium di-octyl Sulfo- Succinate
- 6.3.7 Vaporisation of Naphthalene Spheres

6.4 Preliminary Study of Droplet Drying

6.5 Summary of Experimental Observations.

CHAPTER SIX

'The combined results of a group of experiments should yield a maximum amount of information for the effort expended'

Harry H. Holscher.

EXPERIMENTAL RESULTS

6.1 *Introduction*

Experiments were chosen to cover a representative range of solvents. Firstly, materials were selected which were known to be widely used as solvents. Water and propanol were selected so that results could be compared with studies by investigators who have experimented with single drops either on suspension devices or in free-flight. The liquids chosen were; distilled de-ionised water, propanol, iso-butanol, n-heptane and monoethanolamine.

In this chapter the technique of interpretation of tapes for the terminal velocity, droplet diameter and evaporation will be discussed and the data presented. All experimental data were analysed and the data plotted where necessary but only representative graphs are shown in this chapter.

6.2 *Drop Diameter and Terminal Velocity.*

Individual liquid drops freely suspended at their terminal velocities in the vertical wind tunnel were filmed with the shutter speed of the video recorder set at 1/10000th of a second, recording at 100 frames per second. The films were viewed on a 14" television screen, using a Panasonic video deck, (Model; NUG45 HQ). Frame by frame advancement of the video tape allowed all the hundred frames recorded per second to be viewed and analysed. Each section was run backwards and forwards to ensure it was properly analysed. Using the calibrated

scale on the wind tunnel the relative position of each droplet was identified and related to its terminal velocity.

The effective magnification was arrived at by first measuring the apparent dimensions of a spherical plastic ball on the television screen and then comparing these with its actual diameter. Measurements were made by placing a transparent acetate of 2 mm grid mesh onto the surface of the television screen, thus counteracting the curvature of the screen surface so that the intersection of the scales coincided with the mid-point of the droplet. Using a pair of dividers, perpex rule and a pair of callipers, droplet diameter was measured to an accuracy of ± 0.5 mm. Whilst measuring droplet dimensions, notes were made about the general droplet behaviour and oscillation, and the movement of the droplet along the axis of the wind tunnel. In some cases, a slight zig-zag motion of the drop was unavoidable due to the velocity profile and wake shedding. If this motion was excessive, data for that experiment were discarded. After these measurements, the tape was re-run and droplet oscillation noted. This exercise was mainly carried out to attempt to find a correlation for droplet shape oscillation frequency.

The equivalent spherical diameter for a drop at time, t, was calculated from the magnification factor and the successive profiles, assuming that the volume of the drop was;

$$V = \frac{\pi}{6}\left(\frac{\Sigma d_x}{N_p}.\frac{\Sigma d_y}{N_p}.\frac{\Sigma d_z}{N_p}\right) \tag{6.1}$$

where d_x, d_y, d_z, are the diameters of the drop in the respective perpendicular axes, and N_p the number of profiles taken of the drop.

The force balance around a liquid drop falling in air was given in Equation 2.11 as;

$$V(\rho_l-\rho_a)g = C_D A(\rho_a v^2) + V\rho_l\left(\frac{\partial u}{\partial t}\right) \tag{6.2}$$

for a droplet at its terminal velocity, $\left(\frac{\partial u}{\partial t}\right) = 0$, therefore v_t the terminal velocity is given by:

$$v_t = \left[\frac{2V(\rho_l - \rho_a)g}{C_D A_f \rho_a}\right]^{0.5} \equiv \left(\frac{4}{3}\frac{d_e(\rho_l - \rho_a)g}{C_D \rho_a}\right)^{0.5} \tag{6.3}$$

where A_f is the cross section area of the equivalent sphere. In the Newtonian region, within which investigations were conducted, C_D is fairly constant, therefore,

$$v_t \alpha d_e^{0.5} \tag{6.4}$$

Representative plots of v_t vs $d_e^{0.5}$ are shown in Figures 6.1-6.4. The drag coefficient, C_D, was calculated thus;

$$C_D = \frac{1}{x_p^2}\left(\frac{4}{3}\frac{(\rho_l - \rho_a)g}{\rho_a}\right) \tag{6.5}$$

where x_p = the slope of v_t vs $d_e^{1/2}$.

Equation 6.3 may be rewritten as:

$$Ar = C_D Re^2 = \frac{4g\rho_a(\rho_d - \rho_a)d_e^3}{3\mu^2} \tag{6.6}$$

where Ar = Archimedes number.

Evidently, for a given fluid sphere, Ar is independent of the velocity v, which appears in the Reynolds number. Several attempts have been made to establish the functional relationship between Archimedes number (Ar) and Re; most of those reported up to 1978 have been reviewed by Clift et al.[43] whereas recent work has been critically evaluated by Khan and Richardson[159] . Based on

experimental data culled from the literature, Khan and Richardson[159] proposed the following relationship:

$$Re = (2.32.Ar^{0.018} - 1.523.Ar^{0.016})^{13.3} \tag{6.7}$$

Finlay[49] suggested that C_D could be related to Re and We thus:

$$C_D = \left(\frac{Re}{P^{0.13}}\right)^n . \left(\frac{\omega}{We.P^{0.13}}\right) \tag{6.8}$$

where n = 1.26 for water and 1.55 for other liquids and ω = a correlation constant. Plots of $(Re/P^{0.13})^n$ against $(1/We.P^{0.13})$ are shown in Figures 6.5- 6.8. C_D values for monoethanolamine, n-propanol, n-heptane, iso-butanol and water drops at their terminal velocity are shown in Table 6.1. Table 6.1 was used to correlate Equation 6.9.

For monoethanolamine, n-propanol, heptane and iso-butanol, C_D was correlated with a modified Finlay's equation;

$$C_D = 0.237.\left(\frac{Re}{P^{0.13}}\right)^{1.55}\left(\frac{1}{We.P^{0.13}}\right) \tag{6.9}$$

the deviation was ±5%.

Srikrishna[21] found that the terminal velocity of liquid drops increased with increasing diameter. However, his reported data were considerably lower than the data predicted by Finlay[49]. This, Srikrishna attributed to the higher temperature of air in his experiments. Srikrishna's[21] correlation of ω and n are shown in Table 6.2.

As discussed in section 2.4.3, mass transfer from evaporating droplets may reduce skin friction due to a thickening of the boundary layer. Obviously, whilst the drops were being recorded in the wind tunnel, they were also evaporating.

However, the experimental data could not be used to assess whether or not mass transfer had any effect on the drag coefficient and hence the terminal velocities.

Table 6.1 Values for drag coefficients, extracted from Figures 6.1-6.8 and correlating equations 6.5 and 6.9

$$C_D = \left(\frac{Re}{P^{0.13}}\right)^n \cdot \left(\frac{\omega}{We.P^{0.13}}\right)$$

Liquid drops	C_D	x_p	R^2	ω
monoethanolamie	0.96	118.32	0.975	0.217
n-propanol	0.98	100.00	0.987	0.189
n-heptane	1.17	83.77	0.950	0.267
iso-butanol	1.27	87.65	0.973	0.256
water	1.10	105.20	0.990	1.310

n=1.55 for all liquids except for water where n=1.26. R^2 = coefficient of correlation.

Table 6.2. Values of ω and n in Equation 6.8 obtained by Srikrishna[21].

Groups of liquids	ω	n	% deviation
n-heptane, acetone, toluene, xylene, tetrachloroethylene.	0.562	1.50	(-6.7% to 21%)
Iso-propyl alcohol, n-hexane, methyl ethyl ketone.	1.269	1.22	(-34% to 13%)

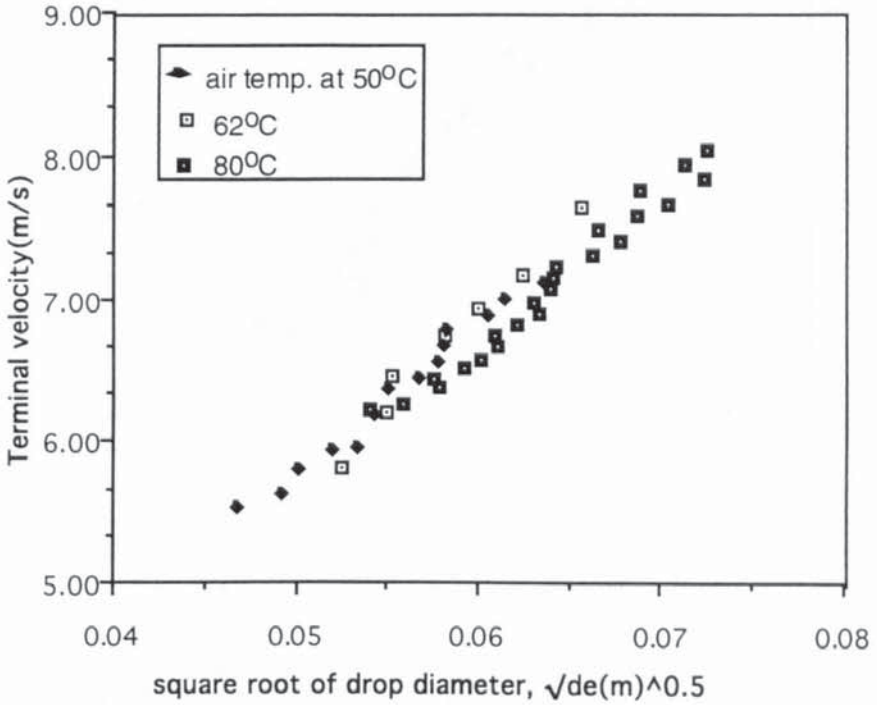

Figure 6.1. **Terminal velocity of distilled de-ionised water drops freely- suspended in an upward flow of air plotted against (drop diameter)$^{0.5}$.**

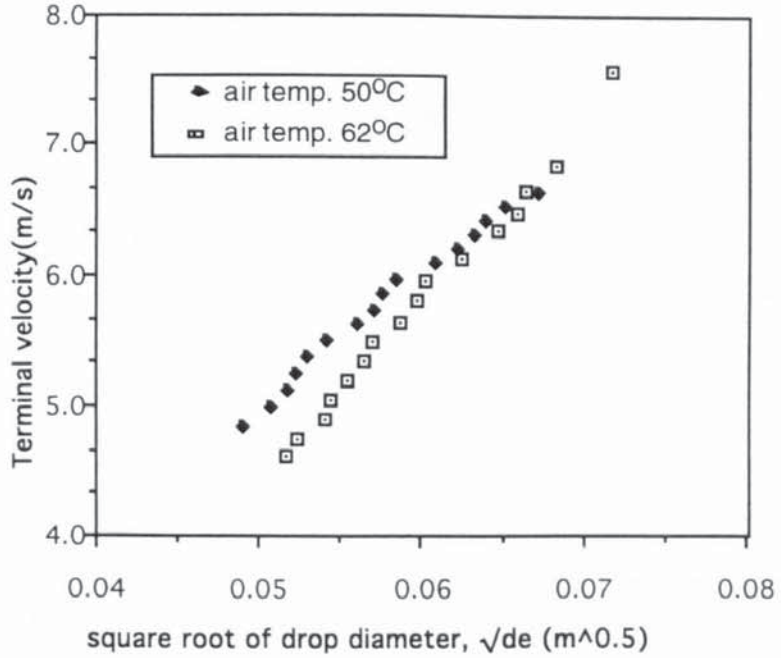

Figure 6.2 **Terminal velocity of propanol droplets freely- suspended in an upward flow of air plotted against(drop diameter)$^{0.5}$.**

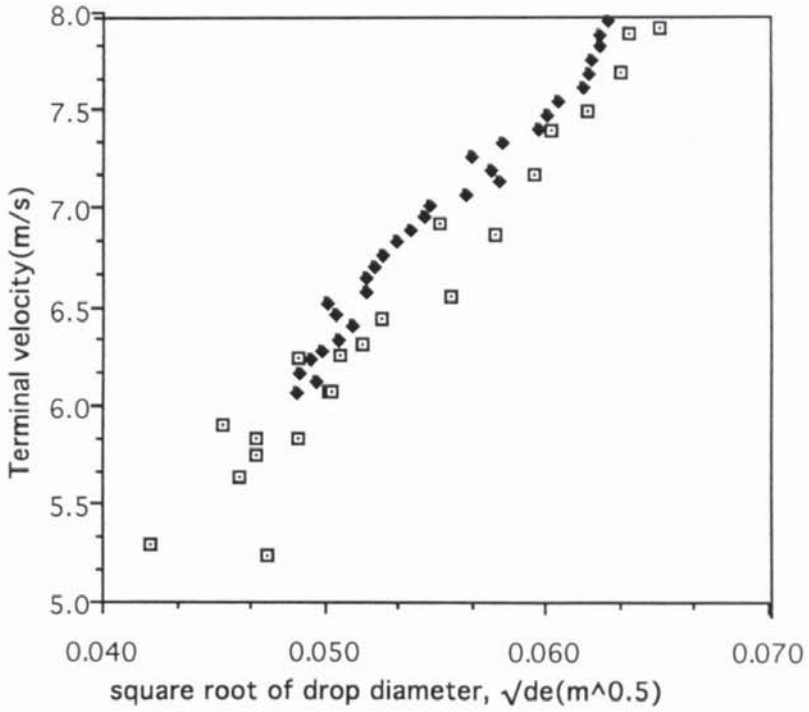

Figure 6.3. **Terminal velocity of monoethanolamine drops in free-flight plotted against (drop diameter)$^{0.5}$. Initial drop diameter ≈ 5 mm.**

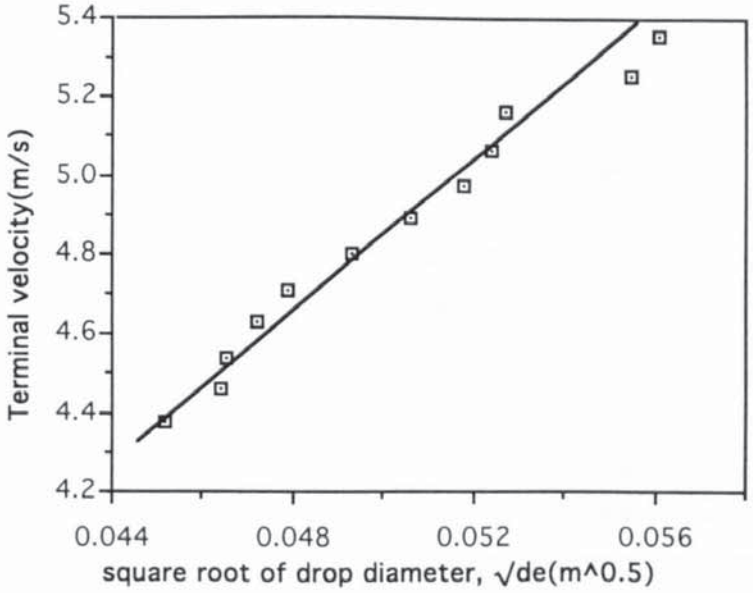

Figure 6.4. **Terminal velocity of iso-butanol drops freely-suspended in an upward flow of air as a function of drop diameter. Air temp. = 62°C**

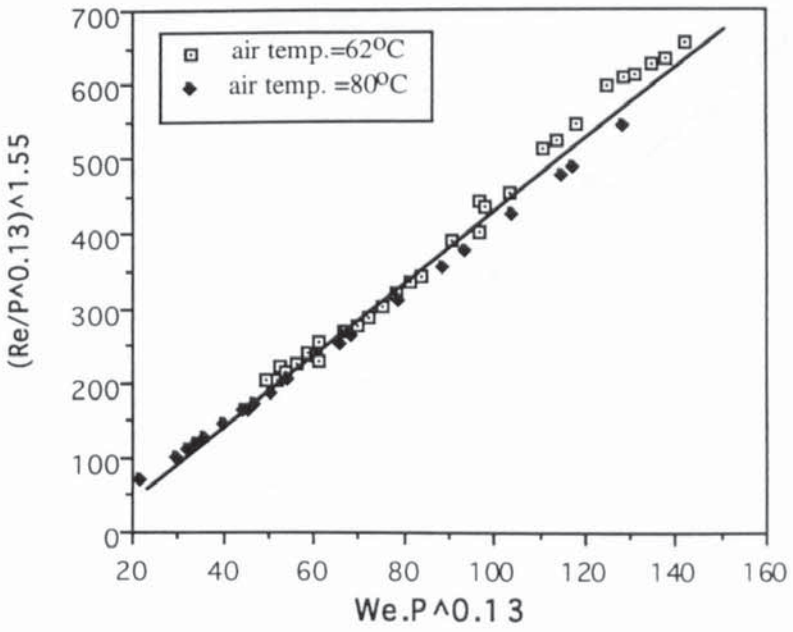

Figure 6.5. **Correlation for terminal velocity of monoethanolamine drops with model by Finlay. Initial drop diameter ≈ 4 mm**

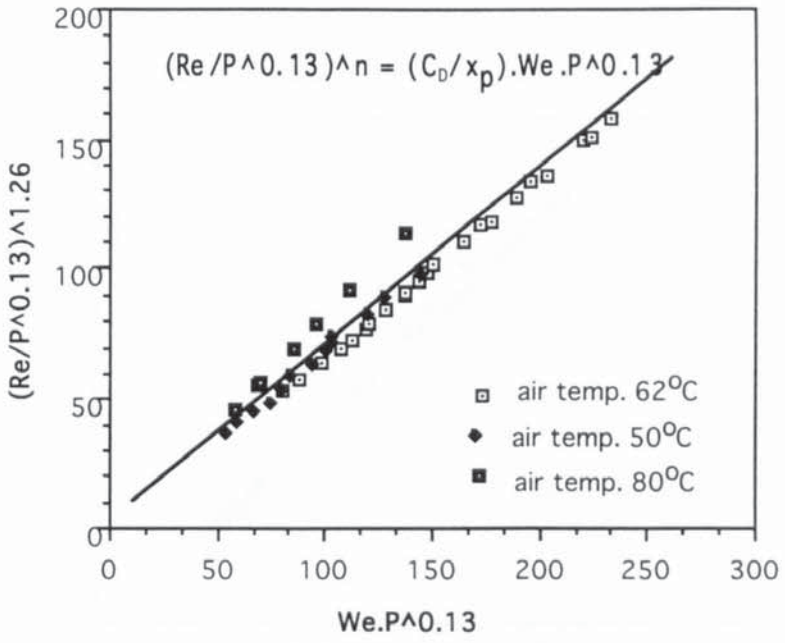

Figure 6.6. **Correlation for terminal velocity of water drops using model by Finlay. Initial drop diameter, 5 mm.**

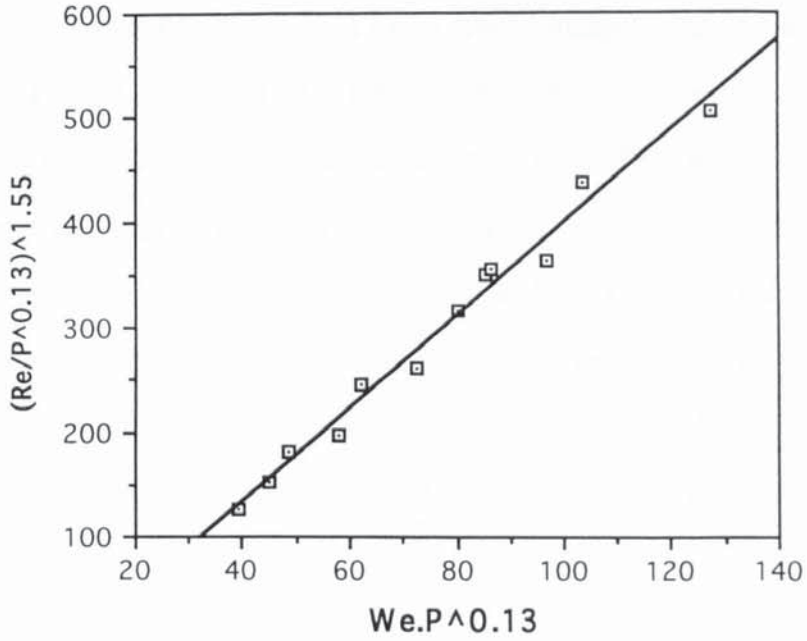

Figure 6.7. **Correlation for terminal velocity of iso-butanol drops using model by Finlay. Air temp., 62°C. Initial drop diameter ≈ 4 mm.**

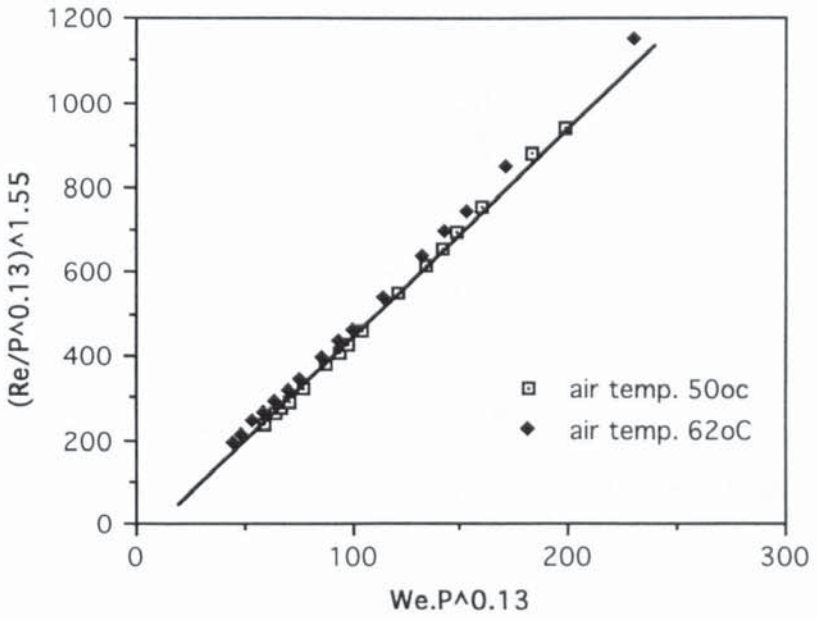

Figure 6.8. **Correlation for terminal velocity of n-propanol drops using model by Finlay. Initial drop diameter ≈ 4 mm.**

6.3 *Evaporation of Liquid Drops*

Individual droplets which had been freely suspended for a fixed time in the wind tunnel were collected in a weighing bottle and weighed to determine the evaporation rates. The procedure for droplet collection is outlined in section 5.5. The weight of each droplet collected after a specified time interval was matched with recordings of its terminal velocity. This allowed droplet evaporation to be compared with droplet size reduction. Results were plotted as mass of droplet versus time and the evaporation rates correlated in terms of the Sherwood and the Nusselt number using the characteristic diameter, d_e, defined by;

$$d_e = \sqrt[3]{\left(\frac{\Sigma d_x}{N}.\frac{\Sigma d_y}{N}.\frac{\Sigma d_z}{N}\right)} \tag{6.10}$$

The Sherwood number was correlated by:

$$Sh = \frac{\dot{m}}{\pi d_e^2 \Delta P}.\frac{d_e}{D_v} \tag{6.11}$$

where $\Delta P = (p_2 - p_1)$, $p_2 = \frac{M_w P_s}{RT_f}$ and $p_1 = \frac{M_w P_{vg}}{RT_f}$.

=» $$Sh = \frac{\dot{m}\, RT_f}{\pi d_e (p_2 - p_1)}.\frac{1}{M_w.\, D_v} \tag{6.12}$$

T_f = the interfacial temperature given by; $(T_s+T_a)/2$

The diffusion coefficient D_v was calculated using the correlation given by Fuller et al.[160] i.e.

$$D_v = \frac{1.0\times10^{-7} T^{1.75}(1/M_A + 1/M_B)^{0.5}}{P\left[(\Sigma v_A)^{1/3} + (\Sigma v_B)^{1/3}\right]^2} \tag{6.13}$$

where (Σv_A) and (Σv_B) = sum of structural volume increments of liquid and air respectively.

6.3.1 *Evaporation of Distilled De-ionised Water Drops.*

The evaporation of individual drops of distilled, de-ionised water was studied at 50°C, 62°C and 80°C in air. The drop injection and experimental procedure were as described in Chapter Five. Results from the evaporation of water drops are shown in Figures 6.9-6.12. The data for these plots are included in Appendix A. Figure 6.9 shows the variation of mass of drop with time during evaporation. The evaporation rates plotted as a function of droplet Reynolds number is shown in Figure 6.10.

Figure 6.11 demonstrates that the initial mass transfer rates were higher than those predicted by the Ranz-Marshall relationship. Figure 6.12 shows the change in mass transfer coefficient with change in drop diameter. Here, the mass transfer coefficient is demonstrated to increase with increase in drop diameter. Plate 6.1 and 6.2 show droplet shape oscillation in free-flight. The image on the right gives the third dimension of the droplet. Drop shape oscillation was random and non-symmetrical. However, it decreased with a decrease in drop size.

6.3.2 *Evaporation of iso-butyl alcohol Liquid Drops.*

Representative results from the evaporation of iso-butyl alcohol drops are shown in Figures 6.13 and 6.14. Figure 6.13 shows the mass transfer rates in terms of Sh compared with the predicted values based on the Ranz-Marshall relationship. Here again evaporation rates from experimental data were initially higher than those predicted by Ranz-Marshall. Due to the lower surface tension of iso-butyl alcohol, (23 mN/m compared with 72 mN/m for H_2O), the maximum stable droplet size that could be formed with the 2 mm nozzle was ≈ 4 mm in diameter. Droplet shape oscillation did not conform to regular oblate-prolate shape oscillations as suggested by many researchers. The frequency of

Plate 6.1 Drop of distilled de-ionised water in wind-tunnel.

Plate 6.2 A Drop of distilled de-ionised water in free-flight showing the three dimensional images

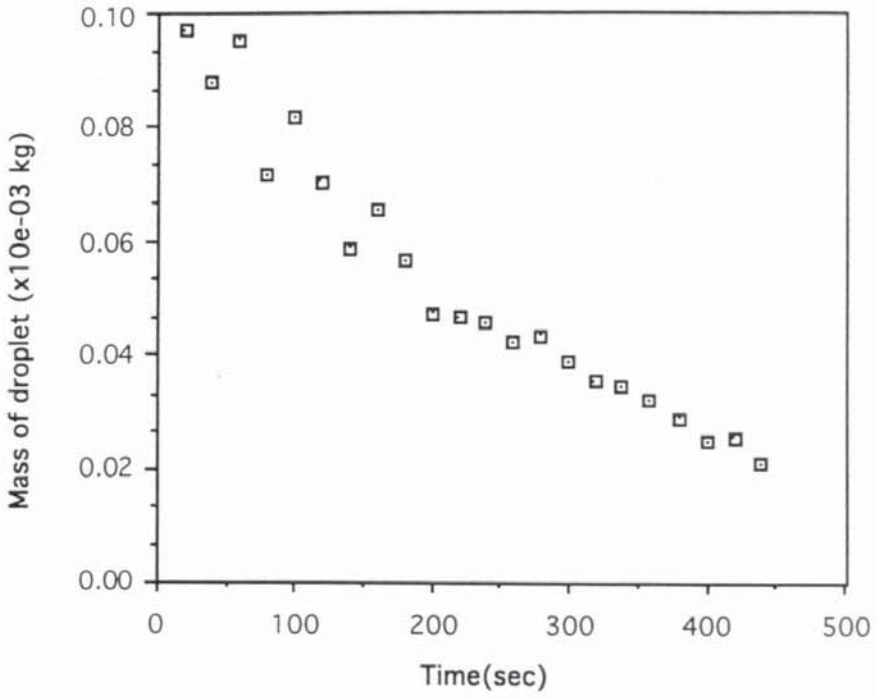

Figure 6.9. **Mass of evaporating distilled de-ionised water droplet freely-suspended in an air stream plotted against time. Initial drop diameter ≈ 5 mm. Air temperature; 62°C**

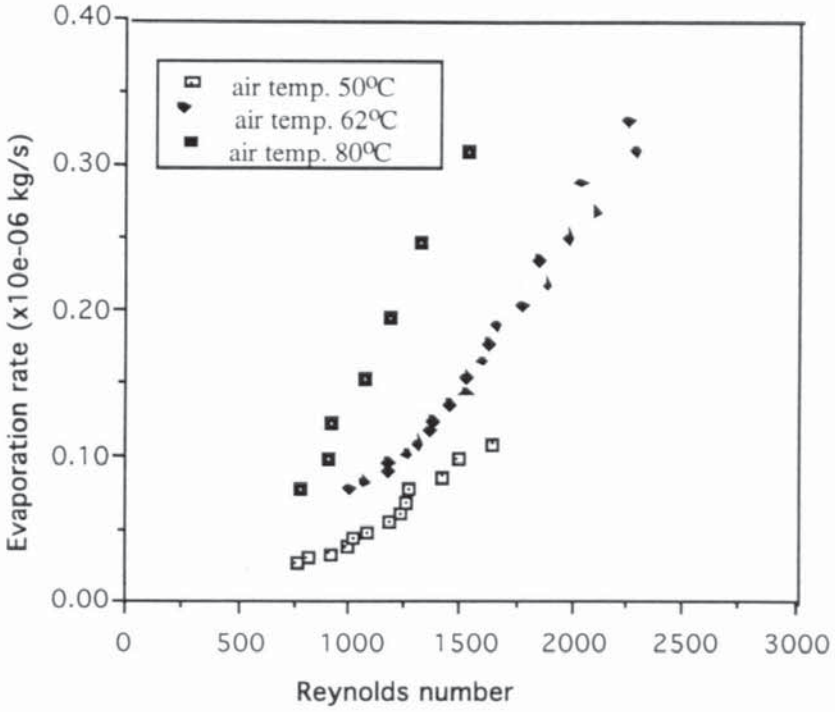

Figure 6.10 **Change in Evaporation rates of distilled de-ionised water droplets with Re. Initial drop diameter ≈ 4 -5 mm.**

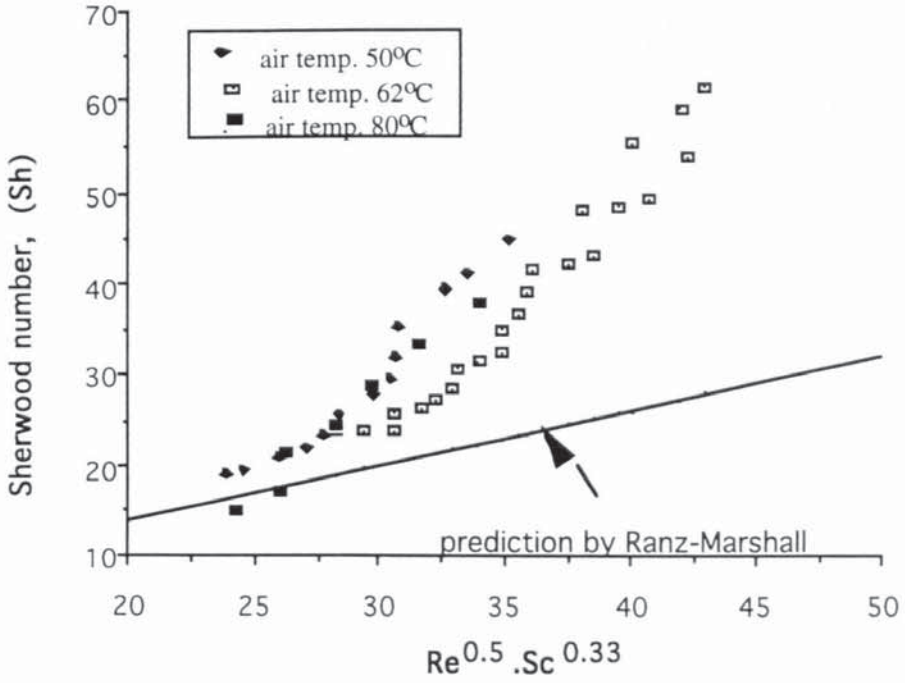

Figure 6.11 **Evaporation rates of distilled de-ionised water drops compared with predictions by Ranz-Marshall. Initial drop diameter ≈ 5 mm.**

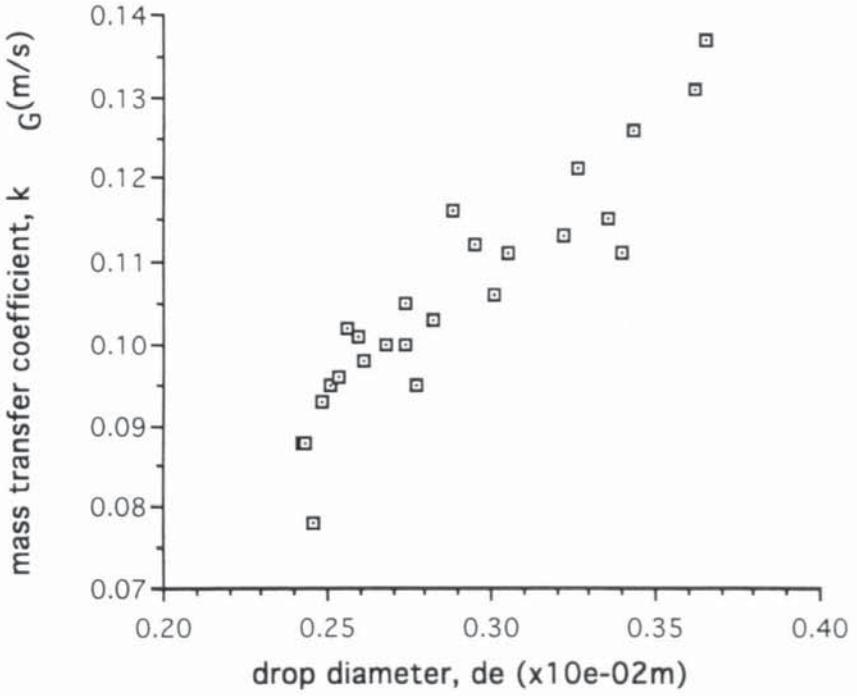

Figure 6.12. **Experimentally determined mass transfer coefficient (k_G) of water drops versus drop diameter. Initial drop diameter ≈ 5 mm. Air temperature 50°C.**

oscillation could not be correlated in terms of cycles per second, but it was observed to be higher than that of H_2O drops. This was attributed to the difference in surface tension/viscosity ratio. A plot of the mass transfer coefficient, k_G, versus droplet diameter is shown in Figure 6.14. The mass transfer rate coefficient is again shown to be linearly proportional to drop diameter. The data for these plots are included in Appendix A.

6.3.3 *Evaporation of Heptane Liquid Drops*

Typical results for the evaporation of heptane droplets at 62°C are shown in Figure 6.15. (4-2 mm) The lower density and surface tension of heptane enabled relatively smaller and lighter drops to be studied. Since droplets found their own position in the wind tunnel due to a balance of buoyancy and aerodynamic forces, heptane droplets floated in the upper section of the drying chamber where the air velocity was lowest. Residence time in the tunnel therefore tended to be very short, i.e. 60 sec, which limited the air temperature that could be used. Figures 6.16 shows the mass transfer coefficients of heptane versus droplet diameter .

6.3.4 *Evaporation of n-Propanol Drops.*

Individual droplets of n-propanol were evaporated at 62°C and 50°C in air. The average initial droplet diameter was approximated by 4.5 mm. The mass of the droplet plotted versus residence time is shown in Figure 6.17. Mass transfer rates in terms of Sh plotted against $Re^{0.5}.Sc^{0.33}$ are shown in Figure 6.18. The results for evaporation rate are similar in pattern to those for water and heptane. The mass transfer coefficient of propanol droplets again decreased as drop diameter was reduced, (see Figure 6.19 & 6.20).

6.3.5 *Evaporation of Monoethanolamine Drops*

Oscillations of monoethanolamine liquid droplets were not as pronounced as those of water and propanol droplets. Drop shape oscillation frequency was lower and less erratic. This was attributed to the higher viscosity of

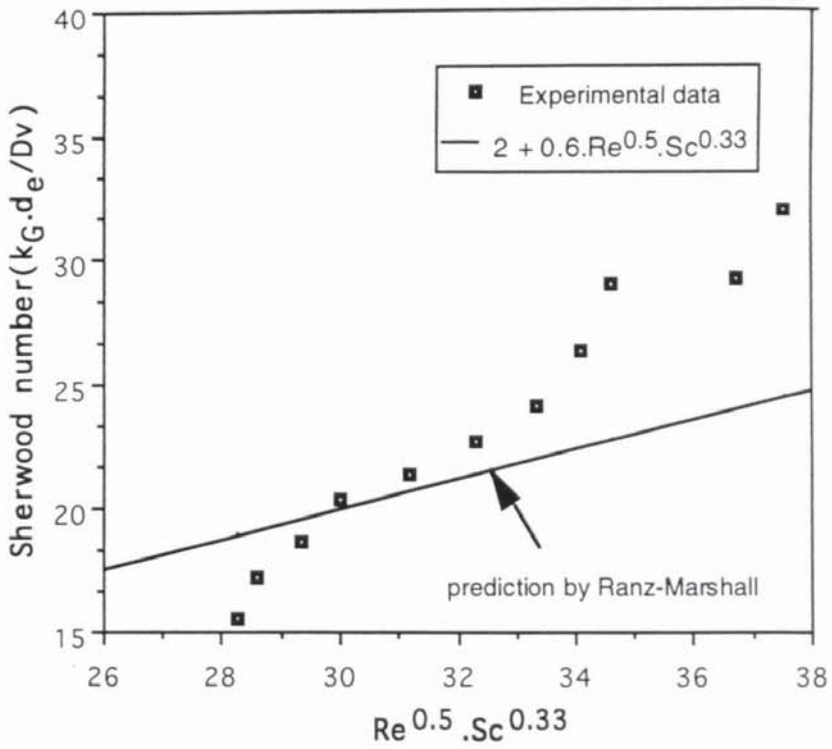

Figure 6.13 **Correlation for Sh of iso-butanol droplets evaporated in free-flight with Ranz-Marshall equation. Initial drop diameter ≈ 4.0 mm Air temperature 62°C.**

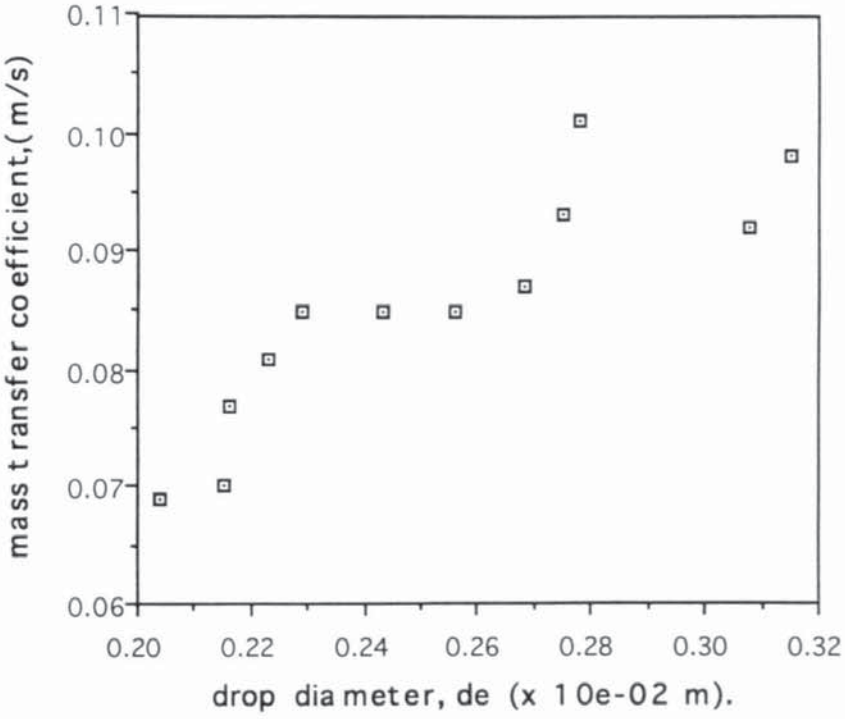

Figure 6.14. **A plot of mass transfer coefficient of oscillating iso-butanol drops versus equivalent drop diameter. Air temperature 62°C. Initial drop diameter, 4 mm.**

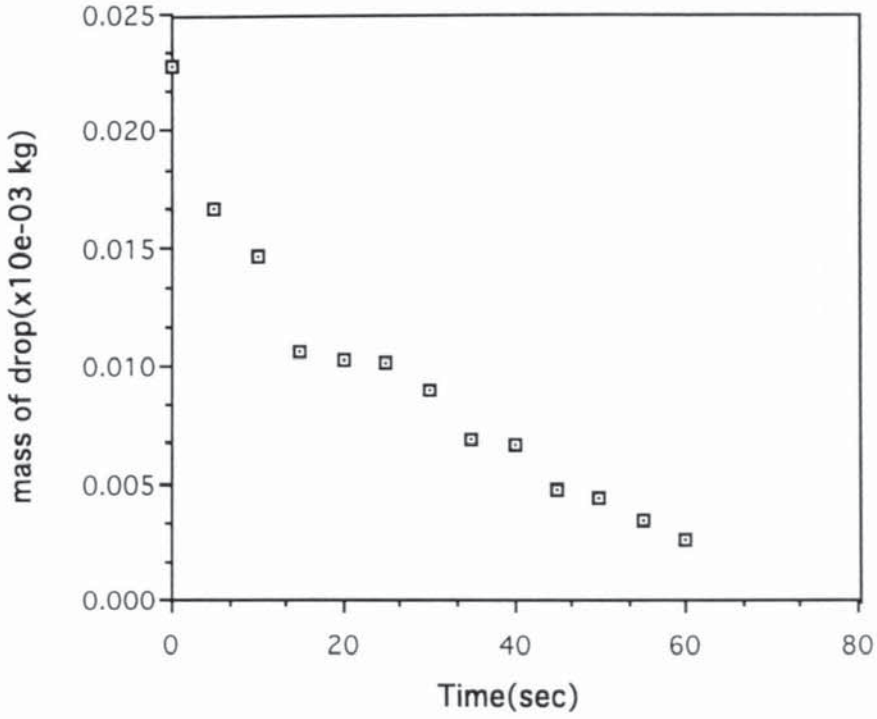

Figure 6.15. **Mass of n-heptane droplets versus time. Initial drop diameter, 4.0 mm. Air temperature 62°C.**

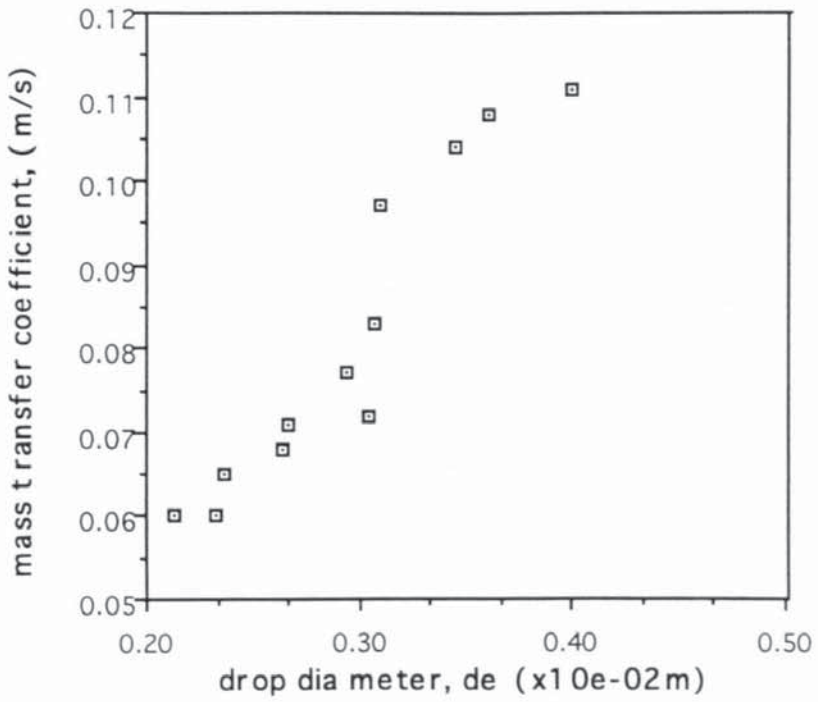

Figure 6.16. **Mass transfer coefficient, k_G, of oscillating liquid drops of n-heptane versus equivalent drop diameter. $k_G = f(d_e)$.**

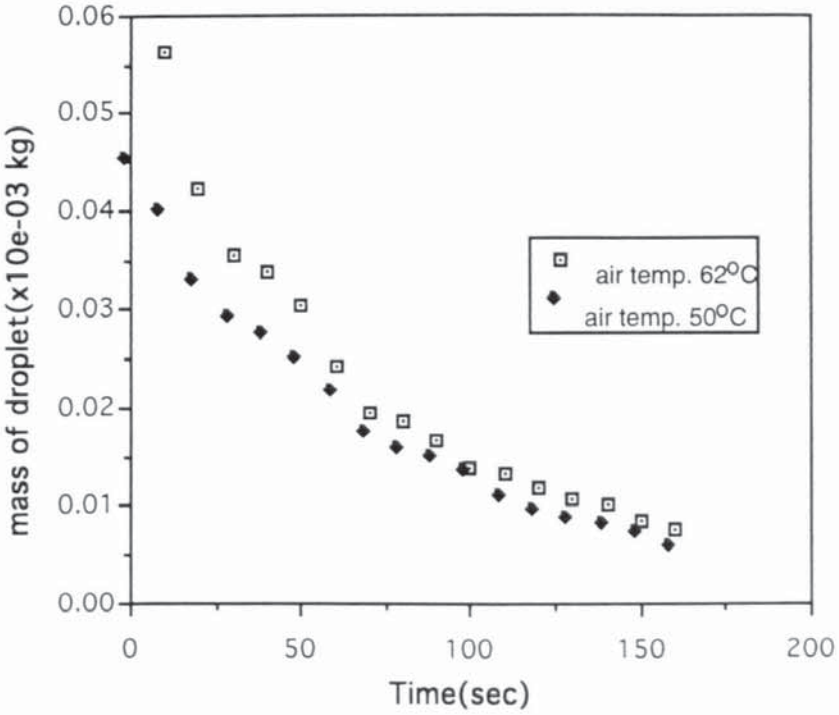

Figure 6.17. **Evaporation of oscillating propanol droplets versus time. Initial drop diameter ≈ 4.8 mm. Reynolds number ≈ 1660**

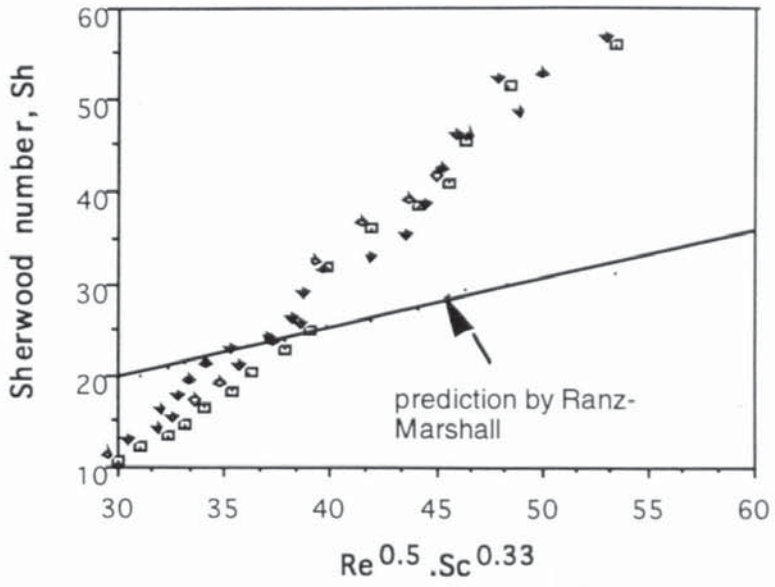

Figure 6.18 **A comparison of mass transfer rates of propanol drops evaporated in free-flight with prediction by Ranz-Marshall.**

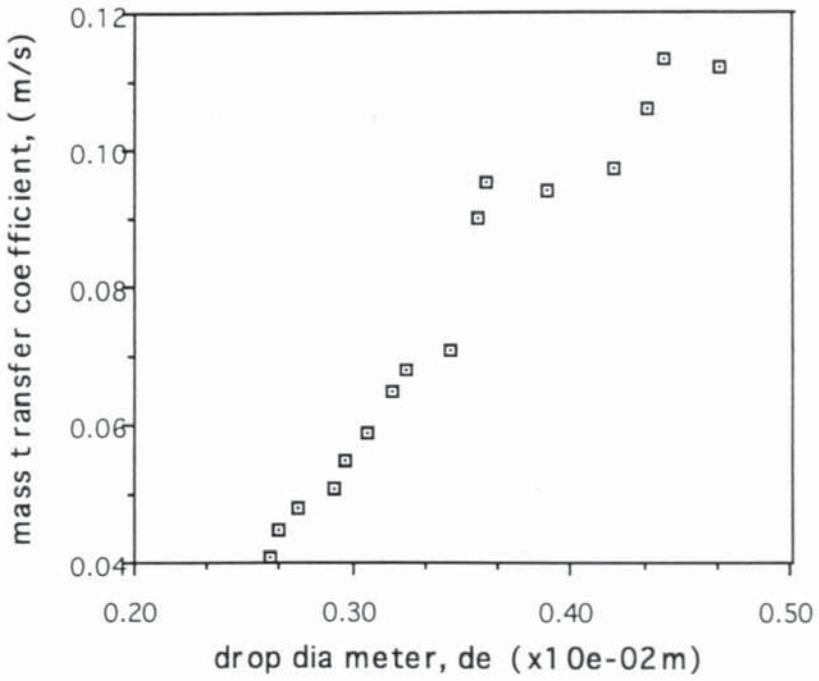

Figure 6.19 **Mass transfer coefficient of propanol drops evaporated in free-flight versus drop diameter. Air temperature = 62°C.**

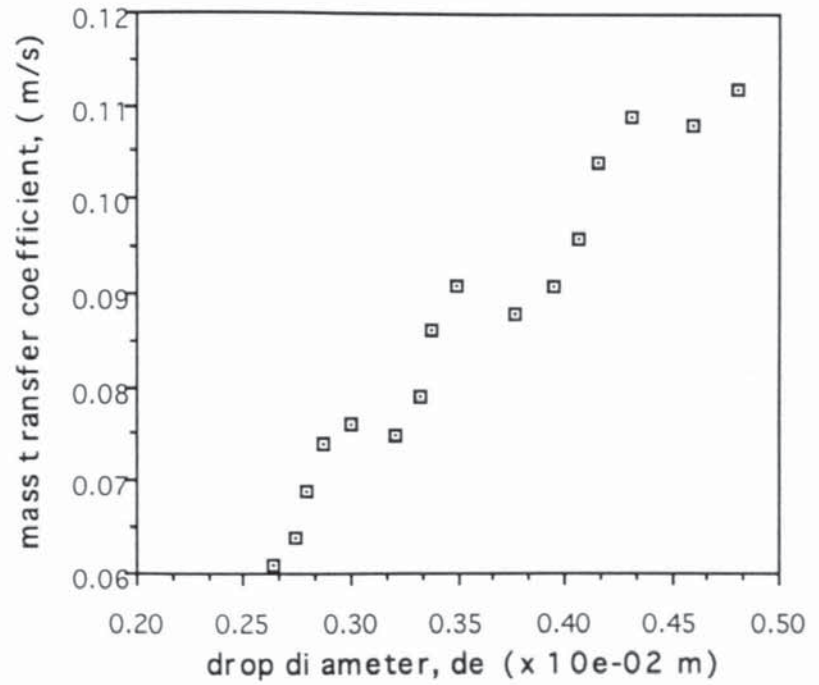

Figure 6.20 **Mass transfer coefficient of oscillating propanol drops evaporated at 50°C versus drop diameter. Initial drop diameter ≈ 4.8 mm.**

monoethanolamine ($1.7x10^{-3}$ Pas). Initial Sh values after drop release were higher than those predicted by the Ranz-Marshall relationship, Figure 6.22. However, they later fell below the predicted values. Mass transfer coefficients with a reduction in drop diameter followed a similar pattern to those of propanol, iso-butyl alcohol, water and heptane.

6.3.6 *Evaporation of Distilled De-ionised Water Doped with Sodium Di-octyl Sulfo -Succinate.*

Evaporation rates of "clean" drops of distilled de-ionised water and water drops doped with a surface active agent are shown in Figure 6.23. The oscillatory behaviour of droplets of water in which 0.001/wt/wt of sodium di-octyl sulfo-succinate was dissolved decreased considerably. This reduction is also reflected in the difference in mass transfer rates between drops of 'clean' and treated water as shown in Figure 6.23. The data plotted in Figure 6.23 clearly confirm the effects of surface dynamics on mass transfer rates. They also demonstrate that droplet sphericity is a function of surface tension as discussed in Chapter Two. With the addition of 0.001wt/wt surfactant, the initial mass transfer rate of distilled de-ionised water was reduced by 40%.

6.3.7 *Vaporisation of Naphthalene Spheres.*

10 mm spherical naphthalene balls were vaporised in free-flight at 74°C in the vertical wind tunnel.

To determine the surface temperature of the vaporising naphthalene, controlled experiments were run at the start of each experiment in which individual naphthalene spheres moulded around three type K thermocouples, inserted at different positions beneath the surface and connected to the temperature output device were vaporised in the wind tunnel. The temperature of the sphere was continuously recorded up to a point at which it suddenly rose to the air temperature (i.e. the thermocouples became exposed to the air stream as a result of naphthalene sublimation). The temperature of the naphthalene just

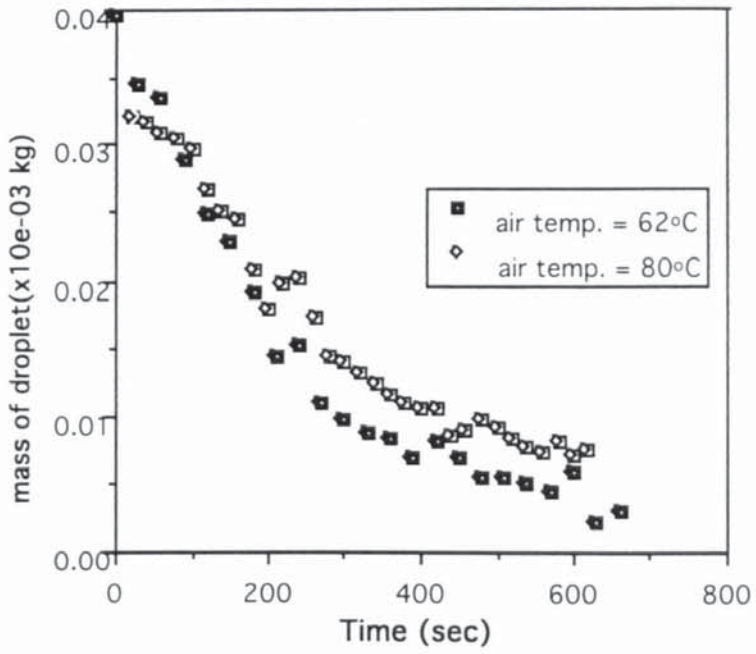

Figure 6.21 **Mass of evaporating monoethanolamine drops versus time.**

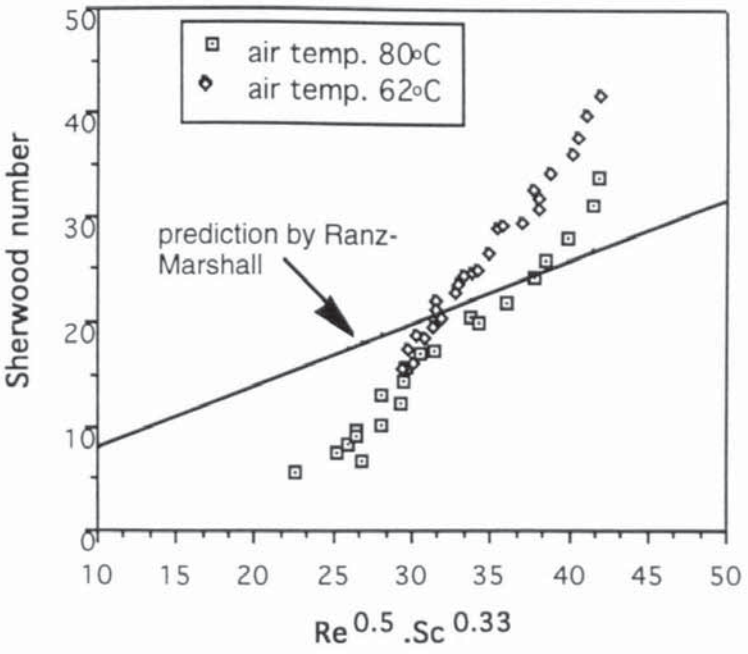

Figure 6.22 **Evaporation rate of monoethanolamine drops expressed as Sh versus $Re^{0.5}.Sc^{0.33}$ and compared with Ranz-Marshall equation.**

before the sudden rise was recorded as the surface temperature. The surface temperature was found to be about 4°C below the air temperature. The same amount of time was allowed for collecting, weighing and return of the vaporising sphere into the wind tunnel for each experiment. This was to annul any error of continuous vaporisation that might be introduced during collection and weighing of the spheres. The error introduced, if any, was thought to be negligible as little or no vaporisation was expected, the surface temperature being reduced to that of ambient air.

Unlike those of oscillating drops, the vaporisation rates of naphthalene spheres, Figure 6.24, were found to decrease linearly with time. The Sherwood number correlated closely with values predicted by the Ranz-Marshall relationship. The data for Figures 6.23 and 6.24 are shown in the Appendix A.

6.4 *Preliminary Studies on Droplet Drying*

Individual drops of solutions ≈ 5 mm in diameter were also observed in the wind tunnel at air temperatures of 62°C and 80°C. Droplet internal circulation was observed when drops of potassium sulphate or ammonium sulphate solution (40/100 wt/wt) were evaporated. Tiny particles of crystals were first formed and these then circulated internally about a horizontal axis before aggregating on the projected frontal end of the drop. Crystal formation commenced from the front end of the drop; they then swirled rapidly to the side of the drop and circulated through the interior back to the front end to repeat the pattern. The circulation process was initially rather chaotic, and it was not apparent whether a particle completed a full cycle of circulation.

The commencement of crystal formation and the induced swirl and turbulence at the front of the drop demonstrated that the rate of evaporation was higher at the front end of the drop facing the incident air and that internal circulation was induced by the transfer of shear across the interface to the adjoining liquid sub-layer. This would cause extensive surface renewal

principally at the front of the drop where much of the mass transfer (evaporation) occurred. Drop oscillation and internal circulation decreased as more crystals were formed and the solute concentration increased, the droplet viscosity increasing until it became rigid. This observation is analogous with internal circulation in liquid-liquid systems reported by Garner and Lane[23] and Kintner[86] who used aluminium dust to enhance observation and illuminated the drop with a thin, flat shaft of light for photographic purposes. It is also analogous with circulation in bubbles in gas-liquid systems in which ammonium chloride was used to aid visual observation[36].

6.5 *Summary of Experimental Observations*

The only explanation for the increased mass transfer rate associated with increased drop diameter is drop shape oscillation and the degree of turbulence. Consequently a way is required of correlating mass transfer data with drop surface behaviour.

Drop oscillation increases the rate of mass transfer above that which would otherwise be observed in its absence. It is, however, difficult to dissociate the increase in mass transfer due to circulation and wake shedding from that due solely to shape oscillation. With the photographic system employed in the present study, the onset of internal circulation of pure liquids could not be studied, although droplet internal oscillation was observed when individual drops of potassium sulphate solution were evaporated in free flight. Two types of drop oscillation observed were the pulsation type in which droplets appear to oscillate in a random fashion. It is possible that instability of the wake behind the drop was the driving force. Another significant observation was that the oscillation was related to the size of drop which in turn was a function of its viscosity and surface tension. Oscillation became less random as the drop size was decreased by evaporation. The causes of drop oscillation may include local variation

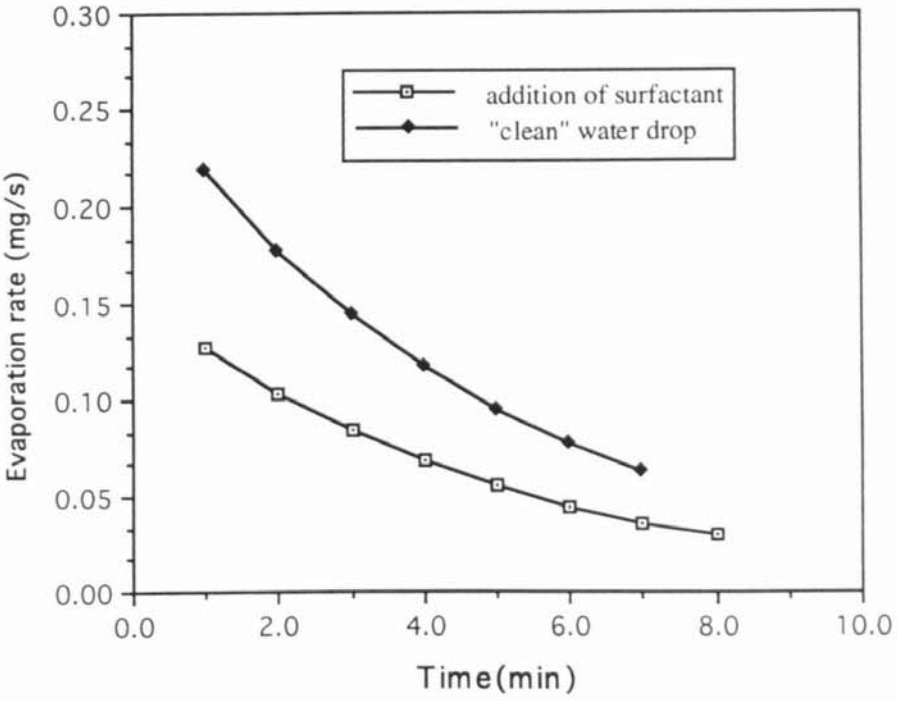

Figure 6.23. **Comparison of evaporation rates of water drops doped with surfactant (0.001 wt/wt) with those of untreated distilled de-ionised water, (data in Appendix A), Air temp. = 68°C.**

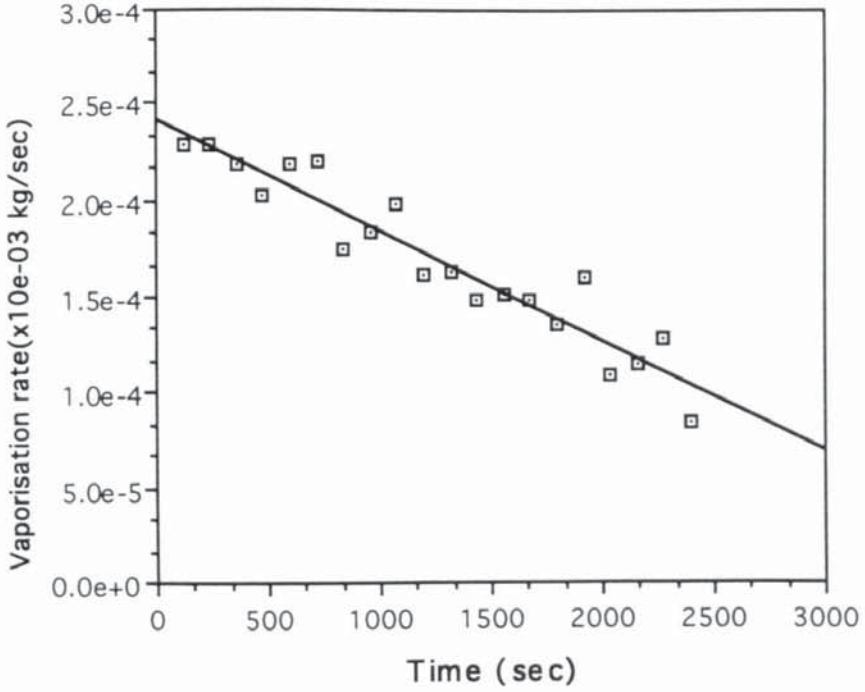

Figure 6.24 **Vaporisation rate of naphthalene spheres. (see data in Appendix A) , Air temp. = 74°C.**

in surface tension, instability during formation, wake turbulence, vortex shedding, turbulence in the continuous phase, the aerodynamic pressure force or indeed a combination of all these factors. A novel way of incorporating these factors into the mass transfer relationship is presented in Chapter Seven.

The Sherwood, Sh of the evaporated droplets were observed to fall below the prediction by Ranz-Marshall at Re<600. This phenomenon has also been reported by Finlay[49], Ahmadzadeh[140], Srikrishna[21], and Walton[162]. Whilst a satisfactory explanation remains to be found for this, it appears that due to reduced dispersion of evaporated vapour at Re below 600, heat is transferred to the vapour from the evaporating liquid and that the simultaneous heat and mass transfer processes described under theoretical conditions giving Nu=Sh=2 are not followed.

CHAPTER SEVEN

7 DISCUSSION OF RESULTS

7.1 Introduction

7.2 Heat and Mass Transfer

7.3 Effects of Surface Active Agents and Liquid Viscosity

7.4 Sublimation of Naphthalene Spheres.

7.5 Approximate Models (Interior Field)

7.6 Development of a New Model:-(Drop Oscillation and Wake Shedding).

7.7 Incorporation of OT into the Mass Transfer Equation for Oscillating Drops

7.8 The Evaporation of a Single Drop injected into an Air Stream.

7.8.1 The Significance of the OT number and Drop Oscillation.

7.9 Limitations of the "OT Number"

CHAPTER SEVEN

"An orderly method of analysing problems and presenting their solutions represents training in logical thinking that is of considerably greater value than mere knowledge of how to solve a particular type of problem."

- Himmelblau, D.M.

DISCUSSION OF RESULTS

7.1. *Introduction*

Experimental studies of the evaporation of single droplets of pure liquids in free-flight have been carried out to gain a fundamental knowledge of the transport processes of heat and mass transfer which take place in numerous liquid-gas operations in the chemical industry. A carefully designed single pass vertical wind tunnel was used to freely suspend individual liquid droplets and to evaporate them under conditions similar to those encountered in many spray liquid-gas contact operations. Results of experiments carried out in this study are presented in Chapter Six. Owing to the experimental difficulties of measuring droplet surface temperature and of collecting freely suspended individual droplets for weighing, experimental study was limited to pure liquid droplets. Experiments were replicated to ensure consistency and reliability of results and video recordings of droplet behaviour were analysed frame by frame in an attempt to correlate droplet behaviour with mass transfer.

In this chapter, the forces giving rise to droplet oscillation and their effect upon heat and mass transfer rates are discussed. A novel dimensionless group is presented to characterise droplet behaviour. A modified Sherwood number for the prediction of the mass transfer coefficient for oscillating droplets is proposed before concluding with a theoretical analysis of fractional evaporation of oscillatory spray droplets in evaporative spray processes.

7.2 Heat and Mass Transfer

The rate of heat and mass transfer is a function of temperature, humidity and transport properties of the air surrounding each droplet. It is also a function of droplet diameter and of the relative velocity between droplet and air. Models to describe the evaporation of single drops are to be found in a range of chemical engineering publications. The most widely used is the Ranz and Marshall[3] equation;

$$Sh = 2 + 0.6\, Re^{0.5} Sc^{0.33} \qquad (7.1)$$

Experimental results obtained in the present research were therefore compared with Equation 7.1. This demonstrated a great divergence between predictions from the model of Ranz-Marshall from experimental data for drops at Re>500, and confirmed the discrepancy reported by Finlay[49], Ahmadzadeh et al.[140] and Akbar[22]. This clearly indicates that the heat and mass transfer rates of oscillating drops depend not only on the temperature, humidity, and transport properties of the surrounding gas but also on the surface hydrodynamics of the droplet.

A drop suddenly exposed to a gas stream experiences the force of the dynamic pressure of the gas which tends to deform its surface. The surface tension of the perturbed droplet counteracts this force and acts to squeeze the liquid drop to minimise surface area. The greater the inward attractive force perpendicular to the surface of the droplet to counteract the dynamic force of the air stream, the less the deformation of the droplet. Thus a higher surface tension promotes drop sphericity and resists deformation.

A deformed droplet experiences a local decrease in pressure at the perturbed surface which corresponds to the increase in air velocity in the vicinity of the extended surface as the air is deflected around it. This local decrease in pressure acts to increase the deformation, i.e. to move the extended surface of the droplet even further. Thus there are forces with opposing effects.

It is observed that the lower the viscosity of the liquid drop, the readier it will oscillate. The oscillatory behaviour of the droplet generates and promotes internal circulation as molecules move continuously from the interior of the droplet to the surface. As the droplet becomes smaller, the surface tension per unit diameter predominates, shape oscillation diminishes and the droplet surface become stable. This phenomenon of droplet oscillation is responsible for the high initial mass transfer rates observed in Chapter Six.

There is at present no satisfactory model to account for drop hydrodynamics and their effects on mass transfer rates. The models presented by Angelo et al.[66] and Kintner[86], and discussed in Chapter Four, are based on surface stretch and predict drop frequency or amplitude of oscillation for a fluid drop travelling through a stagnant continuous phase as observed in two dimensions only. Consequently, they do not account for the dynamic effect of the continuous phase on the droplet surface and on the stability of the droplet. In addition, the concept of eccentricity used in the above models relies on the ratio between the horizontal stretch (in terms of the major axis) and the vertical stretch (in terms of the minor axis) (d_h/d_v), thereby ignoring the deformation in the third direction.

The rate of dispersed phase mass transfer for oscillating drops was found to depend on the "frequency" of oscillation. "Frequency" used here does not imply a periodic harmonised change but random movements of drop surface. Surface oscillatory motion in the early stages after drop release did not conform to any symmetric periodic change. It was made up of random wobbles of lower frequency and higher amplitude. The frequency increased and the amplitude decreased as the drop decreased in size. Attempts to find a simple relationship between frequency of oscillation and mass transfer were hampered by the unperiodic oscillatory motion of the droplet surface. An alternate analysis was therefore sought with recourse to the forces within the droplet and the dynamic force of the continuous phase.

The evaporation data reported in Chapter Six demonstrate that neither mass transfer rates from oscillating droplets nor the Sherwood Number correlate with $Re^{0.5}Sc^{0.33}$.

Oteng-Attakora et al[161] reported the effects of drop oscillation in an earlier study and attempted to correlate the Sherwood number as an exponential function of $Re^{0.5}.Sc^{0.33}$. Walton[162] in a recent study, supported pure liquid drops on a rotating thermocouple in a horizontal wind tunnel. Using a magnifying lens he observed random and irregular drop movement, described as 'wagging'. Some of Walton's mass transfer data, reproduced in Figure 7.1 confirm the observed higher initial mass transfer rates of oscillating droplets. Walton, however, plotted d_e^2 against time, Figure 7.2, and obtained a linear relationship. The data were correlated with an equation previously used by Audu[130] namely

$$Sh = \frac{\partial m}{\partial t} \cdot \frac{1}{A_e} \frac{R_c T_a}{M_w(p_2-p_1)} \cdot \frac{d_e}{D_v}. \qquad (7.2)$$

Equation 7.2 can be written in the form :

$$k_G = \rho \frac{\partial}{\partial t}(V) \cdot \frac{1}{A_e} \cdot \frac{R_c T_a}{M_w(p_2-p_1)} \qquad (7.3)$$

which implies,

$$k_G \alpha \frac{\partial}{\partial t}(d_e^3) \cdot \frac{1}{A_e} \qquad (7.4)$$

since $\rho \frac{R_c T_a}{M_w(p_2-p_1)} \approx$ constant andthe surface area of the equivalent sphere $A_e = \pi d_e^2$. Let $y = d_e^2$,i.e. $d_e^3 = y^{3/2}$, hence;

$$\frac{\partial}{\partial t}(d_e^3) = \frac{\partial}{\partial t}(y^{3/2}) = \frac{3}{2} y^{1/2} \frac{dy}{\partial t} \qquad (7.5)$$

upon substitution,

$$\frac{\partial}{\partial t}(d_e^3) = \frac{3d_e}{2}.\frac{\partial}{\partial t}(d_e^2) \tag{7.6}$$

if $\frac{\partial}{\partial t}(d_e^2)$ is a constant, as suggested by Walton, then Equation 7.4 becomes;

$$k_G \alpha \frac{1}{d_e} \tag{7.7}$$

It would be expected that if change of surface area ($\approx d_e^2$) with time was constant, then the rate of mass and heat transfer per unit area would decrease as the drop diameter increased. This was not found in the present study and indeed not in the study by Walton[162]. A closer look at results presented by Walton, Figure 7.1, and his correlation, Equation 7.8:

$$Sh = Ae^{-x}10^{(BRe^{0.5}Sc^{0.33})} \tag{7.8}$$

demonstrate that k_G initially decreased exponentially with decrease in drop diameter. However, in Figure 7.1, Walton presents d_e^2 as a linear function of time, contradicting results presented in Figure 7.2 and Equation 7.8. Hence the correlation does not have the general applicability intended.

7.3 *Effects of Surface Active Agents and Liquid Viscosity.*

Surface active agents are substances which, although present in small amounts, exert a marked effect on the surface behaviour of a system. Their ability to cause these changes is associated with the tendency to migrate to the surfaces between two phases. An addition of 1 part of sodium octyl sulfo-succinate to 1000 parts wt/wt of distilled de-ionised water drops decreased considerably, (i) the size of droplet formed from the same nozzle and (ii) surface oscillatory

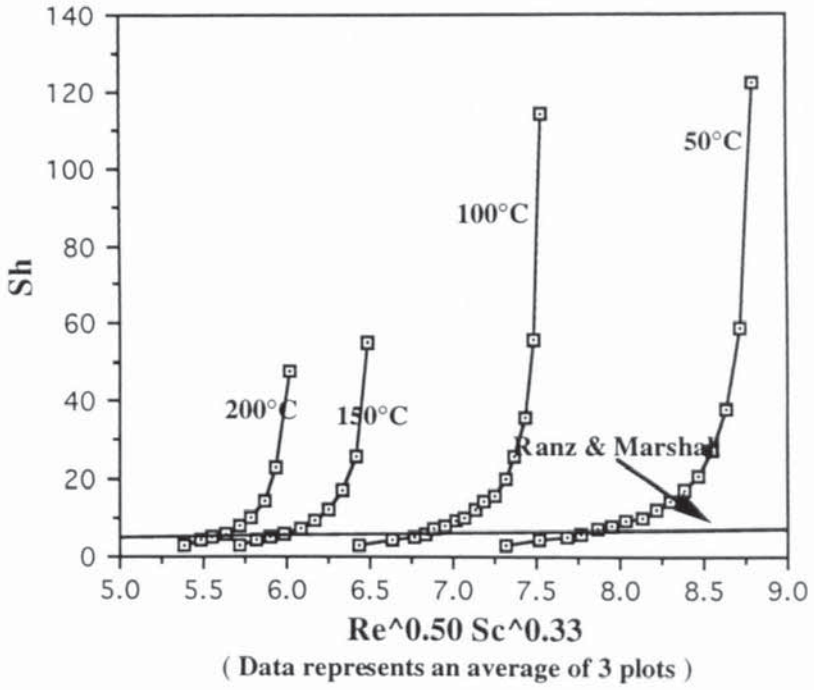

Figure 7.1. **Correlation of mass transfer data. Walton[162], 1994**

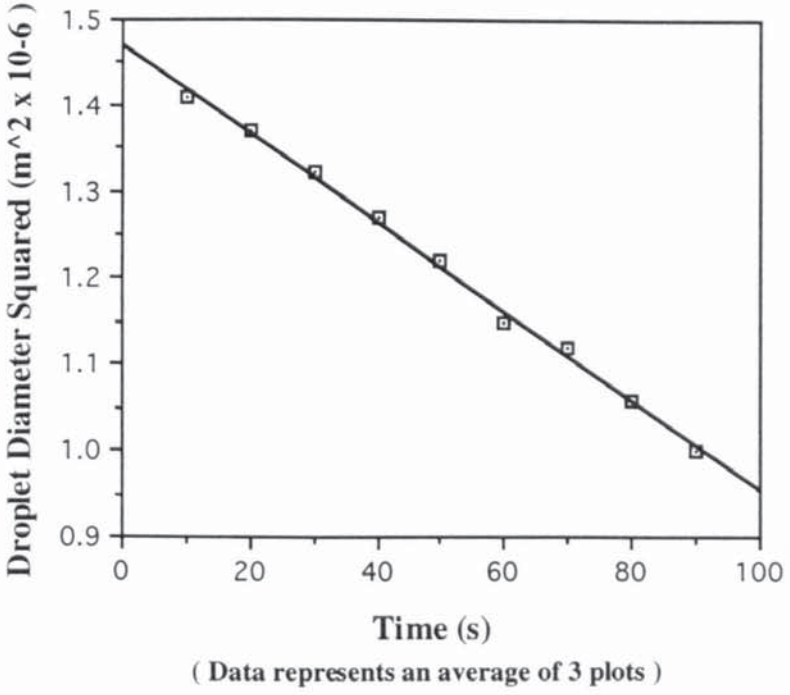

Figure 7.2 **Drop diameter squared versus time.(Walton[162],1994)**

behaviour. A radical lowering of the frequency and amplitude of oscillation was noted. Such reduction in oscillation lowered considerably the mass transfer rates as shown in Figure 6.23. However apart the change in surface tension of the liquid, no measurable change could be detected in any physical property of the liquid phase.

Frumkin and Levich[39] have explained the mechanism underlying the observed reduction in mass transfer rate associated with the addition of surface agents. The surface active matter accumulates on the downstream surface of a drop since on reaching the interface at upstream positions it is dragged by passing fluid to downstream locations. Because of the difference in concentration created, there is thus an interfacial tension gradient. The latter gradient opposes surface flow.

The equation which describes the effect of interfacial tension gradient on surface flow is obtained from a force balance at the interface. This balance is at any point on the interface[164];

$$\delta\gamma/\delta x = \tau_{xy2} + \tau_{xy1} \qquad (7.9)$$

where γ, x and y are the interfacial tension, a vector distance parallel to the interface and the direction normal to the interface respectively. τ_{yx2} and τ_{yx1} are the viscous shears acting in the x-direction at the interface and produced by flow outside and within the drop respectively . Equation 7.9 indicates that surface flow and, hence, circulation within the drop will be retarded appreciably and may even be prevented (i.e. $\tau_{yx1} = 0$) when the interfacial tension gradient and external viscous drag are of the same order. Davies[165] proposed the use of the equation

$$\% \text{ circulation} = \left(\frac{100}{1 + 1.5\left(\frac{\mu_d}{\mu_c}\right)}\right) - \left(\frac{32C_s^{-1}}{r_d.g.\Delta\rho}\right) \qquad (7.10)$$

in which the "surface compression modulus", C_s^{-1}, is a factor expressing the degree of reduction from full Hadamard circulation[32] due to surfactant addition. However, observed Re in the present study were too large for Hadamard's model to be strictly satisfied.

7.4 Sublimation of Naphthalene Spheres.

Individual naphthalene spheres with rigid surfaces were vaporised to confirm the effect of surface behaviour on mass transfer rates. It was noted that the mass transfer rates for naphthalene vaporisation closely approached published predictions in the literature i.e. equations 4.46 and 4.47, with maximum deviation of 10% at Re > 7000, and 2% at Re < 2000. This finding confirms the effect of rigid drop behaviour upon mass transfer rates.

The essential difference between a naphthalene sphere and a liquid droplet is the mobile interface and internal circulation of the latter. The total interfacial area for mass transfer from naphthalene spheres to the surrounding fluid remains constant except for slight changes due to sublimation. These changes leave the naphthalene in a somewhat ellipsoidal shape indicating that transfer rates are a maximum at the 'leading pole' of the solid and decrease to a minimum at the edges. Beyond the edges the rates increase again owing to reversed flow. For liquid drops however, interfacial area is continuously created on the upstream half of the mobile phase and continuously destroyed on the downstream.

In liquid drops the surface tension forces act in a direction tangential to the interface. During drop oscillation, the surface undergoes "dilatation" which suggests that there must be another force acting normal to the interface. The mass transfer rate is enhanced because a sphere has the smallest area per unit volume; therefore, any deviation from drop sphericity as observed in drop oscillation produces alternate creation and destruction of interfacial area which results in interfacial turbulence and consequently higher mass transfer rates.

However, such observations do not accurately describe the physical situation. In order to be of practical value, the factors affecting a physical situation should be measured and presented in a model. This is the subject of the following section. It deals with the analysis and development of a novel dimensionless group, the Oteng-Attakora number (OT), based on the forces responsible for droplet oscillation and presents a mathematical correlation of the forces responsible for mass transfer.

7.5 *Approximate Models (Interior Field.)*

(i) Complete Mixing Model.

The simplest model for the transport processes in the interior of the drop is to assume the internal motion of the drop is so vigorous that complete mixing is achieved[139]. The temperature profile in the drop is essentially flat and resistance to heat and mass transfer exits only in the continuous phase. For the complete mixing model the energy transport can be described by

$$-\frac{4}{3}\pi r_2^3 C_{pd}\frac{\partial T_m}{\partial t}\Big| = 4\pi r_2^2[h_c(T_m - T_\infty) + \lambda k_G(C_s(T_m) - C_\infty) + \sigma_\Sigma(T_m^4 - T_\infty^4)] \tag{7.11}$$

assuming that

$$\frac{\partial T_m}{\partial t} = u_\infty \frac{\partial T_m}{\partial x} \quad \text{and} \quad \frac{k_G}{h_c} = \frac{Le}{\rho C_p} \tag{7.12}$$

the energy transport equation can be reduced to

$$Nu \equiv \frac{h_c d_e}{k} \equiv \frac{d_e}{k}\left[\frac{\frac{1}{6}\frac{\partial T_m}{\partial x} d_e \rho_d u_\infty(x) - \sigma_\Sigma(T_m^4 - T_\infty)}{(T_m - T_\infty) + \frac{Le.\lambda}{\rho C_p}(C_s(T_m) - C_\infty)}\right] \tag{7.13}$$

Since the drop temperatures along the falling distance are known, the Nu can be evaluated.

(ii) Non-mixing Model.

The non-mixing model assumes there is no internal motion and the energy equation is reduced to simply a transient heat conduction equation. The equations which describe the heat transport in the non-mixing drop are

$$\frac{\partial T}{\partial t} = \alpha_d\left(\frac{\partial^2 T}{\partial r^2} + \frac{2}{r}\frac{\partial T}{\partial r}\right) \text{ for } 0 < r \leq r_2 \tag{7.14}$$

with initial condition, T = To, and boundary conditions

$$\left.\frac{\partial T}{\partial r}\right|_{r->0} = 0 \tag{7.15}$$

$$-k_d\left.\frac{\partial T}{\partial r}\right|_{r_2} = h_c(T_s - T_\infty) + \lambda k_G(C_s - C_\infty) + \sigma_\Sigma(T_s^4 - T_\infty^4) \tag{7.16}$$

Neither the complete-mixing nor the non-mixing model is realistic because they are based on the extreme situations of the drop internal motion. Therefore, a new model is proposed which considers both the effects of oscillation and internal circulation on the mixing in the drop.

7.6 *Development of a New Model:-(Drop Oscillation and Wake Shedding.)*

Drop oscillation results from the combined effect of wake vortex shedding and of the inherent tendency of a deformed droplet to exhibit dampened oscillation. Hydrodynamic forces tend to flatten the drop, whilst the interfacial tension tends to pull it into a spherical shape. The frequency of vortex shedding is estimated from the Strouhal number, Sr, (cf. Chapter Two).

Natural drop oscillatory frequency can be estimated from Lamb's formula[22];

$$f_n = \sqrt{\frac{48\sigma}{\pi^2 d_e^3(2\rho_a + 3\rho_d)}} \tag{7.17}$$

and for drops in air;

$$f_n \approx \sqrt{\left(\frac{\sigma}{d_e^3 \rho_d}\right)} \tag{7.18}$$

The terminal velocity of a spherical particle falling under gravity is usually derived from a balance between buoyancy and drag forces, in an infinite medium; thus:

$$\frac{\pi}{6} d^3 g \Delta\rho_p = C_D \frac{\pi d^2}{8} \rho_a v_\alpha^2 \tag{7.19}$$

It was shown in Figures 6.1-6.4 and in Equation 6.3 that the air velocity supporting a drop in free-flight is;

$$v_a \approx \sqrt{\frac{(d_e \Delta\rho g)}{\rho_a}} \tag{7.20}$$

If drop shape frequency, f_N, is assumed to be a function of natural frequency, f_n, it can be shown that, Sr, if related to drop oscillation, is given by;

$$Sr = \left(\frac{\sigma}{d_e^3 \rho_a}\right)^{1/2} \frac{d_e}{v_a} = \sqrt{\frac{\sigma}{\rho_d d_e^3}} . d_e . \sqrt{\frac{\rho_a}{d_e \rho_d g}} \tag{7.21}$$

$$= \sqrt{\frac{\sigma}{\rho_d g d_e^2}} . \sqrt{\frac{\rho_a}{\rho_d}} \tag{7.22}$$

$$Sr = \sqrt{\frac{1}{E_o}\left(\frac{\rho_a}{\rho_d}\right)} \tag{7.23}$$

An approximate criterion for internal circulation is that due to Bond[34], i.e. Eo>4. From Equation 7.23, it can be inferred that vortex shedding contribute to drop oscillation as much as internal circulation. A complementary view of droplet

internal circulation is provided from consideration of the forces at play during the drying process, (Figures 7.3 & 7.4).

Traditionally Re is defined by $\rho v d_e/\mu_a$. In the case of internal circulation, an internal Reynolds number may be defined as:

$$Re_{int}=\frac{\rho_d v_{int} d_e}{\mu_d} \tag{7.24}$$

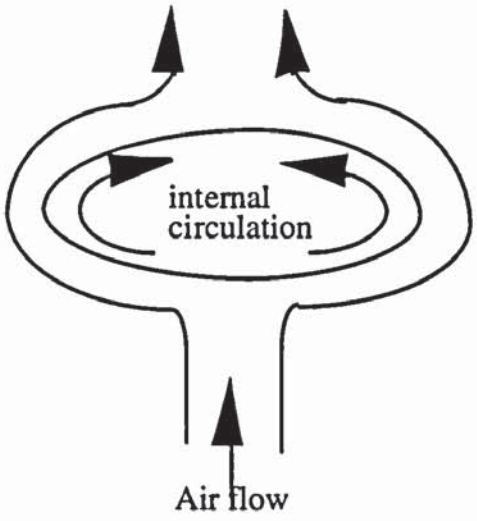

Figure 7.3. **Oscillating droplet with internal circulation**

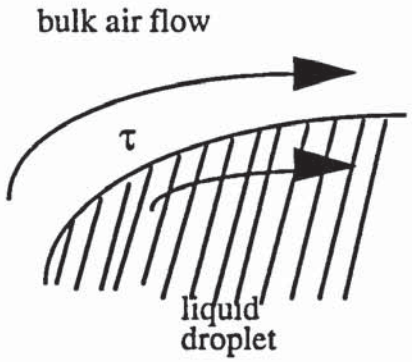

Figure 7.4 **Shear force at drop surface**

Interaction between the liquid and gas phase is through shear, τ, the force per unit area; therefore $\tau \alpha \rho_a v_a^2$ in the gas phase and $\tau \alpha \rho_d v_{int}^2$ in the liquid phase. Hence $v_{int} \approx \sqrt{(\tau/\rho_d)}$ or $v_a \approx \sqrt{\rho_a/\rho_d}$). (For droplets of water, Garner and Lane[23] observed v_{int} values of $\approx$ 1% of terminal velocity.)

Consequently ,

$$Re_{int}=\rho_d \frac{\sqrt{\frac{\tau}{\rho_d}}}{\mu_d} d_e \tag{7.25}$$

On the basis of force per unit area, the relevant forces are;

τ	$\frac{\mu_d}{d_e}\sqrt{\frac{\tau}{\rho_d}}$	$\frac{\sigma}{d_e}$	(7.26)
External shear	internal viscous force	surface tension	

Any equation to describe the phenomenon of droplet oscillation in a liquid-gas system must include all the properties of the droplet and the conditions of gas flow that affect drop behaviour. These factors might include τ, μ_d, d_e, ρ_d, σ. It is difficult to establish a model based solely on theoretical reasoning that incorporates the interaction between the gas motion, droplet oscillation, and drop trajectory, because of the complexity of shape oscillation and internal circulation. The difficulty in solving simultaneously the gas flow field, the change in droplet shape due to surface tension, viscosity, and the pressure variation around a moving small droplet is immense. However, these properties may be arranged into a useful relationship by dimensional analysis[166], which formulates physical properties in an equation and shows the manner in which they are inter-related. The relevant physical properties represent the starting point for the determination of a complete set of dimensionless groups. The properties are grouped into two units, the core matrix and the residual matrix. Application of the Gaussian algorithm which uses matrix calculation transforms the core matrix into a unit matrix. The procedure for constructing the dimensional matrix and determining a complete set of Π groups is demonstrated in Table 7.1. Each element of the residual matrix forms the numerator of a fraction whilst its denominator consists of the fillers from the unit matrix with the exponents indicated in the residual matrix, i.e.

$$\Pi_1 = \frac{\mu_d}{(\rho_d d_e \sigma)^{1/2}} \tag{7.27}$$

$$\Pi_2 = \frac{\tau d_e}{\sigma} \tag{7.28}$$

Table 7.1 **Dimensional matrix; Gaussian Algebra.**

	core matrix			residual matrix	
properties	ρ_d	d_e	σ	μ_d	τ
M	1	0	1	1	1
L	-3	1	0	-1	-1
T	0	0	-2	-1	-2
z_1	1	0	1	1	1
$z_2 = 3M+L$	0	1	3	2	2
$z_3 = -T/2$	0	0	1	1/2	1
$z'_1 = z_1-z_3$	1	0	0	1/2	0
$z'_2 = z_2-3z_3$	0	1	0	1/2	-1
z_3	0	0	1	1/2	1

Π_1 and Π_2 are then transformed to provide more commonly known expressions or dimensionless groups which are more suitable to manipulate and which describe droplet oscillation. Dividing the square root of Π_2 by Π_1 yields Π_3 thus;

$$\frac{\Pi_2^{1/2}}{\Pi_1} = \frac{\sqrt{\tau d_e}}{\mu_d}.\sqrt{\rho_d d_e} \tag{7.29}$$

$$= \frac{d_e.\sqrt{\tau \rho_d}}{\mu_d} \tag{7.30}$$

$$\Pi_3 = \frac{\rho_d d_e}{\mu_d}.\sqrt{\frac{\tau}{\rho_d}} \tag{7.31}$$

Hence Π_1 and Π_3 are given by;

$$\Pi_1 = Oh_d = \frac{\mu_d}{(\rho_d d_e \sigma)^{1/2}} \qquad \Pi_3 = Re_{int} = \frac{\rho_d d_e}{\mu_d}\sqrt{\frac{\tau}{\rho_d}}$$

Oh_d, the droplet property group or Ohnesorge number, has been referred to by Wallis[167] as the stability group. This group characterises the resistance of the drop to oscillation, i.e. deformation, whilst Re_{int} characterises the flow phenomena inside the drop. Based on the above considerations, it is possible to formulate a new dimensionless group, the OT number, to characterise droplet behaviour that will embrace the phenomena of drop oscillation and internal circulation. This is achieved by combining Π_1 and the square of Π_3 to give the OT number;

$$OT = Re_{int}^2 . Oh_d = \left(\frac{\rho_d d_e v_{int}}{\mu_d}\right)^2 . \left(\frac{\mu_d}{(\rho_d d_e \sigma)^{1/2}}\right) \tag{7.32}$$

since $v_{int} \approx v_a \sqrt{\frac{\rho_a}{\rho_d}}$, OT can be written;

$$OT = \frac{\rho_a v_a^2}{\mu_d} . \left(\frac{\rho_d d_e^3}{\sigma}\right)^{1/2} \tag{7.33}$$

But vortex shedding is characterised by $Sr = \left(\frac{\sigma}{d_e \rho_d}\right)^{1/2} . \frac{d_e}{v_a}$, therefore

$$OT = \frac{\rho_a v_a^2}{\mu_d} \left(\frac{1}{Sr} . \frac{d_e}{v_a}\right) \tag{7.34}$$

and after re-arranging;

$$OT = \left(\frac{\rho_a v_a^2}{\mu_d}\right) . d_e^{1.5} \sqrt{\left(\frac{\rho_d}{\sigma}\right)} \tag{7.35}$$

It was shown in Equation 7.23 that wake shading is a function of Eo which generates internal circulation when Eo>4. It is evident from Equation 7.34 that the OT-number includes all the factors and properties which effect drop behaviour.

Liquid flowing under shear in low flow does so in layers maintaining a velocity gradient, ($\tau=\mu_d du/dy$). At a given shear the ease of flow is inversely proportional to the liquid viscosity or rheology. It is apparent that, the OT number characterises droplet surface movement in terms of its internal flow, (Re_{int}), its stability, (Oh_d), and the effects of vortex shedding, (Sr). The higher the OT number, the greater the degree of droplet oscillation. Whilst quantitative analysis of droplet frequency proved impossible in the present work, the OT number gives an appropriate indication of drop oscillation based on the forces acting within and outside the droplet.

Another way of interpreting the OT number is as the ratio of the force balance between the forces outside of the droplet causing deformation and those at the surface to the ratio of the forces within the droplet and its surface. This may be written;

$$OT = \left(\frac{\rho_s v^2 d_e}{\sigma}\right) \Big/ \left(\frac{\mu_d}{\sqrt{\rho_d d_e \sigma}}\right) \tag{7.36}$$

which in effect is the ratio of the Weber number to the Ohnesorge number. Both the Weber and the Ohnesorge numbers are used to characterise droplet disintegration, a process based on the aerodynamic interaction and turbulence which generate waves at the surface of liquid jets and sheets before break-up.

7.7. Incorporation of OT into the Mass Transfer Equation for Oscillating Drops

The approach adopted in order to correlate heat and mass transfer from oscillating drops was to draw an analogy with published work on single droplet evaporation and to correlate the Sherwood number as:

$$Sh = Sh_o + K.OT^x Re^y Sc^{0.33} \tag{7.37}$$

where Sh_o = Sh at virtually zero relative motion between the drop and continuous phase. i.e. under natural convective conditions, and $Sc^{0.33}$ is related to the boundary layer thickness for momentum mass transfer, (Equation 3.14).

By multiplying the top and bottom of Equation 7.35 by $\rho_a\mu_a^2 d_e$, OT is re-cast in the form:

$$OT = \left[Re^2 \left(\frac{\mu_a^2}{\mu_d \rho_a} \right) \left(\frac{\rho_d}{\sigma . d_e} \right)^{0.5} \right] \tag{7.38}$$

Let

$$\psi = K. \left[\left(\frac{\mu_a^2}{\mu_d \rho_a} \right) \left(\frac{\rho_d}{\sigma . d_e} \right)^{0.5} \right]^x Sc^{0.33} \tag{7.39}$$

such that Equation 7.37 may be written:

$$Sh_1 \approx \psi . Re^{\beta} \tag{7.40}$$

where $Sh_1 = Sh\text{-}Sh_o$ and β is the exponent to the Re number = (2x+y).

The Ranz and Marshall[3] correlation predicts;

$$k_G \alpha \frac{(d_e . v_a)^{0.5}}{d_e} \tag{7.41}$$

The droplet velocity within the wind tunnel reveals that ;

$$v_a \approx \sqrt{\frac{(d_e \Delta \rho g)}{\rho_a}} \tag{7.42}$$

and therefore in general, k_G for oscillating droplets incorporating the OT number is given by:

$$k_G \alpha \frac{(d_e.d_e^{0.5})^{\beta}}{d_e.d_e^{0.5x}} \quad \text{or} \quad d_e^{1.5\beta-(0.5x+1)} \tag{7.43}$$

Log-log graphs of Equation 7.40 and of Equation 7.43 yield $\beta = (2x+y)$ and $\varphi = 1.5\beta-(0.5x+1)$ respectively; see Appendix B for graphs and Table 7.2,). The analyses give values of x and y as;

$$Sh = Sh_o + K.OT^{0.15}Re^{1.07}Sc^{0.33} \tag{7.44}$$

The intercept C_1, on the y-axis of a log-log plot of Equation 7.40 gives $\ln(\psi)$. Hence $\psi = \exp(C_1)$. But ψ is given by;

$$\psi = K.\left[\left(\frac{\mu_a^2}{\mu_d\rho_a}\right)\left(\frac{\rho_d}{\sigma.d_e}\right)^{0.5}\right]^{0.15} Sc^{0.33} \tag{7.45}$$

therefore

$$K = \frac{\exp(C_1)}{\left[\left(\frac{\mu_a^2}{\mu_d\rho_a}\right)\left(\frac{\rho_d}{\sigma.d_e}\right)^{0.5}\right]^{0.15} Sc^{0.33}} \tag{7.46}$$

Implicit in Equation 7.40 is the assumption that d_e, the equivalent diameter of the drop is constant. This assumption was made as a matter of convenience in order to find an approximate value of β. Consequently, Equation 7.44 over-estimates Sh. A statistical analysis on the experimental data using Equation 7.44 as basis yields:

$$Sh = 2 + 0.02OT^{0.15}Re^{0.88}Sc^{0.33} \tag{7.47}$$

Table 7.2. **Values of φ and β from Equation 7.40 and 7.43.**

Pure liquid	φ	β	x	y
Evaporation at 50°C air temperature				
Propanol	0.86	1.30	0.18	0.94
Distilled de ionised water	0.89	1.30	0.12	1.06
Evaporation at 62°C air temperature.				
Propanol	1.24	1.56	0.20	1.16
Distilled de-ionised water	0.83	1.30	0.24	0.82
Heptane	1.14	1.43	0.01	1.41
Iso-butanol	0.89	1.30	0.12	1.06
Monoethanolamine	0.91	1.31	0.09	1.13
Evaporation at 80°C air temperature.				
Distilled de-ionised water	1.02	1.40	0.16	1.08
Monoethanolamine	1.05	1.40	0.10	1.20

The ability of the model to accurately predict evaporation rates can be assessed by comparing model predictions with data that have been experimentally determined. Equation 7.47 is compared with experimental data in Figure 7.5. It is obvious that the model greatly improves the correlation of mass transfer data.

To determine the experimental value of Nu, the surface temperature of the drop was assumed uniform at Ts. Ts was calculated using the program SURFACE_TEMPERATURE, (see Appendix C). The vapour pressure at the surface was assumed equal to the saturated vapour pressure at Ts. Physical Properties of air in the vicinity of the drop surface were, however, based on the interfacial temperature defined as $(T_a+T_s)/2$.

The experimental Nusselt number for heat transfer was determined by the introduction of the latent heat of vaporisation thus:

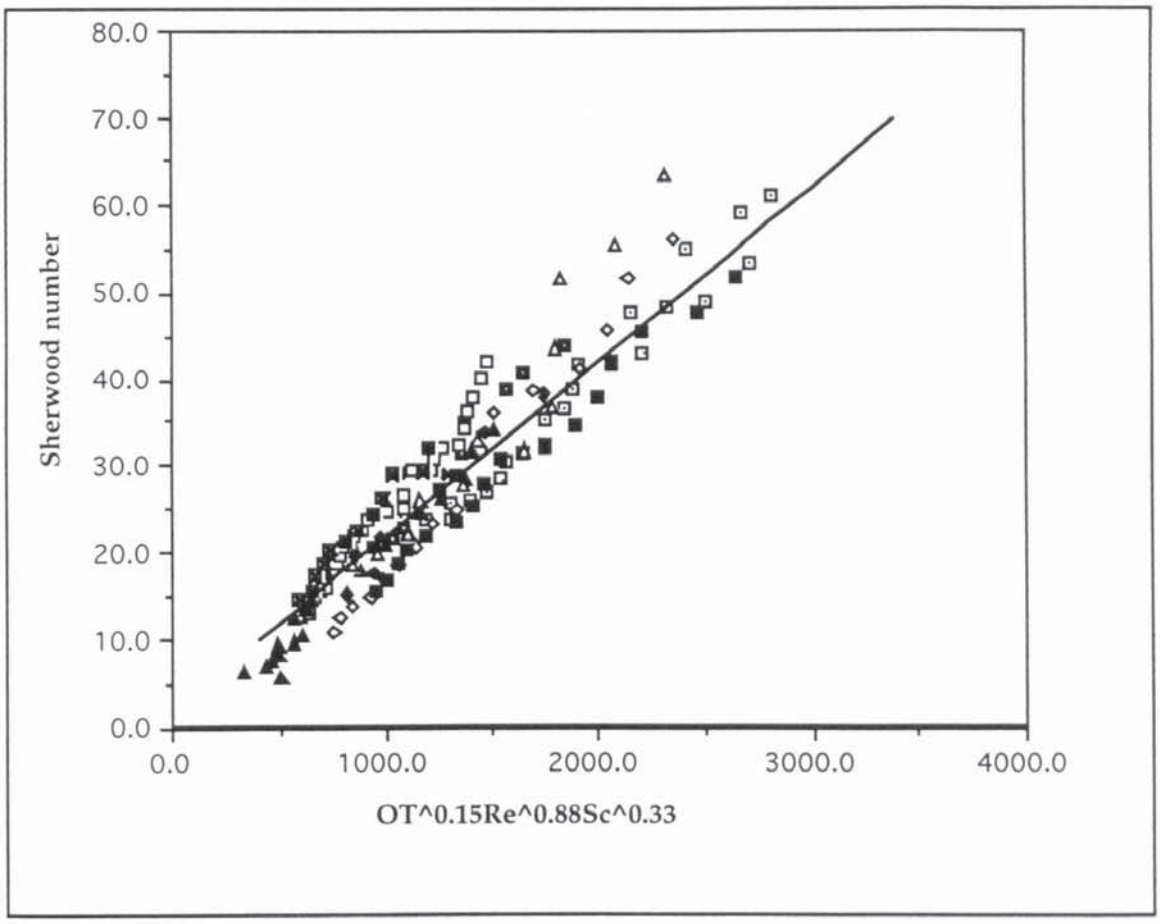

Figure 7.5. **Correlation of mass transfer data incorporating the OT number. Maximum deviation ± 7%, correlation coefficient 0.917.**

Key to Figure 7.1

- water drops (AT= 62°C)
- water drops (AT=80°C)
- water drops (AT= 50°C)
- propanol drops (AT= 62°C)
- propanol drops (AT= 50°C)
- monoethanolamine drops(AT= 62°C)
- monoehanolamine drops(AT= 80°C)
- heptane drops(AT=55°C)
- iso-butanol drops(AT =62°C)
- Correlation of Sh OT number

AT = evaporating air temperature

$$Nu = \frac{\dot{m}\lambda}{\pi d_e k \Delta T} \tag{7.48}$$

By analogy with the mass transfer correlation, the Nusselt number was correlated in the form:

$$Nu = 2 + 0.02OT^{0.15}Re^{0.88}Pr^{0.33} \tag{7.49}$$

Equation 7.49 was corrected for sensible heat loss by introduction of the Spalding number as:

$$Nu(1 + B)^{0.7} = 2 + 0.02OT^{0.15}Re^{0.88}Pr^{0.33} \tag{7.50}$$

The 0.88 power dependency of Re in the OT model compares reasonably well with theoretical consideration by Prandtl for heat and mass transfer in turbulent zones. Values ranging between 0.8 and 1.0 have also been reported by Finlay[49] and Hattangady[136]. The higher power dependence on Re can be explained by the pulsating behaviour of the droplets surface. Under these conditions the boundary layer has no time to fully develop and therefore presents very little resistance to mass transfer.

7.8 The *Evaporation of a Single Drop injected into an Air Stream.*

Spray droplets leaving an atomiser are ejected into the continuous phase at a relatively high initial velocity before eventually being slowed down by the external resistance of the continuous phase. For the movement of a single droplet discharged with an initial velocity, v_o, force balance equations for counter-current flow can readily be set up, (see Figure 7.6) Neglecting the effect of gravity, the equation of motion is;

$$m\frac{\partial v}{\partial t} + F_d = 0 \tag{7.51}$$

where m, the mass of droplet = $\pi/6\ d_e^3\rho_d$ and F_d is air resistance given by:

$$F_d = \frac{\pi}{8} C_D \rho_a v_a^2 d_e^2 \tag{7.52}$$

Even in a low pressure atomiser, the high initial velocity with which the liquid jet is discharged increases the air resistance on a droplet to a value which renders the

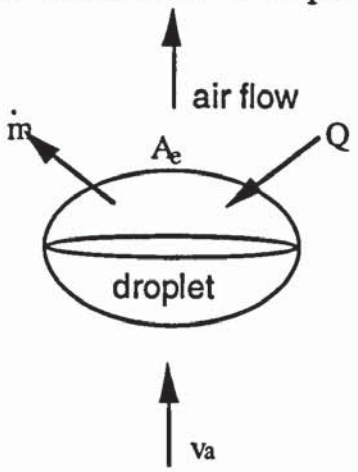

Figure 7.6 **Counter-current flow of droplet in an air stream.**

gravitational force negligible during the first period of the droplet travel. Hence, in the analysis of the movement of a droplet immediately after atomisation, the effect of gravity can be neglected.

Upon substitution of Equation 7.52 into 7.51,

$$-\frac{1}{3} d_e^3 \rho_d \frac{\partial v}{\partial t} = \frac{1}{4} C_D \rho_a v^2 d_e^2 \tag{7.53}$$

we may introduce a dimensionless velocity;

$$\left(\frac{v}{\nu/d_e}\right) \equiv Re \tag{7.54}$$

i.e.

$$\partial Re = \frac{d_e \partial v}{\nu} \tag{7.55}$$

and a dimensionless time;

$$\theta \equiv \left(\frac{t}{\frac{4}{3} \cdot \frac{\rho_d}{\rho_a} \cdot \frac{d_e^2}{\nu}} \right) \tag{7.56}$$

i.e.

$$\partial\theta = \partial t \left(\frac{3\rho_a \nu}{4\rho_d d_e^2} \right) \tag{7.57}$$

Equation 7.53 therefore reduces to;

$$-\frac{\partial Re}{\partial \theta} = C_D . Re^2 \tag{7.58}$$

The time elapsed for the drop to slow from Re_1 to Re_2 is given by:

$$\int_{\theta_1}^{\theta_2} \partial\theta = -\int_{Re_1}^{Re_2} \frac{\partial Re}{c_D . Re^2} \tag{7.59}$$

Now

$$\frac{\partial E_v}{\partial t} = \left(2\pi d_e D_v \frac{\Delta P . M_w}{RT} \left(1 + \frac{K}{2} Sc^{0.33} OT^{0.15} Re^{0.88} \right) \right) \tag{7.60}$$

From Equation 7.38, $OT = \left[Re^2 \left(\frac{\mu_a^2}{\mu_d \rho_a} \right) \left(\frac{\rho_d}{\sigma d_e} \right)^{0.5} \right]$. Hence using this relationship the enhanced evaporation is given by;

$$\frac{\partial (Ev)}{\partial t} = \beta_1 \pi K d_e D_v Sc^{0.33} \frac{\Delta P}{RT} Re^{1.18} \tag{7.61}$$

where $\beta_1 = \left[\left(\frac{\mu_a^2}{\mu_d \rho_a} \right) \left(\frac{\rho_d}{\sigma d_e} \right)^{0.5} \right]^{0.15}$

Ranz and Marshall used the following assumptions;

(i) stable droplet internal structure, (ii) spherical droplet shape in air flow in order derive Equation 7.62;

$$\frac{\partial(Ev)}{\partial t} = 0.6\pi d_e D_v \frac{\Delta P}{RT} Sc^{0.33} Re^{0.5} \tag{7.62}$$

Equation 7.62 underestimate mass transfer rates from oscillating droplets as much as 50% at Re>1000 in comparison with Equation 7.61.

From Equation 7.55 and 7.56, ∂t can be written as;

$$\partial t = -\left(\frac{4\rho_d d_e^2}{3\,\rho_a v}\right)\frac{\partial Re}{C_D Re^2} \tag{7.63}$$

Equation 7.63 is evaluated on the assumption that the change in velocity after drop release from the atomiser is far greater than the change in d_e, i.e. $\Delta v >> \Delta d_e$. Therefore d_e in Equation 7.63 is to be taken constant. The rate of evaporation immediately after atomisation can be written,

$$-\frac{\partial(E_v)}{\partial Re} = \frac{8\pi d_e^3 \rho_d}{3.Sc}\Delta H\left[\frac{1}{C_D Re^2} + \frac{K.\beta_1 Sc^{0.33}}{2C_D Re^{0.82}}\right] \tag{7.64}$$

where $\Delta H = \frac{\Delta P.M_w}{\rho_a RT}$.

On integration, Equation 7.64 becomes;

$$Ev = \frac{8\pi d_e^3}{3.}.\frac{\rho_d}{Sc}\Delta H\left[\int_{Re_2}^{Re_1}\frac{\partial Re}{C_D Re^2} + \frac{K.\beta_1 Sc^{0.33}}{2}\int_{Re_2}^{Re_1}\frac{\partial Re}{C_D Re^{0.82}}\right] \tag{7.65}$$

mass transfer due to molecular diffusion

enhanced mass transfer due to drop movement

Inspecting Equation 7.65, $\frac{8\pi d_e^3}{3Sc}\rho_d \Delta H \int_{Re_1}^{Re_2} \frac{\partial Re}{C_D Re^2}$ depicts mass transport due to molecular diffusion whilst $\frac{K.4\pi}{3}.d_e^3 \frac{\rho_d}{Sc^{0.67}}.\Delta H.\beta_1 \int_{Re_1}^{Re_2} \frac{\partial Re}{C_D Re^{0.82}}$ represents enhanced mass transport due to: (1) increased turbulence in the boundary layer as a result of movement of the drop, i.e. drop oscillation and relative velocity conditions, and (2) extension of drop surface area.

It is evident from the above expression that at higher Re the contributuion of molecular diffusion to mass transfer becomes diminishingly small. At Re>2000, in the case of distilled de-ionised water for instance, (c.f. Table A1 in the Appendix), the contribution of molecular diffusion to mass transfer was less than 3%

The mass fractional evaporation per change in Re may be obtained by dividing the mass transfer equation, Equation 7.65, by the mass of drop, ($m = \pi/6\, d_e^3 \rho_d$) and simplifying; i.e.

$$x_w = \left(\frac{16.}{Sc}\Delta H\right).\left[\int_{Re_2}^{Re_1} \frac{1}{c_D.Re^2}\partial Re + \frac{K.\beta_1}{2.}Sc^{0.33}\int_{Re_2}^{Re_1} \frac{1}{c_D.Re^{0.82}}\partial Re\right] \qquad (7.66)$$

The total amount of mass transfer from a drop depends upon the rate of evaporation and the contact time, the latter depending upon the velocity of fall and the length of path or penetration through the dryer. The length of path or penetration is given by:

$$Y = \int_0^t v.\partial t \qquad (7.67)$$

Introducing a dimensionless velocity and time (see Equation 7.52 to 7.56) we can write;

$$Y = \frac{4}{3} d_e \cdot \frac{\rho_d}{\rho_a} \int_0^{\theta} Re.\, \partial\theta \tag{7.68}$$

i.e.

$$Y = \frac{4}{3} d_e \frac{\rho_d}{\rho_a} \int_{Re_1}^{Re_2} \frac{1}{C_D Re} \partial Re \tag{7.69}$$

The fractional evaporation per unit distance from atomiser is therefore given by;

$$x_{ws} = \beta_2 \cdot \left[\frac{1}{Sc} \int_{Re2}^{Re1} \frac{1}{Re} \partial Re + \frac{K.\beta_1}{2.Sc^{0.67}} \int_{Re2}^{Re1} Re^{0.18}\, \partial Re \right] \tag{7.70}$$

where $\beta_2 = \dfrac{12.\Delta P.M_w}{d_e \rho_d RT}$.

7.8.1 *The Significance of the OT number and Drop Oscillation.*

There is at present no practical design method that incorporates drop hydrodynamics based on measurable physical properties in the prediction of mass transfer rates in any evaporative spray process. Drops have always been considered in forced convective drying as if they presented a uniform spherical surface for evaporation. The attempt by some investigators to correlate drop shape oscillation employing the concept of eccentricity is impracticable. The new dimensionless group, the OT number, relates drop oscillations to their effect on mass transfer based on measurable physical properties of the liquid which control and influence such behaviour.

The effect of drop oscillation on turbulence is akin to the effect of surface roughness upon flow in pipes. The rapid movement of drop surface increases turbulence in the boundary layer hence reducing the resistance to mass transfer.

The effect of droplet surface area extension is evident from consideration of the molecules of a freshly-formed liquid surface free from stress. The chemical potential of the molecules in the surface is higher than that in the bulk phase of the liquid on account of their unsymmetrical environment. Consequently some of the molecules leave the surface so as to increase the intermolecular spacing in the plane of the surface and to provide an extra attractive tension between molecules

in the surface layer. This reduces the surface area and hence the chemical potential. If a droplet is subjected to stress such that drop oscillation is promoted, as is encountered in forced convective evaporation, (e.g. spray evaporative processes where the driving force is in the direction of the continuous phase), the extension in surface area is accompanied by an aggregate of molecules to the surface since molecules must migrate to occupy the extended surface. This raises the chemical potential at the surface, i.e. the "escaping tendency " thereby promoting mass transport.

Equation 7.70 provides a generalised model for the evaporation of a droplet released from an atomiser. When a droplet is discharged from an atomiser, its initial velocity may be expected to be in the turbulent range. As the velocity falls the flow will pass through the semi-turbulent stage and may finally become laminar. In order to determine fully the motion of the droplet it is necessary to apply equations describing these three regimes; turbulent, semi-turbulent and laminar, between the limiting values of Reynolds number to which they apply: e.g. laminar flow may be assumed up to a value of Re = 2; semi-turbulent flow extends from Re = 2 to Re = 500; turbulent flow applies to values of Re above 500 and for this range the OT equation incorporating droplet oscillation may be used. As mentioned in the introduction, Masters[1] schematic presentation of a spray dryer layout is somewhat misleading. A better presentation is as shown in Figure 7.7. Stage 2 is evaporation and stage 3 Drying. Stage 3 commences once droplets have been concentrated beyond saturation and a skin or crust has formed. Moisture transfer at this stage is from within the droplet. Here the receding interface model may be used to estimate crust thickness and mass transfer. It is therefore important that the evaporation rate prior to skin or crust formation be accurately estimated.

It is evident from industrial spray processes that a greater % of volatile loss occurs immediately after atomisation, i.e. at higher OT and Re numbers. It is important to note that materials which adhere to the surface of a drop or provide

surface rigidity, e.g. polymers or binders, could be used to further reduce mass transfer rates and to reduce flavour loss. They may also improve particle attrition or friability and prevent particle inflation.

7.9 *Limitations of The "OT Number"*

The OT number is based on the simplifying assumption that drop viscosity and surface tension are not highly sensitive to slight changes in temperature, and that at Re≥500 turbulence persists right up to the surface of the droplet. The correlation has been validated experimentally over the following ranges:

Re: 500 to 2500

d_e: 1.00 to 5.00 mm

However, the mechanisms of droplet behaviour at higher velocities and drop diameter < 1.0 mm are thought to be similar to that observed in the present study.

In liquid spray processes, droplet diameter does not remain constant. There is also considerable back-mixing or vertical recirculation of air rather than the straight line flow assumed in the above model. Although the exact degree and nature of this back-mixing are usually not known and are difficult to account for in calculations of evaporating times, when mixing takes place the droplet is exposed to a parallel flow of fast-moving air in the vicinity of the nozzle with the velocity of the enhanced air diminishing with increasing axial distance. The movement of droplets following release from a centrifugal pressure nozzle is two-dimensional in parallel air flow, or three dimensional in rotary air flow. The entrainment effect assists rapid spray evaporation by creating intimate spray air contact, enhanced drop oscillation, and also maintains droplet velocity well in excess of droplet terminal velocities with the result that mass transfer rates are altered compared with prediction. However, the above approach serves a useful purpose in providing a method whereby the important transport variables are

examined. These are air initial velocity, droplet size, droplet density, surface tension and viscosity.

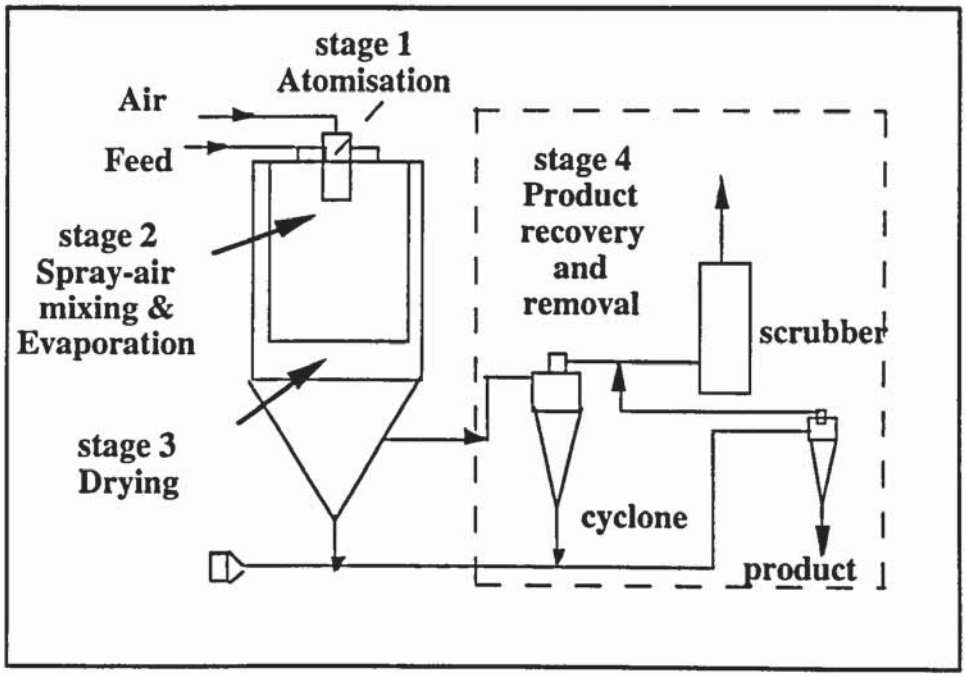

Figure 7.7 A co-current open-cycle spray dryer.

CHAPTER EIGHT

CONCLUSIONS AND RECOMMENDATIONS FOR FUTURE WORK

Heat and mass transfer rates to, and from, single drops have been successfully investigated by freely suspending individual drops (approximately 5 mm diameter) of a range of pure liquids in an air stream in a Vertical Wind Tunnel. This was achieved by inversion of the air velocity profile such that the turbulence generated simulated conditions within industrial equipment, especially those used for evaporative spray processes. A method of accounting for the effects of oscillation has been developed which does not rely solely upon empirical expressions and should therefore facilitate prediction of mass transfer rates in a variety of situations.

Specific Conclusions:

The following major conclusions arise from this study:

1) The Vertical Wind Tunnel was satisfactory for studying liquid droplets at Re>=500. Drops could be suspended for residence times up to 10 min. The camera speed of 1/10000 sec provided sharp images whilst the electrically-controlled injector achieved droplet repeatability within 2% maximum deviation in weight. However, droplets at Re<500 could not be studied with the apparatus, because the centrifugal fan, (see Figure 5.1) of the Vertical Wind Tunnel was of fixed speed and at Re<500 the droplet was carried away by the air stream. The Vertical Wind Tunnel was not equipped with any device that would continuously measure the surface temperature gradient of individual drops in free-flight; consequently, it was not ideal for drop drying studies. Once a drop of a slurry or suspension is evaporated beyond saturation, the surface temperature no longer approximates to that of the wet-bulb since heat is then transferred within the drop by

conduction at a rate which is a function of crust thickness. The temperature gradients within the drop upon which heat transfer calculations for drying studies could be based must then be experimentally determined.

2) Liquid drops in free-flight at Re>500 experienced oscillation, i.e. they had mobile surfaces across which turbulent eddies, by transmission of shear stress, caused extension in surface area and internal circulation. The extended surface area was not uniformly-distributed; consequently, such oscillations produced interfacial turbulence, which thinned the boundary layer and increased mass transfer rates, about 50% above those predicted by Ranz-Marshall in Equation 7.56. i.e.

$$Sh = 2 + 0.6Re^{0.5}Sc^{0.33}.$$

Droplet oscillation was random and not symmetrical; hence, no simple correlation of drop frequency of oscillation could be determined. The amplitude of oscillation and mass transfer coefficients, however, increased in proportion to drop diameter, indicating that for oscillating drops the larger the drop the greater the degree of oscillation and the effects on mass transfer rates.

3) The forces responsible for drop oscillation and internal circulation were: the dynamic pressure force of the gas stream, wake shedding behind the droplet, and surface tension and viscous forces within it. Their relative contributions, considered in Section 7.5, are characterised by the OT number given as:

$$OT = \left(\frac{\rho_a v_a^2}{\mu_d}\right).d_e^{1.5}\sqrt{\left(\frac{\rho_d}{\sigma}\right)}$$

This correlation suggests that interfacial convection is transferred by continuity of stress to the adjoining sublayers such that drop oscillation is inevitably accompanied by internal circulation. The Sh number was correlated incorporating the OT-number as:

$$Sh = 2 + 0.02OT^{0.15}Re^{0.88}Sc^{0.33}$$

The heat transfer rate was correlated by analogy and corrections were made for sensible heat loss using the Spalding number. i.e.

$$Nu(1 + B)^{0.7} = 2 + 0.02OT^{0.15}Re^{0.88}Pr^{0.33}$$

4) Variations in the drag coefficient with Reynolds number were correlated by:

$$C_D = 0.237.\left(\frac{Re}{P^{0.13}}\right)^{1.55}\left(\frac{1}{We.P^{0.13}}\right)$$

to within ±5% maximum deviation. Correlated drag coefficients were larger than for rigid spheres of equivalent diameter by about 50%. The difference was attributed to drop shape oscillation which complicated drop motion.

5) For liquid drops doped with 0.001 wt/wt surface active agent, drop size, internal circulation and drop shape oscillation were reduced. The mass transfer rates were also decreased by 40% confirming the enhancement of mass transfer by drop oscillation.

General Conclusions:

Whereas the frequency of drop oscillation could not be quantitatively correlated, this study shows that a description of evaporation from drops in free-flight based upon sound scientific principles can lead to a better understanding of drop hydrodynamics than studies based upon drops supported on a suspension device. In addition, it shows that drop physical properties play a greater role in droplet evaporation than previously thought by earlier workers. Whilst a mathematical model based on the perturbation theory to predict drop oscillation frequency as a function of operating parameters and drop physical properties would be of practical value, it seems likely that some form of empirical correlation will always remain in use until better understanding is gained of the complexity of drop hydrodynamics and turbulence in mass transfer processes. This study has provided an improved understanding of the mechanisms of mass transfer from oscillating droplets and their effects on mass transfer rates.

RECOMMENDATIONS FOR FURTHER WORK

With the existing apparatus.

(1) The effect of turbulence intensity on drop oscillation and on heat and mass transfer mechanisms could be further investigated. Turbulence is characterised by fluctuations which are continually mixing, fragmenting, disappearing and reforming. The intensity of this fluctuation could be measured by relating the magnitude of the "velocity fluctuation" (i.e. the root-mean-square value, $\sqrt{\acute{u}^2}$) and its scale, which is a statistical measure of the eddies. The ratio $\sqrt{\acute{u}^2}/U$, where U is the free stream velocity, gives the intensity of turbulence. This can be measured by means of a hot wire anemometer. Such a study would be useful in testing the bases for the proposed correlation. i.e. the effect of

turbulence and wake shedding on drop oscillation. It may also be useful in predicting the frequency and amplitude of drop oscillation by integrating the force field generated by turbulence over the drop surface.

(2) The interesting phenomena of crystallisation summarised in section 6.4 would be worthy of further study. Further work could also be carried out on the effect of polymers or surface binders on drop oscillation in relation to product morphology and flavour retention. It is estimated that about 60% of flavour loss occurs immediately after atomisation, at a period when drop oscillation is rife. Polymers such as polyethylene glycol may provide surface rigidity and help reduce flavour loss.

With an improved apparatus.

(1) The effects of drop oscillation on skin formation around drops containing dissolved substances could be investigated. In many drying processes, the mechanism of moisture movement after skin or crust formation is crucial in determining the drying rate and the quality of the product. A skin or crust around a drop may trap moisture in the interior of the droplet and present a barrier to mass transfer (Oteng-Attakora[169]). The effect, if any, of oscillation during this period in completely unknown. The present apparatus could be improved to accommodate such a study and to measure droplet surface temperature gradient by fitting an infra-red temperature sensor focused on the drop under study. Materials to study should include skimmed milk and custard.

(2) Finally, a theoretical study could be carried out using computational fluid dynamics, incorporating droplet oscillation to predict drop trajectory, residence time and evaporation rates. Sharma[176] used the following

assumptions, beside others, to produce a model to predict drop trajectory, residence time and evaporation rates:

(i) a rigid porous crust is formed immediately upon commencement of drying (i.e. no constant rate period),

(ii) the drops constituting the spray are spherical and experience no change in shape and size during drying.

However, these assumptions are invalidated immediately after atomisation.

The use of multi-nozzle dryers is commonplace in industry, and the shear force and turbulence in the vicinity of the atomiser are such that higher initial mass transfer rates are experienced due to drop oscillation. Therefore, for a rigorous spray dryer model, droplet oscillation must be incorporated for Re>500 and before skin or crust formation.

NOMENCLATURE

Symbols used in this thesis have the meaning listed below unless stated otherwise in the text.

A	=	surface area (m^2)
a_1	=	$(R_p^2 h_c k_{tc})/[\rho_{co} x(\lambda - C_c)]$
a_2	=	$(k_{tc} - R_p h_c)$
a_3	=	$R_p h_c$
a_4	=	$(C_{pc})/[3x(\lambda - C_c)]$
A_e	=	equivalent surface area of sphere of same volume (m^2)
A_f	=	cross sectional area of equivalent sphere (m^2)
Amp	=	amplitude of oscillation (m)
B_M	=	mass ratio defined by $B_M = \frac{(x_{vs} - x_{vo})}{(1 - x_{vs})}$
b	=	empirical amplitude coefficient defined in Equation 3.28.
b_1	=	$[R_p(R_p - z)k_G]/D_{eff}.z$
b_2	=	$D_{eff} - R_p k_G$
b_3	=	$R_p k_G$
C_1	=	correlation constant
C_{Ai}	=	concentration of A at interface ($kmol/m^3$)
Co, Ci	=	initial concentration ($kmol/m^3$)
$C\alpha$, C_∞	=	concentration of solute in gas stream ($kmol/m^3$)
C_c	=	heat of crystalisation per mass of water evaporated (J/kg)
C_D	=	drag coefficient
C_{DM}	=	drag coefficient of drop undergoing mass transfer
C_{do}	=	drag coefficient for a sphere
C_{fp}	=	drag coefficient of a flat plate.
C_p	=	heat capacity (J/kg.K)
C_{pd}	=	heat capacity of drop (J/kg.K)
C_{pc}	=	heat capacity of crust (J/kg.K)
c_S	=	humid heat (kJ/kg)
C_s	=	concentration of solute at drop surface ($kmol/m^3$)
C_{sol}	=	electrochemical species concentration.
d	=	jet diameter
D	=	dimensional diameter of a sphere (m)
d_c	=	crust diameter
d_e	=	diameter of droplet of equivalent volume of a sphere
D_{eff}	=	effective diffusivity coefficient (m/s)

d_h, a = equitorial dimensional length (m)

d_{max} = length of major axis, (m).

d_{min} = length of minor axis, (m).

d_p = bubble diameter, (m).

D_p = particle diameter (m)

d_v = vertical dimensional length, (m)

D_v = molecular diffusivity coefficient (m^2/s)

e = number of electrons

E = eccentricity; ratio of semi-major and semi-minor axes.

E_d = eddy diffusivity (m^2/s),

E_r = evaporation rate (kmol/s)

E_T defined as $E_T = \frac{mC_p}{4\pi k_v}$,

E_v = evaporation (kg)

F = Faraday current

f_n = natural frequency of oscillating (Hz)

f_N = droplet oscillation fequency (Hz)

f_D = drag force (N)

F_t,F_t1 = designated wind factors

G = gas flow rate

g = gravitational constant (m/s^2)

h = combined heat transfer coefficient due to convection and radiation

h = height of hemispherical segment, Equations 4.7 to 4.9.

H = humidity of continuous phase

h_c = convective heat transfer coefficient (W/m^2-K)

H_d = down stream humidity

h_r = radiant heat transfer coefficient (W/m^2K)

ΔH = humidity gradient defined as ($\Delta PM_w/\rho_a RT$)

Hs = humidity at saturated surface

Hu = upstream humidity

J_D = Colburn factor for mass transfer

k = thermal conductivity ($W/m^2.K$)

k_d = thermal conductivity of drop ($W/m^2.K$)

k_v = heat capacity of vapour

k_{tc} = thermal coefficient of crust (W/m.k)

K = correlation factor

k_c = mass transfer coeficient defined by (N_A/C_{Ai}-Cα)

k_G, = gas film transfer coefficient (m/s)

L = length of jet

l = wavelength

l_{opt} = optimum wavelength for liquid disintegration

m = mass of drop (kg)

M^1 defined as $M^1 = 1 - 0.4(1 - T_s/T_a)$

m_o = initial mass of drop (kg)

M_w = molecular weight (kg mol/kmol)

N defined as $N = 1 - 0.4\left(1 - \ln\frac{(1 + B^1)}{B^1}\right)$

N_A = mass flux (kmol/m^2.s)

N_{AO} = mass flux at natural convection (kmol/m^{2}s)

Np = number of profiles of drop

OD = oscillation number defined as $OD = (\pi\mu_d d_e/\sigma T^1)$

p = pressure (N/m^2)

Pa = outer pressure of continuous phase on droplet surface (N/m^2)

P_c = vapour pressure of water at core interface (N/m^2)

p_1 = partial pressure of vapour in gas stream (N/m^2)

Pi = pressure inside of the droplet defined as change in energy per unit volume. (N/m^2)

p2 = saturated vapour pressure (N/m^2)

Ps = pressure on droplet surface due to surface tension forces (N/m^2)

Q_f = heat flux (W/m^2.s)

q = wave growth rate

q_{rad} = heat transfer due to radiation (W)

R = Universal gas constant (J/kg mol K)

R^1 = resistance to mass transfer

r_1 = radius of evaporating sphere

r_2 = radius of the outside of the film of gas

R_e = external drop radius

r_e = radius of drop of equivalent spherical volume

R_o = jet orifice radius

R_p = Particle radius (m)

s = rate of surface renewal

s = free drop surface, Equations 4.7 to 4.9

s_b = specific surface area

t = time

T = temperature (K)

T^1 = period of oscillation

T_a = air temperature (K)

T_{amb} = ambient temperature (K)

T_c, T_z = core temperature of droplet (K)

T_g = gas temperature (K)

T_{tot} = time for complete evaporation

tr = transfer area

T_s = droplet surface temperature (K)

T_m = mean temperature within drop(K)

T_∞ = average temperature of continuous phase (K)

Tu = turbulent intensity defined by $Tu = \frac{1}{3}\frac{\sqrt{(\bar{v}_z'^2 + \bar{v}_r'^2 + \bar{v}_\theta'^2)}}{\bar{v}}$

u = drop velocity (m/s)

$\bar{v}$ = time smooth velocity (m/s)

$\bar{v}'$ = velocity fluctuation(m/s)

v = velocity of continuous phase (m/s)

u_∞ = velocity at far upstream (m/s)

V = volume of droplet (m^3)

v_a = air velocity (m/s)

v_{int} = internal velocity of circulating drop (m/s)

v_t = terminal velocity of droplet (m/s)

W = weight of water evaporated (kg)

x = mass fraction of water, falling distance of drop.

x_{vs} = mass fraction of vapour at droplet surface

x_{vo} = mass fraction of vapour in continuous phase

x_w = fractional evaporation of drop

x_{ws} = fractional evaporation per distance

x_p defined as $x_p = \left[\frac{1}{C_D}\left(\frac{4}{3}\frac{(\rho_l - \rho_a)g}{\rho_a}\right)\right]^{1/2}$

y = distance perpendicular from surface, Equation 3.4

Y = path or length of penetration of drop

z = plane within particle.

Z defined as $Z = \frac{k_a C_p}{k_v}\Delta T$

GREEK SYMBOLS

α = thermal diffusivity(m^2/s)

β = correlation index

β_1 = defined as $\left[\left(\frac{\mu_a^2}{\mu_d \rho_a}\right)\left(\frac{\rho_d}{\sigma d_e}\right)^{0.5}\right]^{0.15}$

β_2 = defined as $\left(\frac{12.\Delta P.M_w}{d_e \rho_d RT}\right)$

τ = shear force at droplet surface (N/m^2)

τ_{zx} = flux of x-directed momentum ($kg.m/m^3$)

∂ = boundary layer thickness defined as (z_1-z_2)

∂_h = hydrodynamic boundary layer thickness.

∂_c = concentration boundary layer thickness

∂_T = thermal boundary layer thickness

θ = dimensionless time , Equation 7.46

$\partial\theta$ = elapse time

σ = surface tension (N/m)

$\sigma\Sigma$ = Boltzmans constant

ρ_l = density of liquid (kg/m^3)

ρ^1 = vapour density(kg/m^3)

ρ_{co} = density of wet core (kg/m^3)

ρ_d = density of droplet (kg/m^3)

ρ_a = density of air (kg/m^3)

λ = latent heat of vaporisation (kJ/kg)

ν = dynamic viscosity (Nsm/kg)

μ_a = viscosity of air (Ns/m^2)

μ_c = viscosity of continuous phase (Ns/m^2)

μ_d = viscosity of droplet (Ns/m^2)

ω = correlation constant

γ = drag coefficient ratio of a flat plat and a sphere

η = amplitude of disturbance

ε = amplitude of surface stretch

ε_o = dimensionless constant defined as $\varepsilon_o = \varepsilon + \frac{3}{8}\varepsilon^2$

ε_1 = crust porosity

φ = probability function defined as $\varphi = se^{-st}$

φ = correlation index, Equation 7.43 and Table 7.2

η_o = initial amplitude of oscillation

ψ defined as $\psi = K.\left[\left(\frac{\mu_a^2}{\mu_d \rho_a}\right)\left(\frac{\rho_d}{\sigma.d_e}\right)^{0.5}\right]^{0.15} Sc^{0.33}$

ψ_1 = crust thickness(m)

ψ_m = surface mass injection ratio.

ψ_p = drop internal motion

DIMENSIONLESS GROUPS

Ar	=	Archimedes number defined by $(C_D Re^2)$
B	=	Spalding number defined by $(Cp\Delta T/\lambda)$
B^1	=	Heat transfer number defined by $B^1 = \dfrac{C_p \Delta T}{\left(\lambda - \dfrac{q_{rad}}{N_A}\right)}$
E_o	=	Eotvos number defined by $\left(\dfrac{\Delta\rho g d_e^2}{\sigma}\right)$
Gr	=	Grashof number defined by $\left(\dfrac{(\beta g)\Delta T D^3 \rho^2}{\mu^2}\right)$
M	=	Morton number defined by $\left(\dfrac{g\Delta\rho\mu^4}{\sigma^2 d_e^2}\right)$
Nu	=	Nusselt number defined by $\left(\dfrac{h_c d_e}{k}\right)$
Nu_o	=	Nusselt number at natural convection conditions.
Oh_d	=	Ohnesorge number defined by $\left(Oh_d = \dfrac{\mu_d}{(\rho_d d_e \sigma)^{1/2}}\right)$
OT	=	Oteng-Attakora number defined by $\left(\left(\dfrac{\rho_a v_a^2}{\mu_d}\right).d_e^{1.5}\sqrt{\left(\dfrac{\rho_d}{\sigma}\right)}\right)$
P	=	Property group defined by $\left(\dfrac{\rho^2\sigma^3}{g\mu^4(\rho_l - \rho_a)}\right)$
Pr	=	Prandtl number defined by $\left(\dfrac{Cp\mu}{k}\right)$
Re	=	Reynolds number defined by $\left(\dfrac{\rho v d_e}{\mu}\right)$
Re_{int}	=	Internal Reynolds number of droplet defined by $\left(\dfrac{\rho_d d_e}{\mu_d}\sqrt{\dfrac{\tau}{\rho_d}}\right)$.
Sc	=	Schmidt number defined by $\left(\dfrac{\nu}{D_v}\right)$
Sh	=	Sherwood number defined by $\left(\dfrac{k_G d_e}{D_v}\right)$
Sh_o	=	Sherwood number under natural convetion conditions
Sr	=	Strouhal number defined by $(f_N d_e/v)$
We	=	Weber number defined by $\left(\dfrac{\rho v^2 d_e}{\sigma}\right)$

REFERENCES

1. Masters, K., (1992), "Handbook Of Spray Drying", 4-481. Pitman Press.

2. Frossling, N.,(1963), "On The Evaporation of Falling Drops". AERE Harwell Translation, 1970.

3. Ranz, W.E., Marshall W.R.(1957), "Evaporation Of Drops". Chem. Eng. Prog. 48, 3, 141.

4. Mujumdar, S.M., Hosseinalipur, B. (1994), "Flow and Thermal Characteristics of Opposing Turbulent Jets. Drying '94. Proc. 9th Int. Drying Symp. Gold Coast. Australia. B 1369

5. Weber C. (1931), Angew Math. Mech. 11. 136-154.

6. Ohnesorge, G. (1936), Angew Math. Mech. 16, 355.

7. Hinze, J.O.(1955), "Fundamentals Of The Hydrodynamic Mechanisms of Splitting in Dispersion Process". A.I.Ch.E, 1, 3, 289-295.

8. Holfelder, O. (1932), "On Fuel Atomisation in Diesel Engines," Forsch Geb. Ingenieurwesens A, 3.

9. Haelein A, (1931), "On the Disruption of Liquid Jets." Forsch Geb. Ingenieurwesens A, . 2, 4.

10. Dombrowski, Johns, W.R., (1963),"The Aerodynamic Instability and Disintegration of Viscous Liquid Sheets". Chem. Eng. Sci., 18, 203-214

11. Fraser, R.P. and Dombrowski, N. (1962), "Drop Formation from Rapidly Moving Sheets". A.I.Ch.E. pp. 672-680.

12. Castleman, R.A. Jr.(1931). "The Mechanism of Atomisation of Liquid". Bureau of standard Journal of Research. 6. 281.

13. Pham Q. I and Keey R.B.(1977), "Experiments on the Residence -Time Distribution of Droplets in a Co-current Spray Chamber". Can. Jr. Chem. Eng. 55. 466.

14. Lane W.R.(1951), "Shattering of Drops in Streams of Air". Ind. Engng Chem. 43, 1312-1317.

15. Morrell, G., (1961). "Critical Conditions for Drop and Jet Shattering", NASA TN D-677.

16. Hanson, A.R., E.G. Domich and H.S. Adams, (1963). "Shock Tube Investigation of the Break-up of Drops by Air Blast", Phys. Fluid, 6, 1070-1080.

17. Rabin, E. Schllenmuller A.R. and Lawhead, (1960). "Displacement and Shattering of Propellant Drops". AFOSR TR 60-75 (AD241473).

18. Klusener, O.(1933), "The Injection Process in Compressionless Diesel Engines". Z.V.D.I. 77, No.7

19. Hinze, J.O. (1949), "Forced Deformation of Viscous Liquid Globules". Appl Sci. Res. A1, 263.

20. Blanchard, D.C., (1950), "The Behaviour of Water Drops at Terminal Velocity in Air". Trans. Am. Geophys. Union, 31, 836.

21. Srikrishna, M., Siviji, K., Narasimhamurty, G.S.R., (1982), "Mechanics of Liquid Drops in Air". Chem. Eng. J., .24, 27-34.

22. Akbar,S.(1988), "A Study of The Drying of Single Droplets in Free-Flight". PhD. Thesis, Aston University. Birmingham. U.K.

23. Garner, F.H and Lane, J.J.(1959), "Mass Transfer to Drops of Liquid Suspended in a Gas Stream". Trans. Inst. of Chem. Eng., 37, 155, 162-172.

24. Constan, G.L. and Calvert, S.(1963), "Mass Transfer from Drops Under Conditions that Promote Oscillation and Internal Circulation". AIChE. 9, 1, 109-115.

25. Green, A.W.,(1975), "An Approximation for the Shapes of Large Rain Drops", J. Applied Meteor., 14, 1578.

26. Hendrix, C.D., Dave, S.B., and Johnson, H.F.,(1967), "Translation of Continuous Phase in the Wakes of Single Rising Drops"AIChE J. 13, 1072-1077.

27. Gunn, R.J. (1949), Geophysics Res., 54. 383-385.

28. Grace, J.R., Wairegi, T., and Nguyen, T.H.,(1976), "Shapes and Velocities of Single Drops and Bubbles moving Freely Through immiscible Liquids". Trans Inst. Chem. Eng. 54, 167-173.

29. LeClair, B.P., (1972), "A Theoretical and Experimental Study of The Internal Circulation in Water Drops falling at Terminal Velocity In Air", J. Atmos. Sci., 29, 728-740.

30. Magono, C., (1954), "On The Shape of Water Drops Falling in Stagnant Air". J. Meteorology, 1.1, 77-79.

31. McDonald, J.E., (1958), "The Shape and Aerodynamics of Large Rain Drops". J. Metero. 11, 478.

32. Hadamard, J.S., (1911), C.R. Acad. Sci. 152. p.1735-1738.

33. Rybczynski, W.,(1911), Bull. Int. Acad. Pol. Sci. Lett., Cl.Sci.Math. Nat., Ser. A. 40-46.

34. Bond, W. N. and Newton D.A.(1928), "Bubbles Drops and Newton's Law", Phil. Mag., 5, 794-800.

35. Garner, F.H. and Skelland A.H.P., (1955), "Some Factors affecting Droplet Behaviour in Liquid-Liquid Systems". Chem.Eng.Sci. 4, 149-158.

36. Garner, F.H. and Hammaerton, D., (1954), "Circulation Inside Gas Bubbles". Chem. Eng. Sci. 3, 1-11.

37. Harpel, J.F., Moore, D.W. and Pearson, J.R.A.,(1967), "The Effect of the Variation of Surface Tension with Temperature on the Motion of Bubbles and Drops".J.Fluid Mech. 27, 361-366.

38. Boussinesq, J.C.R.(1913) Acad. Sci. 156, 1124-1130.

39. Frumkin, A. and Levich, V. G., (1949), Zh. Fiz. Khim. 21, 118-1204.

40. Redfield, J.A. and Houghton, G.(1965), "Mass Transfer and Drag Coefficients for Single Bubbles at Reynolds Numbers of 0.02-5000". Chem. Eng. Sci. 20, 131-139.

41. Oseen, C.W., cited in Massey, B.S.,(1970), Mechanics of Fluids, 293, City Press Ltd.

42. Kalra, T.R., and Uhlherr, P.H.T.,(1971), Proc. 4th. Aust. Conf. Hydraul. Fluid Mech., Melbourne.

43. Clift, R. Grace, R. E. and Weber M.E.,(1978), Bubbles, Drops and Particles, 102. Academic Press.

44. Teneda, S., (1956), "Experimental Investigation of the Wakes Behind a Sphere at Low Reynolds Numbers". Phys. Soc. Jpn. 11, 1104-1108.

45. Goldburg, A., and Florsheim, B.H.,(1966), Phys. Fluids 9, 45-50.

46. Seeley, L. E., Hummel, R.L., and Smith, J.W.,(1975), "Experimental Velocity Profiles in Laminar Flow around Spheres at Intermediate Reynolds numbers". J. Fluid Mech. 68, 591-608.

47. Spilhaus, A.F.,(1948), J. Meterol. Vol.5., 108.

48. Narasimhamurty, G.S.R., (1955), The Motion of Deformable Bodies in Fluids, Trans. Ind. Inst. chem. Eng. Vol. 7, Part II, 123-128.

49. Finlay, B.A.,(1957), "A Study Of Liquid Drops In An Air Stream". PhD. Thesis, University of Birmingham.

50. Ingebo, P.D. (1962), 8th Symposium on Combustion, 104, Williams and Willeins.

51. Eisenklam, P., Weston, J.A. and Arunachalam, S.A.,(1967), 11th Int. Symp. on Combustion, Pittsburgh, Pennsylvania.

52. Chuchottaworn, P., Fujinami, A. and Asano, K.,(1983), "Numerical Analysis of the Effect of Mass Injection or Suction on Drag Coefficients of a Sphere"J. Chem Eng. Japan. 16. 18.

53. Chuchottaworn, P., Asano, K., (1985), "Calculation of Drag Coefficient of an Evaporating or a Condensing Droplet". J. Chem. Eng. Japan, 18, 91.

54. Morimoto, M., Chuchottaworn, P., Fujinami, A. and Asano, K., Proc. 3rd Int. Conf. on Liquid Atomisation and Spray Systems.(ICLASS-85), Imperial College, London.

55. Beek, W.J. and Muttzall, M.K.(1980), "Transport Phenomena", 55-58. John Wiley and Sons Ltd.

56. Davies, J.T.,(1972), "Turbulence Phenomena", 128. Academic Press.

57. Bird, B.R., Stewart, W.E. and Lighfoot, E.N., (1960), "Transport Phenomena", 140. Wiley International Edition. John Wiley and Sons Inc.

58. Sherwood, T.K., Pigford, L.R. and Wilke, R.C., (1975), "Mass Transfer", 103-129. Internal Student Edition. McGraw-Hill Inc.

59. Nernst, W.Z.,(1904), Z. Phys. Chem. 47:52.

60. Whitman, W.G. and Lewis, W. K.,(1924), Absorption Symposium, "Principles of Gas Absorption". Ind, Eng. Chem., 16. 1215.

61. Higbie, R.,(1935), "The Rate of Absorption of a Pure Gas into a Still Liquid During Short Periods of Exposure". Trans. AIChE., 31, 365.

62. Gilliland, E.R. and Sherwood, T. K., (1934), "Diffusion of Vapours into Air Streams". Ind. Eng. Chem., 26, 516.

63. Vivian J.E. and King C.J.,(1964), "Diffusivities of Slightly Soluble Gases in Water". AIChE, 10. 221.

64. McManamey, W.J., Davies J.T., Woollen, J.M. and Coe J.R.(1973), "The Influence of Molecular Diffusion on Mass Transfer Between Turbulent Liquids". Chem. Eng. Sci., 28, 1061.

65. Brunson, R.J. and Wellek, R.M., (1970), "Mass Transfer within Oscillating Liquid Drops". Can. Chem. Eng., 48, 267.

66. Angelo, J.B., Lightfoot, E.N. and Howard, D.W.,(1966), "Generalisation of the Penetration Theory for Surface Stretch: Application to forming and Oscillating Drops" AIChE, 12. .4. 751-759.

67. Handlos, A.E. and Baron, T.,(1957), "Mass and Heat Transfer for Drops in Liquid-Liquid Extraction". AIChE, 3. 1. 127-136.

68. Orlander, D.R.,(1966), "The Handlos-Baron Drop Extraction Model". AIChE. 12. 1018.

69. Patel, J.M. and Wellek, R.M.,(1967), "Handlos and Baron Model: Short Contact Times". AIChE, 13., 384.

70. Dankwerts, P.V.,(1951), "Significance of Liquid-Film Coefficients in Gas Absorption". Ind. Eng. Chem., 43, 1460.

71. Marchello, J.M. and Toor, H.L.,(1963), "A Mixing Model for Transfer Near a Boundary". Ind. Eng. Chem. Fund., 2, 8.

72. Lewis, J.B.,(1953), "Liquid-Liquid Extraction; Part VIII, The Extraction of Uranyl Nitrate in a Wetted Wall Column". Trans. Inst. Chem. Eng., 31, 323, 325.

73. Lewis, J.B. and Pratt, C, R.,(1953), Nature, 171, 1155.

74. Sternling, C.V. and Scriven, L.E.,(1959), "Interfacial Turbulence: Hydrodynamic Instability and the Marangoni Effect". AIChE., 5, 4, 514-523

75. Sawistowski, H, "Interfacial Phenomena", (1971), Recent Advances in Liquid-Liquid Extraction, 293. (Edited by Hanson, C.)Pergamon Press.

76. Ruckenstein, E. and Suciu, D.G.,(1969), "Simulation of Physical Models for Turbulent Mass Transfer". Chem. Engng. Sci., 24. 1395-1397.

77. Ruckenstein, E.,(1963), "Some Remarks on Renewal Model". Chem. Engng. Sci., 18, 233.

78. Thompson, J., (1855), Phil. Mag., 4, 10, 330.

79. Marangoni, C., (1865), *Sull' espanione delle goccie di un liquido galleggiante sulla superficie di altro liquido*, Fusi, Pavia, (Cited in Recent Advances in Liquid-Liquid Extraction. Pergamon Press).

80. Marangoni, C.,(1871), Annln. Phys., 143, 337.

81. Sherwood, T.K. and Wei, J.C.,(1957), "Interfacial Phenomena in Liquid Extraction". Ind. Eng. Chem. 49, 1030.

82. Rose, R.M., and Kintner, R.C.,(1966), "Mass Transfer From Large Oscillating Drops". AIChE, 12, 530.

83. Schroeder, R.R., and Kintner, R.C.,(1965), " Oscillation of Drops Falling in a Liquid Field". AIChE, 11, 5.

84. Haberman, W. L. and Morton, R.R.,(1953), David Taylor Model Basin Report, 802.

85. Al-Hassan, T.S.,(1979), PhD. Thesis. Aston University, Birmingham.

86. Kintner, R.C.,(1963), Advan. Chem. Eng., 4, 51.

87. Sawistowski, H and Golz, G.E.,(1963), "The Effect of Interface Phenomena on Mass Transfer Rates in Liquid-Liquid Extraction". Trans. Inst. Chem. Eng. 41, 174.

88. Ellis, S.R.M. and Biddulph, M.(1966), "Interface Turbulence Measurements". Chem. Eng.Sci., 21, 1107.

89. Berg, J.C., and Acrivos, A., (1965), "The Effect of Active Agents on Convective Cells Induced by Surface Tension". Chem Engng. Sci., 20, 737.

90. Pearson, J.R.A.(1958), " On Convection Cells Induced by Surface Tension" J. Fluid Mech., 4, 489.

91. Plevan, R.E. and Quinn, J.A.(1966), The Effect of Monomolecular Films on the Rate of Gas Absorption into a Quiescient Liquid". AIChE, 12, 894.

92. Lindland, K.P. and Terjesen, S.G.,(1956), "The Effect of a Surface-Active Agent on Mass Transfer in Falling Drop Extraction". Chem. Eng. Sci. 5, 1.

93. Thompson, D.W., (1970), "Effect of Interfacial Mobility on Mass Transfer in Gas-Liquid Systems". Ind. Eng. Chem. Fundam., 9, 243.

94. Davies J.T., and Radiel E.K.,(1963), Advan. Chem. Eng. vol. 4. 1.

95. Davies, J.T.,(1972), "Turbulence Phenomena of Free Surfaces". AIChE, 18. 169.

96. Davies, J.T. and Haydon, D.A.,(1975). Proc. 2nd Int. Congr. Surface Activity, London. 1, 417.

97. Orell, A.and Westwater, J.W.,(1961), "Natural Convection Cells Accompanying Liquid-Liquid Extraction". Chem. Engng. Sci., 16, 127.

98. Orell, A. and Westwater, J.W.,(1962), "Spontaneous Interfacial Cellular Convection Accompanying Mass Transfer: Ethylene Glycol-Acetic Acid-Ethyl Acetate". AIChE. 8, 350.

99. Davies, J.T., and Rideal, E.K.(1963), Interfacial Phenomena. Academic Press, London and New York.

100. Maxwell, J.C.,(1890), Collection of Scientific Papers, Cambridge, 11, 625.(Cited in 118)

101. Srezvenski, V.,(1882), Zh.R.Ph.Kh, O. 14, 420.

102. Powell, R.W.,(1940), "Further Experiments on the Evaporation of Water From Saturated Surfaces". Transt.Inst. Chem Engnr. 36.

103. Lurie, M., and Michailoff, N.,(1936), "Evaporation from Free Water Surfaces". Ind. Eng. Chem., 28., 3, 345.

104. Mathers, W.G., Madden, A.J., Piret, E.L.,(1957), "Simultaneous Heat and Mass Transfer in Free Convection", Ind, Eng. Chem., 49, 961.

105. Tsubouchi, T. and Sato, S.,(1960), "Heat Transfer Between Single Particles and Fluids in Relative Forced Convection". Chem. Eng.Prog. Symp. Ser. 30. 285.

106. Yuge, T.,(1960), "Experiment on Heat Transfer From Spheres Including Combined Natural and Forced Convection". Trans. A.S.M.E., 82, Series C, 214.

107. Steinberger, R.L. and Treybal, R.E.(1960), " Mass Transfer From A Solid Soluble Sphere to a flowing Liquid stream" . A.I.Ch.E.J., 6, 2, 227.

108. Maisel, D.S., Sherwood, T.K.,(1950), " Evaporation Of Liquid Into Turbulent Gas Stream", Chem. Eng. Prog., 46, 3, 131.

109. Pasternak, I.S., Gauvin, W.H.,(1960), " Turbulent Heat & Mass Transfer from Stationary Particles". Can. J Chem Eng. 38, 35.

110. Pasternak, I.S., Gauvin, W.H.,(1961), " Turbulent Convective Heat & Mass Transfer from Accelerating Particles" A.I.Ch.E.J., 7, 254.

111. Rowe, P.N.M., Claxton, K.T. and Lewis, J.B.,(1965), " Heat and Mass Transfer from a Single Sphere in an Extensive Flowing Fluid". Trans. Inst. Chem. Engrs. 43, T-14-T31.

112. Skelland, A.H.P., Cornish, A.R.H.,(1963), " Mass Transfer From Spheroids to An Air Stream". A.I.Ch.E.J., 9, 1, 73.

113. Acrivos, A.,(1977), "Combined Laminar Free And Forced Convection Heat Transfer In Extended Flow". A.I.Ch.E.J. 4., 285.

114. Sandoval-Robles, J.G., Riba, J.P. and Couderc, J.P.,(1980), " Mass Transfer Around A Sphere". Trans. IChemE., 58, 132.

115 Sandoval-Robles, J.G., Delmas H, J.P. and Couderc, J.P.,(1981), "Influence of Turbulence on Mass Transfer Between a Liquid and a Solid Sphere". A.I.Ch.E.J 27, 5, 819.

116. Hughes, R.R., Gilliland, E.R.,(1952), "The Mechanics of Drops". Chem. Eng. Progr., 48, 497.

117. Langmuir, L.,(1918), Phy. Rev., 12, 368.

118. Fuchs, N. A., (1959), " Evaporation and Droplet Growth in Gaseous Media", Pergamon Press. London.

119. Ingebo, R.D.,(1952), "Vaporisation Rates and Heat-Transfer Coefficients For Pure Liquid Drops". Chem. Eng. Prog., 48, 403.

120. Bedingfield, C.H. Jr., Drew, T.B.,(1950), " Analogy Between Heat Transfer and Mass Transfer, A Psychrometric Study". Ind. Eng. Chem., 42, 6, 1164.

121. Morse, H.W., (1910). "Evaporation From The Surface Of A Solid Sphere"., Proc. Am. Acad. Sci., 45, 363.

122. Houghton, H.G.,(1933), " A Study Of The Evaporation of Small Water Drops". Physics, 4, 419.

123. Jeffreys, H., (1918), Phil. Mag. 35, 270.

124 Frazier, G.C.,(1977), "Water Droplet Vaporisation In Humid Atmosphere". Can. J. Chem. Engr,. 55, 678.

125. Duguid, H.A., Stampfer, J.F. Jr.,(1971), J. Atmos. Sci., 28, 1238.

126. Kinard, G.E., Manning, F.S., Manning W.P.,(1963), "A new Correlation for Mass Transfer from Single Spheres", Brit. Chem. Eng., 8, 326.

127. Garner, F.H., Suckling, R.D.,(1958), "Mass Transfer from a Soluble Solid Sphere". A.I.Ch.E.J. 4, 1, 114

128 Bose, A. K., Pei, D.,C. T., (1964), " Evaporation Rates in Spray Drying". Can. J., Chem. Eng., 42, 259.

129. Hsu, T.N., Sato, K., Sage, B.H.,(1954), "Material Transfer in Turbulent Gas Streams; Influence of Shape on Evaporation of Drops of n-Heptane". Ind. Eng. Chem., 46, 5, 870.

130. Audu, T.K.O.,(1973), "Studies of the Drying of Particulate Slurries", Ph.D. Thesis, University of Aston in Birmingham. England.

131. Hassan, H.M.,(1991), "Mechanisms of Drying of Skin Forming Materials, PhD. Thesis, University of Aston in Birminghan.

132. Woodland, D.J., Mack, E.,(1933), " Effect of Curvature of Surface on Surface Energy; Rate of Evaporation of Liquid Droplets, Thickness of Saturated Vapour films". J. Amer. Chem. Soc., 55, 3149.

133. Gudris, N., Kulikova, L.,(1924), Z. Physik., 25, 121.

134. Kinzer, G.D., Gunn, R.,(1951), "The Evaporation, Temperature and thermal Relaxation-Time of Freely Falling Water Drops". J. Meteor., 81. 71.

135. Jones, S.J.R. , Smith, W.,(1962), "Mass Transfer from Solids Freely Suspended in An Air Stream", Proc. Symp. Interaction Between Fluids and Particles. IChemE., London, 190.

136. Hattangady, K.S.,(1973), "Evaporation of Drops Into A High Pressure Gas Stream". Ph.D. Thesis, Birmingham University.

137. Garner, F.H., Lihou, D.A.,(1964), "Mass Transfer To and From Drops In Gaseous Streams". Dechma Monographien, 55, 155.

138. Miura, K., Miura.,T., Ohatani, S.,(1977), "Heat and Mass Transfer to and from Droplets". A.I.Ch.E. Symp. Ser. 73, 95.

139. Yao, S.C., Schrock, V.E. (1976), "Heat and Mass Transfer from Freely Falling Drops". Trans. ASME. Journal of Heat Transfer, Series C, 98, 120.

140. Ahmadzadeh, J., Harker, J.H.,(1974), "Evaporation of Drops in Free-Fall". Trans. Inst. Chem. Eng., 52, 1, 108.

141. Dloughy, J., Gauvin, W.H.,(1960), "Heat and Mass Transfer in Spray Drying", A.I.Ch.E.J. 6, 1, 29.

142. Dickinson, D.R., Marshall, W.R.,(1968), "The Rate of Evaporation of Sprays". A.I.Ch.E.J. 14, 4, 541.

143. Manning, W.P., Gauvin, W.H.,(1960), "Heat and Mass Transfer to Decelerating Finely Atomised Spray", A.I.Ch.E.J. 6, 184.

144. Marshall, W.R. Jr.,(1955), " Heat and Mass Transfer in Spray", Trans. A.S.M.E., 77, 1377.

145. Ranz, W.E.,(1956), " On The Evaporation of a Drop of Volatile Liquid in High-Temperature Surroundings", Trans. A.S.M.E., 78, 909.

146. Spalding, D.B., (1953), 4th Int. Symp. On Combustion, 847, Williams and Williams, Baltimore. Maryland.

147. Pei, D.C.T., Gauvin, W.H., (1962), " Natural Convection Evaporation From Spherical Particles in High-Temperature Surroundings", A.I.Ch.E.J., 9, 3. 375.

148. Maltosz, R.L., Leipziger, S., Torda, T.P.,(1972), "Investigation of Liquid Drop Evaporation in a High Temperature and Pressure Environment". Int.J. Heat & Mass Transfer, 15, 831.

149. Lee, K., Ryley, D.J.,(1968), " The Evaporation of Water Drops in Superheated Steam", ASME. Jl. of Heat Transfer, Series C, 90, 445.

150. Trommelen, A.M., Crosby, E.J.,(1970), "Evaporation and Drying of Drops in Saturated Vapours", A.I.Ch.E.J. 16, 5, 857.

151. Yuen, M.C., Chen, L.W.,(1978), "Heat Transfer Measurements of Evaporating Liquid Droplets", Int. J. Heat & Mass Transfer, 21, 537.

152. Renkzibulut, M., Yuen, M.C.,(1983), "Experimental Study of Droplet Evaporation in a High-Temperature Air Stream", J. Heat Transfer. 105, 385.

153. Shepherd, C.B., Hadlock, C., Brewer, R.C.,(1938), "Drying Materials in Trays; Evaporation of Surface Moisture" Ind. Eng. Chem., 30, 388.

154. Geankoplis, C.J.,(1978)., "Transport Process and Unit Operations", 527. publ: Allan and Bacon Inc.

155. Harmathy, T.Z.,(1969), "Simultaneous Moisture and Heat Transfer in Porous Systems with Particular Reference to Drying", Ind. Eng. Chem. Fund., 8, 92.

156. Cheong,H.W., Jeffreys, G.V., Mumford, C.J.,(1986), "A Receding Evaporation Interface Model for the Drying of Slurry Droplets", A.I.Ch.E.J. 15, 5, 1334.

157. Audu, T.O.K., and Jeffreys, G.V.,(1975), "The Drying of Drops of Particulate Slurry". Trans. I.Chem.E., 53, 165-172.

158. Esubiyi, A.O.,(1980), "Drying of Portland Cement Raw Material Slurries", PhD. Thesis, University of Aston in Birmingham. England.

159. Khan, A.R., Richardson, J.F.,(1987), "The Resistance to Motion of a Solid Sphere in a Fluid". Chem. Eng. Commun., 62, 135.

160. Fuller, E.N., Schettler, P.D., Giddings, J.C.,(1966), "A New Method for Prediction of Binary Gas-Phase Diffusion Coefficients". Ind. Eng. Chem., 58, 5, 19.

161. Oteng-Attakora, G., Walton, D.E., Mumford, C.J.,(1994), " Enhanced Heat and Mass Transfer of Oscillating Droplets Under Forced Convection". IChemE Research Event, 2, 1056.

162. Walton, D.E.,(1994), "The Morphology of Spray-Dried Particles", Ph.D. Thesis, University of Aston in Birmingham. England.

163. Lord Rayleigh (1931), The Proceedings of London Mathematical Society, 10, 4.

164. Griffith, R.M., (1960), "Mass Transfer From Drops and Bubbles", Chem. Eng. Sci., 12, 198-213

165. Davies, J.T., (1960), "The Importance of Surfaces in Chemical Engineering". Trans. Inst. Chem. Engrs.(London), 38, 289.

166. Zlokarnik, M., (1991), "Dimensional Analysis and Scale-up in Chemical Engineering". Springer-Verlag".

167. Wallis, G.B., (1974), "The Terminal Speed of Single Drops Or Bubbles in an Infinite Medium". Int.J. Multiphase Flow, 1, 491.

168 Oteng-Attakora, G., Mumford, C.J., Smith, E.L., (1994), "Mechanism of Droplet Oscillation; Effect on Mass Transfer". Proc. 9th Int. Drying Symp. (Australia), A, 375.

169 Oteng-Attakora, G., (1994), "Evaporation from Droplets in Free-Flight; Effect of Skin-Forming Materials". IChemE Research Event, 2, 477.

170 Yen, Y.C., Thodos, G., (1962), "Mass, Heat, and Momentum Transfer in the Flow of Gases Past Single Spheres". A.ICh.E. J., 8, 34.

171 Linton, W., H., Sherwood, T. K., (1950), " Mass Transfer from Shapes to Water in Streamline and Turbulent Flow". Chem. Engng. Prog., 46, 258.

172 Garner, F.H., Grafton, R.W., (1954), Proc. R. Soc. A224, 64.

173 Calderbank, P.H., Johnson, S.L., Loudon, J. (1970), "Mechanisms and Mass Transfer of Single Bubbles in Free Rise through Some Newtonian and Non Newtonian Liquids". Chem. Eng. Sci., 25, 235.

174 Karamanev, D.G., (1994), "Rise of Gas Bubbles in Quiescent Liquids". A.I.Ch.E.J, 40, 8, 1418.

175 Johnson, A. I. Besic, F. and Hameilec, A. E., (1969). "Mass Transfer from a Single Rising Bubble". Can. J. chem. Eng., 47, 559.

176 Sharma, S., (1990), " Spray Drier Simulation and Air Flow Pattern Studies". Ph.D Thesis

177 Downing G.C.,(1966), "The Evaporation of Drops of Pure Liquid at Elevated Temperatures: Rates of Evaporation and Wet-bulb Temperatures" A.I.Ch.E.J., 12, 4, 760.

APPENDIX A

LIST OF APPENDIX A

METHOD OF ESTIMATING DROPLET WEIGHT

Individual drops collected using the Drop Collection Device were weighed on a Mettler AE50 chemical balance. The weight measurements were compared with the weight equivalent given by the product of the droplet volume (as calculted from measurement from the TV screen) and its density. Where there was a great variation in the two weights, possibly due to out-of-line measurements or splashing of the drop against the walls of the Drop Collection Device, the result was discarded. Droplet weight considered satisfactory were those within ±10% of measured and calculated weights.

Table A.1 **EVAPORATION OF DISTILLED DE-IONISED WATER DROPLETS IN FREE-FLIGHT AT 62°C**

AIR TEMP = 62°C, WET BULB = 32°C
humidity of air = 0.018 kg H_2O/kg air,
density of water=998kg/m^3. Latent heat = 2411.19kJ/kg
viscosity = 0.86E-03Pa.s. Surface tension = 0.072N/m
Cp = 4.16kJ/kg.K. B=0.0561, Ts = 32.75°C
Dv = 2.7E-05 m^2/s

Time(sec)	mass of drop (x E-03 kg)	Evap. rate (x E-06 kg/s)	Equiv. dia (x E-02 m)	Terminal Vel. (m/s)	OT number	OT^{15}
0	0.0972					
20	0.0881	0.3263	0.525	8.03	3597.25	3.42
40	0.0959	0.3043	0.508	7.94	3346.03	3.38
60	0.0715	0.2839	0.523	7.84	3404.08	3.39
80	0.0819	0.2648	0.474	7.75	2872.78	3.30
100	0.0703	0.2470	0.496	7.66	3003.38	3.32
120	0.0587	0.2304	0.471	7.58	2723.38	3.28
140	0.0651	0.2149	0.444	7.49	2430.73	3.22
160	0.0566	0.2005	0.460	7.41	2505.72	3.23
180	0.0475	0.1869	0.439	7.31	2274.45	3.19
200	0.0465	0.1743	0.414	7.23	2038.16	3.14
220	0.0456	0.1626	0.411	7.15	1974.38	3.12
240	0.0422	0.1517	0.408	7.07	1909.07	3.11
260	0.0436	0.1414	0.398	6.98	1791.41	3.08
280	0.0386	0.1320	0.402	6.90	1779.58	3.07
300	0.0354	0.1231	0.386	6.82	1635.90	3.03
320	0.0344	0.1148	0.371	6.74	1504.90	3.00
340	0.0319	0.1071	0.372	6.67	1476.55	2.99
360	0.0290	0.0998	0.362	6.57	1378.17	2.96
380	0.0245	0.0931	0.351	6.51	1291.77	2.93
400	0.0253	0.0868	0.332	6.44	1162.23	2.88
420	0.0205	0.0810	0.335	6.37	1154.81	2.88
440	0.0206	0.0755	0.313	6.27	1008.41	2.82
460	0.0171	0.0705	0.293	6.22	898.05	2.77

Sh number (Experimental)	Sh (preicted by OT model)	Sh (predicted by Ranz-Marshall	ln(dp) (m)	ln(kg) (m/s)	Re.No	$Re^{0.5}$
61.17	62.23	28.81	-5.249	-1.195	2376.01	28.81
58.98	55.49	28.36	-5.282	-1.198	2272.58	27.22
53.49	56.38	27.89	-5.254	-1.324	2308.53	27.42
55.01	50.15	27.44	-5.351	-1.199	2069.55	26.07
49.04	51.92	27.00	-5.306	-1.359	2140.12	26.47
48.14	48.59	26.58	-5.357	-1.326	2011.98	25.73
47.68	45.00	26.16	-5.417	-1.276	1872.57	24.89
42.97	46.11	25.75	-5.383	-1.414	1917.74	25.17
41.97	43.24	25.32	-5.429	-1.391	1806.01	24.48
41.50	40.16	24.92	-5.488	-1.344	1684.82	23.72
38.96	39.40	24.53	-5.494	-1.401	1655.61	23.53
36.62	38.61	24.15	-5.501	-1.456	1624.98	23.33
35.01	37.06	23.75	-5.527	-1.475	1564.17	22.92
32.31	37.01	23.38	-5.516	-1.566	1563.27	22.92
31.39	35.02	23.01	-5.556	-1.555	1483.72	22.38
30.46	33.16	22.64	-5.596	-1.545	1408.94	21.86
28.39	32.82	22.30	-5.595	-1.616	1396.04	21.77
27.15	31.42	21.91	-5.621	-1.635	1340.05	21.37
26.11	30.13	21.59	-5.652	-1.643	1287.37	20.98
25.76	28.10	21.26	-5.708	-1.601	1204.13	20.36
23.78	28.06	20.94	-5.697	-1.691	1203.37	20.35
23.77	25.70	20.57	-5.767	-1.622	1105.21	19.59
23.70	23.81	20.28	-5.833	-1.559	1025.76	18.94

$Re^{0.88}$	ln(sh)	ln(Re)	Nu	Nu (predicted by OT model)	OT/Axis
1001.24	4.11	7.85	55.84	58.84	2842.09
898.95	4.08	7.82	53.84	56.07	2703.41
911.45	3.98	7.78	48.82	56.96	2748.09
827.89	4.01	7.75	50.21	50.67	2433.38
852.68	3.89	7.71	44.76	52.46	2523.03
807.58	3.87	7.68	43.94	49.10	2354.77
758.13	3.86	7.64	43.52	45.46	2173.21
774.20	3.76	7.61	39.22	46.59	2229.41
734.37	3.74	7.57	38.31	43.68	2084.20
690.82	3.73	7.54	37.88	40.57	1928.62
680.27	3.66	7.50	35.56	39.80	1890.14
669.19	3.60	7.47	33.42	39.00	1849.97
647.10	3.56	7.43	31.96	37.44	1771.93
646.77	3.48	7.40	29.49	37.39	1769.27
617.72	3.45	7.36	28.65	35.37	1668.58
590.23	3.42	7.33	27.80	33.49	1574.51
585.48	3.35	7.29	25.91	33.15	1557.38
564.76	3.30	7.26	24.78	31.74	1486.82
545.18	3.26	7.22	23.83	30.43	1421.38
514.04	3.25	7.19	23.52	28.38	1319.11
513.75	3.17	7.16	21.71	28.34	1317.12
476.68	3.17	7.12	21.70	25.95	1197.49
446.40	3.17	7.09	21.63	24.04	1102.07

de^0.5 ($m^{1/2}$)	We number	P^0.13	Re/P^1.26	We*P^13
0.0725	5.03	31.50	232.12	158.60
0.0713	4.76	31.50	219.46	149.99
0.0723	4.78	31.50	223.84	150.44
0.0689	4.23	31.50	195.05	133.32
0.0704	4.33	31.50	203.46	136.27
0.0687	4.02	31.50	188.24	126.77
0.0666	3.70	31.50	171.95	116.59
0.0678	3.75	31.50	177.19	118.12
0.0662	3.48	31.50	164.29	109.74
0.0643	3.21	31.50	150.52	101.26
0.0641	3.12	31.50	147.24	98.40
0.0639	3.03	31.50	143.82	95.50
0.0631	2.88	31.50	137.07	90.75
0.0634	2.85	31.50	136.97	89.66
0.0622	2.67	31.50	128.24	84.11
0.0609	2.51	31.50	120.15	78.94
0.0610	2.46	31.50	118.77	77.40
0.0602	2.32	31.50	112.80	73.18
0.0593	2.21	31.50	107.24	69.66
0.0576	2.05	31.50	98.58	64.46
0.0579	2.02	31.50	98.50	63.72
0.0559	1.83	31.50	88.49	57.60
0.0541	1.68	31.50	80.55	53.03

Table A.2

EVAPORATION OF DISTILLED DE-IONISED DROPLETS IN FREE-FLIGHT AT 50°C

Air temperature = 50°C, wet bulb temp. = 23°C
density of water = 997kg/m3, viscosity of water = 9.142e-04 Pas,
humidity of air = 0.007kg H20/kg air
surface tension = 0702 N/m, Latent heat = 2411.19 kJ/kg
Ts = 24.05°C Dv = 2.5E-05 m^2/s

Time(sec)	mass of drop(g)	dia.(cm)	vel(m/s)	Re. No.	Evap. rate(mg/s)
0	0.0365	0.412	7.09		
30	0.0301	0.387	6.86	1646.58	0.1099
60	0.0274	0.375	6.75	1494.21	0.0978
90	0.0217	0.347	6.50	1425.69	0.0870
120	0.0214	0.345	6.48	1268.91	0.0774
150	0.0206	0.341	6.44	1260.12	0.0689
180	0.0187	0.330	6.34	1236.36	0.0613
210	0.0156	0.311	6.15	1178.02	0.0546
240	0.0143	0.302	6.06	1076.05	0.0486
270	0.0131	0.293	5.97	1030.29	0.0432
300	0.0111	0.277	5.81	986.16	0.0384
330	0.0090	0.259	5.61	907.84	0.0342
360	0.0080	0.249	5.50	817.55	0.0304
390	0.0060	0.226	5.25	770.84	0.0271

OT number	$OT^{0.15}$	$de^{0.5}$ ($m^{1/2}$)	Sh number (experimental)	Sh(predicted by OT model)	Sh(predicted by Ranz-Marshall)
1833.60	3.09	0.0642	44.04	38.85	23.44
1559.20	3.01	0.0622	40.43	35.02	22.43
1441.86	2.98	0.0612	38.88	33.32	21.95
1187.41	2.89	0.0589	34.76	29.45	20.82
1173.72	2.89	0.0588	31.32	29.24	20.76
1137.08	2.87	0.0584	28.79	28.66	20.58
1049.07	2.84	0.0574	27.21	27.24	20.14
902.14	2.78	0.0557	24.92	24.79	19.33
839.10	2.75	0.0549	22.83	23.69	18.96
780.05	2.72	0.0541	21.47	22.65	18.60
679.56	2.66	0.0527	20.49	20.80	17.92
570.69	2.59	0.0509	18.96	18.71	17.11
517.39	2.55	0.0499	18.57	17.63	16.67

ln(sh)	ln(Re)	Nu number (experimental)	$(Re/P)^{1.26}$	We.P	ln(kg) (m/s)
3.79	7.41	26.63	146.23	97.05	-1.26
3.70	7.31	25.27	129.39	88.25	-1.28
3.66	7.26	23.20	121.96	82.85	-1.29
3.55	7.15	22.31	105.31	74.17	-1.32
3.44	7.14	19.94	104.39	71.35	-1.42
3.36	7.12	17.97	101.91	68.01	-1.49
3.30	7.07	16.52	95.89	63.49	-1.52
3.22	6.98	15.61	85.55	58.43	-1.55
3.13	6.94	14.30	80.99	53.74	-1.60
3.07	6.89	13.10	76.65	48.45	-1.64
3.02	6.81	12.32	69.06	45.42	-1.63
2.94	6.71	11.75	60.52	40.50	-1.64
2.92	6.65	10.88	56.20	36.57	-1.62

Table A.3

EVAPORATION OF DISTILLED DE-IONISED WATER DROPLETS IN FREE-FLIGHT AT 80°C

Air temperature = 80°C
wet bulb tmperature = 23°C

density of air = 1.0 kg/m3 viscosity of air = 2.10e-05 Pas.
Viscosity of water = 8.6e-04 Pas, surface tension of water = 0.072 N/m
density of water = 995 kg/m^3. Latent Heat = 2411.19 kJ/kg.
diffusivity = 2.7 e-05 m/s^2. Ts = 31.10°C

Time(sec)	mass of drop (x E-03 kg)	Evap. rate (x E-06 kg/s)	Equiv. dia (x E-02 m)	Terminal velocity (m/s)	Re.No.
0	0.0415	0.3078	0.431	7.48	1568.53
30	0.0307	0.2446	0.390	7.12	1319.93
60	0.0243	0.1944	0.360	6.84	1174.45
90	0.0201	0.1546	0.338	6.63	1068.25
120	0.0149	0.1229	0.306	6.31	919.88
150	0.0143	0.0977	0.302	6.27	901.19
180	0.0109	0.0776	0.276	5.99	786.90

OT number	ln(sh)	ln(Re)	Sh Number (experimental)	Sh predicted by Ranz-Marshall	Sh predicted by OT model
2260.04	3.63	7.36	37.85	22.59	2.73
1682.79	3.50	7.19	33.26	20.89	2.61
1385.17	3.35	7.07	28.57	19.82	2.54
1182.76	3.19	6.97	24.20	19.00	2.48
921.86	3.06	6.82	21.26	17.77	2.42
890.85	2.84	6.80	17.13	17.61	2.41
710.63	2.70	6.67	14.89	16.59	2.35

	$Re/P^{1.26}$	We.P	Nu (experimental)	Nu by OT model	
	137.55	112.87	33.82	36.39	
	110.67	92.34	29.72	30.26	
	95.53	79.03	25.53	26.75	
	84.77	69.64	21.63	24.23	
	70.22	57.06	18.99	20.76	
	68.42	55.51	15.31	20.33	
	57.68	46.33	13.31	17.72	

Table A.4

EVAPORATION OF PROPANOL DROPLETS IN FREE-FLIGHT AT 62°C

Air temp.= 62°C, wet bulb = 30°C. Vapour pressure = 3572.34Pa
density of liquid = 804kg/m^3, viscosity of liquid= 1.95e-03 Pas
surface tension = 25.26e-03 N/m. latent heat = 787.41kJ/kg
diffusivity = 11.00e-06 m^2/s Ts = 31.05°C

Time (sec)	mass of drop (x E-03 kg)	Equiv. dia (x E-02 m)	Terminl vel. (m/s)	Re.No	OT. No	Evap. rate (x E-06 kg/s)
	0.0562	0.515	7.01	2031.22	1775.46	
10	0.0423	0.468	6.32	1667.38	1253.80	0.7126
20	0.0356	0.443	6.15	1532.78	1090.12	0.6195
30	0.0339	0.435	5.99	1468.99	1009.39	0.5386
40	0.0304	0.420	5.87	1388.71	918.44	0.4682
50	0.0243	0.390	5.67	1245.83	767.00	0.4070
60	0.0194	0.362	5.52	1126.00	650.27	0.3539
70	0.0187	0.358	5.37	1082.20	604.32	0.3076
80	0.0167	0.345	5.22	1013.43	539.93	0.2325
90	0.0139	0.324	5.08	928.29	466.95	0.2021
100	0.0131	0.318	4.94	885.22	428.80	0.1757
110	0.0117	0.307	4.80	828.65	382.81	0.1528
120	0.0106	0.297	4.66	778.69	343.60	0.1328
130	0.0100	0.291	4.53	742.55	315.46	0.1155
140	0.0084	0.275	4.40	680.91	273.01	0.1004
150	0.0076	0.266	4.28	640.82	245.84	0.0873
160	0.0073	0.262	4.15	613.16	226.57	0.0759

Sh predicted by Ranz-Marshall	Sh number (experimental)	Sh predicted by OT model	ln (kg) (m/s)	ln(sh)	ln(Re)	$de^{0.5}$ (√m)
31.08	55.67	47.02	-2.189	4.02	7.62	0.0717
29.89	51.23	42.93	-2.178	3.94	7.42	0.0684
29.30	45.26	40.98	-2.245	3.81	7.33	0.0665
28.54	40.79	38.58	-2.333	3.71	7.29	0.0660
27.14	38.17	34.36	-2.363	3.64	7.24	0.0648
25.90	35.75	30.88	-2.355	3.58	7.13	0.0625
25.43	31.46	29.58	-2.408	3.45	7.03	0.0602
24.67	24.68	27.60	-2.639	3.21	6.99	0.0598
23.70	22.79	25.18	-2.681	3.13	6.92	0.0587
23.19	20.21	23.95	-2.741	3.01	6.83	0.0570
22.50	18.24	22.36	-2.824	2.90	6.79	0.0564
21.88	16.38	20.97	-2.894	2.80	6.72	0.0554
21.41	14.52	19.96	-2.982	2.68	6.66	0.0545
20.59	13.37	18.28	-3.045	2.59	6.61	0.0540
20.03	12.02	17.20	-3.094	2.49	6.52	0.0524
19.64	10.59	16.44	-3.188	2.36	6.46	0.0516

	Nu	Nu predicted by				
	(experimental)	OT model	We.P	(Re/P)^1.55		
	35.27	46.54	230.68	1150.28		
	33.68	37.53	170.72	847.10		
	31.00	34.31	152.72	743.49		
	27.38	32.77	142.55	696.08		
	24.68	30.87	132.06	638.02		
	23.10	27.54	114.44	539.19		
	21.63	24.80	100.70	460.97		
	16.55	23.77	94.15	433.47		
	14.93	22.21	85.70	391.53		
	13.79	20.30	76.40	341.74		
	12.23	19.33	70.85	317.48		
	11.03	18.07	64.44	286.58		
	9.91	16.97	58.79	260.25		
	8.79	16.18	54.50	241.77		
	8.09	14.85	48.54	211.38		
	7.27	14.00	44.43	192.41		

Table A.5

EVAPORATION OF PROPANOL DROPS IN FREE- FLIGHT AT 50°C

Air temp. = 50°C, Wet bulb temp = 27°C
Drop surface temp. = 27°C
Vapour pressure = 2774.58 Pa. diffusivity = 11.0e-06 m^2/s
latent heat = 787.41. kJ/kg.

Time(sec)	mass of drop (g)	Ev.rate(mg/s)	equiv. dia.(cm)	vel. (m/s)	Reynolds no.
0	0.0454		0.480	6.74	1780.72
10	0.0401	0.5207	0.460	6.60	1709.80
20	0.0329	0.4618	0.431	6.38	1549.23
30	0.0294	0.4095	0.415	6.26	1464.77
40	0.0275	0.3632	0.406	6.19	1416.80
50	0.0252	0.3221	0.395	6.10	1356.43
60	0.0218	0.2856	0.376	5.95	1261.88
70	0.0174	0.2533	0.349	5.73	1127.70
80	0.0158	0.2246	0.338	5.64	1074.73
90	0.0149	0.1992	0.332	5.58	1043.74
100	0.0134	0.1767	0.321	5.48	989.93
110	0.0110	0.1567	0.300	5.30	897.09
120	0.0096	0.1389	0.287	5.18	838.16
130	0.0088	0.1232	0.279	5.11	802.54
140	0.0083	0.1093	0.274	5.06	779.44
150	0.0074	0.0969	0.264	4.96	736.03
160	0.0060	0.0859	0.246	4.79	662.84

OT. No	Sh number (experimental)	Sh predicted by OT model	Sh predicted by Ranz-Marshall	ln(kg) (m/s)	ln(sh)
1413.44					
1330.06	51.64	48.38	32.30	-2.190	3.94
1128.23	47.72	46.34	31.69	-2.228	3.87
1027.46	45.17	41.66	30.26	-2.217	3.81
971.91	41.57	39.23	29.48	-2.263	3.73
903.79	37.69	37.85	29.03	-2.339	3.63
801.11	34.40	36.13	28.44	-2.402	3.54
664.05	32.00	33.46	27.51	-2.426	3.47
612.80	30.57	29.70	26.11	-2.398	3.42
583.60	27.99	28.24	25.54	-2.454	3.33
534.24	25.31	27.38	25.20	-2.535	3.23
453.26	23.25	25.91	24.59	-2.585	3.15
404.66	21.99	23.39	23.51	-2.575	3.09
376.35	20.40	21.81	22.79	-2.606	3.02
358.44	18.63	20.86	22.34	-2.668	2.92
325.74	16.84	20.25	22.05	-2.750	2.82
273.48	15.50	19.10	21.48	-2.794	2.74

ln(Re)	dia^0.5 (√m)	We.P	(Re/P)^1.55	Nu number (experimental)	Nu predicted by OT model
7.48	0.068	198.39	938.00	39.53	40.33
7.44	0.066	182.64	880.74	36.52	38.65
7.35	0.064	160.06	755.89	34.57	34.79
7.29	0.064	148.50	692.99	31.82	32.77
7.26	0.063	142.03	658.13	28.85	31.64
7.21	0.061	133.99	615.18	26.33	30.21
7.14	0.059	121.64	549.99	24.49	28.00
7.03	0.058	104.65	462.04	23.40	24.90
6.98	0.058	98.12	428.84	21.42	23.69
6.95	0.057	94.36	409.83	19.37	22.98
6.90	0.055	87.90	377.55	17.79	21.76
6.80	0.054	77.05	324.10	16.83	19.68
6.73	0.053	70.35	291.70	15.62	18.37
6.69	0.052	66.37	272.71	14.26	17.59
6.66	0.051	63.83	260.64	12.89	17.08
6.60	0.050	59.11	238.49	11.87	16.14

Table A.6 **EVAPORATION OF HEPTANE LIQUID DROPLETS IN FREE-FLIGHT AT 55°C**

Air temp. = 55°C wet bulb temp= 27°C

Liquid density=679kg/m^3, viscosity of liquid= 3.486E-04Pas.
surface tension = 23.28E-03 N/m, diffusivity = 7.4e-06m^2/s
Latent heat 357.56 kJ/kg. Cp=1.655kJ/kg.K. B = 0.165
Ts = 27.75°C Vapour pressure = 6626.47 Pa

Time(sec)	mass of drop (x E-03 kg)	Evap. rate (x E-06 kg/s)	Equiv. dia (x E-02 m)	Terminal velocity (m/s)	Re. No	OT No.
0	0.0228		0.400			
5	0.0166	1.1124	0.360	5.76	1167.76	3756.63
10	0.0146	0.9289	0.345	5.47	1062.76	3178.36
15	0.0106	0.7757	0.310	5.40	942.73	2638.33
20	0.0103	0.6478	0.307	5.38	930.15	2580.90
25	0.0101	0.5409	0.305	5.37	922.37	2546.23
30	0.0090	0.4517	0.294	5.22	864.27	2276.99
35	0.0068	0.4216	0.267	5.06	760.84	1851.69
40	0.0066	0.3520	0.264	4.91	729.99	1714.23
45	0.0047	0.2940	0.236	4.77	633.96	1367.43
50	0.0044	0.2455	0.232	4.62	603.62	1250.30
55	0.0034	0.2050	0.213	4.49	538.59	1038.87
60	0.0026	0.1712	0.194	4.36	476.34	851.48

Sh number (experimental)	Sh predicted by OT model	Sh predicted by Ranz-Marshall	ln(sh)	ln(Re)	ln(kg) (m/s)	dia^0.5 (√m)
63.28	48.59	29.77	4.15	7.06	-2.201	0.063
55.13	43.82	28.49	4.01	6.97	-2.233	0.060
51.24	38.60	26.95	3.94	6.85	-2.264	0.059
43.21	38.05	26.79	3.77	6.84	-2.327	0.056
36.32	37.71	26.68	3.59	6.83	-2.491	0.055
31.46	35.16	25.89	3.45	6.76	-2.628	0.055
32.33	30.74	24.42	3.48	6.63	-2.564	0.054
27.30	29.39	23.96	3.31	6.59	-2.637	0.052
25.51	25.39	22.46	3.24	6.45	-2.694	0.051
21.67	24.10	21.97	3.08	6.40	-2.745	0.049
19.71	21.44	20.86	2.98	6.29	-2.822	0.048
18.07	18.94	19.74	2.89	6.17	-2.824	0.046

	Nu number (experimental)	Nu predicted by OT model	We.P	(Re/P)^1.55		
	28.16	29.34	127.770	505.56		
	26.12	26.52	103.705	436.87		
	22.76	23.43	96.857	362.80		
	21.16	23.11	86.387	355.33		
	17.84	22.91	85.233	350.73		
	14.99	21.40	80.014	317.09		
	14.52	18.79	72.472	260.24		
	13.35	17.99	61.972	244.07		
	11.28	15.62	57.831	196.14		
	10.53	14.86	48.497	181.78		
	8.95	13.29	45.030	152.34		
	8.14	11.81	38.983	125.94		

Table A.7 **EVAPORATION OF ISO-BUTANOL LIQUID DROPLETS IN FREE-FLIGHT AT 62°C**

Air temp = 62°C, wet bulb =27°C
liquid density = 802kg/m^3, viscosity = 3.44E-03 Pas
surface tension = 23e-03 N/m. diffusivity in air = 9.9E-06m^2/s
Latent heat = 673.34 J/g, Cp=1.51kJ/kg.K, Spalding number, B=0.0866
Ts = 37.65°C

Time(sec)	mass of drop (x E-03 kg))	Evap. rate (x E-06 kg/s)	Equiv. dia (x E-02 m)	Terminal vel. (m/s)	Re.No.	OT^0.15
0			0.315			
5	0.0122	0.2495	0.308	5.36	950.84	2.35
10	0.0090	0.2234	0.278	5.26	912.36	2.32
15	0.0087	0.2001	0.275	5.17	809.40	2.26
20	0.0081	0.1792	0.268	5.07	785.18	2.24
25	0.0071	0.1605	0.256	4.98	751.61	2.21
30	0.0060	0.1437	0.243	4.89	704.98	2.18
35	0.0051	0.1287	0.229	4.80	656.87	2.14
40	0.0047	0.1153	0.223	4.71	607.42	2.10
45	0.0043	0.1032	0.216	4.63	581.45	2.08
50	0.0041	0.0924	0.215	4.54	552.26	2.05
55	0.0036	0.0828	0.204	4.46	540.01	2.04
60	0.0023	0.0741	0.176	4.38	503.19	2.00

Sh number (experimental)	Sh predicted by OT model	Sh predicted by Ranz-Marshall	ln(sh)	ln(Re)	ln kg (m/s)	$de^{0.5}$ (√m)
31.96	31.95	24.51	3.46	6.86	-2.32	0.0561
29.26	31.16	24.05	3.38	6.82	-2.39	0.0555
29.04	27.52	22.77	3.37	6.70	-2.29	0.0527
26.29	26.64	22.46	3.27	6.67	-2.38	0.0524
24.16	25.44	22.01	3.18	6.62	-2.44	0.0518
22.65	23.81	21.38	3.12	6.56	-2.46	0.0506
21.37	22.15	20.71	3.06	6.49	-2.47	0.0493
20.31	20.45	19.99	3.01	6.41	-2.46	0.0479
18.67	19.56	19.60	2.93	6.37	-2.51	0.0472
17.26	18.56	19.16	2.85	6.31	-2.56	0.0465
15.54	18.14	18.96	2.74	6.29	-2.66	0.0464
14.65	16.90	18.38	2.68	6.22	-2.67	0.0452

	Nu number (experimental)	Nu predicted by OT model	We.P	(Re/P)^1.55		
	22.52	19.46	86.20	382.69		
	20.62	18.66	81.16	358.95		
	20.46	16.58	70.77	298.15		
	18.52	16.08	67.33	284.44		
	17.02	15.39	63.30	265.81		
	15.96	14.46	58.30	240.69		
	15.06	13.51	53.33	215.71		
	14.31	12.54	48.39	191.07		
	13.16	12.03	45.53	178.56		
	12.16	11.46	42.40	164.85		
	10.95	11.22	40.73	159.22		
	10.33	10.51	37.28	142.72		

Table A.8

EVAPORATION OF MONOETHANOLAMINE IN FREE-FLIGHT AT 62°C

Air temp. 62°C. Wet bulb temp = 25°C
liquid density = 1016kg/m^3, viscosity = 17.87e-03Pa.
surface tension = 0.052 N/m, diffusivity = 11.006e-06m^2/s
latent heat = 914.83 kJ/kg.
drop surface temperature = 40°C. Cp = 1.5kJ/kg.K. B= 0.0121

Time(sec)	mass of drop (x E-03 kg))	Evap. rate (x E-06 kg/s)	Equiv. dia (x E-02 m)	Terminal vel (m/s)	Re. No.	OT Number.
0	0.0321		0.400	7.89	1791.55	133.93
20	0.0316	9.72E-02	0.396	7.85	1751.10	128.61
40	0.0308	9.18E-02	0.394	7.83	1737.54	126.95
60	0.0305	8.67E-02	0.391	7.80	1715.63	124.29
80	0.0297	8.19E-02	0.389	7.79	1707.34	123.29
100	0.0265	7.74E-02	0.386	7.75	1685.02	120.62
120	0.0250	7.31E-02	0.372	7.61	1592.56	109.79
140	0.0244	6.91E-02	0.365	7.54	1547.29	104.64
160	0.0207	6.53E-02	0.362	7.51	1528.79	102.56
180	0.0178	6.16E-02	0.343	7.31	1409.27	89.55
200	0.0196	5.82E-02	0.326	7.13	1307.82	79.07
220	0.0202	5.50E-02	0.336	7.24	1371.69	85.61
240	0.0172	5.20E-02	0.340	7.28	1392.32	87.76
260	0.0145	4.91E-02	0.322	7.09	1285.81	76.86
280	0.0140	4.64E-02	0.305	6.89	1181.59	66.76
300	0.0132	4.33E-02	0.301	6.85	1161.24	64.86
320	0.0123	4.14E-02	0.295	6.78	1127.91	61.78
340	0.0115	3.91E-02	0.288	6.70	1089.16	58.29
360	0.0109	3.70E-02	0.282	6.63	1053.50	55.14
380	0.0105	3.49E-02	0.277	6.57	1025.93	52.76
400	0.0105	3.30E-02	0.274	6.53	1007.11	51.15
420	0.0086	3.12E-02	0.274	6.53	1007.11	51.15
440	0.0089	2.94E-02	0.256	6.32	912.36	43.39
460	0.0098	2.78E-02	0.259	6.36	927.98	44.63
480	0.0091	2.63E-02	0.268	6.46	973.30	48.32
500	0.0083	2.48E-02	0.261	6.38	938.24	45.46
520	0.0078	2.34E-02	0.253	6.28	896.47	42.13
540	0.0073	2.22E-02	0.248	6.22	869.31	40.03
560	0.0081	2.09E-02	0.243	6.15	841.27	37.90
580	0.0072	1.98E-02	0.251	6.26	885.71	41.29
600	0.0076	1.87E-02	0.242	6.14	835.55	37.47
620	0.0065	1.76E-02	0.246	6.19	858.21	39.18

Sh.No.	Sh predicted by OT-model	Sh predicted by Ranz-Marshall	ln kg (m/s)	ln d (m)	ln(sh)	ln(Re)
41.72	35.62	30.08	-1.99	-5.52	3.73	7.49
39.82	34.75	29.76	-2.03	-5.53	3.68	7.47
37.82	34.46	29.65	-2.07	-5.54	3.63	7.46
36.03	34.00	29.48	-2.11	-5.55	3.58	7.45
34.15	33.82	29.41	-2.16	-5.55	3.53	7.44
32.55	33.35	29.23	-2.20	-5.56	3.48	7.43
31.92	31.42	28.48	-2.18	-5.59	3.46	7.37
30.75	30.47	28.10	-2.20	-5.61	3.43	7.34
29.28	30.09	27.94	-2.24	-5.62	3.38	7.33
29.20	27.62	26.90	-2.19	-5.68	3.37	7.25
29.00	25.55	25.99	-2.15	-5.73	3.37	7.18
26.54	26.85	26.57	-2.27	-5.69	3.28	7.22

24.82	27.27	26.75	-2.35	-5.68	3.21	7.24
24.73	25.10	25.79	-2.30	-5.74	3.21	7.16
24.41	23.00	24.80	-2.25	-5.79	3.20	7.07
23.62	22.59	24.61	-2.28	-5.81	3.16	7.06
22.75	21.92	24.28	-2.29	-5.82	3.12	7.03
22.00	21.15	23.89	-2.30	-5.85	3.09	6.99
21.25	20.44	23.53	-2.32	-5.87	3.06	6.96
20.43	19.90	23.25	-2.34	-5.89	3.02	6.93
19.54	19.53	23.05	-2.37	-5.90	2.97	6.91
18.47	19.53	23.05	-2.43	-5.90	2.92	6.91
18.63	17.68	22.04	-2.35	-5.97	2.92	6.82
17.40	17.98	22.21	-2.43	-5.96	2.86	6.83
15.92	18.86	22.70	-2.55	-5.92	2.77	6.88
15.42	18.18	22.32	-2.56	-5.95	2.74	6.84
15.02	17.37	21.86	-2.56	-5.98	2.71	6.80
14.48	16.84	21.56	-2.57	-6.00	2.67	6.77
13.98	16.30	21.24	-2.59	-6.02	2.64	6.73
12.76	17.16	21.74	-2.71	-5.99	2.55	6.79
12.54	16.19	21.18	-2.69	-6.03	2.53	6.73

	Nu number	Nu predicted by	(Re/P)^1.55	dia^0.5	We.P	
	(Experimental)	OT-model		(√m)		
					27.31	
	34.32	29.06	654.95	0.0632	142.18	
	32.75	28.37	632.17	0.0629	138.19	
	31.11	28.13	624.60	0.0628	134.99	
	29.63	27.76	612.43	0.0625	131.43	
	28.08	27.62	607.85	0.0624	128.64	
	26.77	27.24	595.58	0.0621	125.21	
	26.26	25.68	545.70	0.0610	118.41	
	25.29	24.92	521.84	0.0604	114.06	
	24.08	24.62	512.20	0.0601	111.10	
	24.02	22.63	451.49	0.0585	103.33	
	23.85	20.96	402.12	0.0571	96.53	
	21.83	22.01	432.96	0.0580	97.85	
	20.42	22.35	443.10	0.0583	97.04	
	20.34	20.60	391.67	0.0568	90.37	
	20.08	18.90	343.58	0.0552	83.87	
	19.43	18.57	334.45	0.0549	81.41	
	18.71	18.04	319.69	0.0543	78.40	
	18.10	17.42	302.83	0.0537	75.21	
	17.48	16.85	287.60	0.0531	72.23	
	16.80	16.41	276.01	0.0527	69.68	
	16.07	16.11	268.21	0.0523	67.58	
	15.19	16.11	268.21	0.0523	66.36	
	15.32	14.62	230.12	0.0506	61.01	
	14.31	14.86	236.26	0.0509	60.59	
	13.10	15.58	254.38	0.0517	61.42	
	12.68	15.03	240.32	0.0511	58.85	
	12.35	14.37	223.94	0.0503	56.06	
	11.91	13.95	213.51	0.0498	53.93	
	11.50	13.51	202.93	0.0493	51.81	
	10.50	14.20	219.79	0.0501	52.65	
	10.31	13.43	200.80	0.0492	49.73	

Table A.9

EVAPORATION OF MONOETHANOLAMINE LIQUID DROPLETS IN FREE-FLIGHT AT 80°C

Air temperature = 80°C, Wet bulb temp = 30°C
Mol. wt= 61.084, Ts = 45°C
diffusivity = 12.002e-06m^2/s.
Vapour Pressure = 1137.93 Pa. Latent heat = 914.83kJ/kg
B = 0.0234

Time(sec)	mass of drop (x E-03 kg)	Equiv. dia de, (x E-02 m)	Terminal Velocity (m/s)	Evap. rate (x E-06 kg/s)	OT Number	Re Number
0	0.0395	0.42	7.36		126.12	
30	0.0345	0.41	7.20	0.145	112.74	1582.69
60	0.0335	0.40	7.16	0.1283	110.27	1479.65
90	0.0288	0.38	6.99	0.1135	97.17	1460.09
120	0.0247	0.36	6.81	0.1004	85.53	1353.40
150	0.0228	0.35	6.72	0.0888	80.05	1253.72
180	0.0190	0.33	6.52	0.0786	68.88	1204.85
210	0.0145	0.30	6.24	0.0695	55.25	1100.94
240	0.0153	0.31	6.29	0.0615	57.54	964.56
270	0.0109	0.28	5.95	0.0544	43.58	988.37
300	0.0098	0.27	5.85	0.0481	39.86	836.56
330	0.0087	0.26	5.73	0.0426	36.10	792.98
360	0.0083	0.25	5.69	0.0377	34.84	747.17
390	0.0069	0.24	5.52	0.0333	29.95	731.47
420	0.0081	0.25	5.67	0.0295	34.24	667.93
450	0.0069	0.24	5.52	0.0261	29.98	723.76
480	0.0054	0.22	5.30	0.0231	24.42	668.37
510	0.0054	0.22	5.30	0.0204	24.53	590.95
540	0.0030	0.18	4.82	0.0111	24.53	592.57

Sh Number (experimental)	Sh predicted by OT model	Nu number (experimental)	Nu predicted by OT model	ln(sh)	ln(dp) (m)
	32.39	24.05	26.04	3.522	-5.463
33.86	30.16	22.25	24.28	3.445	-5.508
31.34	29.74	19.86	23.95	3.331	-5.517
27.97	27.46	18.48	22.14	3.259	-5.568
26.03	25.35	17.20	20.47	3.187	-5.619
24.22	24.33	15.63	19.66	3.092	-5.645
22.02	22.16	14.68	17.95	3.029	-5.705
20.67	19.36	14.19	15.74	2.995	-5.794
19.98	19.85	12.35	16.12	2.856	-5.777
17.39	16.78	12.20	13.70	2.844	-5.889
17.18	15.92	11.20	13.01	2.758	-5.924
15.77	15.01	10.31	12.29	2.676	-5.964
14.52	14.70	9.24	12.05	2.566	-5.978
13.01	13.46	8.69	11.07	2.505	-6.039
12.24	14.55	7.29	11.93	2.329	-5.985
10.27	13.47	6.81	11.08	2.260	-6.038
9.58	11.98	6.52	9.90	2.218	-6.120
9.19	12.01	5.87	9.92	2.113	-6.118
4.99	12.01	3.54	9.92	1.607	-6.118

	ln(Re)	ln(kg)	dia^0.5	We.P	Re/P	
		(m/s)	(√m)			
	7.37	-2.205	0.0651	129.03	540.46	
	7.30	-2.238	0.0637	117.95	486.91	
	7.29	-2.342	0.0634	115.88	476.97	
	7.21	-2.364	0.0618	104.72	424.05	
	7.13	-2.385	0.0602	94.57	376.63	
	7.09	-2.454	0.0594	89.69	354.12	
	7.00	-2.456	0.0577	79.52	307.92	
	6.87	-2.402	0.0552	66.67	250.85	
	6.90	-2.558	0.0557	68.87	260.51	
	6.73	-2.458	0.0526	55.14	201.18	
	6.68	-2.508	0.0517	51.35	185.16	
	6.62	-2.551	0.0507	47.43	168.85	
	6.60	-2.647	0.0503	46.10	163.38	
	6.50	-2.647	0.0488	40.84	141.92	
	6.58	-2.876	0.0502	45.46	160.72	
	6.50	-2.892	0.0488	40.88	142.06	
	6.38	-2.853	0.0469	34.69	117.38	
	6.38	-2.959	0.0469	34.82	117.88	
	6.38	-3.465	0.0469	34.82	117.88	

Table A.10

EVAPORATION OF DISTILLED DE-IONIZED WATER TREATED WITH A SURFACTANT

(Sodium di-octylsulfono succinate)
CONCENTRATION = 0.001(wt/wt)

Air temp.=68°C, Wet bulb temp =30°C
Air humidity = 0.017 kg H_2O/kg dry air
density of treated water = 995kg/m^3. Surface tension = 0.033N/m
viscosity of treated water = 8.0E-04Pas. Latent heat = 2411.19J/g
Ts = 33.45°C

Time (mun)	mass of drop (x10e-3kg)	Equiv. diameter (de, x10e-02m)	Evaporation rate. (x10e-06 kg/s)	Terminal velocity (m/s)	Reynolds number (Re)	Sherwood number (Expt. Sh)
0	0.0364	0.449		7.11	1707.93	
1	0.0323	0.420	0.1268	6.84	1536.95	34.75
2	0.0231	0.388	0.1030	6.57	1363.80	30.17
3	0.0172	0.359	0.0837	6.31	1211.93	26.54
4	0.0163	0.332	0.0680	6.07	1078.15	23.30
5	0.0110	0.306	0.0552	5.83	954.43	20.46
6	0.0086	0.283	0.0448	5.60	847.87	18.01
7	0.0066	0.262	0.0364	5.38	754.11	15.82
8	0.0027	0.242	0.0296	5.28	683.60	13.90

Table A11

EVAPORATION OF 'CLEAN' DISTILLED DE-IONISED WATER

Air temp.=68°C, Wetbulb temp =30°C
Air humidity = 0.017 kg H2O/kg dry air
density of water = 995kg/m^3. Surface tension = 0.072N/m
viscosity of water = 8.0E-04Pas. Latent heat = 2372.65J/g

Time (mun)	Evaporation rate (x10e-06 kg/s)	Equiv. diameter (x10e-02 m)	Mass of drop (x10e-03 kg)	Term. velocity (m/s)	Reynolds number (Re)	Sherwood number (Expt. Sh)
1	0.2184	0.493	0.0626	7.84	2067.84	
2	0.1772	0.471	0.0546	7.58	1910.05	54.50
3	0.1438	0.429	0.0413	7.31	1677.75	46.29
4	0.1167	0.400	0.0334	7.07	1512.98	41.24
5	0.0947	0.386	0.0301	6.82	1408.40	35.90
6	0.0768	0.348	0.0220	6.57	1223.20	30.18
7	0.0623	0.335	0.0196	6.37	1141.66	27.15

Table A.12

VAPORISATION OF NAPHTHALENE SPHERES

Air temperature = 74 °C.
Surface temperature of spheres =70°C
Heat of sublimation = 72.5 kJ/kmol

Time (sec)	Equiv. diameter (x10e-02 m)	mass of sphere (x10e-03 kg)	Terminal velocity (m/s)	Vaporisation rate (x10e-03kg/sec)	Vap Rate(Cor) (x10e-03kg/sec)
0	0.983	0.4834	9.86		
120	0.965	0.4559	9.77	2.29E-04	2.31E-04
240	0.945	0.4284	9.67	2.29E-04	2.24E-04
360	0.925	0.4023	9.57	2.18E-04	2.17E-04
480	0.906	0.3780	9.47	2.03E-04	2.10E-04
600	0.885	0.3517	9.36	2.19E-04	2.03E-04
720	0.862	0.3253	9.23	2.20E-04	1.97E-04
840	0.843	0.3043	9.13	1.75E-04	1.90E-04
960	0.822	0.2823	9.02	1.83E-04	1.83E-04
1080	0.798	0.2585	8.88	1.98E-04	1.76E-04
1200	0.778	0.2391	8.77	1.62E-04	1.69E-04
1320	0.756	0.2195	8.65	1.63E-04	1.63E-04
1440	0.735	0.2017	8.53	1.48E-04	1.56E-04
1560	0.712	0.1836	8.39	1.51E-04	1.49E-04
1680	0.689	0.1659	8.26	1.48E-04	1.42E-04
1800	0.665	0.1496	8.11	1.36E-04	1.35E-04
1920	0.636	0.1304	7.93	1.60E-04	1.29E-04
2040	0.614	0.1173	7.79	1.09E-04	1.22E-04
2160	0.589	0.1035	7.63	1.15E-04	1.15E-04
2280	0.558	0.0881	7.43	1.28E-04	1.08E-04
2400	0.536	0.0780	7.28	8.42E-05	1.01E-04

Sherwood number (Expt. Sh)	Reynolds number (Re)	Mass transfer coefficient, kg(m/s)	Predicted Sh Ranz-Marshall	Nusselt number (Expt. Nu)	Predicted Nu Ranz-Marshall
52.62	5185.79	0.0434	58.94	36.42	40.41
52.02	5044.01	0.0437	58.15	36.00	39.88
51.51	4888.01	0.0441	57.28	35.65	39.29
50.97	4733.66	0.0446	56.40	35.28	38.70
50.35	4588.57	0.0450	55.56	34.85	38.13
49.83	4429.96	0.0456	54.63	34.49	37.50
49.39	4258.39	0.0464	53.60	34.18	36.81
48.69	4118.38	0.0468	52.74	33.70	36.23
48.08	3965.45	0.0474	51.79	33.28	35.59
47.61	3793.05	0.0483	50.70	32.95	34.85
46.87	3651.36	0.0488	49.78	32.44	34.23
46.22	3497.58	0.0495	48.76	31.99	33.54
45.47	3352.86	0.0501	47.78	31.47	32.88
44.79	3196.72	0.0510	46.70	31.00	32.16
44.07	3043.08	0.0518	45.62	30.50	31.42
43.37	2885.47	0.0528	44.47	30.02	30.65
42.95	2698.80	0.0547	43.08	29.73	29.71
42.00	2559.98	0.0554	42.00	29.07	28.99
41.20	2405.24	0.0567	40.78	28.51	28.16
40.75	2217.87	0.0592	39.24	28.20	27.12

APPENDIX B

LIST OF APPENDIX B

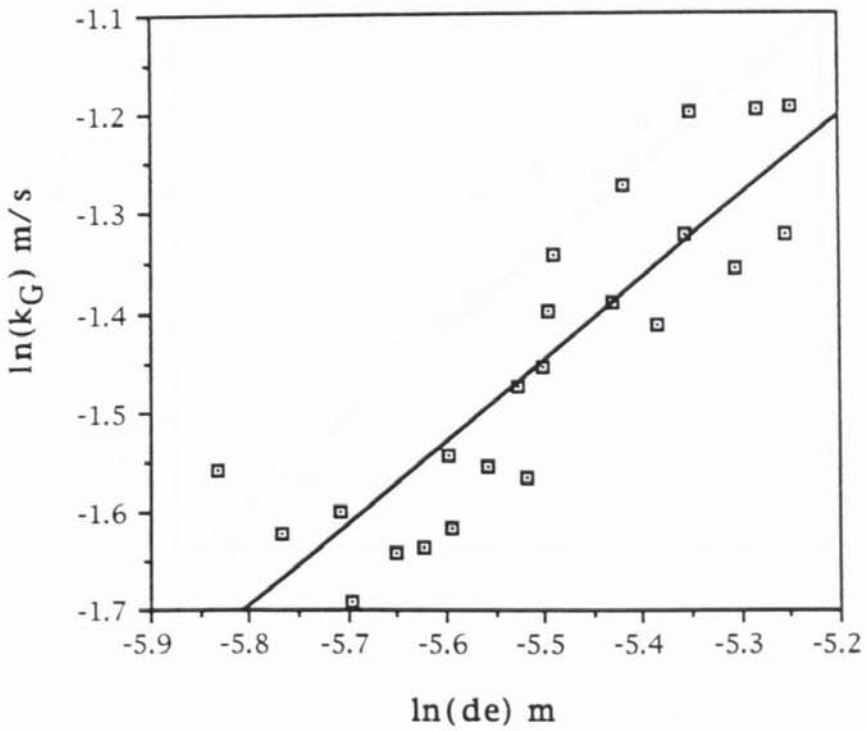

Figure B1. A plot of $\ln(k_G)$ vs ln(de) of distilled de-ionised water droplets evaporated in free-flight. Air temperature 62°C. (correlation coefficient, R^2= 0.8).

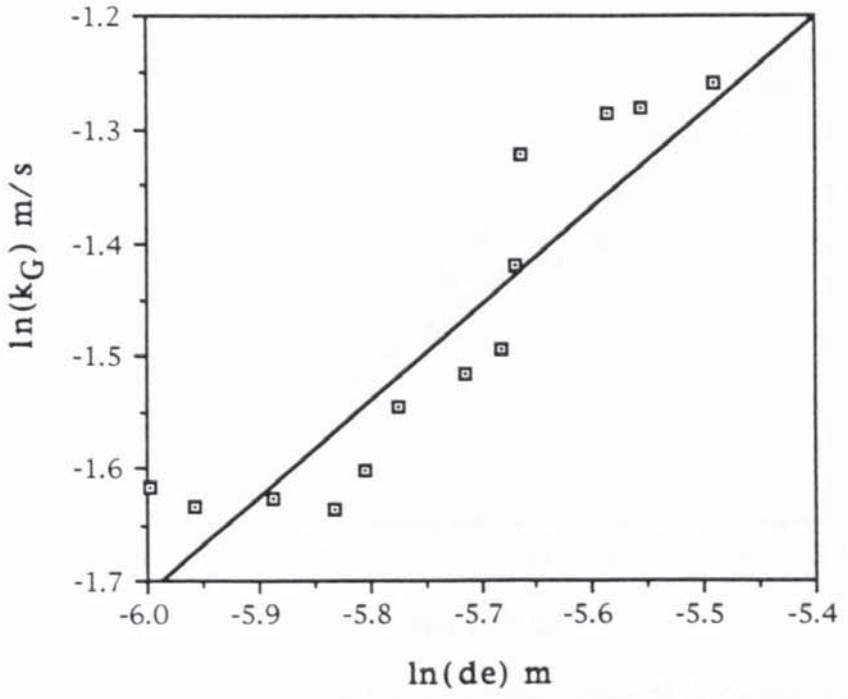

Figure B2. A plot of $\ln(k_G)$ vs ln(de) of distilled de-ionised water droplets evaporated in free-flight. Air temperature, 50°C. (correlation coefficient, R^2=0.84)

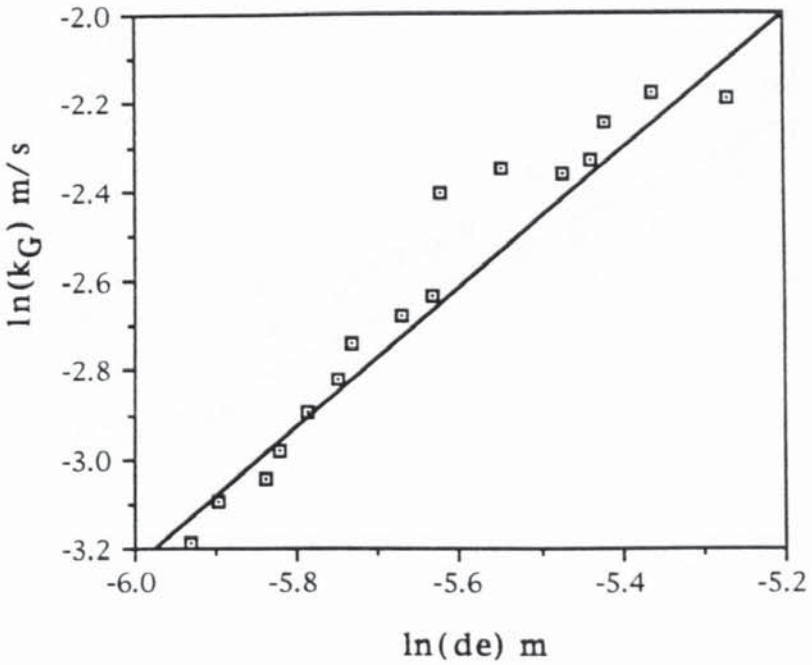

Figure B3. A plot of $\ln(k_G)$ vs ln(de) of n-propanol droplets evaporated in free-flight. Air temperature, 62°C. (correlation coeffeicient, $R^2 = 0.94$)

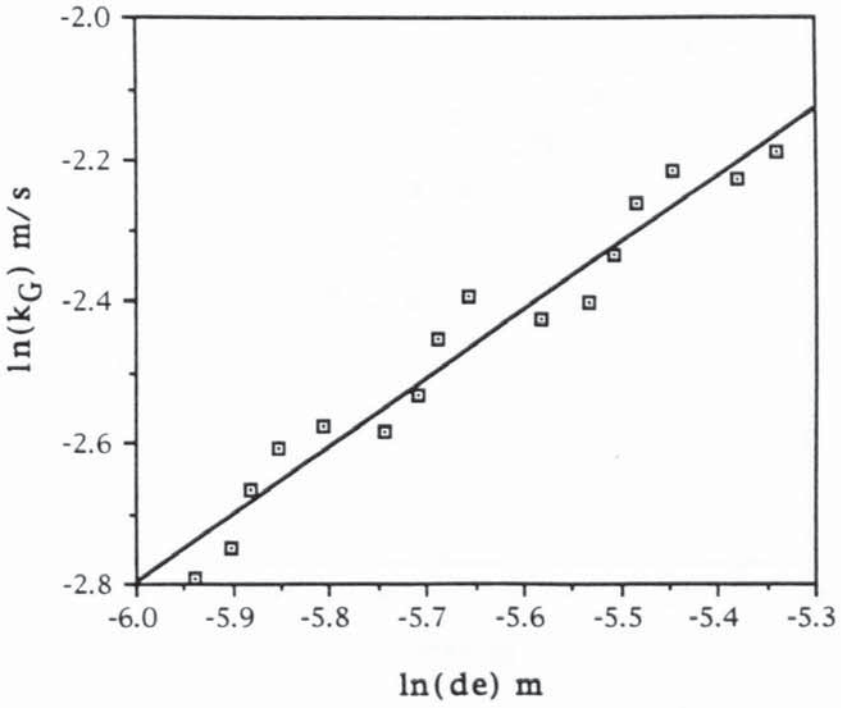

Figure B4. A plot of $\ln(k_G)$ vs ln(de) of n-propanol droplets evaporated in free-flight. Air temperature, 50°C. (correlation coefficient, $R^2 = 0.95$)

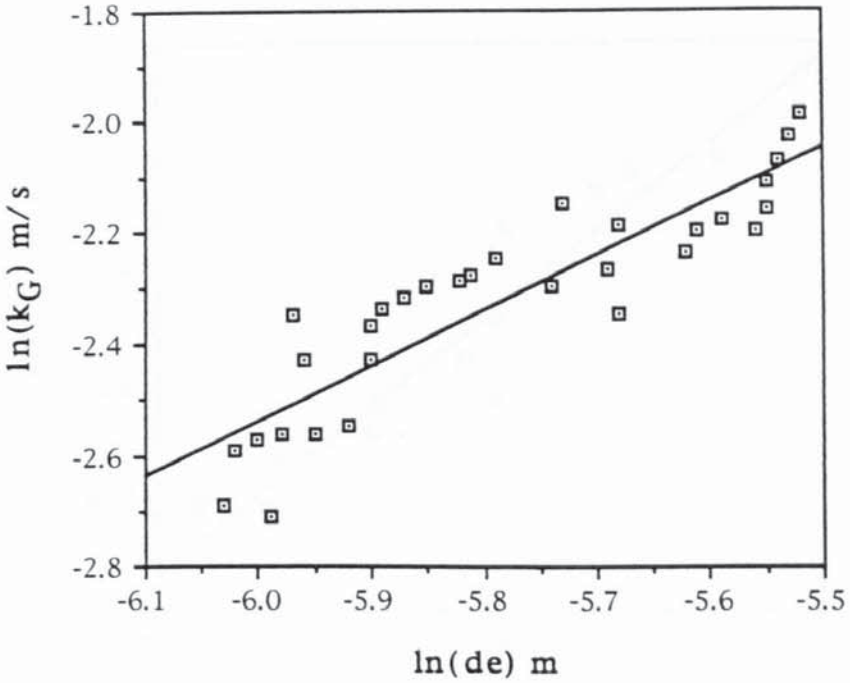

Figure B5. A plot of $\ln(k_G)$ vs ln(de) of monoethanolamine liquid droplets evaporated in free-flight at 62°C air temperature. (correlation coefficient, $R^2 = 0.81$)

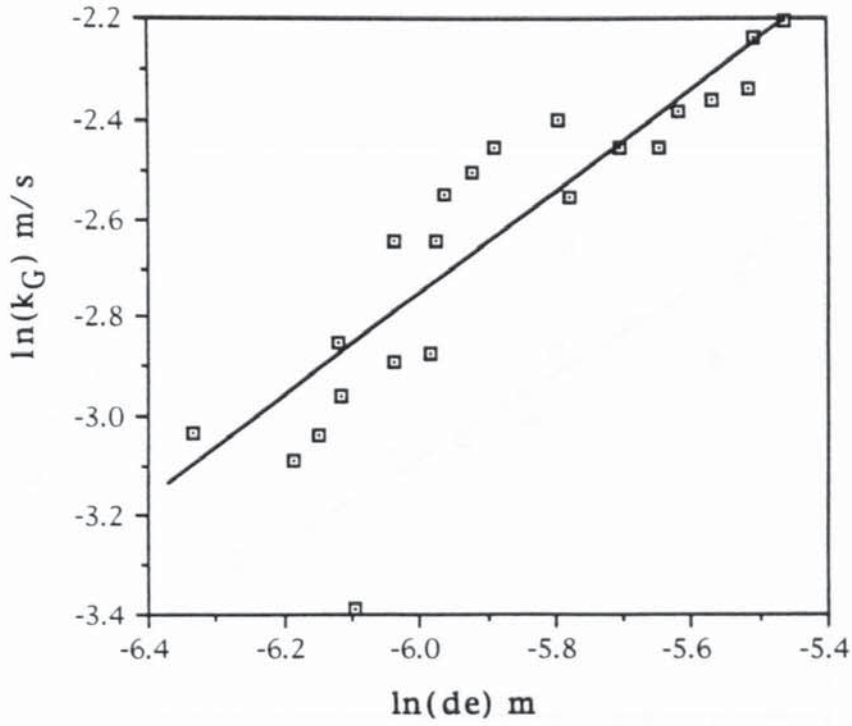

Figure B6. A plot of $\ln(k_G)$ vs ln(de) of monoethanolamine liquid drops evaporated in free-flight at 80°C air temeperature. (correlation coefficient, $R^2 = 0.8$).

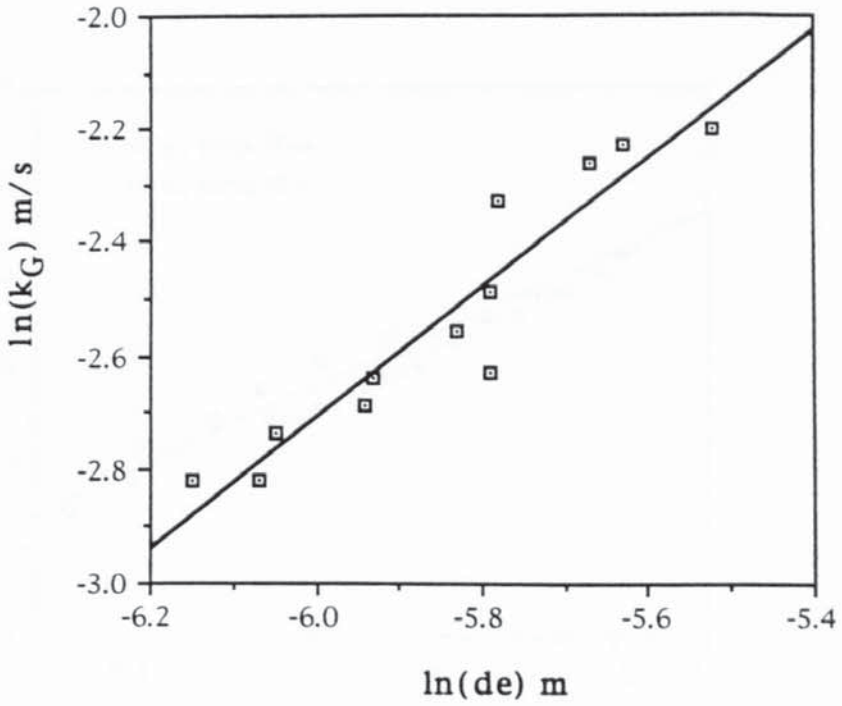

Figure B7. Aplot of $\ln(k_G)$ vs ln(de) of heptane liquid drops evaporated in free-flight. Air temperature, 62°C. (correlation coefficient, $R^2 = 0.9$).

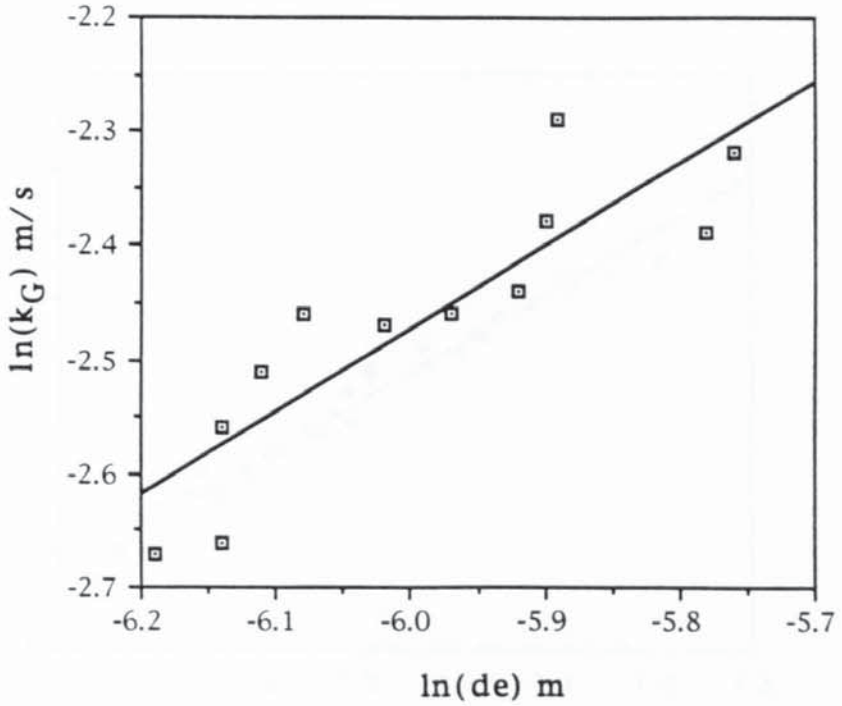

Figure B8. A plot of $\ln(k_G)$ vs ln(de) of iso-butanol drops evaporated in free-flight. (correlation coefficient, $R^2 = 0.8$).

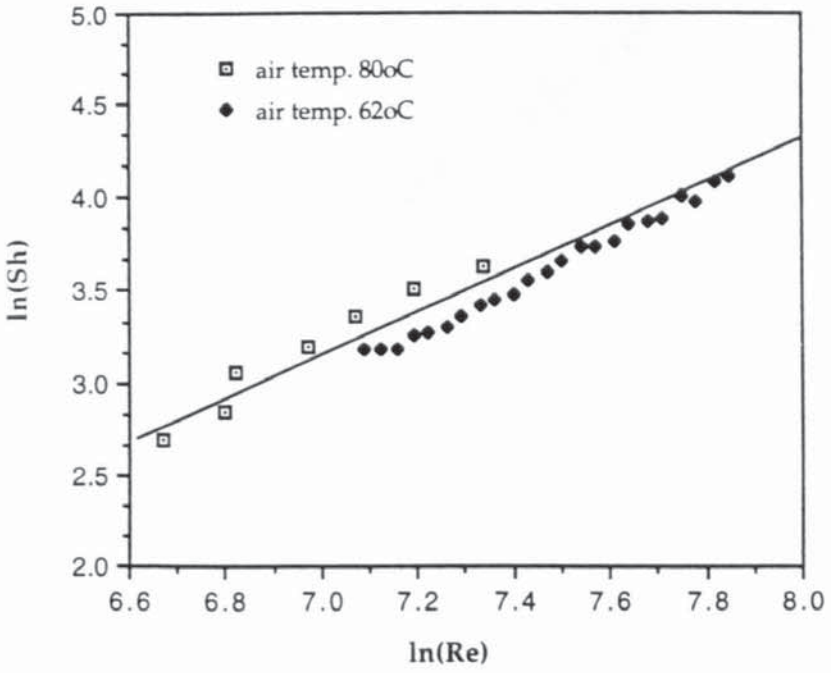

Figure B9. Correlation of ln(Sh) with ln(Re) of distilled de-ionised water droplets evaporated in free-flight. ($R^2 = 0.96$)

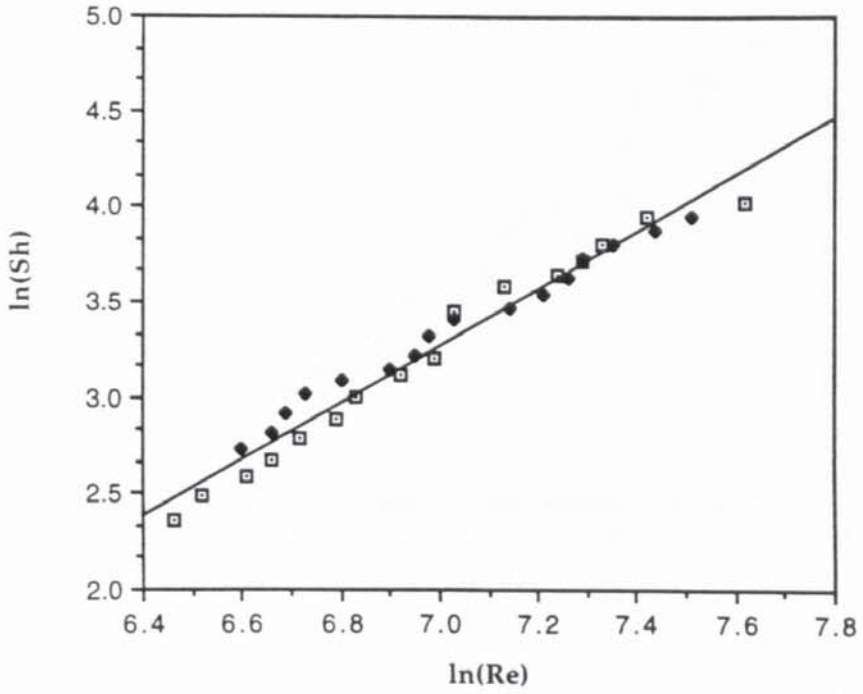

Figure B10. Correlation of ln(Sh) with ln(Re) of n-propanol drops evaporated in free-flight.($R^2 = 0.98$)

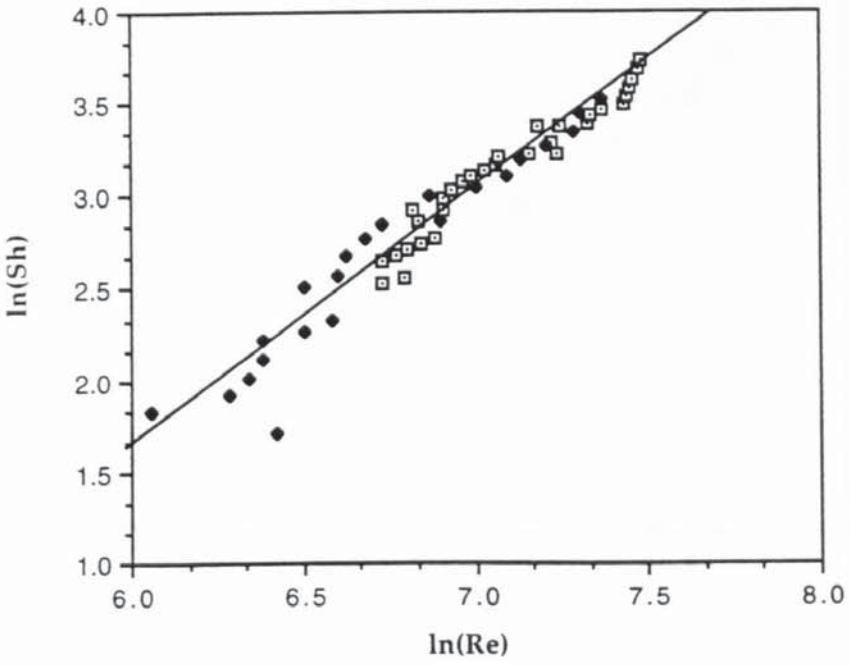

Figure B11. Correlation of ln(Sh) with ln(Re) of monoethanolamine liquid drops evaporated in free-flight. (R^2 = 0.944)

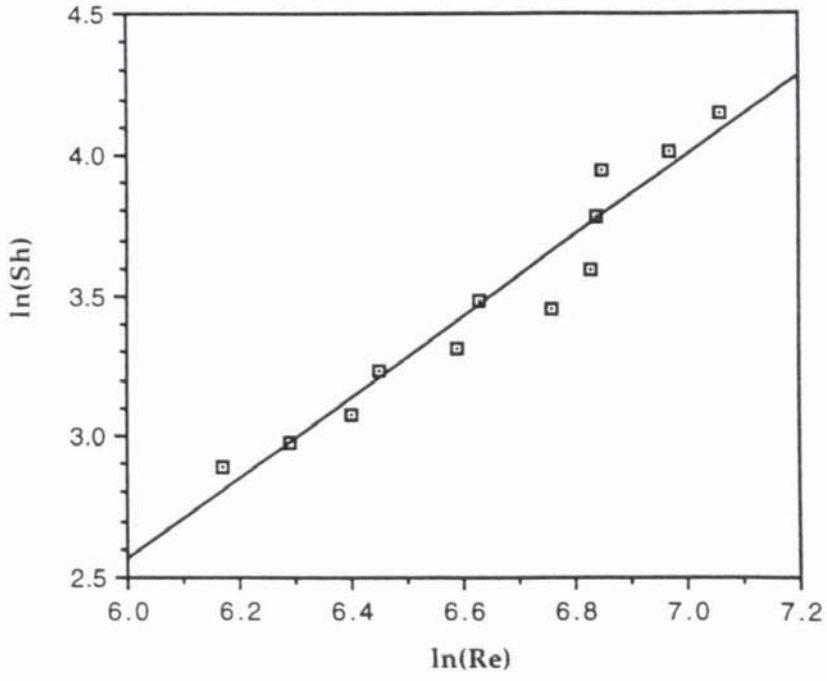

Figure B12. Correlation of ln(Sh) with ln(Re) of heptane drops evaporated in free-flight at 62°C. (R^2 = 0.936)

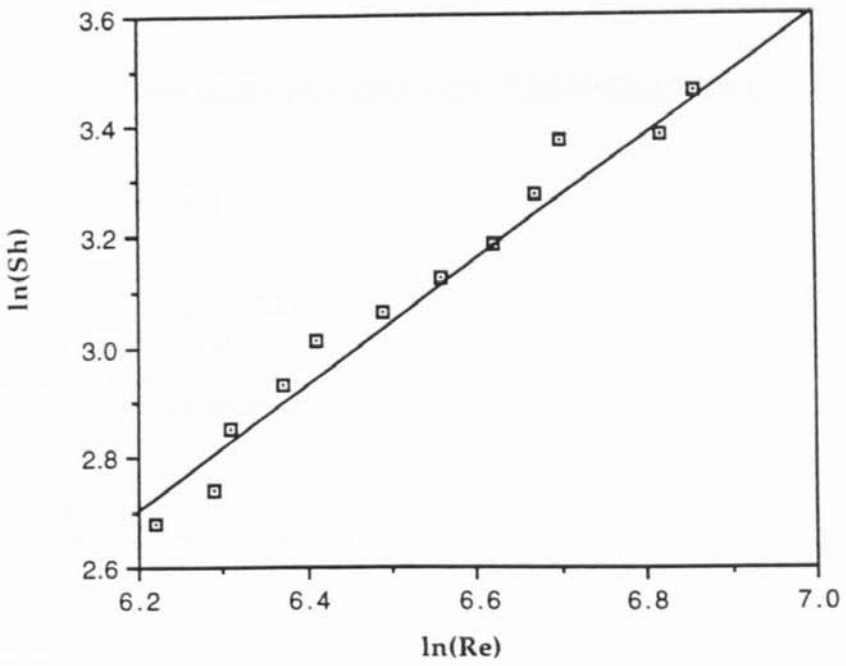

Figure B13. Correlation of ln(Sh) with ln(Re) of iso-butanol liquid droplets evaporated in free-flight. (R^2 = 0.97)

APPENDIX C

PROGRAM SURFACE_TEMPERATURE

```
uses Crt,printer;{graph;}
CONST

molair = 29; cpa= 1.0;eva= 20.1;
R = 8314.34; dyn_vis = 18.22e-06;
PT = 101315.0; Pr = 0.703;
string_length =20; MaxRe = 50;

type
word1 = 1..string_length;
string20 = packed array [word1] of char;
var
count:integer;
set_one, List: set of char;
Ch,liquid,W,I,P,H,M : char;
water,n_propanol,heptane,Iso_butanol,
monoethanolamine: string20;
OrigMode,LastCol,LastRow: Word;
Done,ioerr: Boolean;
pvap,pva,Hw,cpvap,str_inc_vol,moladd,pva1,clause,
s,Dv,Sc,Ts,x1,x2,claus,lat,Hwg,conv,Ta,Tb,Twb,B,pvap1,
AntA,AntB,AntC,moliq,evliq,Ts1,vis,den,sur_ten,x4,tf :real;
{-------------------------------------------------------------------------------}
procedure Initialize;
{ Initialize the video mode, LastCol, LastRow,}
{ Paint the help line. }
begin
CheckBreak:=False;       { turn off Contrl-C checking }
OrigMode:=LastMode;      { Remember original video mode }
TextMode(Lo(LastMode)+Font8x8); { use 43 or 50 lines on EGA/VGA }
LastCol:=Lo(WindMax)+1;  { get last column, row }
LastRow:=Hi(WindMax)+1;
GoToXY(1,LastRow);       { put message line on screen }
TextBackground(Black);
TextColor(White);
Write(' Alt-Print ',
'Alt-E-Evaporation rate ',
#27#24#25#26'-Cursor ',
'Alt-R-Repeat ',
'Esc-Exit');
Dec(LastRow,80 div LastCol);  { don't write on message line }
end; { Init }
{-------------------------------------------------------------------------------}
procedure MakeWindow;
{ Make a window, with background and foreground colors }
var
X,Y,Width,Height: Word;
begin
Width:=(LastCol-12)+2;     { window size }
Height:=(LastRow-18)+2;
```

```
 X:=1;{Random(LastCol-Width)+1;}    { random position on screen }
 Y:=9;{Random(LastRow-Height)+1;}
 Window(X,Y,X+Width,Y+Height);
 TextBackground(3);
 TextColor(14);
 ClrScr;end;
 {-------------------------------------------------------------------------------}
 Procedure get_info;
 begin
 List:= [ 'W', 'P', 'I', 'H', 'M'];
 REPEAT
 Set_one:=[];
 writeln;
 writeln('          SELECT LIQUID EVAPORATED    ');
 writeln('-------------------------------------------------------------------------------');
 writeln;
 Writeln('     W : Distilled De-ionised Water ');writeln;
 writeln('     P : n-Propaonl '); writeln;
 writeln('     I : Iso-butanol ');writeln;
 writeln('     H : Heptane ');writeln;
 writeln('     M : Monoethanolamine ');liquid:=ReadKey;
 liquid:=upCase(liquid);
 if liquid = #27 then begin
 case liquid of
 #27: Done:=True;
 end;
 clrscr;
 TextMode(origMode);
 Halt;
 end;
 {-------------------------------------------------------------------------------}
  writeln;writeln; set_one:= set_one + [liquid];
  {$I-}
  IF list>=set_one then
  begin
repeat
  writeln(' Enter air temperature and the Wetbulb in oC');
  read(Ta,Ts1);
 ioerr:=(IOresult<>0) or ((ta-ts1)<0);
if ioerr then
    begin
      writeln(#7,'...Invalid entry, Re-enter temperatures....');
    end;
until not ioerr;
{$I+}
  WRITELN; Ts:=(Ts1+273); Ta:=(Ta+273);
 {$I-}
 repeat
  writeln(' Enter humidity of air and Cp of vapour');
  read(Hwg,cpvap);
  ioerr:=IOresult<>0;
if ioerr then
    begin
      writeln(#7,'...Invalid entry...');
    end;
until not ioerr;
{$I+}
```

```
   end
   else
      begin
      writeln;
      writeln('NOT A LEGAL SELECTION. Press any key to restart ');
      ch:=ReadKey; clrscr; end; {legal message}
   until list>=set_one;
   end; {Get_Info}
{-------------------------------------------------------------------------------}
Procedure Vapour_Pressure;
begin
   if liquid='P' then
      begin
AntA:= 17.5439; AntB:= 3166.38;
AntC:=(-80.15); moliq:= 60.1;
evliq:= 70.82; tb:=370.2; vis:=1.95e-03;
den:=804; sur_ten:=25.26e-03;
      end;

   if liquid='W' then
      begin
AntA:= 18.3036; AntB:= 3816.44;
AntC:=(-46.13); moliq:= 18;
evliq:= 12.7; tb:= 373; vis:=8.6e-04;
den:=998; sur_ten:=0.072;
      end;

   if liquid='I' then begin
AntA:= 16.8712; AntB:= 2874.73;
AntC:=(-100.30); moliq:= 74.123;
evliq:= 91.28; tb:= 380.8; vis:= 3.44e-03;
den:=802; sur_ten:=23.0e-03;
      end;

   if liquid='M' then
      begin
AntA:= 17.8174; AntB:= 3988.33;
AntC:=(-86.93); moliq:= 60.0841;
evliq:= 70.82;  tb:=443.3;  vis:=17.87e-03;
den:=1016; sur_ten:=0.052;
      end;

   if liquid='H' then
      begin
AntA:= 15.8757; AntB:= 2911.32;
AntC:=(-56.51); moliq:= 100.26;
evliq:= 147.18;  tb:=371.4; vis:=3.486e-04;
den:=679; sur_ten:=23.28e-03;
      end;
end;

{-------------------------------------------------------------------------------}
Procedure calc;
begin
Twb:=(Tb-93);
pval:=AntA-(AntB/(Twb+AntC));
pva:=exp(pval);
```

```
pvap:=133.32*pva;
clause:= (Twb*Tb/(Tb-Twb))*Ln(PT/Pvap);
B:=ln(pva)+(clause/Twb);
count:=0;
repeat
count:=count+1;
pvap:=exp(B-(clause/Ts));pvap1:=133.32*pvap;
claus:= (Ts*Tb/((Tb-Ts)*moliq))*Ln(PT/Pvap1);
lat:=R*claus/1000;
moladd:=sqrt((1/moliq)+(1/molair));    {sum of molecular weights}
str_inc_vol:=exp(0.33*ln(eva))+exp(0.33*ln(evliq)); {Structural incremental volume}
Dv:= 1.0e-07*exp(1.75*ln(Ts))*moladd/sqr(str_inc_vol); {Diffusivity}
Sc:=dyn_vis/Dv;
x1:=exp(2/3*ln(sc/pr));
Hw:=(Moliq/molair)*Pvap1/(PT-Pvap1);
s:= cpa+(cpvap*Hw);
   begin
   if Ta<>Ts then
     begin
     x2:= lat*((Hw-Hwg)/(Ta-Ts));
     conv:=abs(1-(s*x1/x2));
     end else
     conv:= 0.05;
   end;
   if conv>0.05 then
    begin
    if x2>(s*x1) Then
    Ts:= Ts-0.15
    else
    Ts:=Ts+0.15;
    end;
  until (conv<=0.05) or (Ta=Ts) or (x2=0) or (count=100);
      tf:=(ta+ts)/2;
      if count=100 then begin
      writeln(' Won"t converge after 100 interactions,');
      write('calculations terminated ');
      writeln('press enter to countinue.');
      readln;end;
end;
{-------------------------------------------------------------------------------}
   function func(x4:real):real;
   begin
   func:=(1/sqr(x4));
   end;
{-------------------------------------------------------------------------------}
   function func1(x4:real):real;
   begin
   func1:=1/(exp(0.82*ln(x4)));
   end;
{-------------------------------------------------------------------------------}
    Procedure Evaporate;
    var
    strip,n,v:integer;
    Re1,Re2,St,st1,y1,sum,sum1,inte1,dia,Tm1,Tm2,
    dia1,time,ini_vel,Fin_vel,inte2,dh,beta1,Time1,
    beta,sc3,xw,xw1,mass, drop_dia,Final_drop_dia,
    Final_drop_mass,Ev1,Ev,Xwmass,web,vt1,Erate2 :real;
```

```
   tot,tot1,sh1,Erate,ReX: array[1..MaxRe] of real;
   begin
   {$I-}
repeat
writeln(' Enter the initial diameter of droplet in mm');
   readln(dia1);
ioerr:=IOresult<>0;
if ioerr then
    begin
      writeln(#7,'...Invalid entry...');writeln;
    end;
until not ioerr;
{$I+}
dia:= 0.001*dia1;
 {$I-}
repeat
   writeln(' Enter the initial and final Re of spray');
   readln(Re1,Re2);
   ioerr:=(IOresult<>0) or ((re1-re2)<0);
if ioerr then
    begin
    writeln(#7,'...Invalid entry, Re1 must be > Re2...');writeln;
    end;
until not ioerr;
{$I+}
   st:=(Re1-Re2);
   if st>2000 then strip:=40;
   if st<=2000 then strip:=20;
   st1:=st/strip;
   x4:=y1;
   dh:=(pT-pvap1)*moliq/(1.07*R*Tf);   {humidity gradient}
   beta1:= (dyn_vis*1.95e-05/vis)*sqrt(den/(sur_ten*dia));
   beta:=exp(0.15*ln(beta1));
   sc3:=exp(0.33*ln(sc)); {schmidt number}
   n:=0;v:=0;sum:=0; Erate2:=0;
   sum1:=0;
    repeat
    n:=n+1;
    x4:=Re1-(st1*v);
    ReX[n]:=x4;
    tot[n]:=func(x4);
    sum:=sum+tot[n];
    tot1[n]:=func1(x4);
    sum1:=sum1+tot1[n];
    Sh1[n]:=2+(0.02*beta*sc3*(exp(1.18*ln(x4))));
    Erate[n]:=(2*dh*1.07*dia*dv*pi)*(1+
    (0.01*beta*sc3*exp(1.18*ln(x4))));
    Erate2:= Erate2+Erate[n];
    v:=v+1;
    until v=strip;
    vt1:=sqrt(4*dia*(den-1.07)*9.81/(3*1.07));
  inte1:= st1*sum; inte2:=st1*sum1;
  Xw1:=inte1+(0.01*beta*sc3*inte2);
  Ev1:=8*pi*den*exp(3*ln(dia))*dh/(3*sc);
  Ev:=ev1*xw1;          {evaporation}
  Xw:=(16*dh/Sc)*Xw1*100;
  mass:=((pi/6)*exp(3*ln(dia))*den)*1000;
```

```
  time:=inte1*4*den*sqr(dia)/(3*1.07*dyn_vis);
  Ini_vel:=Re1*dyn_vis/dia;
  web:=1.07*sqr(Ini_vel)*dia/sur_ten;
  if (xw<100) and (web<15) then begin
  XwMass:= xw*mass/100;
  Final_drop_mass:= mass-Xwmass;
  drop_dia:=6*Final_drop_mass/(pi*den*0.001);
  Final_drop_dia:=10*exp(0.33*ln(drop_dia));
  Fin_vel:=Re2*dyn_vis/(0.01*Final_drop_dia);
  end
  else
  begin
  if (xw>100) and (web<15) then begin
  writeln(' droplet is completely evaporated!!!');
  Writeln(' Initial mass := ',mass:4, 'g');
  writeln(' initial velocity of spray:= ',ini_vel:3:1, 'm/s');
  writeln(' Residence time = ', time:3:1, 'sec');writeln;writeln;
  writeln(' **** Select Option From Menu ****');
  end;
  if web>15 then begin
  writeln(' droplet exceeds weber stability limit, i.e We>15 ');
  writeln(' initial velocity of spray:= ',ini_vel:3:1, 'm/s');
  writeln(' drop diameter = ', dia1:3:2, 'mm');
  writeln;writeln;
  writeln(' **** Select Option From Menu ****');
  end;
  end;
  if (xw<100) and (web<15) then begin
  Writeln(' Initial drop mass := ',mass:4:4, 'g');
  writeln(' initial velocity of spray:= ',ini_vel:3:1, 'm/s');
  writeln(' Final drop mass := ',Final_drop_mass:4:4, 'g');
  writeln(' Final Drop Dia := ' ,Final_drop_dia:3:1, 'mm');
  writeln('-------------------------------------------------------------------------------------------');
  for n:=1 to n do begin
  delay(1000);
  writeln(' Sh = ',Sh1[n]:5:2,' Re = ',ReX[n]:5:1, ' Evap.Rate =',Erate[n]:5,'kg/s');
  writeln; end;
  writeln(' Final Erate = ',Erate[n]:5);
  end;end;
{-------------------------------------------------------------------------------------------}
Procedure Results;
begin
CLrSCR;
WRITELN;
WRITE('   SURFACE CONDITIONS OF DROPLETS EVAPORATED');
writeln(' AT ',(TA-273):4:1,'oC AIR TEMP. ');
writeln;
WRITELN('       AND AT ',Ts1:4:2, 'oC WET-BULB TEMPERATURE' );
writeln;
writeln('     DROPLET SURFACE TEMPERATURE AND DIFFUSIVITY     ');
WRITELN(' -------------------------------------------------------------------------------');
writeln('  DROPLET SURFACE TEMPERATURE,   Ts = ',(Ts-273):4:2,'oC');
writeln;
writeln('  LATENT HEAT OF VAPORISATION,   Lv  = ',lat:4:2,' kJ/kg');
writeln;
writeln('  DIFFUSION COEFFICIENT,         Dv = ',Dv:2, ' m^2/s');
writeln;
```

```
writeln('  VAPOUR PRESSURE AT Ts,        Pv = ',pvap1:4:3, 'Pa');
writeln('-------------------------------------------------------------------------------');
end;


Procedure Print;
begin
WRITELN(Lst);
WRITE(lst,'   SURFACE CONDITIONS OF DROPLETS EVAPORATED AT ');
WRITELN('',(TA-273):4:1,'oC');
writeln(Lst);
WRITELN(Lst,'       AIR TEMP., AT ', Ts1:4:2,'oC WET BULB. ');
writeln(Lst);
writeln(lst,'     DROPLET SURFACE TEMPERATURE AND DIFFUSIVITY     ');
WRITELN(lst,'-------------------------------------------------------------------------------');
writeln(lst,'  DROPLET SURFACE TEMPERATURE,   Ts = ',(Ts-273):4:2,'oC');
writeln(lst);
writeln(lst,'  LATENT HEAT OF VAPORISATION,   Lv  = ',lat:4:2,' kJ/kg');
writeln(lst);
writeln(lst,'  DIFFUSION COEFFICIENT,        Dv = ',Dv:2, ' m^2/s');
writeln(lst);
writeln(lst,'  VAPOUR PRESSURE AT Ts,        Pv = ',pvap1:4:3, 'Pa');
writeln(lst,'-------------------------------------------------------------------------------');
writeln(lst, chr(12));
end;
{-------------------------------------------------------------------------------}
Procedure Redo;
begin
   Initialize;
   MakeWindow;
   get_info;
   Vapour_Pressure;
   calc;
   results;
   end;
   {-------------------------------------------------------------------------------}
   begin { program body }
   Initialize;
   MakeWindow;
   get_info;
   Vapour_Pressure;
   calc;
   results;
   Done:=False;
   repeat
   Ch:=ReadKey;
   case Ch of
   #0:                { Function keys }
      begin
      Ch:=ReadKey;
      case Ch of
      #19: Redo;              { Alt-R }
      #45: Done:=True;        { Alt-X }
      #72: GotoXY(WhereX,WhereY-1); { Up }
      #75: GotoXY(WhereX-1,WhereY); { Left }
      #77: GotoXY(WhereX+1,WhereY); { Right }
      #80: GotoXY(WhereX,WhereY+1); { Down }
```

```
    #25: Print;              { Print }
    #18: Evaporate;          { Evap-calc}
    end;
  end;
  #3: Done:=True;            { Ctrl-C }
  #13: WriteLn;              { Enter }
  #27: Done:=True;           { Esc }
  else
  Write(Ch);
  end;
  until Done;
  TextMode(OrigMode);
  end.
```

APPENDIX D

LIST OF PUBLICATIONS

1. "Mechanism of Liquid Oscillation; Effect on Mass Transfer Rates". Proc. International Drying Symposium'94, A, 435. Australia.
(with E.L Smith, and C.J. Mumford)

2. "Enhanced Heat and Mass Transfer of Oscillating Droplets Under Forced Convection". Proc. IChemE Research Event, 1994, 2, 1054. London.
(with D.E. Walton and C.J. Mumford)

3. "Evaporation of Drops Freely Suspended in an Air Stream". Proc. IChemE Research Event, 1993, 1, 489. Birmingham.
(with C.J. Mumford)

4. "Evaporation from Droplets in Free-Flight; Effect of Skin-Forming Materials". Proc. IChemE Research Event, 1994, 1, 477. London.
(with C.J. Mumford)

5. "The Enhanced Evaporation of Liquid Drops in Free-Flight".
(Submitted for publication, Drying Technology, 1995)
(with E.L Smith and C.J. Mumford).